THE UNDERWATER SEPARATION OF DIAMANTIFEROUS MARINE GRAVELS

by

T J ROSSOUW

BSc (Eng) UCT

A thesis submitted in complete fulfilment
of the requirements for the degree of Master of Science

Department of Civil Engineering
University of Cape Town

September 1988

DEDICATION

To my parents, who endured, yet supported,
my many career changes.

DECLARATION

I, Trevor John Rossouw, declare that this thesis is essentially my own work and has not been submitted for a degree at another university.

Signed by candidate

T J ROSSOUW

September 1988

SYNOPSIS

Three underwater separation devices have been designed, constructed, tested and analysed to determine their suitability for the underwater separation of diamantiferous marine gravels.

The research facility where the devices were tested was constructed at the University of Cape Town's Hydrotransport Research facility.

The first device tested was a *converging elutriator* which separates the oversize gravel from the smaller diamond-bearing gravel, using their varying particle settling velocities in an upward flowing fluid.

The *cyclosieve* and *spirosieve* are two other choices that both use rotational flow to create a centrifugal force, which forces the gravel onto a screening surface.

The test work carried out investigated the effect of various variable parameters on the separation efficiency of each device.

Test results and observations are presented and discussed. It was concluded from these results that both the converging elutriator and the cyclosieve, in their present forms, were unsuitable underwater separation devices. It was also concluded that the spirosieve was the most favourable device tested thus far, because it fulfilled most of the design criteria.

Finally, it was recommended that a large scale spirosieve should be constructed and tested, while continuing tests on the original spirosieve model.

ACKNOWLEDGEMENTS

Professor John Lazarus, for his support, encouragement and inventive ideas.

De Beers Marine, for the financial support and the opportunity to undertake this project.

Mr Mike Dingle, for his knowledge and encouragement at all times.

Mrs Cheryl Wright, for her typing and reading skills.

Mrs Pat Jordaan, for her typing of all the reports, again and again and again.

The staff, and especially my fellow postgraduate students, for the stimulating working environment.

The technical staff, Messrs G Bertuzzi, D J Botha and R Edge, as well as N Hassen and A Siko, for many hours of practical assistance.

Pam, for her encouragement, support and endurance, especially over the last few weeks of this thesis.

Mr Rob Cooke, for his encouragement and proof reading.

To my family and friends for their support.

TABLE OF CONTENTS

LIST OF FIGURES

LIST OF TABLES

NOMENCLATURE

General

C_v	Solids volumetric concentration	%
d_p	particle diameter	m
g	gravitational constant	m/s^2
R_e	Reynolds Number	
R_{ep}	particle Reynolds Number	
t	time	sec
S_s	solids relative density	
ρ_s	solids density	kg/m^3
ρ_ℓ, ρ	liquid density	kg/m^3
μ	viscosity	Pa.s
ν	kinematic viscosity	m^2/s

Converging Elutriator

D	diameter of the elutriation column	m
d_n	diameter of the primary outlet nozzle	m
h	height of primary outlet nozzle	m
Q_p	primary flow rate	m^3/s
Q_s	secondary flow rate	m^3/s
SF	Shape Factor	
V_{an}	annular velocity	m/s
V_{ec}	elutriation column velocity	m/s
V_p	primary circuit velocity	m/s
V_{pn}	primary outlet nozzle velocity	m/s
V_s	secondary circuit velocity	m/s
V_t	terminal settling velocity	m/s
V_t'	hindered settling velocity	m/s
α	a function of Reynolds number (Richardson & Zciki, 1954)	

Cyclosieve

d_i	primary inlet diameter	m
F_c	centrifugal force	N
F_g	gravitational force	m
n	revolutions of the spirosieve	o
Q_s	secondary/fines flow rate	m^3/s
Q_p	primary inlet flow rate	m^3/s
r	local radius at any point	m
R	radius of cyclosieve screen	m
s	height that particles fall	m
v	primary inlet velocity	m/s
$V_{(r)}$	inward radial velocity	m/s
$V_{(t)}$	tangential velocity	m/s
$V_{(tr)}$	terminal radial settling velocity	m/s
Ω	angular velocity	rad/s

Spirosieve

b	height of an internal volume of liquid	m
d	width of an internal volume of liquid	m
f	friction factor	
L	length of an internal volume of liquid	m
p	wetted perimeter	m
Δp	pressure differential	Pa
Q	flow rate	m^3/s
R	radius at which the screen is located	m
v	velocity within the spirosieve	m/s
τ_o	shear stress	Pa

If the deepsea prospecting being undertaken at present shows ocean mining to be feasible, an underwater separation device will be required at a depth of up to 200 m. Figure 1 shows a schematic layout of the probable location of the separation device.

1. The Advantages of Underwater Separation

The major advantages of underwater separation are :

1. A smaller diameter delivery hose between the seabed and the surface can be used.

2. Blockage of the delivery hose by large rocks is less likely.

3. Wear rate of the delivery hose is reduced.

4. Less material needs to be processed aboard the ship.

5. Less water is required for conveying.

6. For air lift pumps a smaller compressor is needed to lift the gravel/water mixture.

2. Research Objectives and Design Criteria

A research facility was commissioned by De Beers Marine to carry out tests on various separation devices. The facility was built in the hydraulic tower of the Department of Civil Engineering, University of Cape Town.

The objectives of this research project are to design, construct, test and analyse several devices for the underwater separation of diamantiferous marine gravels, situated at up to 200 m below the surface of the sea.

The design criteria of the device are as follows :

1. The device must separate the gravel at 16 mm.

2. It must be simple, robust and easily maintained on a daily basis.

3. It is to be small and easily handled by a crane.

4. The device must be able to handle between 300 m^3/hr and 500 m^3/hr of solid/water mixture, with a delivered solids concentration of approximately 6% by volume or 15% by weight.

5. Discharge of the oversize coarse material should be continuous, but batchwise would be satisfactory.

6. Discharge of the undersize will be to an airlift system consisting of a 100 mm diameter pipeline.

The only "restraint" to the research is that one of the devices to be tested has already been designed and manufactured.

3. Thesis Objectives

The main objectives of this thesis are :

1. To present the experimental results and observations of tests carried out on the various separation devices.

2. To analyse and discuss the results and observations.

3. To draw conclusions on the suitability of each device for underwater separation.

4. Thesis Outline

The first chapter of this thesis consists of a literature review of relevant land based and underwater separation devices. Conclusions are drawn concerning the suitability of the reviewed separation devices for underwater separation. The underwater separation devices tested are then presented and discussed in detail.

The following three chapters describe the test rigs in the research facility, their instrumentation and system operation. The calibration of the instrumentation, measurement techniques and the accuracy of the measurements taken are then presented. This is followed by a description of the various types of materials tested and their preparation.

The experimental procedure is also explained and is followed by the experimental test results and observations. A detailed discussion of these results and observations is then presented.

Conclusions and research recommendations complete the investigation.

The References and Appendices follow and form the final part of the thesis document.

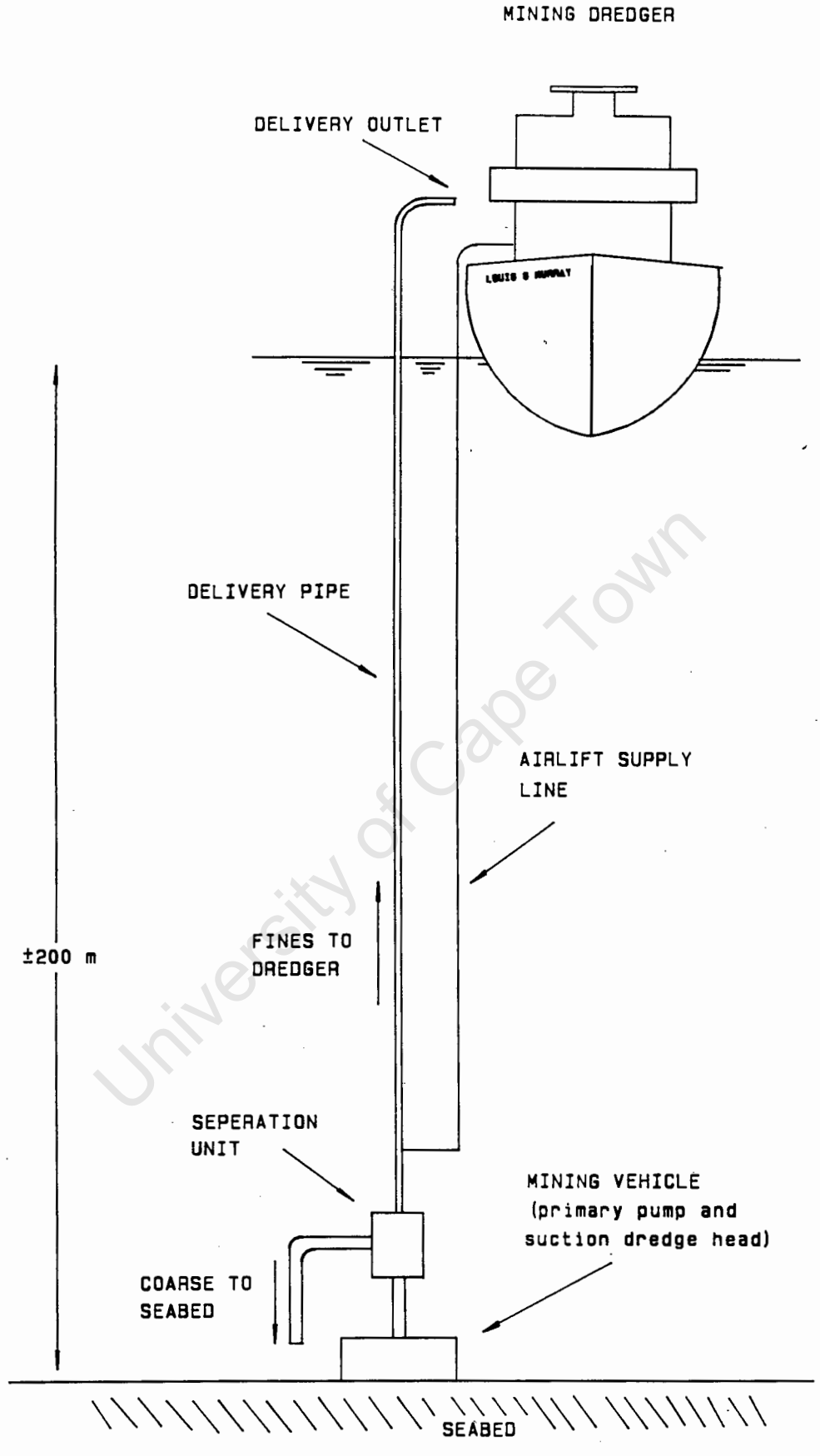

Figure 1 : Layout of the probable location of the separation device.

CHAPTER 1

LITERATURE REVIEW

INTRODUCTION

In this review various methods of separation, i.e. screening/scalping and classification, are presented. Although the separation devices discussed are predominantly land based, they could all operate in principle in a submarine environment.

1.1 SCREENING AND SCALPING DEVICES

Screening is a continuous process whereby particles differing in size are separated from each other by a perforated surface. Scalping is similar to screening but refers to the removal of a small amount of oversize material from a feed that is predominantly fines (Kelly & Spottiswood, 1982).

There are many types of screening and scalping devices in operation but generally they can be classified as stationary or dynamic, depending on whether their screening surface is stationary or moving. The screening surface can be made in a variety of types, shapes, sizes and materials. Table 1.1 shows some of the screening surfaces that are commerically available.

1.1.1 Static Screen

Figure 1.1 from Van Dooremalen (1973), shows the general arrangement of a static screen used aboard gravel dredgers for separating coarse gravel from undersize sand. The screen surface is usually made up of woven mesh and inclined at an angle between 10° and 30°, depending on the feed rate and required screening efficiency.

The main purpose of the screen is to separate the undersize in the feed and to pass it through the screen deck, so the efficiency may be stated as follows :

$$\text{Efficiency} = \frac{\text{Percentage of feed which passed through}}{\text{Percentage of feed which is undersize and should pass through}}$$

(Bovingdon, 1975)

The solid/water mixture is fed onto the screen at its highest point and moves down the screen surface under gravity. The undersize that passes through the apertures is directed overboard while the gravel is fed into storage hoppers.

Tests carried out by Mineralaal Technologisch Institute, IHC Holland have shown that a screening efficiency of up to 90% can be achieved (Van Dooremalen, 1973). However, the major disadvantage of this screening unit is that the apertures are very susceptible to blockage.

1.1.2 Vibrating Screen

The vibrating screen shown in Figure 1.2 from Bovingdon (1975), is very similar to the static screen except that the inclined angle of the screen is usually less (12° to 18°) or even horizontal. The material moves across the screening surface due to the vibrating motion and, to a larger extent, gravity.

The screening efficiency is greatly improved due to the process of stratification. Stratification is a phenomenon whereby vibration causes small particles to work their way to the bottom of the bed while large particles rise to the top (Figure 1.3 from Bovingdon 1975). The vibrating motion also reduces the amount of blockages that occur on a static screen.

1.1.3 "Underwater" Vibrating Screen

An improvement in screening efficiency can be obtained with both static and vibrating screens by directing water on to the moist material during screening. Water is added to eliminate the adhesive forces arising in a moist mixture of material having various particle sizes. These forces arise between particles as a result of the surface tension of the water and the capillary attraction of the water in the pores. Figure 1.4 from Kelly & Spottiswood (1982), shows that screening is most efficient when the mixture is either completely dry or thoroughly wet.

IHC Holland has developed an "underwater" vibrating screen for the separation of gravel from a gravel-sand-water mixture (see Figure 1.5, Van Dooremalen 1973). The whole unit is mounted on the deck of the ship and the solid/water mixture is fed into a boiling or distribution box before it flows onto the screen. The screen is horizontal and is totally submerged in water. The material moves across the screen due to the vibrating action, with the sand passing through the screen and being directed overboard or to the sand collection hoppers. The gravel that remains on top of the screening surface is also transported with some of the water to the gravel hoppers (Van Dooremalen, 1973).

The advantages of this type of screen are :

- high efficiency
- practically insensitive to change in feed rate
- low power consumption
- not subject to blockage.

The disadvantages are :

- very large device
- requires auxilliary power for vibrating.

1.1.4 Trommel

The trommel is a multiphase, revolving cylindrical screening unit (Figure 1.6, Kelly & Spottiswood 1982). The cylindrical screens with different size mesh apertures are of varying diameters and can, therefore, fit inside each other. They are inclined at an angle so that the material that is fed into the inlet can pass over and through the rotating screens. The rotating action also helps to break up agglomerations of small clay particles and to detach small particles from larger ones, thus improving the effectiveness of the screening operation.

The trommel is often used on the smaller diamond mining vessels for separating the diamond-bearing gravel from the waste material. The reel is fitted with a 50 mm aperture conical screen at the inlet. This screen scalps all the larger rocks from the gravel/water mixture and discharges them overboard.

The major screening portion of the trommel is fitted with three sizes of cylindrical screens. The first (innermost) allows all particles less than 12 mm to pass through while the larger material is retained and collected for further processing. The second retains the intermediate 6 mm - 12 mm gravel. The final screen (outermost) allows the water and particles less than 1,5 mm to pass to waste.

The gravel that flows off each screen is collected and sorted below deck on standard diamond sorting jigs (Anon, S A Shipping News, 1979).

1.1.5 Sieve Bend (DSM Screen)

The sieve bend or Dutch State Mines Screen (Figure 1.7, Bain & Bonnington 1970) is a widely adopted type of dewatering screen but is also used effectively for screening. Its screening efficiency is less than that of a vibrating screen but it takes up far less space than a conventional screen of equivalent capacity.

Figure 1.8 from Bain & Bonnington (1970), shows the principle of solids separation. The solid/water mixture enters the feed box from the feed inlet and falls targentially onto the curved screen. The mixture flows at right-angles to the slots between the wedge shaped bars. The water and smaller particles experience a retardation upon striking the wedge bars and are deflected through the slots. The oversize material remains on top of the bars and is discharged at the end of the screen (Bain & Bonnington, 1970).

1.1.6 Grizzly

The grizzly is essentially a scalping device and is similar in design to a static or vibrating screening unit (Figure 1.9, Kelly & Spottiswood 1982). The main difference being that instead of woven mesh or perforated plate, profile bars are used for the separation. The profile bars, as shown in Table 1.1 from Kelly & Spottiswood (1982), are made of thick, heavy steel and usually run parallel to the direction of feed with large openings between bars.

This type of separation device is widely used in the production of various size quarry stone used in the construction industry.

1.2 CLASSIFICATION DEVICES

Classification is the separation of particles according to their settling rate in a fluid. Because water is the fluid most commonly used in mineral processing, wet classification will only be considered.

Although classification generally aims to separate particles by size, particle density and shape also have a significant effect. The operation is, therefore, more realistically viewed as one of sorting rather than sizing (Kelly & Spottiswood, 1982).

1.2.1 Hydrocyclone

Hydrocyclones have been used in industry since 1950. Firstly in mineral processing and mining but lately in the chemical industry, petrochemical, textile and metal working industries. Their diameters range from 10 mm to 2,5 m and separation sizes range from 2 μm to 250 μm.

Separation within a hydrocyclone is based on the effect of centrifugal forces created within the cyclone body. The hydrocyclone has no moving parts so the necessary vortex is produced by pumping the solid/fluid mixture tangentially into a

stationary cono-cylindrical body. Figure 1.10 from Svarovsky (1984), shows a schematic diagram of a conventional hydrocyclone. The cylindrical part is closed by a cover at the top. The liquid overflow pipe or "vortex finder" is located in the centre of the cover and protrudes some distance into the cyclone body. The overflow leaves through the opening in the apex of the inverted cone.

Except for the region near the tangential inlet, the motion of the fluid within the cyclone body has circular symmetry and is shown in Figure 1.11 from Svarovsky (1984). Most of the incoming fluid moves in a helical flow into the outer portion of the inverted cone thus creating high centrifugal forces. From here a portion of the fluid and the smaller particles begin to feed across to the centre. Some of the outer downward flowing fluid and the larger particles exit through the underflow orifice in the apex of the cone. The smaller particles and fluid in the centre now begin to flow upwards in the inner helical flow and out through the vortex finder (Svarovsky, 1984).

The major advantages of separation by means of a hydrocyclone are that it operates continuously with no moving parts, has low maintenance and is inexpensive and easy to install.

1.2.2 Elutriator

An elutriator is basically a vertical cylindrical tube with water fed into it near the bottom to produce an upward flowing fluid. The solids or solid/water mixture is fed into the cylinder near the top. The large particles having a greater hindered settling velocity than the upward flowing water velocity, settle to the bottom of the cylinder and are removed through a valve. The smaller and slower settling particles are transported upwards and leave via the overflow. Figure 1.12 from Kelly & Spottiswood (1982), shows a continuous flow elutriator used in the mineral processing industry.

The advantages of the elutriator are the same as those of the hydrocyclone. The major disadvantage is that the cut size can have a very wide range if the feed material has a large variation in particle shape.

1.2.3 Cone Separator

The cone separator is a device for separating particles into three particle size ranges (Figure 1.13, World Mining, 1969). The device was developed by Humphreys Engineering Company and consists of a feed distributor (2), a dome or cone shaped separating head (3) with a torus shaped rim (4), and three concentrically arranged hoppers for collecting products (5),(6) & (7).

The solid/water mixture is fed onto the separating head (3) from the feed inlet (1). The mixture flows downwards and outwards over the separating head, becoming thinner as it reaches the outer edge. At the transition between the cone shape and torus (4) the coarser solid particles are thrown off tangentially. The particles fall at different trajectories depending on their size and shape.

The remaining smaller particles stay in the bulk of the water which, due to the Coanda effect, follows the curvature of the torus and discharge into the inner hopper (6).

The Coanda effect is the tendency of a fluid moving through a channel to follow the channel wall. Thus three products, coarse, intermediate and fines, are separated and discharged at the bottom outlets (World Mining, 1969).

The disadvantages of this unit are that the separation efficiency is also shape dependent and would vary according to the flow rate and concentration.

1.3 UNDERWATER MANGANESE NODULE COLLECTION AND SEPARATION UNIT

Prospecting of the seabed at water depths of approximately 5 000 m has revealed large deposits of polymetallic nodules. These nodules, consisting mainly of manganese, are found in the soft cohesive seafloor sediment. Nodule sizes range from 4 mm to in excess of 150 mm in diameter and in concentrations exceeding 15 kg/m^2. Full scale mining of these minerals has not yet begun due to the lack of

agreement on International Law of the Sea, relating to the security and rights of concession, and because there are still sufficient land based reserves (Smale-Adams & Jackson, 1978-1979).

In anticipation of a future mining operation Brochett and Petters have proposed a design for an underwater collection and separation unit that incorporates the principle of screening and scalping using profile bars.

The unit, as shown in Figure 1.14 from Brockett & Petters (1980), would be approximately 23 m in width and would act as a giant vacuum cleaner. As the collector moves across the seafloor, nodules are removed up the inclined duct portion of the dredge head by the scouring action of high velocity water jets. Located under the entrance of each dredge head are a series of parallel profile bars with appropriate spacing for scalping the oversize nodules. The cohesive sediment that is washed from the nodules by the water jets, is removed in the sediment separating screen as shown in Figure 1.15 (Brockett & Petters, 1980). The sediment contaminated water passes through the screen while the nodules too large to pass through the screen are directed onto the optional secondary separation bars for further screening, or directly onto the transport conveyor. They are moved across the conveyor by water jets, to the central collector section, from where they are pumped to the surface for further processing (Brockett & Petters, 1980).

1.4 CONCLUSIONS

Due to the lack of published literature on *underwater separation methods* the following initial conclusions can be made :

1. To date there has not been a need for the development of an underwater separation process besides the manganese nodule collector and screening unit of Brockett & Petters

   or

2. Research and development of underwater mining operations is seldom, if ever, published because it is a largely capital intensive venture and a high degree of competitiveness must, therefore, exist between interested concerns.

   However, from the literature presented, it can be concluded that :

3. The screening and scalping units could be modified to operate in an underwater environment with all having one or more of the following disadvantages :

   - large unit
   - mechanical
   - difficult to handle from the surface
   - require auxilliary power
   - not easily maintained.

4. Although the hydrocyclone is well suited to underwater separation in general it is, however, not suited to separating material with such a large particle size range, maximum particle size or cut size that is required in this mining operation.

5. The separation efficiency of the cone separator would be greatly reduced in an underwater environment, especially as the upright orientation of the unit could not always be maintained, thus affecting the trajectories of the particles.

6. From all the separation units considered the elutriator, in principle, has the greatest potential as an underwater operation device because it fulfills more of the required design criteria than any other unit.

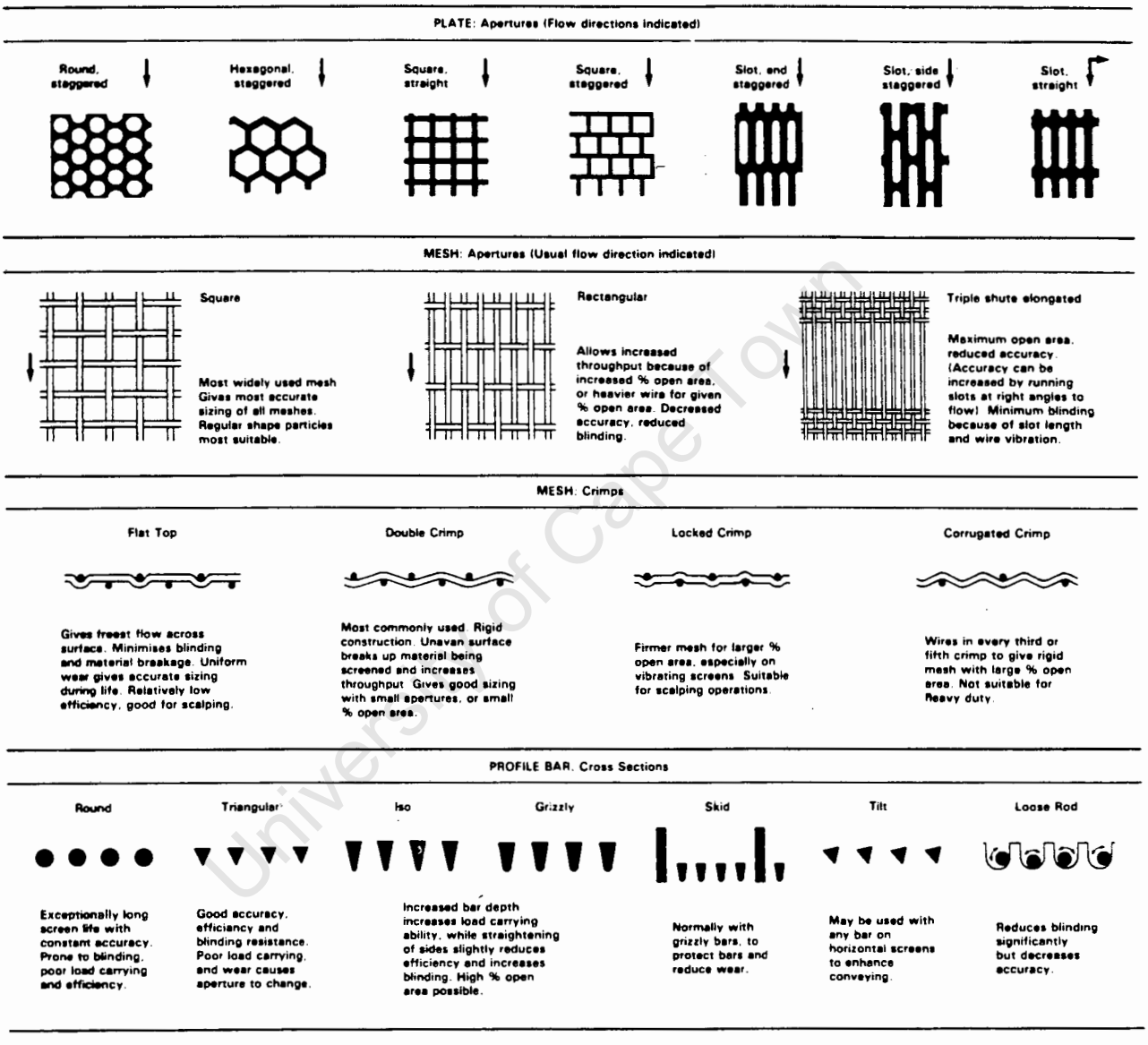

Table 1.1 : Screening surfaces (Kelly & Spottiswood, 1982)

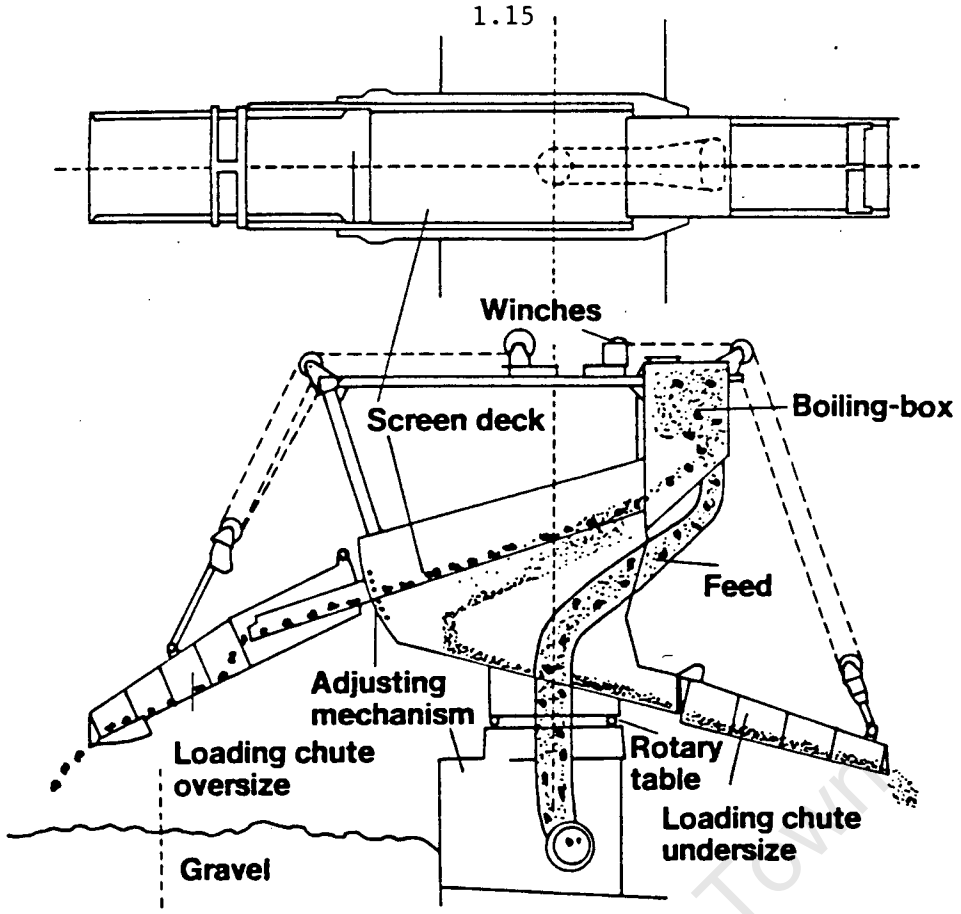

Figure 1.1 : Static screen (Van Dooremalen, 1973)

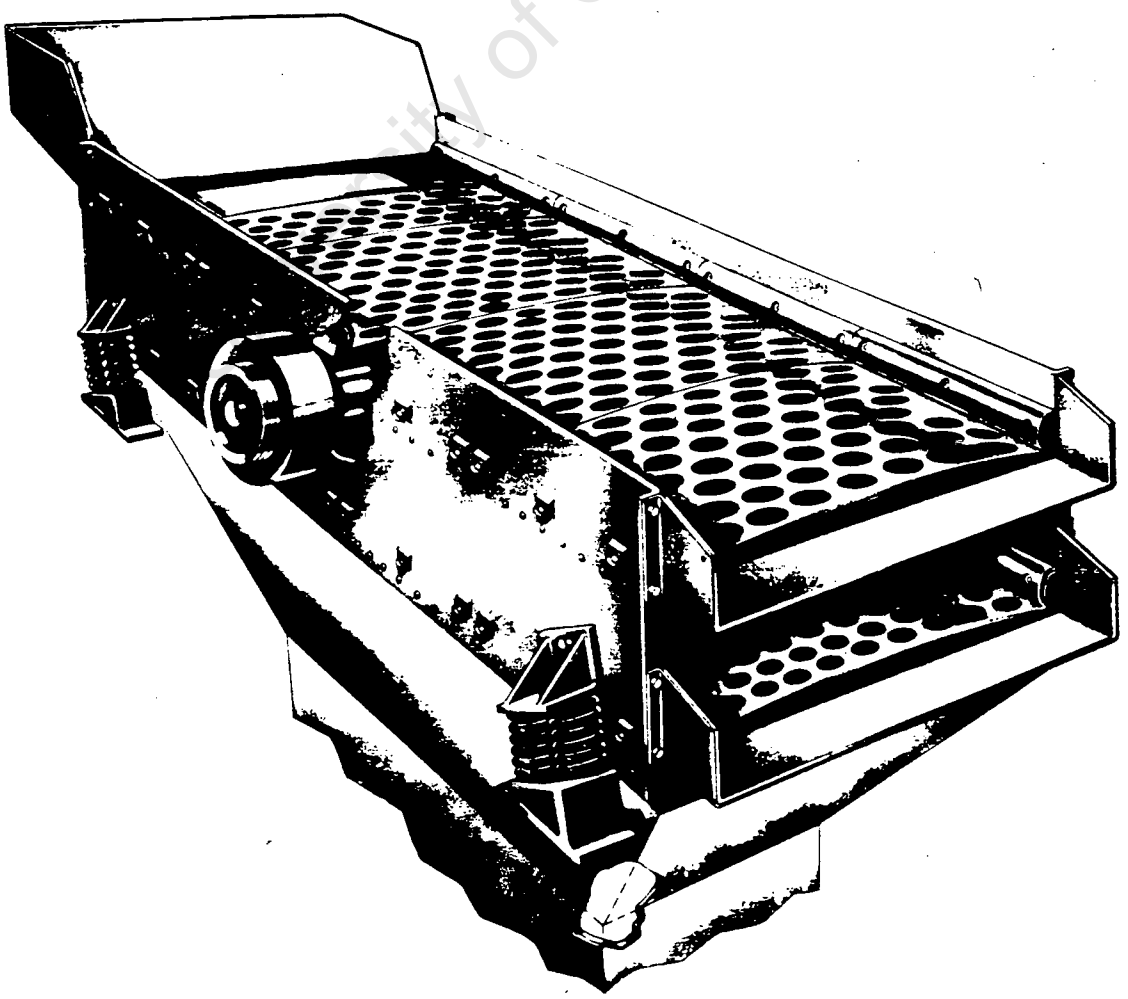

Figure 1.2 : Vibrating screen (Bovingdon, 1975)

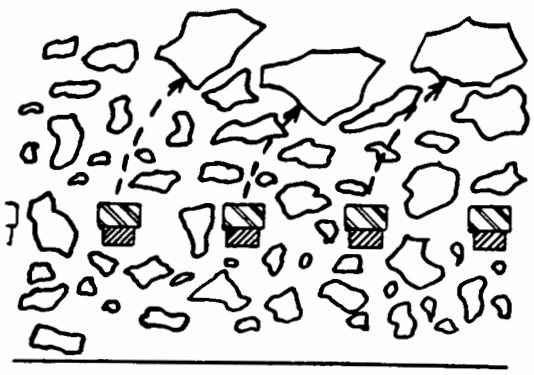

Figure 1.3 : Stratification (Bovingdon, 1975)

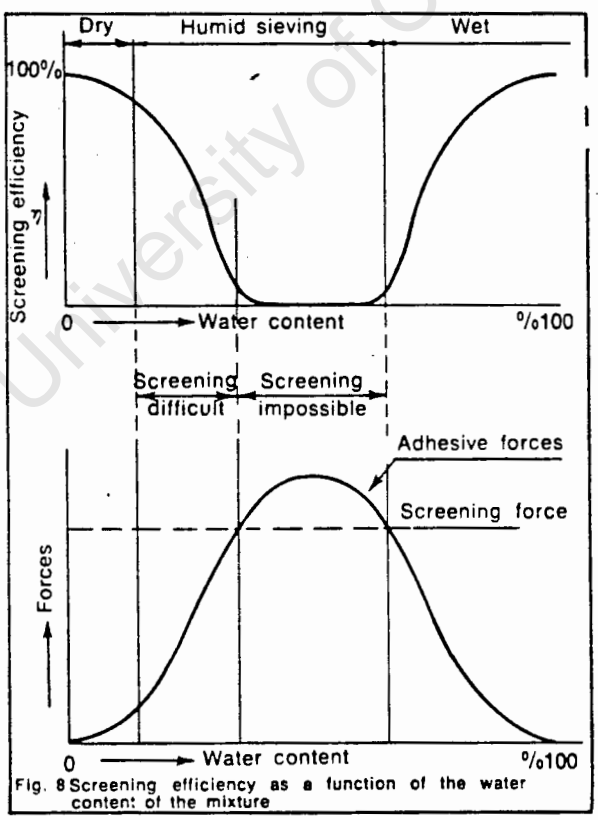

Figure 1.4 : Screening efficiency with the addition of water (Kelly & Spottiswood, 1982)

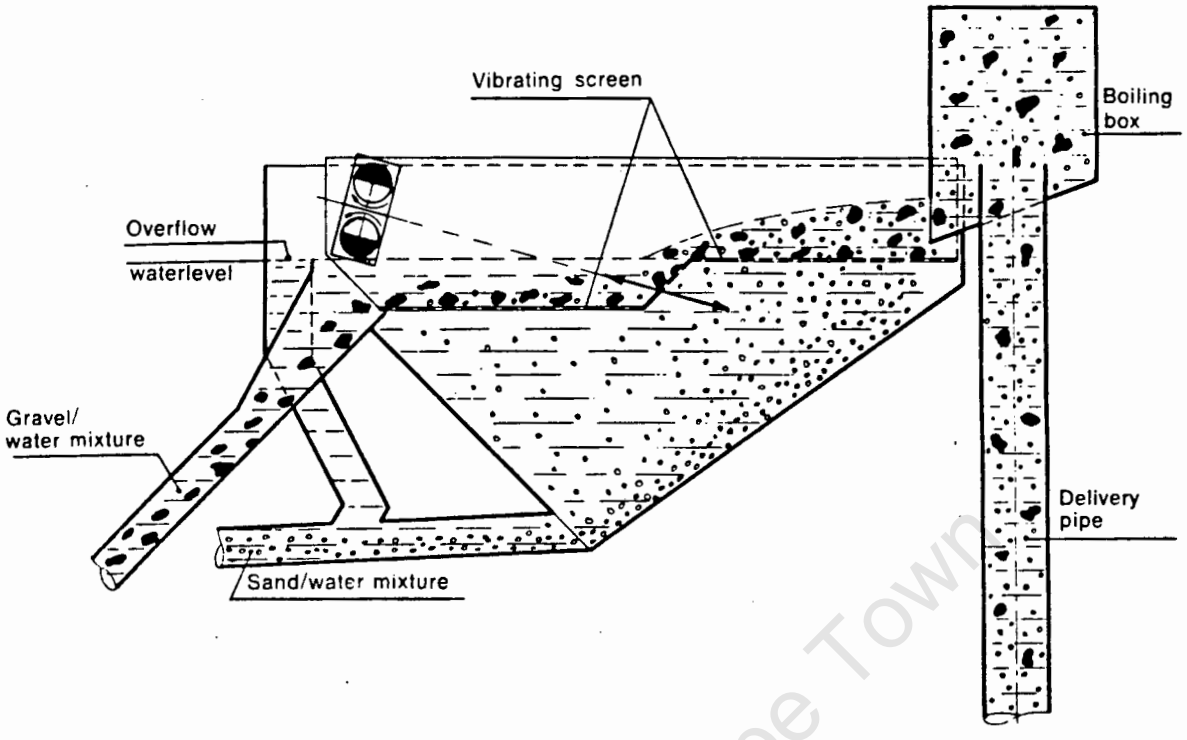

Figure 1.5 : "Underwater" vibrating screen (Van Dooremalen, 1973)

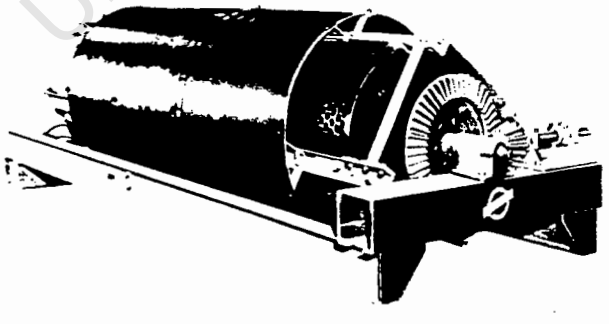

Figure 1.6 : Trommel (Kelly & Spottiswood, 1982)

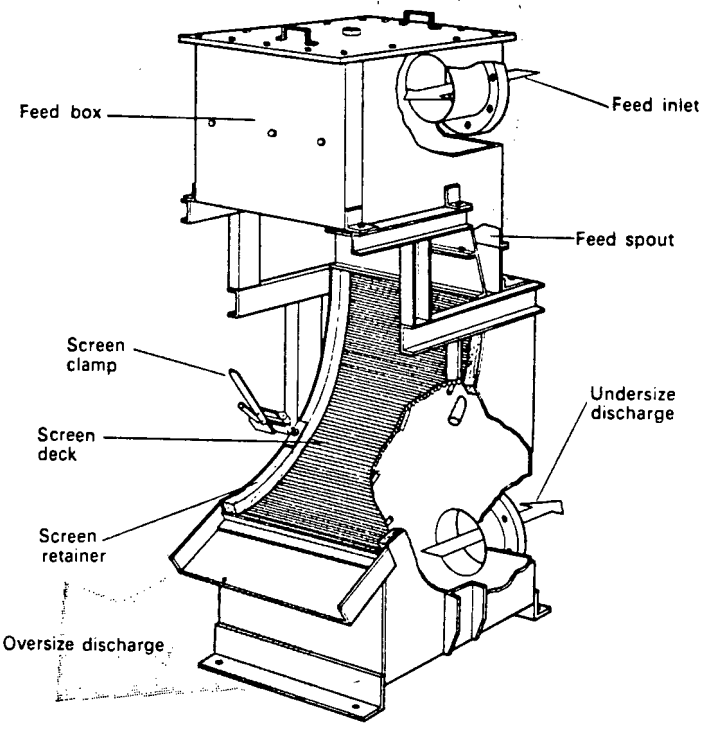

Figure 1.7 : Sieve bend (Bain & Bonnington, 1970)

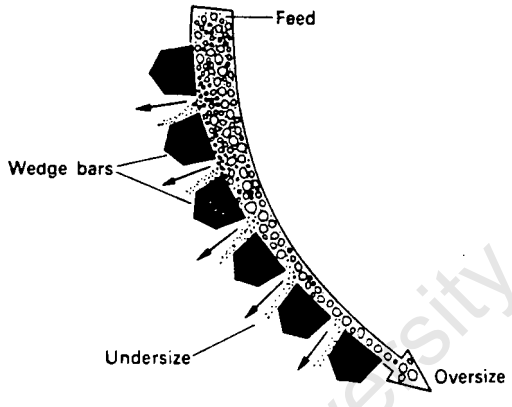

Figure 1.8 : Separation principle (Bain & Bonnington, 1970)

Figure 1.9 : Grizzly (Kelly & Spottiswood, 1982)

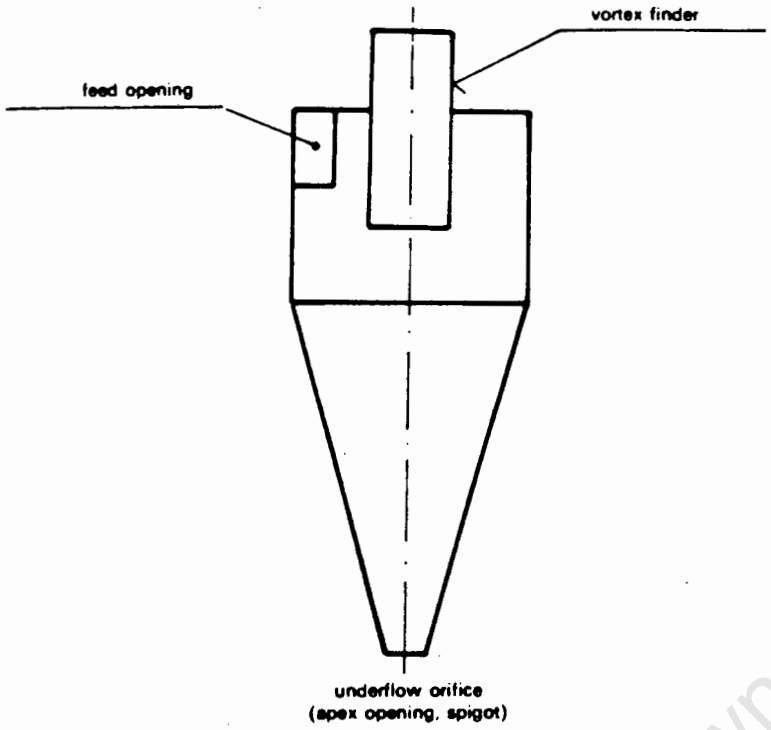

Figure 1.10 : Conventional hydrocyclone (Svarovsky, 1984)

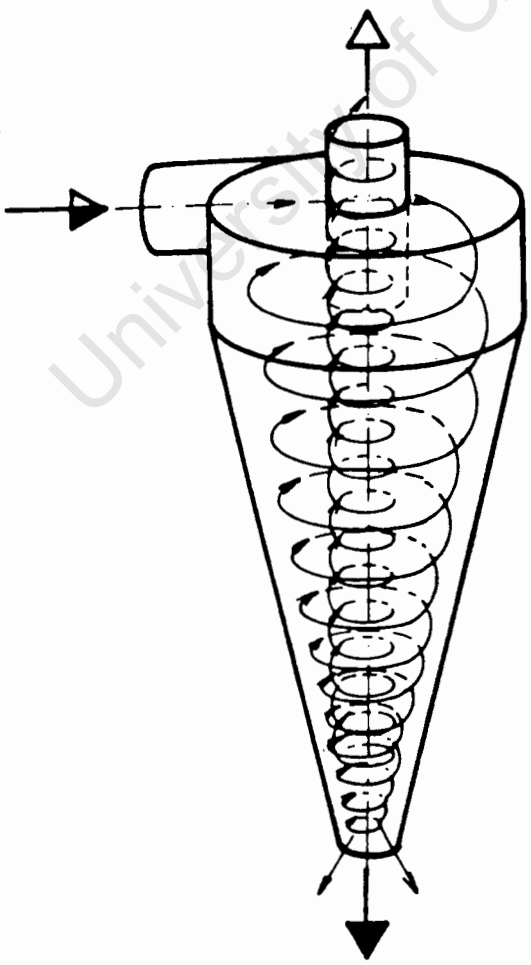

Figure 1.11 : Hydrocyclone fluid motion (Svarovsky, 1984)

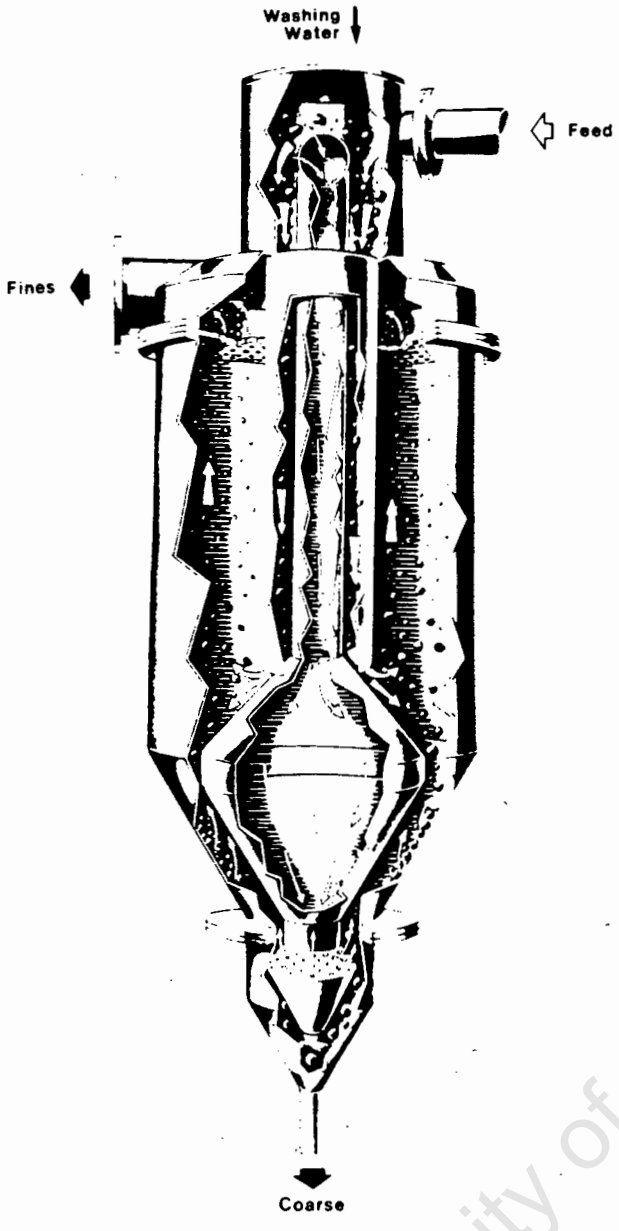

Figure 1.12 : Elutriator
(Kelly & Spottiswood, 1982)

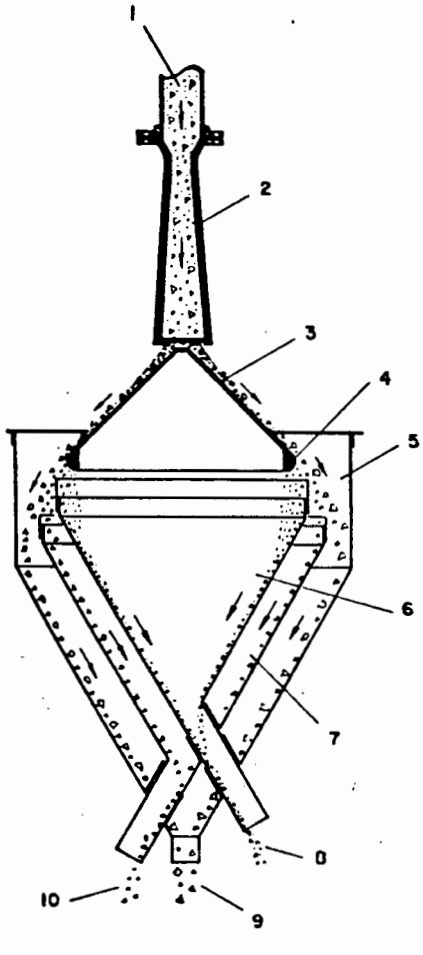

Figure 1.13 : Cone separator
(World Mining, 1969)

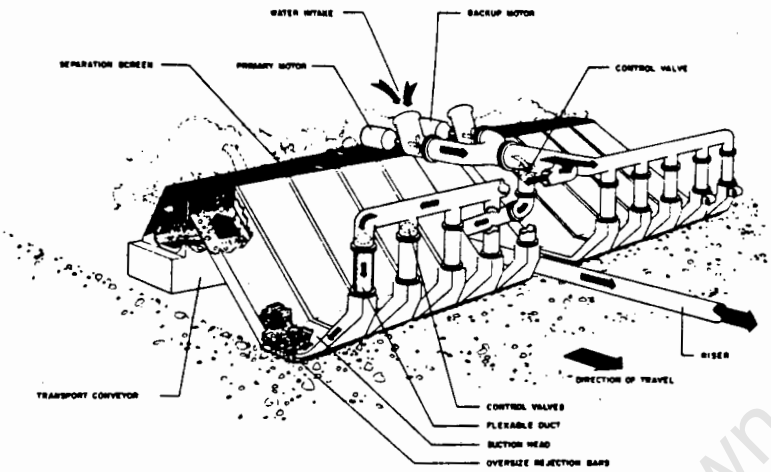

Figure 1.14 : Underwater mining unit (Brockett & Petters, 1980)

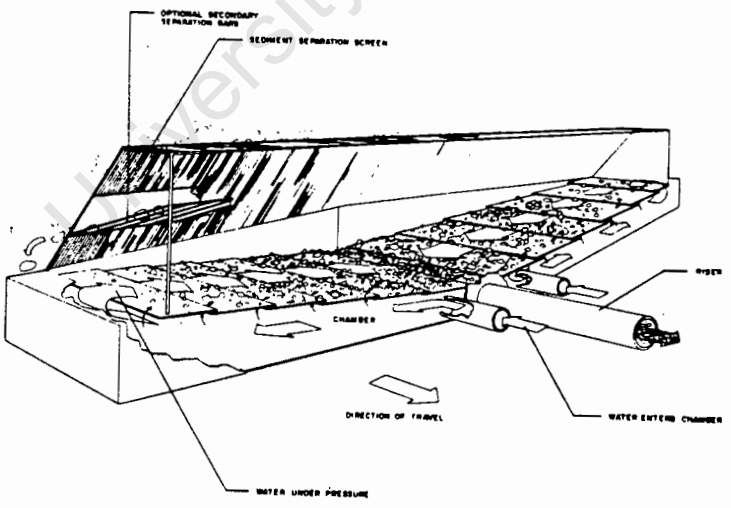

Figure 1.15 : Screening device (Brockett & Petters, 1980)

CHAPTER 2

SEPARATION DEVICES TESTED

INTRODUCTION

Three different separation devices have been designed, constructed and tested to determine their separation efficiency and suitability for the underwater separation of diamantiferous marine gravels.

The three devices are :

1. Converging elutriator
2. Cyclosieve
3. Spirosieve.

In this chapter the three devices will be described with reference to initial designs, description of the device, operation, theory of separation flow patterns and variables to be investigated.

2.1 CONVERGING ELUTRIATOR

From the information gained in the literature review it was decided to design a separation device based upon the classification principles of the elutriator.

The underlying concept is to separate the oversize gravel from the smaller diamond-bearing gravel, using their varying particle settling velocities in an upward flowing fluid.

2.1.1 Initial Conceptual Designs

1. Figure 2.1(a) from Lazarus (September 1986), shows a conceptualised proposal for an elutriator incorporating a number of parallel screening bars in series (two are shown at section BB and CC). The solid/water mixture is drawn into the suction inlet by the pump. The mixture passes up the elutriator and at the various screens the larger gravel is retained. This material falls down the disposal chambers where the water is stationary. The smaller gravel that passes through the screens is carried upwards and through the converging sections where the mixture velocity is higher.

   The non-return valves at the bottom of the disposal chambers are kept closed by suction until the weight of material causes them to open. When sufficient material has been disposed to reduce the weight of stones on the non-return valves, the valves are automatically closed by suction pressure and the cycle repeats.

2. In order to increase the screening area, Figure 2.1(b) shows a modified version of Figure 2.1(a) with an annular disposal chamber and one set of screens. The screens are in the shape of concentric circles displaced one above the other.

3. Figure 2.1(c) shows the previous design with the screens removed. The separation is now entirely due to the variable settling velocities of the different sized gravel. An additional pump for coping with the excess water, after screening has taken place, may be inserted below the solids handling pump shown. This extra pump is for the removal of excess water through a screen in the pipe wall. The reverse non-return valves are still required to prevent upward flow of large solids in the disposal chamber.

4. In Figure 2.1(d) the reverse non-return valves have been removed because it was felt that these would become blocked with gravel when closing. A second pump has been introduced to remove the gravel for the seabed and deliver it into the inlet of the elutriator. The elutriator is now comprised of a converging circular pipe over its entire length.

2.1.2 Description of the Converging Elutriator

Figure 2.2 shows the geometric design and dimensions of the converging elutriator that was constructed and tested in the research facility.

The primary outlet nozzle consists of a 210 mm diameter steel pipe. This is surrounded by a 600 mm diameter circular steel pipe on top of which is placed a 600 mm to 350 mm converging PVC section. Between the converging section and the primary outlet nozzle is an annular chamber. The height to which the primary outlet nozzle extends into the converging section can be increased by adding extra lengths of piping.

The converging section leads into the 350 mm diameter straight section of the elutriator, known as the elutriation column. This section is 2 m in length and made up of four circular cylinders. Two of these cylinders are constructed from clear perspex, so that visual observations of particle behaviour can be made.

Another converging PVC section joins the elutriation column to the start of the pipe which will lead to the surface ship. In the research facility this pipe has a 181 mm internal diameter. All the sections have flanges and backing rings, and are bolted together to form a continuous converging elutriator.

An additional pump for removing the excess water, after separation has taken place, may be incorporated after the last converging section.

2.1.3 Operation of the Converging Elutriator

The primary pump causes a sub-ambient pressure at the bottom of the suction inlet, drawing a solid/water mixture through the pump and into the high velocity primary outlet nozzle (velocity will be approximately 3,5 m/s).

When the mixture reaches the first converging section the overall velocity decreases because of its large area. The larger rocks with high settling velocities are dispersed radially outwards and fall freely into the annular disposal chamber. The water flow in the disposal chamber is upwards due to entrainment by the mixture being ejected from the high velocity primary outlet nozzle. Any smaller particles that may leave the outlet jet before entering the straight section of the elutriator, should move upwards with this flow.

The secondary pump (conventional or airlift) draws the solid/water mixture from the top of the converging elutriator. The upward velocity in the annular disposal chamber and the elutriation column, can be controlled by the flow rate through the secondary pump.

In the constant diameter elutriation column, further separation takes place. The larger rocks are forced radially outwards into the slower moving stream of water near the pipe wall. From here they settle under the action of gravity and pass out via the disposal chamber.

Finally, the smaller particles are drawn out of the elutriator at the top, where the velocity is once again increased by the last converging section.

2.1.4 Theory of Separation in the Converging Elutriator

1. Terminal Settling Velocity

Separation in the converging elutriator can be achieved because different size particles have different terminal settling velocities in a fluid.

The terminal settling velocity of a particle is the maximum constant velocity at which it will settle in a specific fluid, i.e. water. The three major factors affecting the terminal settling velocity of a specific particle are :

i) Size

ii) Density

iii) Shape.

If the density and shape are kept constant an increase in particle size will result in an increase in the terminal settling velocity. If size and shape are constants then an increase in particle density also results in an increase in the particle terminal settling velocity. There are many ways to describe the shape of a particle but generally the more spherical a particle is, the higher will be its terminal settling velocity.

In this thesis the shape of a particle will be described by the particle shape factor. The shape factor (SF) being defined as the terminal settling velocity of the particle divided by the terminal settling velocity of a sphere with the same volume and density, i.e. shape factor of a sphere would be 1.

In the underwater separation of diamantiferous marine gravels, the major concern is with size separation. If the upward velocity in the converging elutriator is kept above the terminal settling velocity of a 16 mm diamond density particle (S_s = 3,5g/cm^3) then theoretically no diamonds will be lost. However, the efficiency of the separation is also dependent on the size of the largest rocks that are removed to the surface with the diamonds.

Figure 2.3(a) shows the relationship between particle size and theoretical terminal settling velocity for spherical particles having a density of 2,7g/m^3 (quartz pebbles) and

3,5g/cm³ (diamonds). This was derived from Figure 2.4 Lazarus (Hydrotransport 8, 1982), which gives the non-dimensional terminal settling velocity as a function of non-dimensional particle size, for a wide range of Reynolds numbers.

From Figure 2.3(a) it can be seen that the terminal settling velocity of a 16 mm spherical diamond is 1,09 m/s. A quartz pebble having the same terminal settling velocity will be approximately 23,5 mm in diameter. This means that for an elutriation column velocity of 1,1 m/s, separation will occur at a particle size of approximately 24 mm.

However, the diamantiferous gravel is not spherical and in some areas flat rocks with very low shape factors are found. Shape factors can vary from 0,35 for a flat stone to 0,85 for a roundish pebble. Figure 2.3(b) shows the terminal settling velocity versus particle size for a shape factor of 1 and 0,7. At an elutriation velocity of 1,1 m/s the separation or cut size is now at 49 mm diameter particles.

It can be concluded that the shape of the marine gravel *will have* an effect on the sharpness of the separation when using the converging elutriator. *How much* an effect will have to be investigated during testing.

2. Hindered Settling Velocity

The terminal settling velocity of an individual particle is reduced by the presence of other particles and decreases with increasing concentration.

This decrease in velocity is called hindered settling. It is caused by collisions between particles (if the particle sizes are non-uniform) as well as the upward flow of water in the area between particles due to the settling of other particles.

Richardson and Zaki (1954) showed that :

$$V_t' = V_t \, (1 - C_v)^{\alpha}$$

where V_t' is the hindered settling velocity, V_t the theoretical settling velocity, C_v the solids volumetric concentration and α a function of the particle Reynolds Number R_{ep} .

$$R_{ep} = \frac{\rho_\ell V_t \, d_p}{\mu}$$

The marine gravel concerned settles according to Newton's Law with $R_{ep} > 500$ and thus $\alpha = 2{,}4$ (Richardson and Zaki, 1954).

At the envisaged C_v of 6% the theoretical terminal settling velocity will decrease by 13,8%. Thus the upward velocity in the converging elutriator could be reduced by 13,8% at 6% concentration. However, because the concentration can fluctuate it may be wiser to use a high velocity to guarantee 100% recovery of the diamond-bearing gravel.

3. Flow Patterns

Although the converging and straight sections of the elutriator are of a set diameter, the geometry of the system can be altered by extending the primary outlet nozzle. Any change to the geometry or flow rates will result in a change in the associated flow pattern.

Figures 2.5 and 2.6 from Lazarus & Rossouw (July 1987), show the range of the positions that the primary outlet nozzle was placed at. In the position, as shown in Figure 2.5, the primary jet flows into a large area where the surrounding water is practically stationary. Figure 2.7 from Blevins (1984) shows the various flow regimes of a round submerged jet. Although the jet is flowing into an infinite reservoir (no boundaries) the initial core and shear layer will be similar to that found at the start of the converging elutriator.

The initial region consists of the core flow and the surrounding shear layer. The turbulent shear layer or mixing layer forms the boundary between the core and the

surrounding stationary water. The jet entrains water by drawing it from this stationary reservoir. This will result in an upward velocity in the annular disposal chamber. The diameter of the jet increases with axial length due to spreading, resulting in a decrease in the overall velocity.

With the high d_n/D ratio of 0,6 the jet may spread to the sides of the converging section before reaching the straight section. This could cause the smaller particles to impinge on the converging section and be deflected down the sides of the annular disposal chamber, where the velocity is very low. If this occurs the primary outlet nozzle will have to be extended further into the converging section.

With the primary outlet nozzle extended to the position shown in Figure 2.6 a smaller diameter will have to be used. This is to allow a larger annular area for the removal of the larger waste rocks. The resultant flow is that of a confined jet with coflow (upward annular flow).

Figure 2.8 from Blevins (1984), shows the general flow regimes of a confined jet with coflow. In Region 1 the inner and outer jet flows are separated by a shear layer. As in the previous flow pattern there is turbulence, mixing and entrainment between the shear layer and the coflow stream. In Region 2 the shear layer has extended

to the duct walls and the fluid is entrained from the surrounding stream rapidly enough to reduce the velocity of the stream. Region 3 is a region of possible eddy formation and recirculation. This only occurs if the d/D ratio and the coflow stream velocity are relatively small. The central jet will then laterally entrain all the fluid in the coflow before the jet has spread to the wall, resulting in recirculating eddies. Region 4 begins after the point of flow reattachment, and it makes the beginning of conventional duct flow (Blevins, 1984).

Recirculating flow is not expected as the d_n/D ratio is fairly large ($d_n/D = 0,44$). The central jet should spread rapidly to the duct walls, resulting in partial conventional duct flow before the top of the elutriator is reached.

2.1.5 Test Variables

In order to determine the separation efficiency of the converging elutriator, the variables that affect the separation process need to be investigated.

These variables are :

- Size of marine gravel
- Shape of marine gravel
- Density of marine gravel

- Geometry of converging elutriator
- Annular velocity
- Elutriation column velocity
- Concentration.

2.2 CYCLOSIEVE

The cyclosieve is a screening device that was designed in Europe. It was constructed in South Africa where the screens were modified to enable the separation of large rocks from smaller diamantiferous marine gravels.

2.2.1 Description of the Cyclosieve

The initial design of the cyclosieve is shown in Figure 2.9 (Lazarus & Rossouw, October 1987).

The cyclosieve comprises a large steel outer cylindrical vessel, containing a smaller diameter, cylindrical perforated screen. The hole configuration of the perforated screen is shown in Figure 2.10 (Lazarus & Rossouw, October 1987). At the bottom of the screen is a cone which leads into a coarse solids outlet pipe.

The tangential inlet is situated at the top of the screen and the fines outlet at the bottom of the outer cylinder. Two clear perspex observation covers are situated on top of the cyclosieve.

Figure 2.11 from Lazarus and Rossouw (March 1988), shows a variation to the initial design of the cyclosieve. The cylindrical perforated screen has been replaced with a conical screen and the coarse outlet has been extended. The hole configuration is the same as that of the cylindrical screen (Figure 2.10).

2.2.2 Operation of the Cyclosieve

The solids/water mixture that is pumped from the seabed by the primary pump is introduced into the cyclosieve via the tangential primary inlet. The flow inside the cyclosieve is rotational with circular symmetry. It is envisaged that the high outward centrifugal forces resulting from the rotational flow will force the solids against the screen. The smaller gravel and diamonds should pass through the holes in the screen and fall to the bottom of the outer chamber. They are removed to the ship via the fines outlet, by the sub-ambient pressure provided by the airlift pump.

The larger waste gravel which does not pass through the screen should fall to the bottom of the cone and exit via the coarse solids outlet.

2.2.3 Flow Conditions, Forces and Particle Behaviour

The cyclosieve can be operated under two very different flow conditions, i.e. aerated and sub-marine.

Figure 2.12 shows the cyclosieve under aerated conditions where the centre of the unit is taken up by air and a thin layer of water rotates over the screen. This flow condition is created when the majority of the primary inlet flow passes through the holes in the screen and out the fines outlet.

The sub-marine flow condition that is shown in Figure 2.13 is created by removing most of the inlet flow via the coarse outlet. This results in a large body of rotating water with a smaller central air core. This is the ideal operating condition because less water is removed to the surface ship.

In the analysis that follows, from Lazarus and Rossouw (October 1987), the friction force between a particle and the screen has been ignored. This is because the friction coefficient is difficult to determine and is believed to be small compared with the other forces involved.

1. <u>Aerated Condition</u>

<u>Forces in the cyclosieve</u>

The gravitational force (F_g) acts downwards ;

$$F_g = mg$$

where m is the mass of a particle.

The centrifugal force (F_c) acts radially outwards ;

$$F_c = m R \Omega^2 = \frac{mv^2}{R} \qquad (\Omega = v/R)$$

where Ω is the angular velocity, v the inlet velocity, and R the cyclosieve radius.

$$\therefore \frac{F_c}{F_g} = \frac{v^2}{Rg}$$

Hence the radial outward force developed in the cyclo sieve is $\frac{v^2}{Rg}$ times as large as the gravity force. This is often expressed as g forces.

The design flow Q = 500 m^3/hr

The inlet diameter d_i = 0,2 m

The cyclosieve radius R = 0,4 (at the screen)

Therefore the inlet velocity v = 4,42 m/s

$$\therefore \frac{F_c}{F_g} = 5 \text{ gravities or g's.}$$

Particle residence time (PRT)

Under aerated conditions a particle has to move through a relatively thin layer of water before reaching the screens. Therefore the PRT is the time taken for the particle and the water to fall the height of the screens (s).

$s = \frac{1}{2} g t^2$

$\therefore \quad t = 0{,}435$ seconds.

Number of rotations (n)

$$n = \frac{vt}{2\pi R} = 0{,}765 \text{ revolutions}$$

$$\text{or } n = \frac{vt180}{\pi R} = 275 \text{ degrees}$$

Path length on screens (PL)

The length of screen that a particle moves over is

PL = 2,08 m

2. Sub-marine conditions

Forces in the cyclosieve

The ratio of centrifugal force to gravitational force is the same as for aerated conditions, i.e.

$$\frac{F_c}{F_g} = 5 \text{ g's}$$

Particle residence time (PRT)

A particle now has to settle through water so the PRT is affected by drag and is dependent on the particle settling velocity (V_t).

Consider a 16 mm spherical particle, with a relative density of 3,5 (d_p = 16 mm).

From Newton's Law for settling :

$$V_t = 0{,}981\, d_p^{½} \sqrt{(\rho_s - \rho) g\, \pi/\rho}$$

$$V_t = 1{,}09 \text{ m/s}$$

The time taken for the particle to reach the bottom of the screens is 0,910 seconds.

Number of rotations (n)

The particle moves radially through the water at its terminal radial settling velocity (V_{tR}) , assuming that there is no secondary inward radial flow as found in a hydrocyclone.

$$V_{tR} = 0{,}981\, d_p^{½} \sqrt{(\rho_s - \rho)\, v^2\, \pi/\rho r}$$

where r is the local radius at any point

V_{tR} = 2,43 m/s (r = 0,4 at the outermost radius)

V_{tR} = 3,44 m/s (r = 0,2 at the innermost radius of the inlet)

The time taken for a particle to reach the screens is

$$t = \frac{d}{V_{tR}}$$

$\therefore$ t = 0,07 seconds

where d = inlet pipe diameter.

The corrected particle residence time (PRT) is 0,840 seconds

n = 1,48 revs

n = 532°

Path length on screens (PL)

PL = 3,83 m

3. Summary

These results are summarised in Table 2.1.

Conditions	$\frac{F_c}{F_g}$	Particle Residence Time (PRT) (seconds)	Number of Revolutions (n)	Path Length (m)
Aerated	5	0,435	0,765	2,08
Sub-marine	5	0,840	1,48	3,83

2.2.4 Test Variables

In the test program to determine the screening efficiency of the cyclosieve, the effect of the following variables needs to be investigated.

- Ratio of primary inlet flow to fines outlet flow
- Screen geometry
- Particle size
- Solids concentration
- Particle size distribution.

2.3 SPIROSIEVE

The spirosieve is a screening device, similar to the cyclosieve, in the fact that it also uses centrifugal action to force the solids onto a cylindrical screen.

2.3.1 Description and Operation of the Conceptual Spirosieve

Figure 2.14 from Lazarus and Rossouw (February 1988), shows the conceptual design of the spirosieve screening device. It comprises a spiralling rectangular conduit divided by a profile bar screen into two smaller conduits, the inner (B) and outer (C). The solids/water mixture containing both large and small gravel is pumped from the seabed and enters at the inlet (A). The mixture flows around the spiral with the solids being forced against the screen (D) by the radially outward centrifugal force.

The smaller particles pass through the screen into the outer chamber (C). The larger particles remain in the inner chamber (B).

At (E) the inner and outer chambers are separated by a solid barrier. The inner chamber containing the coarse particles is diverted in one direction (say downwards and to waste) together with a portion of the water. The outer chamber containing the fines is directed upwards and is carried to the surface ship by means of a pump.

2.3.2 Description and Construction of the Spirosieve Model

A model of the spirosieve was designed and constructed so that tests could be performed to analyse its screening efficiency and suitability to underwater separation. The model was constructed from perspex so that visual observations of the separation process could be made.

The design and dimensions of the model are shown in Figure 2.15. The spiralling conduit measures 45 mm x 98 mm and is contained within two perspex cylinders. The screen is made from a standard 3 mm mesh, with rectangular openings, as shown in Figure 2.16. It is located at 135 mm radius and divides the main conduit into two smaller conduits. A solid wedge is located within the first spiral, on the inner wall of the outer cylinder. This wedge reduces the outer radius from 171 mm to 135 mm so that the screen can be introduced. The screen has a length of 2,76 m.

The tangential circular inlet is 54 mm in diameter and changes to the rectangular conduit via a sudden expansion. The turbulence in the sudden expansion causes it to act as a mixing chamber for the solid/water mixture. The coarse and fine outlets are also circular with internal diameters of 54 mm.

Two 4 mm diameter pressure tapping holes are located in the outer cylinder, at the beginning and end of the screen. These are used to measure the head loss over the entire length of the spirosieve.

2.3.3 Screening Process and Flow Patterns

The spirosieve model has been designed to operate in a system that provides a maximum flow of 13,6 ℓ/s, resulting in a maximum spirosieve velocity of 3,1 m/s. It is this velocity in the spiralling conduit that induces the outward centrifugal flow needed to bring about the screening. The maximum ratio of centrifugal force to gravity force is :

$$\frac{F_c}{F_g} = \frac{v^2}{Rg} = 7{,}3 \text{ gravities or g's}$$

where R is the radius at which the screen is located.

Due to the outward centrifugal force the solids are forced onto the screen as shown in Figure 2.17. The small particles close to the screen pass through the holes and continue up the spirosieve in the outer chamber. The remaining solids continue

to flow over the screen and up the spiralling conduit, in the inner chamber. The particles closest to the screen collide with the vertical bars causing vibrations in the vertical bed. These vibrations result in stratification, where small particles make their way to the screen while large particles move to the top of the bed, thus improving the screening efficiency.

One factor that may cause a reduction in the screening efficiency is the effects of secondary flow. The secondary flow can be considered to consist of two vortices of opposite sign, each occupying one half of the cross section, as shown in Figure 2.18. This is caused by the fluid being driven outwards across the core flow of the pipe, and a secondary flow in the radial plane is established as this fluid returns back along the pipe walls (Blevins, 1984).

These secondary flows may not necessarily be present because of the high degree of turbulence caused by the screen and solids. If, however, they do exist, the larger solids against the screen may prevent any fines from passing back through the screen.

2.3.4 Variable Parameters

The parameters that can be varied to determine their effect on the screening efficiency of the spirosieve are as follows :

- Velocity or centrifugal force
- Particle size
- Particle density
- Concentration of solids
- Particle size distribution
- Screen length
- Orientation of the spirosieve.

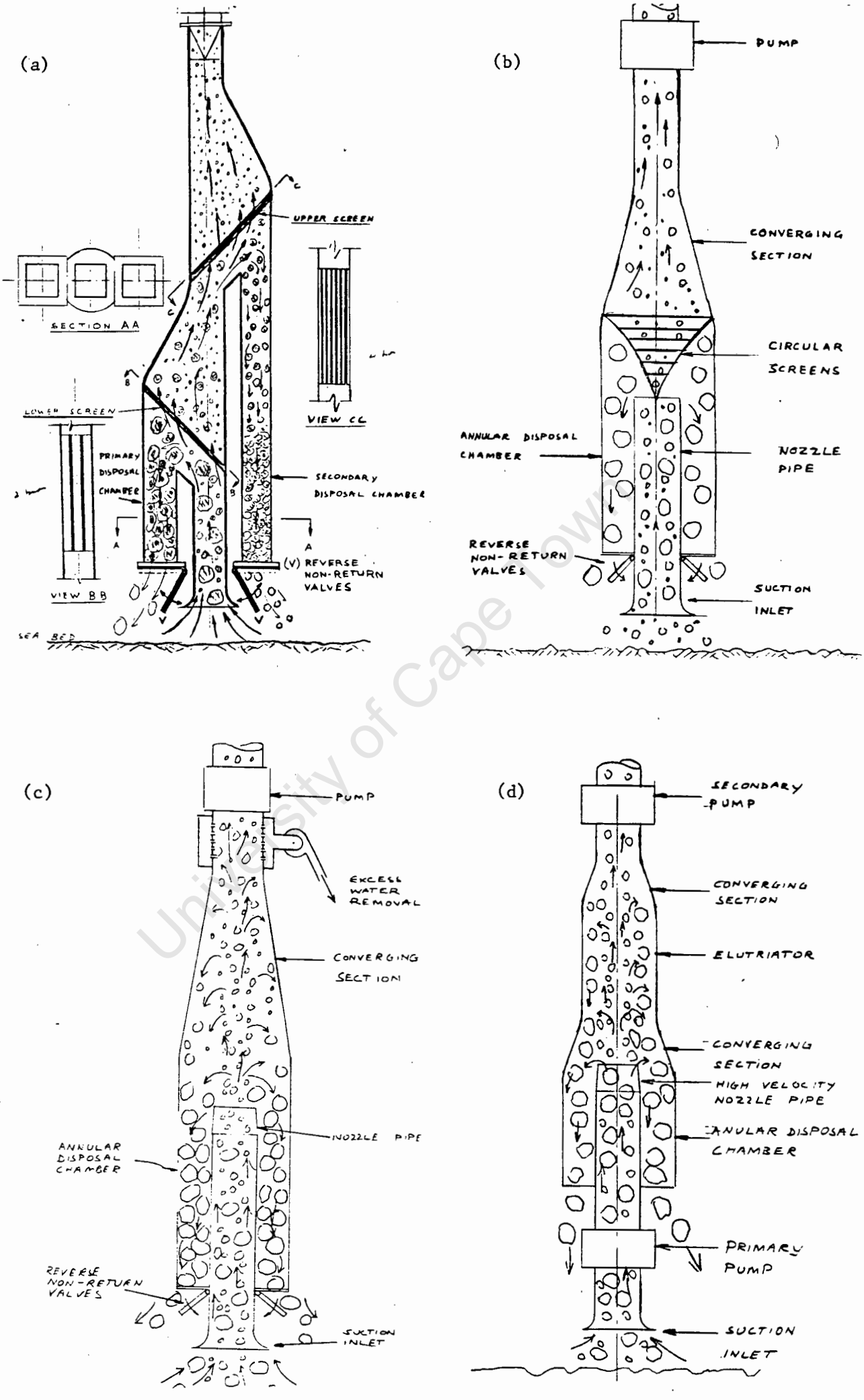

Figure 2.1 : Initial conceptual designs (Lazarus, Sept. 1986)

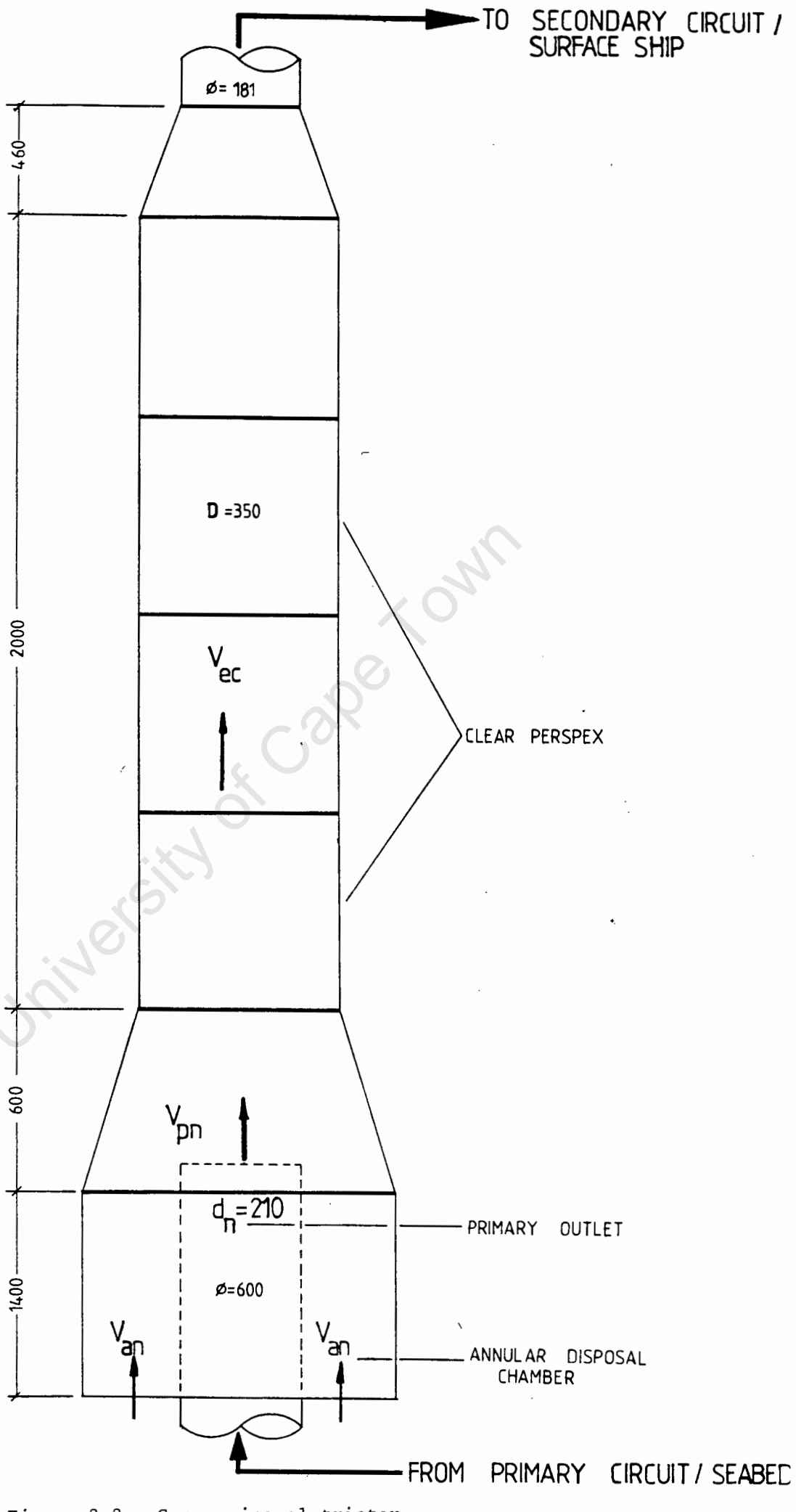

Figure 2.2 : Converging elutriator

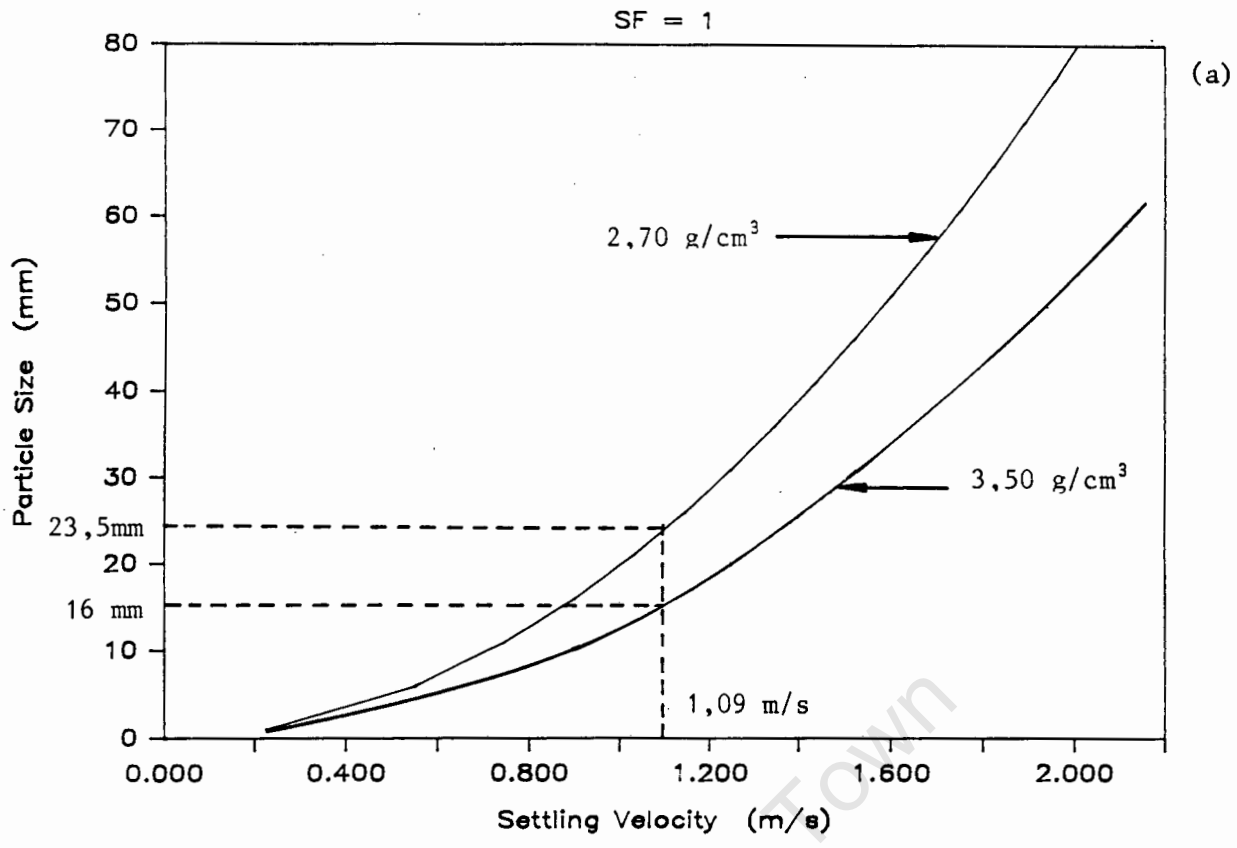

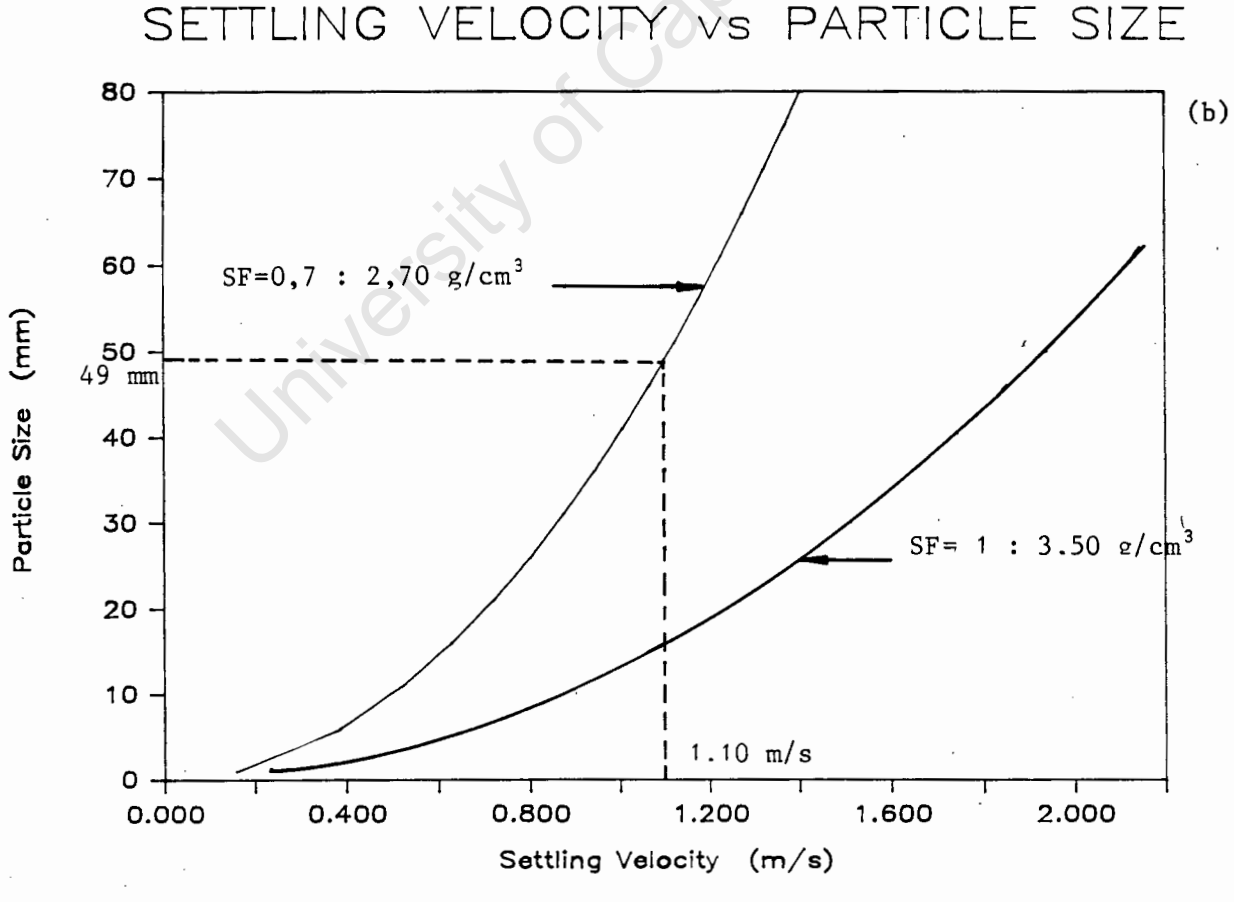

Figure 2.3 : Particle size vs. settling velocity

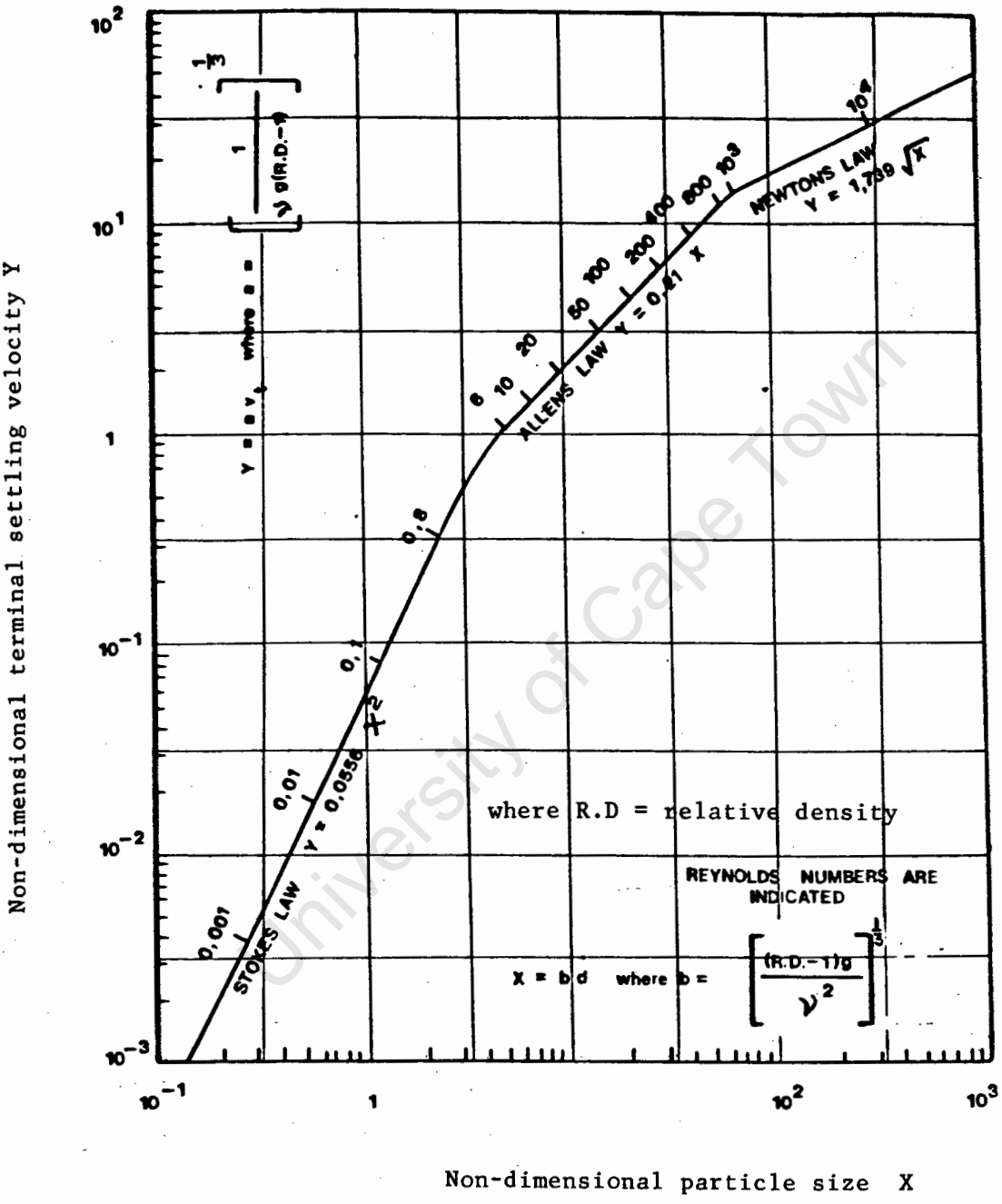

Figure 2.4 : Non-dimensional particle size vs. non-dimensional terminal settling velocity (Lazarus, 1982)

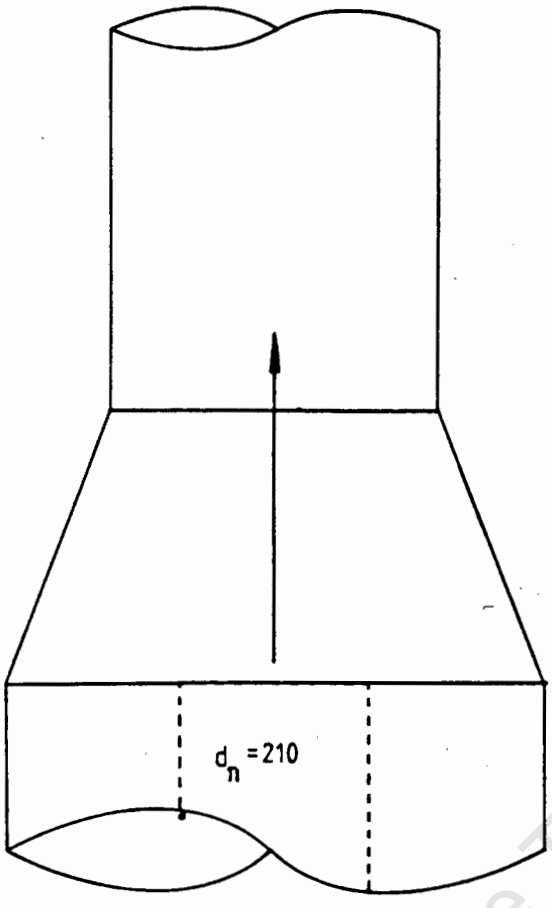

Figure 2.5 : Primary outlet nozzle position
(Lazarus & Rossouw, July 1987)

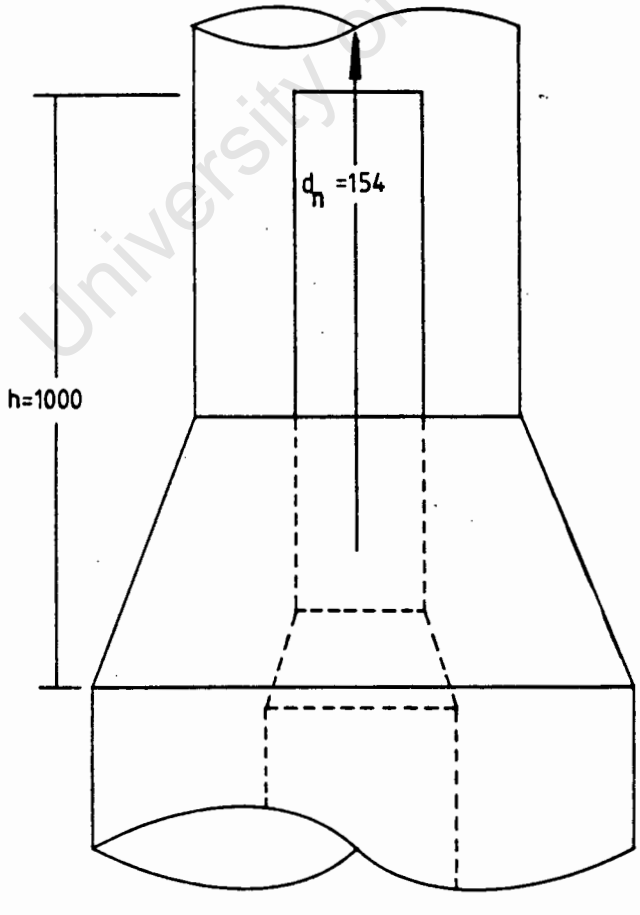

Figure 2.6 : Final primary outlet nozzle position
(Lazarus & Rossouw, July 1987)

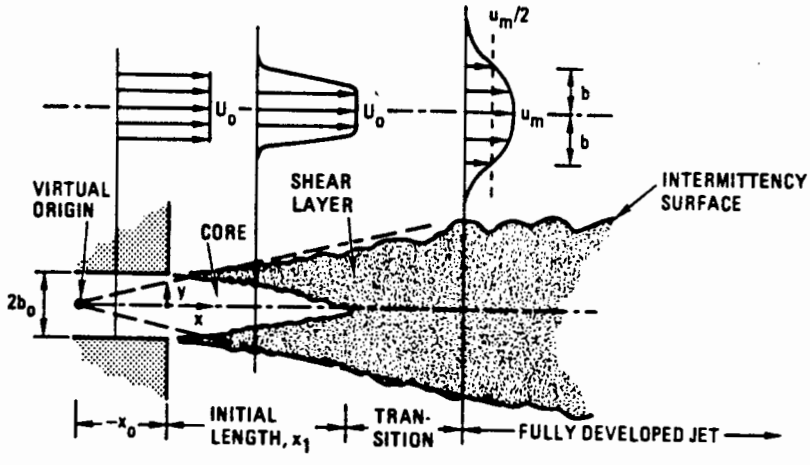

Figure 2.7 : A round submerged jet (Blevins, 1984)

FLOW REGIMES OF A CONFINED JET WITH COFLOW

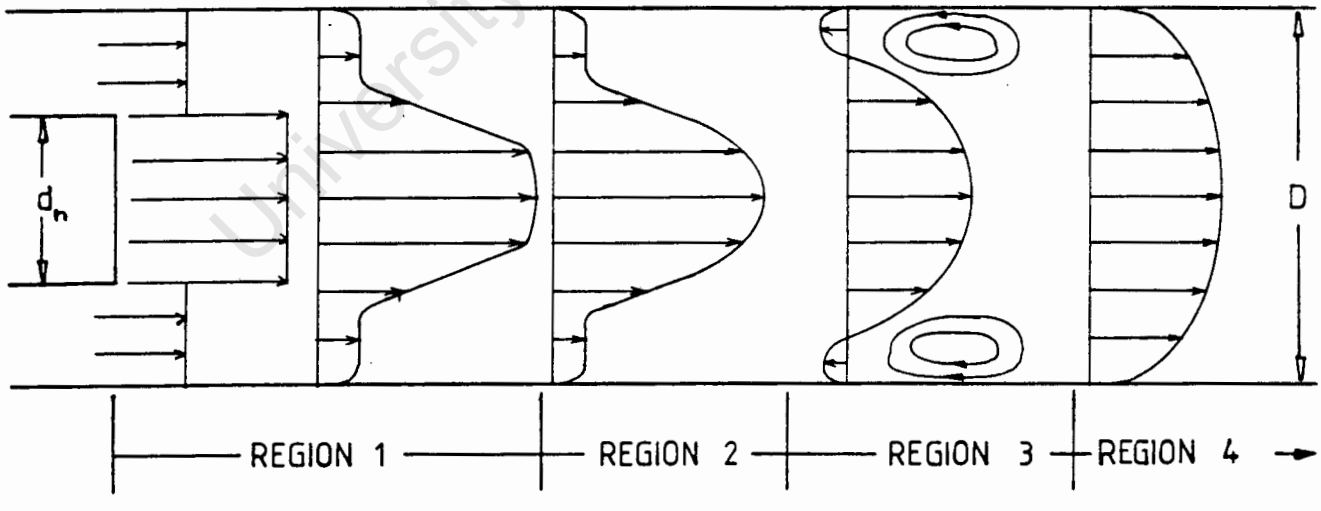

Figure 2.8 : Flow regimes of a confined jet with coflow (Blevins, 1984)

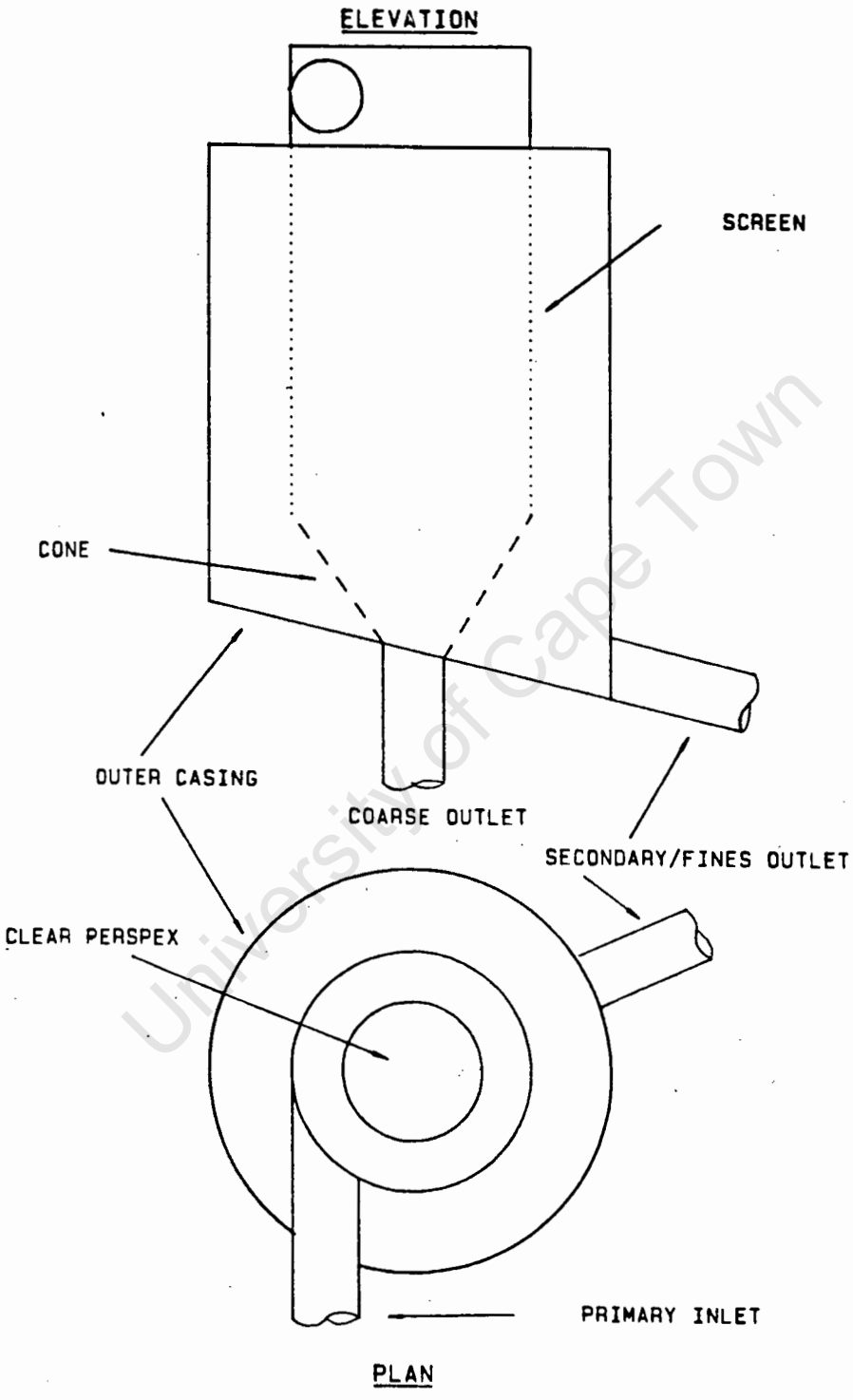

Figure 2.9 : Initial design of the cyclosieve
(Lazarus & Rossouw, October 1987)

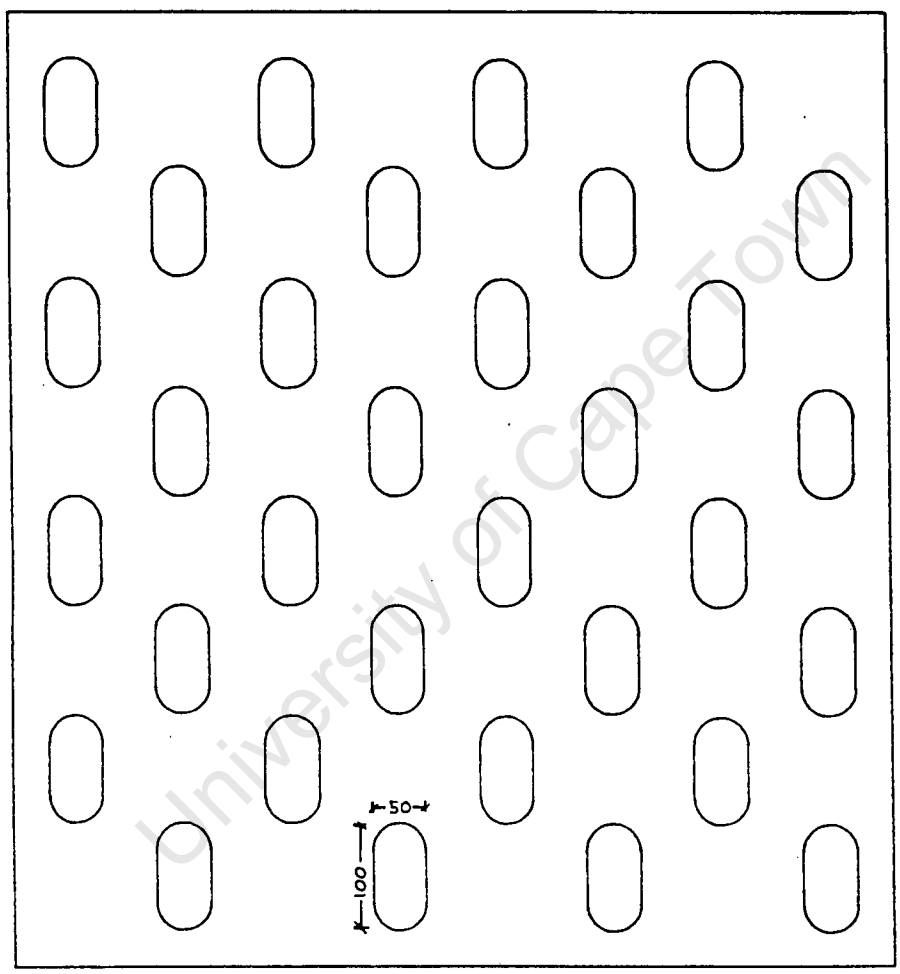

Figure 2.10 : Hole configuration of the perforated screen (Lazarus & Rossouw, October 1987)

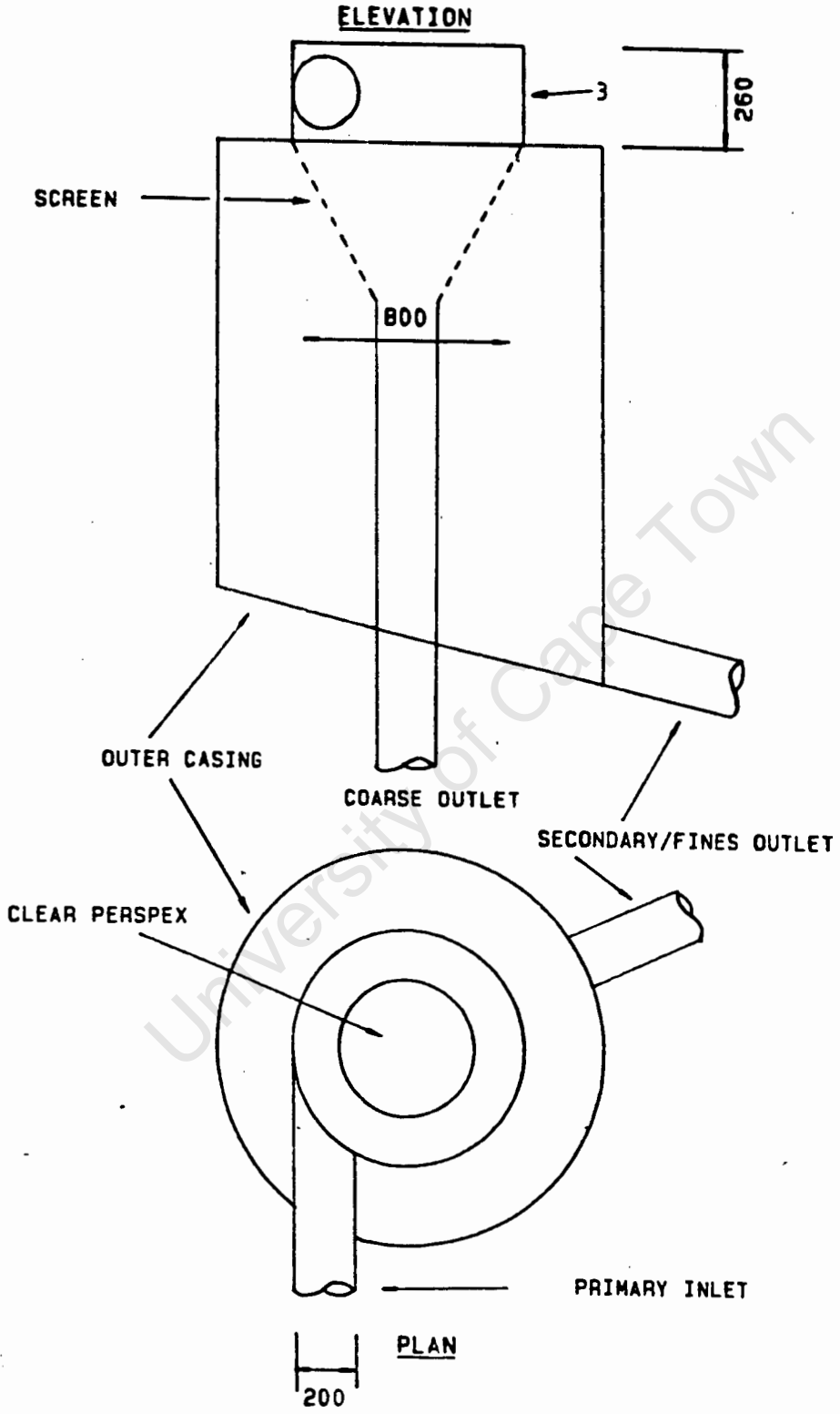

Figure 2.11 : Cyclosieve with conical screen
(Lazarus & Rossouw, March 1988)

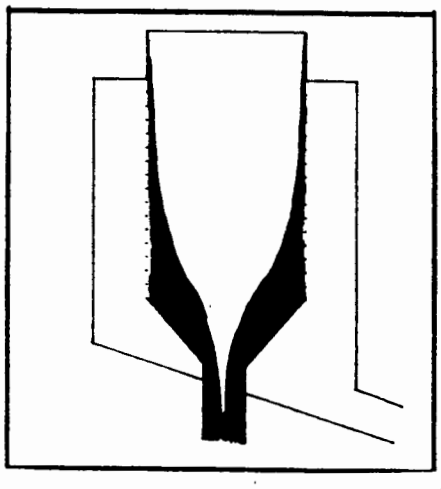

Figure 2.12 : Aerated conditions

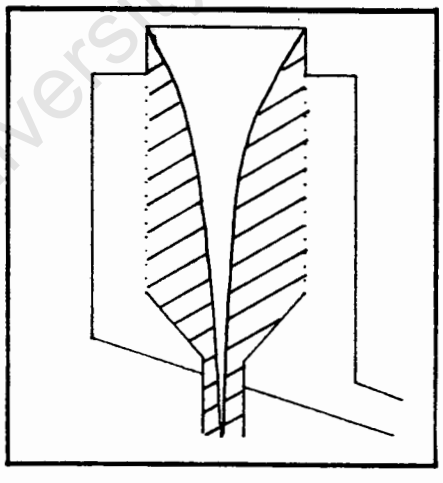

Figure 2.13 : Sub-marine flow conditions

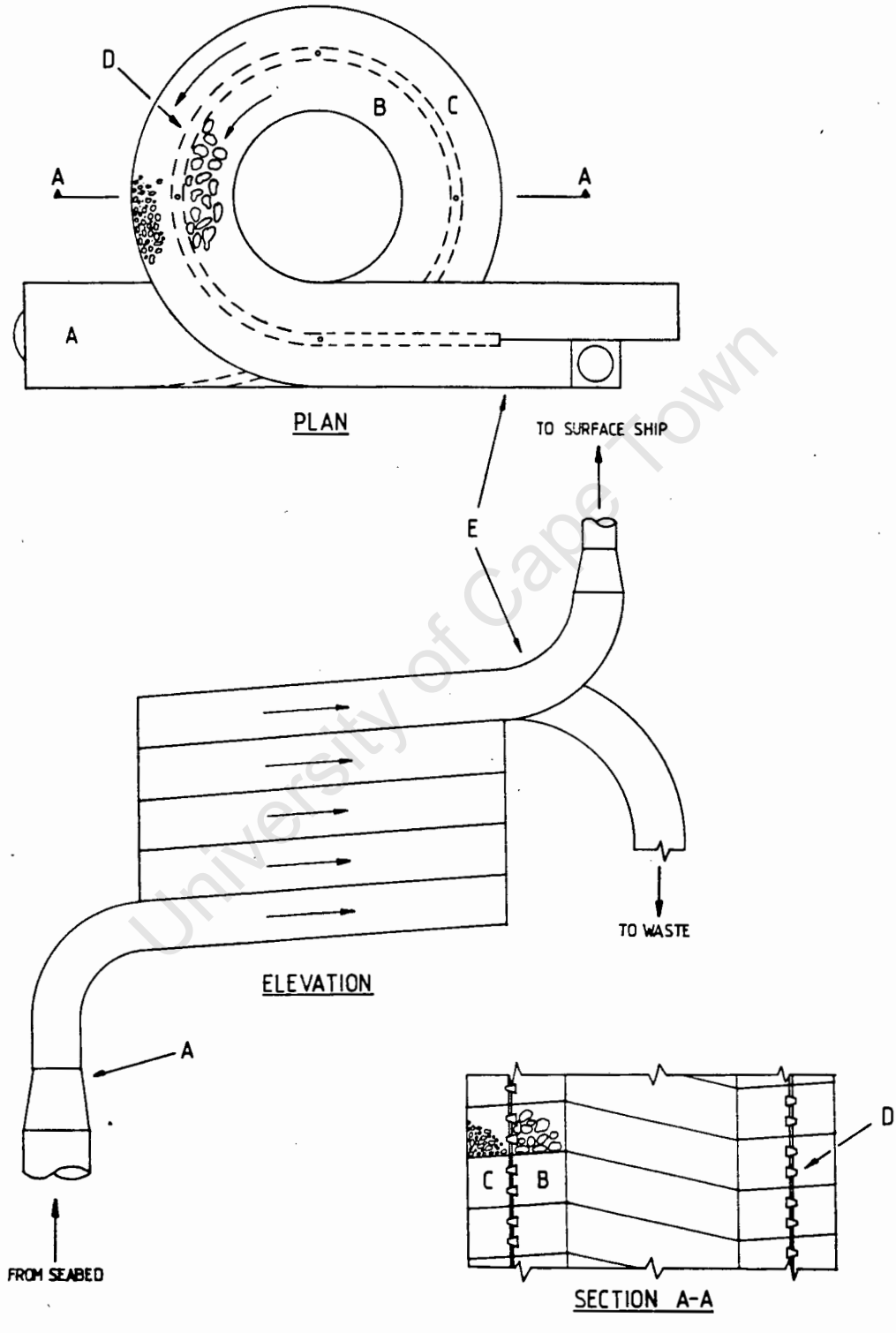

Figure 2.14 : Conceptual design of the spirosieve (Lazarus & Rossouw, February 1988)

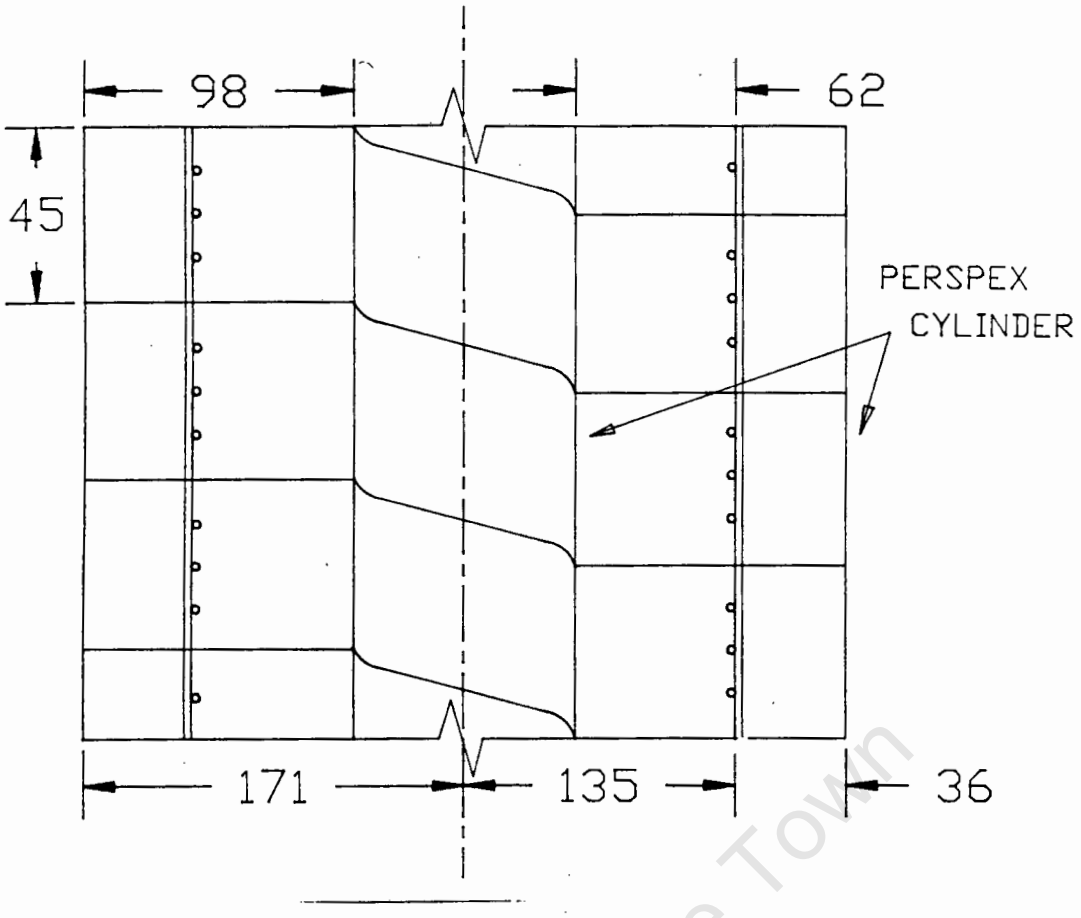

Figure 2.15 : Spirosieve model design

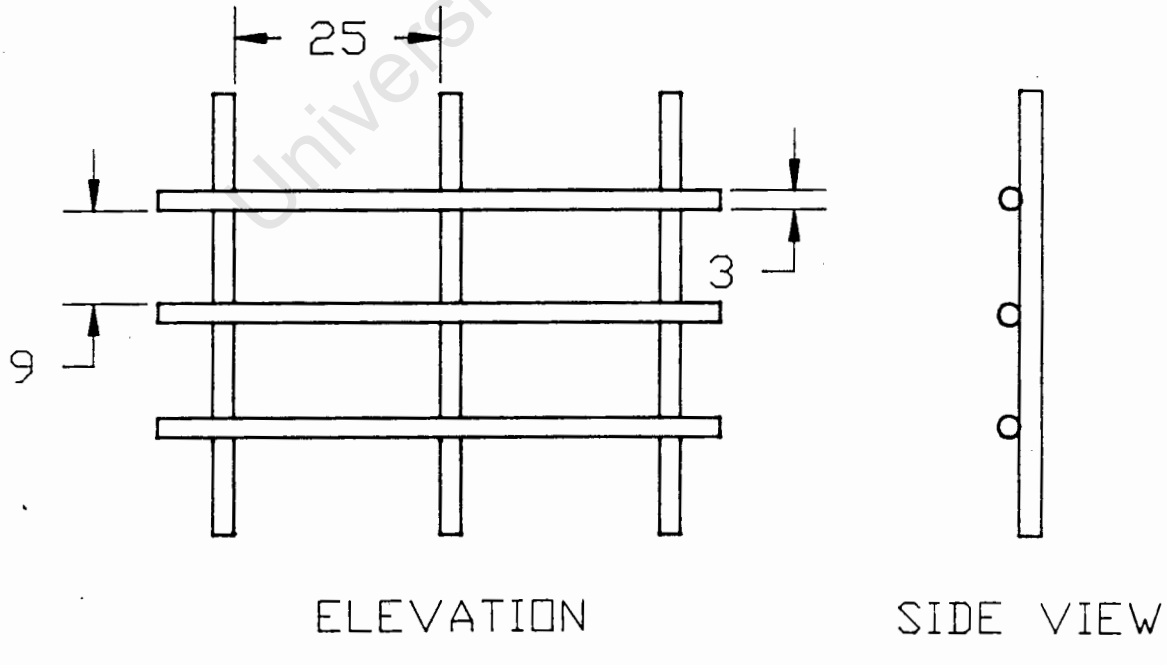

Figure 2.16 : Screen design

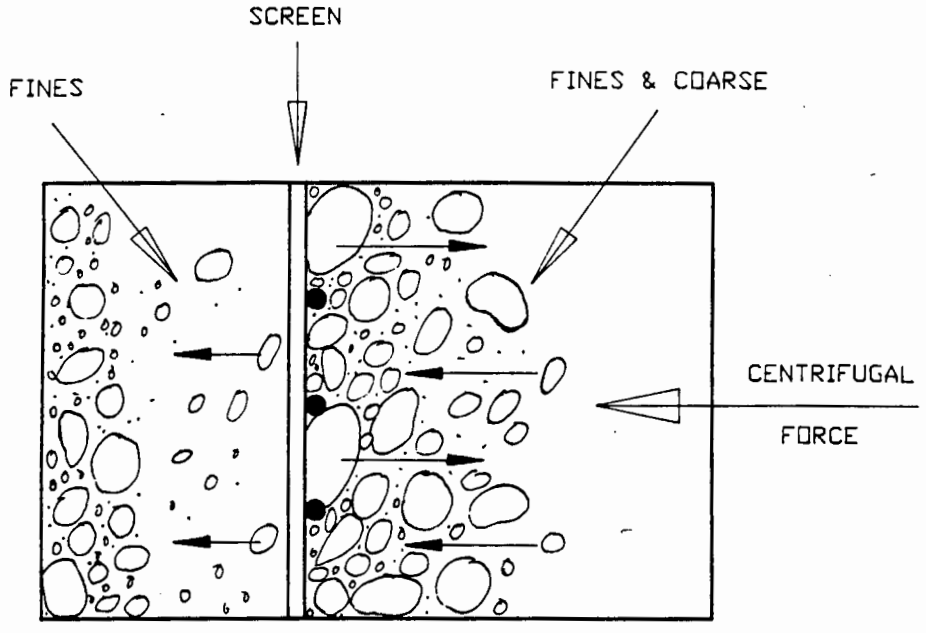

Figure 2.17 : Screening process

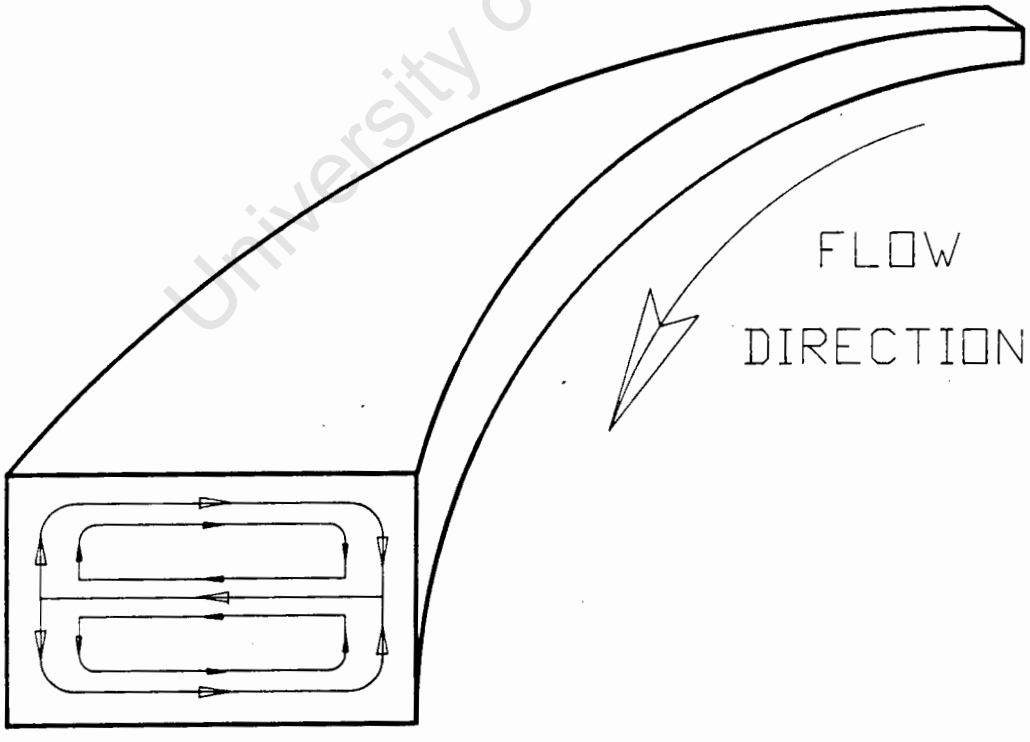

Figure 2.18 : Secondary flow (Blevins, 1984)

CHAPTER 3

THE TEST FACILITY

INTRODUCTION

To allow tests to be carried out on the underwater separation of diamantiferous mine gravels, three test rigs have been constructed in the hydraulics tower of the Civil Engineering Department. They are :

1. A 150 mm internal diameter (i.d.) clear perspex settling tube for determining the settling velocities and shape factors of various particles.

2. A 181 mm i.d. test rig for pumping solid/water mixtures through the converging elutriator and cyclosieve.

3. A smaller, 75 mm i.d. solids handling system for carrying out tests on the spirosieve model.

In this chapter, the three test rigs will be described in detail, with reference to their major components and operation.

3.1 SETTLING TUBE

3.1.1 Description

The settling tube is situated in the stairwell of the hydraulics tower and comprises a 13 m high, 150 mm i.d. circular perspex pipe (Figure 3.1). A collector chamber with a removable side is located at the bottom of the pipe. The collector chamber can be isolated from the pipe above by a gate valve. The settling tube is marked at 2 m intervals so that the distance travelled by the settling particles can easily be determined.

3.1.2 Operation

With the removable side of the collection chamber closed and the gate valve open, the settling tube is filled with water from the top. Particles can now be placed in the water at the top of the tube to determine their terminal settling velocity.

When the collection chamber is full of particles, the valve is closed so as to isolate the chamber from the water above. The side of the chamber is then removed and the particles can be retrieved. The removable side is replaced, the valve is opened and testing can continue.

3.2 181 mm TEST RIG

3.2.1 Description

The 181 mm internal diameter test rig comprises a primary circuit and a secondary circuit, and was used for testing both the converging elutriator and the cyclosieve.

With the converging elutriator in position the overall layout is as shown in Figure 3.2. Figure 3.3 shows the overall layout of the system with the cyclosieve installed.

3.2.2 Major Components

1. Test Tank

   The main test tank has a volume of approximately 13 m^3 and contains the solid/water mixture that is to be pumped through the system.

2. Centrifugal Pumps

   Both the primary and secondary circuits are supplied by 200 x 200 mm solids handling centrifugal pumps. Each pump is powered by a 45 kW variable speed hydraulic drive.

3. Pipeline

   The straight sections of both circuits are constructed of 181 mm i.d. Polyvinyl Chloride (PVC) pipes. All bends and short transitions between bends are constructed of mild steel, to reduce the wear rate.

4. Volume Measuring Tank

The volume measuring tank consists of a 1,6 m^3 cylindrical vessel with a perspex viewing window. It is used for calibrating the flow measuring devices, i.e. bend meters and doppler flow meters.

5. Sample Baskets

Two square sample baskets are used to collect the fine and coarse material after separation has taken place. The baskets are covered in 2 mm mesh so as to allow the water to drain off the solids.

6. Pneumatic Activators

Three pneumatic activators are used to divert the flow of the solids/water mixture. The first is used to divert clear water to the volume tank when calibrating the flow meters. The other two activators are used to divert the fines and coarse material to the sample baskets.

3.2.3 Operation with the Converging Elutriator

With reference to Figure 3.2 from Lazarus and Rossouw (July 1987), the primary circuit draws the solid/water mixture from the tank (A), through the suction nozzle (B), into the primary pump (C), up the vertical riser (D), down the downcomer (E), up the primary outlet nozzle (F) and into the converging elutriator (G).

The secondary circuit draws the solid/water mixture (smaller particles) up the converging elutriator (G), down the downcomer (H), through the secondary pump (I), up the riser (J), down the downcomer (K), through the flow diverter (L), into either the sample tank (M) or back into the tank via a flexible hose, located directly behind the converging elutriator.

A wire mesh sample basket (O) is located in the tank used for sampling the smaller particles in the secondary circuit.

A divertor is located in the disposal chamber of the converging elutriator and is used to sample the larger rocks which pass down the annular disposal chamber. These rocks are collected in another sample basket (P) below valve (1).

Valves (2) and (3) are used to introduce water into both circuits from a constant head tank. Valve (4) is used to empty the tank. At the top of the primary downcomer (E) is a 90 mm ball valve (5) in a sealed column. This is used to introduce selected particles into the primary circuit.

3.2.4 Operation with the Cyclosieve

With reference to Figure 3.3, the primary circuit draws the solid/water mixture from the tank (A), through the suction nozzle (B), into the primary pump (C), up the vertical riser (D), down the downcomer (E), through the tangential primary inlet (F) and into the cyclosieve (G).

The secondary circuit removes a portion of the solid/water mixture (only fines) from the cyclosieve (G), via the downcomer (H), through the secondary pump (I), up the riser (J), down the downcomer (K), through the flow divertor (L), into either the sample tank (M) or back into the tank (A) via a flexible hose (N). A wire mesh sample basket (O) is located in the tank (A).

The remaining solids/water mixture (coarse material) passes out of the bottom of the cyclosieve (G) via the coarse outlet, through a gooseneck divertor (Q), into either the coarse sample chamber or back into the tank.

The fines are sampled by diverting the flexible hose into the fines sample basket (O), while the coarse material is collected in the other sample basket (P), below valve (7).

Valves (2) and (3) are used to introduce water into both circuits from a constant head tank. Valve (1) is used to empty the tank. At the top of the primary downcomer (E) is a 90 mm ball valve (5) in a sealed column. This is used to introduce selected particles directly into the primary circuit. A knife gate valve (6) at the bottom of the cyclosieve is used to close off the coarse outlet.

3.3 75 mm TEST RIG

3.3.1 Description

The 75 mm internal diameter test rig is comprised of a suction/delivery circuit and a jetting circuit as shown in Figure 3.4 from Lazarus and Rossouw (February 1988). The jetting circuit uses high velocity water jets to agitate the solids into suspension, while the suction/delivery circuit draws the suspended solid/water mixture from the main tank and introduces it into the spirosieve model.

3.3.2 Major Components

1. Test Tank

   The main test tank has a volume of approximately 2 m^3 and contains the solid/water mixture that is to be pumped through the system.

2. Centrifugal Pump

   The suction/delivery circuit is supplied by a 100 x 100 mm solids handling centrifugal pump. The pump is powered by a 20 kW variable speed hydraulic drive.

3. Jetting Pump

   The jetting circuits are supplied by a 125 x 75 mm centrifugal pump which is powered by a 75 kW electric motor.

4. Pipeline

The suction/delivery pipeline is constructed from 75 mm i.d. galvanised mild steel.

The suction pipeline of the jetting circuit is constructed from 125 mm i.d. mild steel, while the delivery pipe is 75 mm i.d. galvanised mild steel.

5. Volume Measuring Tank

The volume measuring tank consists of a 0,3 m^3 cylindrical vessle with a perspex viewing window. It is used for measuring flow rates.

6. Sample Baskets

Two cylindrical 2 mm apperture wire mesh sample baskets are situated beside the volume measuring tank. They are used for sampling the fines and coarse material after separation has taken place.

7. Divertors

Two gooseneck diverters are used to direct the solid/water mixture into either the test tank, sample baskets or volume measuring tank.

3.3.3 Operation

Figure 3.4 shows an overall layout of the research apparatus (consisting of two circuits, i.e. the suction circuit and the jetting circuit).

The suction circuit consists of test tank (A) leading to the dredge head (B). This dredge head is coupled to a remote height adjustment (C) through which the suction pipe (D) is joined to the solids handling pump (E). The delivery pipe (F) is connected to the spirosieve (H) by means of 50 mm flexible hose (G).

Both the outlets at the top of the spirosieve are coupled to 50 mm flexible hoses; one carries the fines (I) and the other the coarse material (J). The flexible hoses (I & J) lead into two gooseneck divertors (K_1 and K_2) whereby the solid/water mixtures can be diverted to either the sample tank (N) or to the sample baskets (M_1 and M_2). The coarse material is sampled in basket M_2 and the fines in basket M_1. After sampling, the solid/water mixture is returned to the test tank (A).

The jetting circuit consists of a suction line (O) leading to a high pressure jet pump (P) and then joining the dredge head via delivery pipe (Q). This circuit is used to agitate the sample into suspension before it is drawn into the suction inlet.

Valve (1) is used to introduce water into the test tank, while valve (2) is for priming the suction/delivery circuit. Valve (3) and (4) are for draining the volume measuring tank and main test tank respectively. Valve (5) is used to adjust the jetting flow rate.

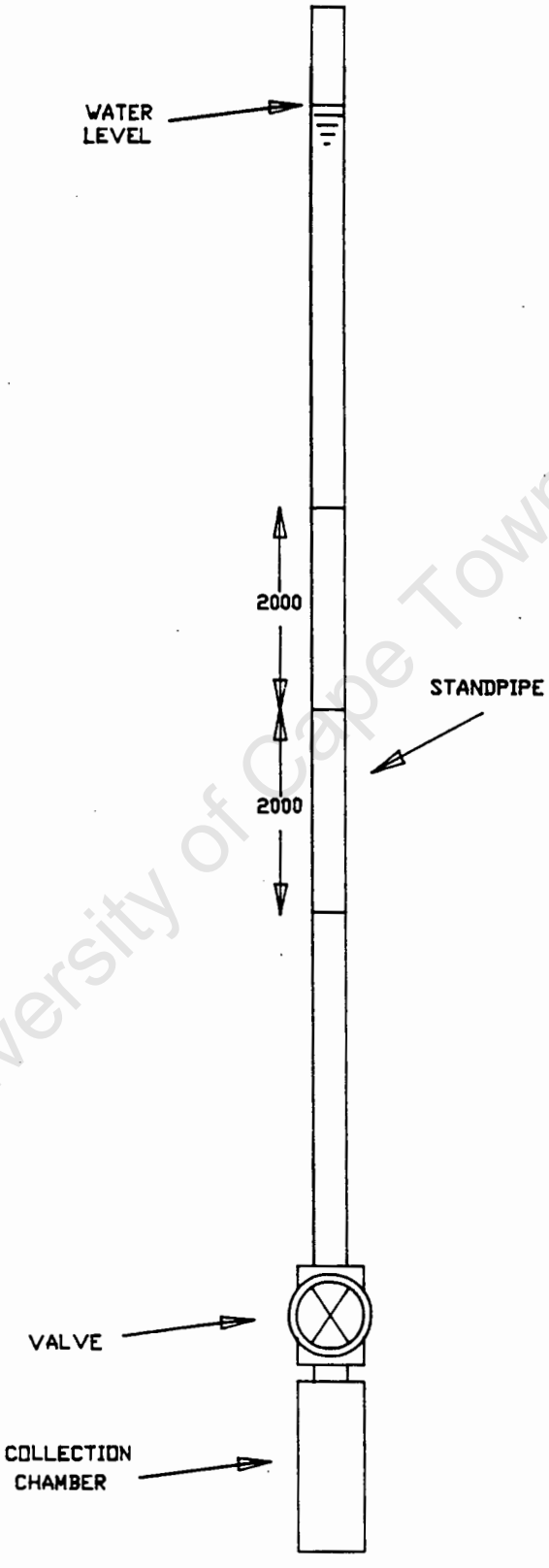

Figure 3.1 : Settling tube

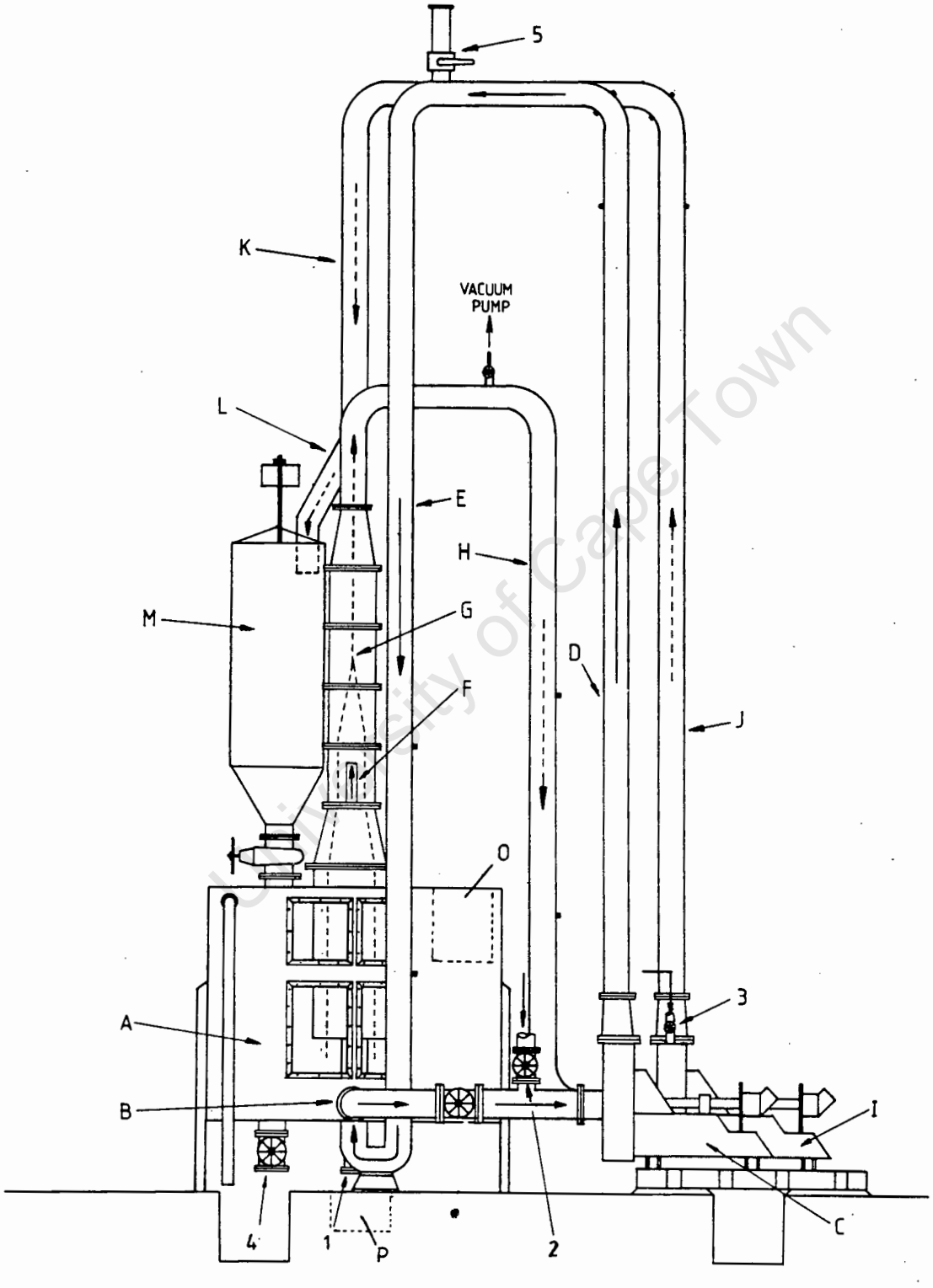

Figure 3.2 : 181 mm Test rig with converging elutriator
(Lazarus & Rossouw, July 1987)

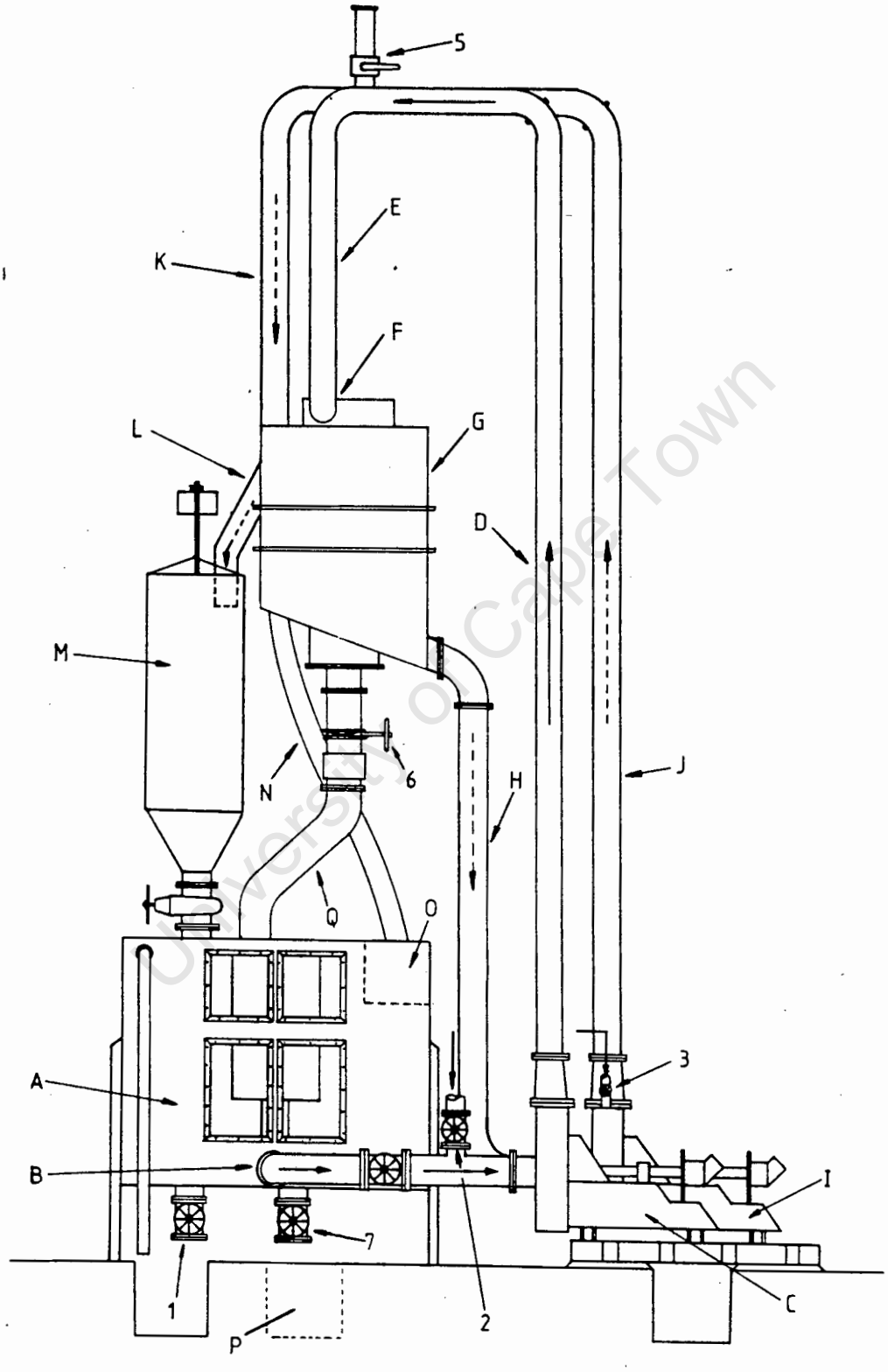

Figure 3.3 : 181 mm Test rig with cyclosieve

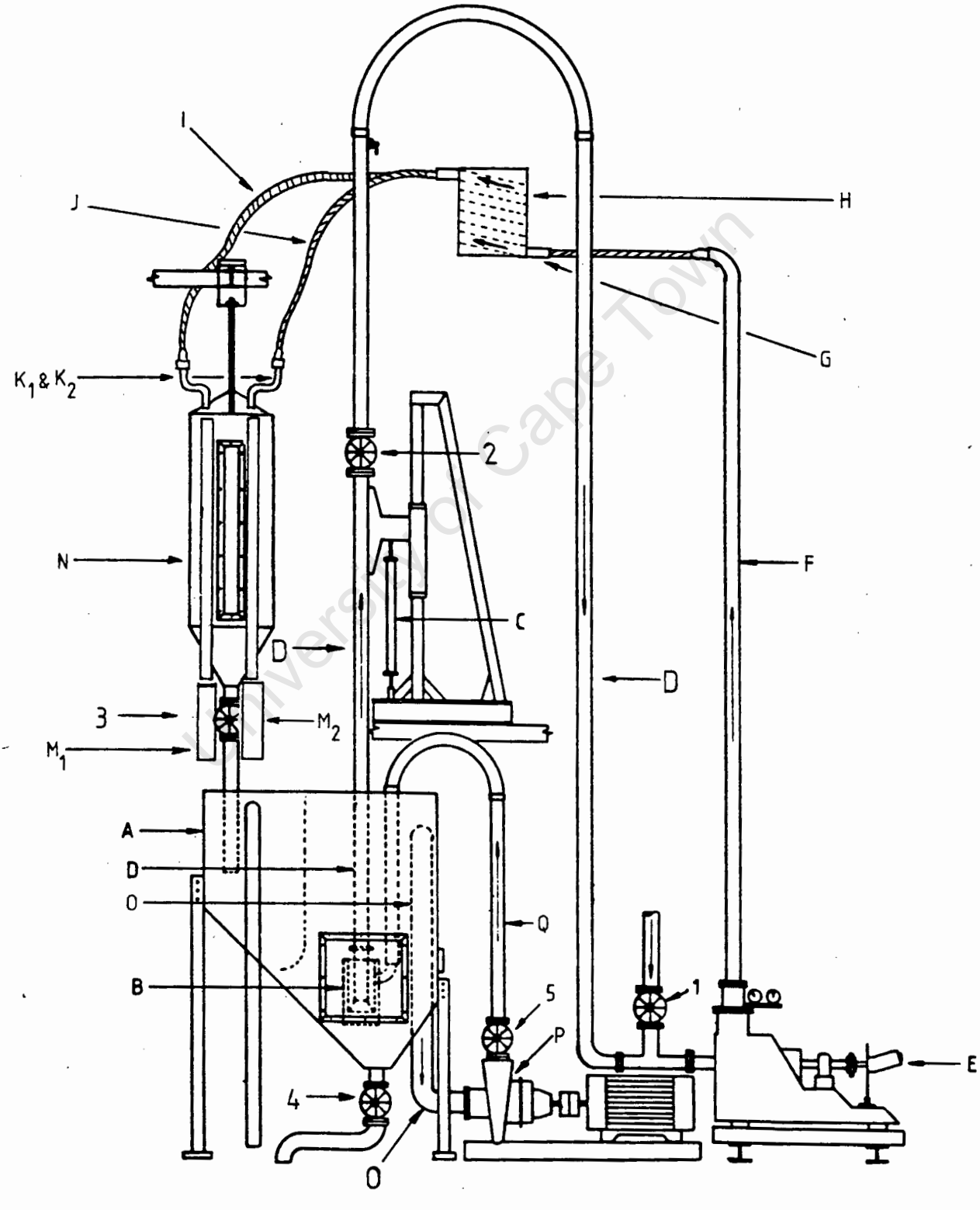

Figure 3.4 : 75 mm Test rig with spirosieve
(Lazarus & Rossouw, February 1988)

CHAPTER 4

INSTRUMENTATION

INTRODUCTION

Various forms of instrumentation have been incorporated into the test facility for the calibration of flow measuring devices, monitoring of flow rates, general data acquisition and presentation.

4.1 DOPPLER FLOW METERS

Two doppler flow meters have been installed in the primary and secondary circuits of the 181 mm test rig. The sonic transducers are located on the risers of each circuit, while the output display terminals are beside the controls of the hydraulic power pack. The output from these meters is *only* used to assist in the setting of the pump speeds to acquire an approximate flow rate (see Appendix A for calibration curves).

4.2 BEND METERS

Bend meters have been incorporated into the primary and secondary circuits of the 181 mm test rig, at the top of each riser. The bend meter consists of two 4 mm holes drilled into the outer and inner radii of a 90° bend. Figure 4.1 shows a bend meter with separation pods for preventing any solids material from entering the pressure

lines. The flow is measured by making use of the differential pressure generated at the high pressure tapping on the outside of the bend, relative to the low pressure tapping on the inside of the bend.

4.3 PRESSURE TRANSDUCERS

Two differential pressure transducers are used for measuring the pressure difference across the bend of each bend meter. The pressure transducers are SenSym LX1801DZ and have a 3,3 m differential range. They are linked to the bend meter tappings via a calibration manometer board. The electrical signals generated at the transducers are fed to a data acquisition unit.

4.4 MANOMETER BOARD

The manometer board comprises air over water and water over mercury manometers. The air over water manometers are used for calibrating the pressure transducers, doppler flow meters and bend meters, as well as relaying pressure readings to the transducers during operation. Figure 4.2 from Rossouw (November 1986), shows the layout of one of the air over water manometers. The water over mercury manometer is used to measure the pressure head loss over the spirosieve and is shown in Figure 4.3.

Separation pod flushing water and air pressure is supplied by the water main (400 kPa) and a compressor (700 kPa).

4.5 D.C. POWER SUPPLY

A 15 volt D.C. power supply is used to supply the required excitation voltage to the differential pressure transducers.

4.6 DATA ACQUISITION UNIT

A Hewlett-Packard 3497 data acquisition unit is used to process the signal from the D.C. power supply and the return signals from the differential pressure transducers. This unit converts the electrical analogue signals to digital signals before relaying them to the computer.

4.7 COMPUTER

The digital signals from the data acquisition unit are processed by a Hewlett-Packard 150 micro-computer. The computer is used for the calibration of the pressure transducers, as well as for monitoring the flow rates and velocities during operation.

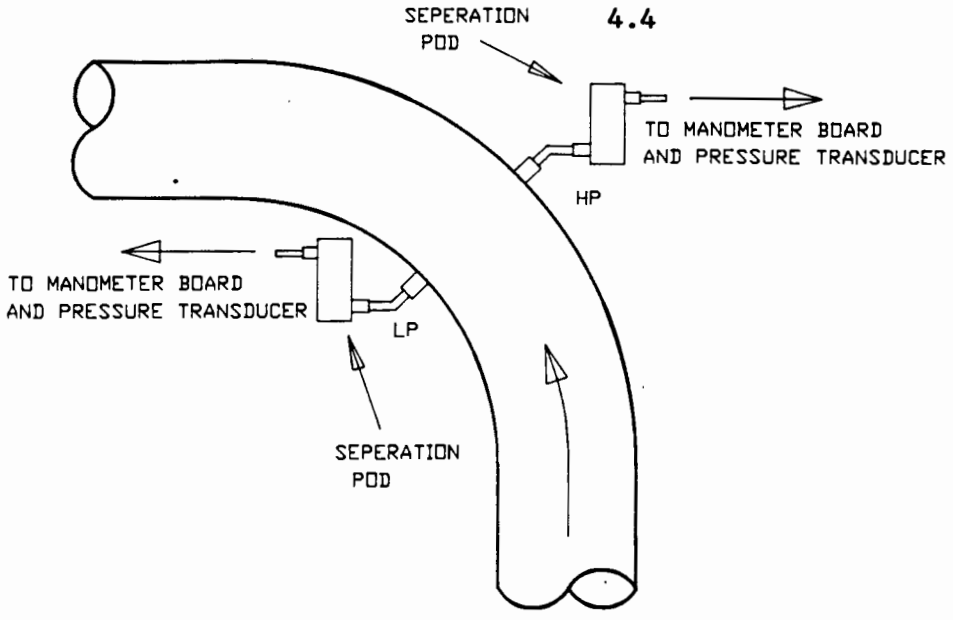

Figure 4.1 : Bend meter with separation pods

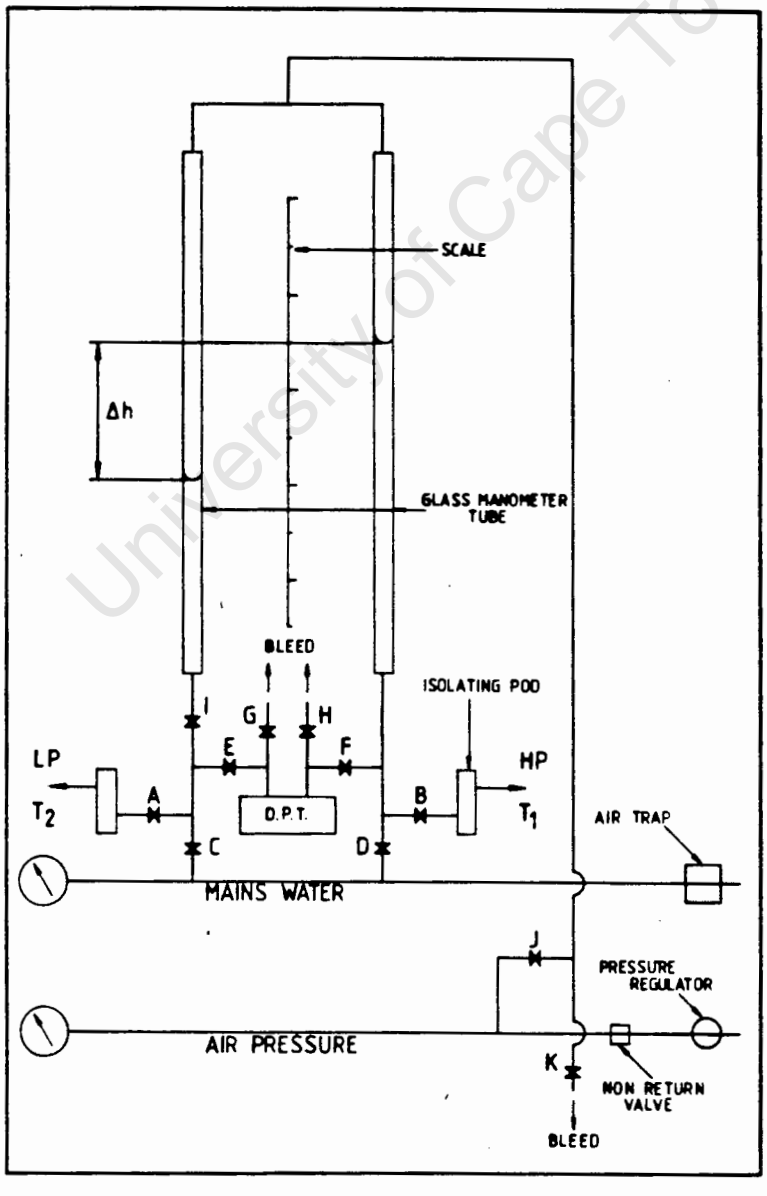

Figure 4.2 : Air over water manometer (Rossouw, Nov. 1986)

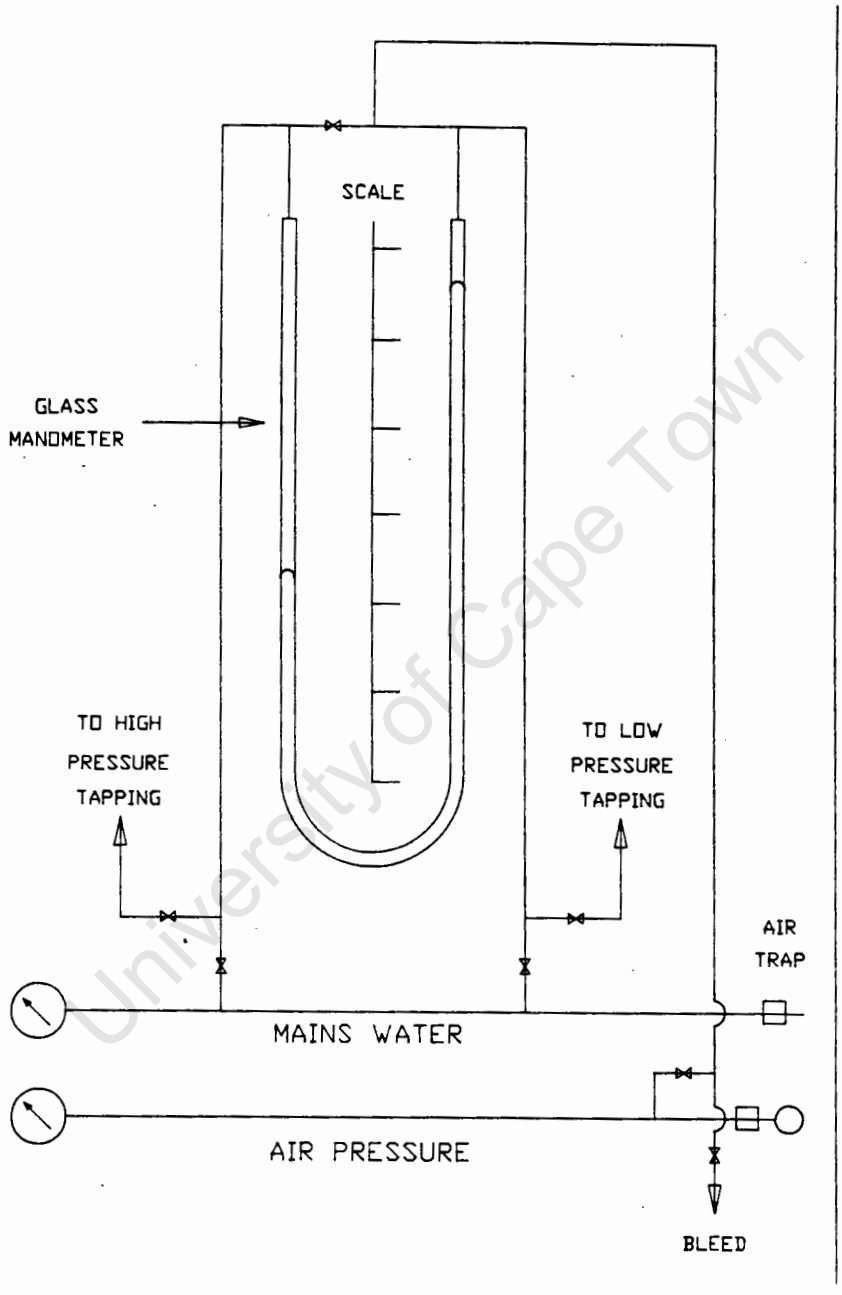

Figure 4.3 : Water over mercury manometer

CHAPTER 5

MEASUREMENT TECHNIQUES, CALIBRATIONS AND ACCURACY OF COLLECTED DATA

INTRODUCTION

To investigate the separation efficiency of each device under various conditions, it was necessary to monitor the following :

1. Flow rates (velocity)
2. Concentration
3. Percentage particles passing.

This chapter discusses the techniques used for the measurement of these components.

Also presented are calibrations and calculations to determine the accuracy of the collected data.

5.1 75mm TEST RIG

5.1.1 Velocity Measurements

The flow rates were monitored using the sample tank and a stop watch. The gooseneck divertors were diverted to the sample tank and the time of the diversion was measured. The time recorded combined with the volumne in the sample tank yields the flow rate

$$Q = \frac{V_T}{t} \qquad (5.1)$$

where V_T = volume in the tank (ℓ)

t = sample time (sec)

Q = flow rate (ℓ/s)

The average velocity in the spirosieve can be calculated by dividing the flow rate by the area of the rectangular conduit

$$v = \frac{Q}{A} \qquad (5.2)$$

where v = velocity (m/s)

A = area (m^2)

Q = flow rate (m^3/s)

1. Calibration

Figure 5.1 shows the calibration curve obtained for the sample tank, where the height (H) measured from a graduated scale on the observation window is related to the volume in the tank. The equation is :

$$V_T = 0{,}195\ H + 70 \qquad (5.3)$$

2. Accuracy of velocity measurements

To determine the accuracy of collected data, the equation used is partially differentiated with respect to each of the measured variables (Lazarus, 1984).

$$\frac{\partial X}{X} = \frac{\partial h}{\Delta H} \qquad (5.4)$$

where ∂h = accuracy obtained when recording data

ΔH = lowest measured value of the data

$\frac{\partial h}{\Delta h} \times 100\%$ = percentage error incurred.

From equation 5.2 and 5.3

$$v = \frac{0{,}195\ H + 70}{1\ 000\ t\ A} \qquad (5.5)$$

Using the procedure as outlined above, the accuracy obtained from the height measurement (H) is given by :

$$\frac{\partial v}{v} = \frac{0{,}195\ \partial H}{0{,}195\ H + 70} \qquad (5.6)$$

and from the time measurement (t) :

$$\frac{\partial v}{v} = -\frac{\partial t}{t} \qquad (5.7)$$

and from the area measurement (A) :

$$\frac{\partial v}{v} = -\frac{\partial A}{A} \qquad (5.8)$$

Data collection errors are as shown in Table 5.1.

Measured Quantity	Accuracy	Lowest Measurement	% error
H	1 mm	320 mm	0,15
t	0,01 sec	20 sec	0,05
A	0,00001 m^2	0,00441 m^2	0,23

TABLE 5.1

The maximum error is therefore 0,43% at a measured velocity of 1,5 m/s.

5.1.2 Solids Concentration

The solids concentration is monitored by diverting the gooseneck divertors to the sample baskets for a measured time period. The sample of material collected is weighed and from the flow rate and solids density, the concentration can be calculated by :

$$C_v = \frac{100\ M_s}{\rho_s\ Q\ t_d} \qquad (5.9)$$

where M_s = mass of solids collected (kg)

ρ_s = solids density = 2 700 kg/m^3

Q = flow rate (m^3/s)

t_d = time of sampling (sec)

Using the method described previously, the accuracy obtained from the mass (M_s) is given by

$$\frac{\partial C_v}{C_v} = \frac{\partial M_s}{M_s} \tag{5.10}$$

and from the time (t_d)

$$\frac{\partial C_v}{C_v} = -\frac{\partial t_d}{t_d} \tag{5.11}$$

and from the flow rate (Q)

$$\frac{\partial C_v}{C_v} = -\frac{\partial Q}{Q} \tag{5.12}$$

Data collection errors are shown in Table 5.2.

Measured Quantity	Accuracy	Lowest Measurement	% error
M_s	0,001 kg	4,364 kg	0,02
t_d	0,01 sec	4,7 sec	0,21
Q	$2{,}8 \times 10^{-5} m^3/s$	$0{,}00662\ m^3/s$	0,43

TABLE 5.2

The maximum concentration error is therefore 0,66%.

5.1.3 Percentage Particle Passing

To determine the screening efficiency during bulk sample tests the percentage particles passing through the screen is calculated at different size ranges.

The coarse and fine particles collected from each sample basket are dried, sieved, weighed and recorded.

The percentage passing in a specific size range is calculated by dividing the mass of material collected in that size range in the fines basket, by the total mass of material in that size range.

The recorded results are presented on a Tromp Curve (Grade Efficiency Curve) as in Figure 5.2. The Tromp curve is a graphical representation of the percentage particles of various sizes that pass through a specific screen.

In Figure 5.2, the data point at (1) indicates that 70% of all particles between 10 mm and 8 mm (next smallest sieve size) passed through the separation devices screen. The last data point (2) indicates the percentage passing between 5 mm and the smallest sieve size used, i.e. 2 mm.

1. Accuracy of measurements

The percentage passing (PP) is given by

$$PP = \frac{100\ M_f}{M_f + M_c} \tag{5.13}$$

where M_f = mass of fines in fines basket (g)

M_c = mass of fines in coarse basket (g)

and the accuracy of the measurement is given by

$$\frac{\partial PP}{PP} = \frac{\partial M_f}{M_f} - \frac{\partial M_f}{M_f + M_c} \tag{5.14}$$

$$\frac{\partial PP}{PP} = - \frac{\partial M_c}{M_f + M_c} \tag{5.15}$$

Data collection errors are shown in Table 5.3.

Measured Quantity	Accuracy	Lowest Measurement	% error
M_f	0,1 g	3,1 g	3,21
M_c	0,1 g	634,7 g	0,01

TABLE 5.3

This results in a maximum error of 3,22% when the percentage passing is at a minimum, i.e. 0%.

The error when 100% material is passing, is approximately 0,09%.

5.2 181 mm TEST RIG

5.2.1 Flow Measurements

The flow rates in the 181 mm diameter test rig were monitored using bend meters as described in Section 4.2. The head loss across the bend was measured using differential pressure transducers.

1. Calibration

Figure 5.3 shows the calibration curve obtained for the sample tank which was used to calibrate the bend meters. The height (H) on the scale is related to the volume (V_T) in the tank by

$$V_T = 0,5\ H + 207 \qquad (5.16)$$

Figures 5.4 and 5.5 show the calibration curves for the primary and secondary pressure transducers. They were calibrated using the air over water manometers which have graduated scales for measuring the head difference Δh . The equations are

$$V_{out} = 1,41 \times 10^{-3}\ \Delta H + 7,58 \qquad (5.17)$$

for the secondary transducer, and

$$V_{out} = 1,42 \times 10^{-3} \Delta H + 7,51 \qquad (5.18)$$

for the primary transducer.

where V_{out} = the voltage output (volts)

ΔH = the head difference (mm)

The primary and secondary bend meters were calibrated using the pressure transducers and the sample tank. The calibration curves are shown presented in Figures 5.6 and 5.7. The equations are :

$$\ln Q_p = 0,518 \ln \Delta H + 1,191 \qquad (5.19)$$

for the primary bend meter, and

$$\ln Q_s = 0,504 \ln \Delta H + 1,317 \qquad (5.20)$$

for the secondary bend meter.

2. <u>Accuracy of measurements</u>

The accuracy of the pressure transducers is taken to be 0,67% as specified by the manufacturers, because the regression coefficient of both calibrations was 1.

The accuracy of the flow measurement is determined by calculating the error due to readings taken via the pressure transducers, and from the bend meter calibrations using the sample tank.

From equation 5.16

$$Q = Q_s = Q_p = \frac{0,5H + 207}{1\,000\ t} \qquad (5.21)$$

By differentiating, the accuracy obtained from the height (H) is given by :

$$\frac{\partial Q}{Q} = \frac{0,5\ \partial H}{0,5H + 207} \qquad (5.22)$$

and from the sample time (t)

$$\frac{\partial Q}{Q} = -\frac{\partial t}{t} \qquad (5.23)$$

Data collection errors are shown in Table 5.4.

Measured Quantity	Accuracy	Lowest Measurement	% error
H	1 mm	1 380 mm	0,06
t	0,01 sec	22,2 sec	0,05

TABLE 5.4

For the primary flow rate, combining equations 5.18 & 5.19

$$\ln Q_p = 0{,}518 \ln \left[\frac{V_{out} - 7{,}51}{1{,}42 \times 10^{-3}} \right] + 1{,}191 \qquad (5.24)$$

the accuracy is given by

$$\frac{\partial Q_p}{Q_p} = \frac{0{,}518\ \partial V_{out}}{V_{out} - 7{,}51} \qquad (5.25)$$

Data collection errors are shown in Table 5.5.

Measured Quantity	Accuracy	Lowest Measurement	% error
V_{out}	0,0504	7,5188	0,30

TABLE 5.5

The maximum error in the primary flow is therefore 0,41% at 40 ℓ/s.

Similarly, for the secondary flow, combining equation 5.17 and 5.20

$$\ln Q_s = 0{,}504 \ln \left[\frac{V_{out} - 7{,}58}{1{,}41 \times 10^{-3}} \right] + 1{,}317 \qquad (5.26)$$

the accuracy is given by

$$\frac{\partial Q_c}{Q_s} = \frac{0{,}504\ \partial\ V_{out}}{V_{out} - 7{,}58} \qquad (5.27)$$

Data collection errors are shown in Table 5.6.

Measured Quantity	Accuracy	Lowest Measurement	% error
V_{out}	0,0521	7,769	0,02

TABLE 5.6

The maximum error in the secondary flow is therefore 0,13% at 50 ℓ/s.

5.2.2 Velocity Measurements

The velocity at any section in the system is calculated by dividing the flow rate by the flow area.

1. Accuracy of measurement

The accuracy of the elutriation column velocity (V_{ec}) is affected by the measurement of both the secondary flow (Q_s) and the diameter (D) of the elutriation column.

$$V_{ec} = \frac{4Q_s}{\pi D^2} \qquad (5.28)$$

by differentiating with respect to Q_s and D, the accuracy is given by

$$\frac{\partial V_{ec}}{V_{ec}} = \frac{\partial Q_s}{Q_s} \qquad (5.29)$$

and

$$\frac{\partial V_{ec}}{V_{ec}} = \frac{2\partial D}{D^2} \qquad (5.30)$$

Data collection errors are shown in Table 5.7.

Measured Quantity	Accuracy	Lowest Measurement	% error
Q_s	$6{,}5 \times 10^{-5}$	0,050 m^3/s	0,13
D	0,002 m	0,350 m	3,27

TABLE 5.7

Similarly, for the primary outlet nozzle velocity (V_{pn}), the accuracy is given by

$$\frac{\partial V_{pn}}{V_{pn}} = \frac{\partial Q_p}{Q_p} \qquad (5.31)$$

and

$$\frac{\partial V_{pn}}{V_{pn}} = -\frac{2\partial d_n}{d_n^2} \tag{5.32}$$

Data collection errors are shown in Table 5.8.

Measured Quantity	Accuracy	Lowest Measurement	% error
Q_p	$1{,}64 \times 10^{-4}$	0,040 m³/s	0,41
d_n	0,002 m	0,154 m	2,60

TABLE 5.8

The equation for the annular velocity (V_{an}) is

$$V_{an} = \frac{Q_s - Q_p}{\pi/4\ (D^2 - d_n^2)} \tag{5.33}$$

and the accuracy in the measurement is

$$\frac{\partial V_{an}}{V_{an}} = \frac{\partial Q_s}{Q_s - Q_p} \tag{5.34}$$

$$\frac{\partial V_{an}}{V_{an}} = \frac{\partial Q_p}{Q_s - Q_p} \tag{5.35}$$

$$\frac{\partial V_{an}}{V_{an}} = -\frac{2D\ \partial D}{D^2 - d_n^2} \tag{5.36}$$

$$\frac{\partial V_{an}}{V_{an}} = \frac{2\, d_n\, \partial d_n}{D^2 - d_n^2} \qquad (5.37)$$

Data collection errors are shown in Table 5.9.

Measured Quantity	Accuracy	Lowest Measurement	% error
Q_s	$9{,}75 \times 10^{-5}$	0,075 m^3/s	0,28
Q_p	$1{,}64 \times 10^{-4}$	0,040 m^3/s	0,47
D	0,002 m	0,350 m	1,42
d_n	0,002 m	0,154 m	0,42

TABLE 5.9

The maximum error in annular velocity measurements is 2,59% at V_{an} = 0,50 m/s.

The equation for the primary inlet velocity (v) of the cyclosieve is given by

$$v = \frac{4Q_p}{\pi d_i^2} \qquad (5.38)$$

The accuracy of the measurement is given by

$$\frac{\partial_v}{v} = \frac{\partial Q_p}{Q_p} \tag{5.39}$$

and

$$\frac{\partial_v}{v} = -\frac{2\partial d_i}{d_i^2} \tag{5.40}$$

Data collection errors are shown in Table 5.10.

Measured Quantity	Accuracy	Lowest Measurement	% error
Q_p	$4{,}1 \times 10^{-4}$ m³/s	0,100 m³/s	0,41
d_i	0,002 m	0,200 m	2,00

TABLE 5.10

5.2.3 Concentration Measurements

The concentration is monitored by diverting the primary and secondary flow to the sample baskets. The sample of material is weighed and from the primary flow rate (Q_p) and solids density, the concentration can be calculated by

$$C_v = \frac{100\ M_s}{\rho_s\ Q_p\ t_d} \tag{5.41}$$

The accuracy in measuring the concentration is calculated as in Section 5.12.

Data collection errors are shown in Table 5.11.

Measured Quantity	Accuracy	Lowest Measurement	% error
M_s	0,001 kg	16,078 kg	0,006
t_d	0,01 sec	5 sec	0,20
Q_p	6,3 x 10^{-4} m^3/s	0,154 m^3/s	0,41

TABLE 5.11

The maximum error is 0,62% at a C_v of 0,72%.

5.2.4 Percentage particles passing

The calculation of the percentage particles passing is the same as that described in Section 5.13.

The error in the measurement is of the order of magnitude as that calculated in Section 5.2.4 (1) i.e. 3,22% at approximately 0% passing and 0,09% at 100% passing.

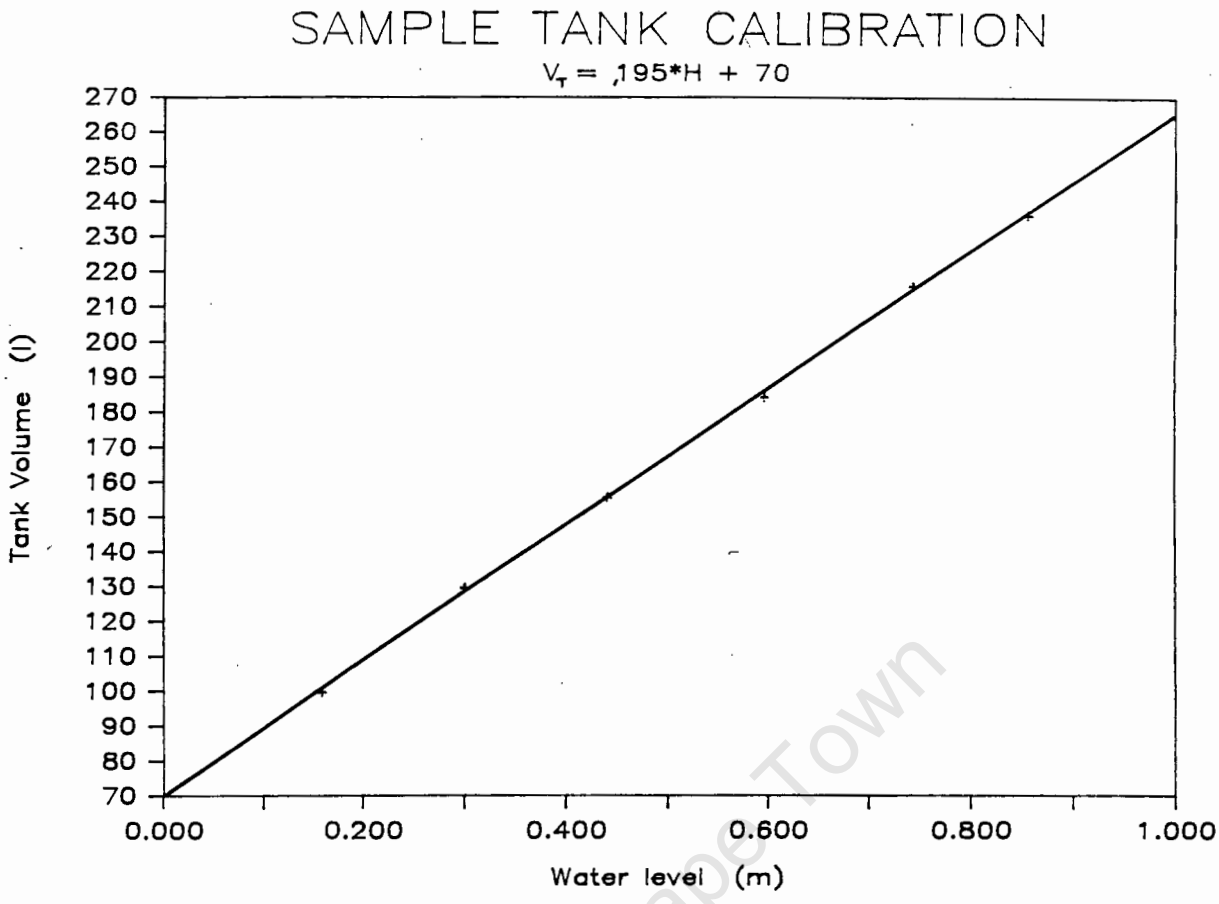

Figure 5.1 : 75 mm Test rig sample tank calibration

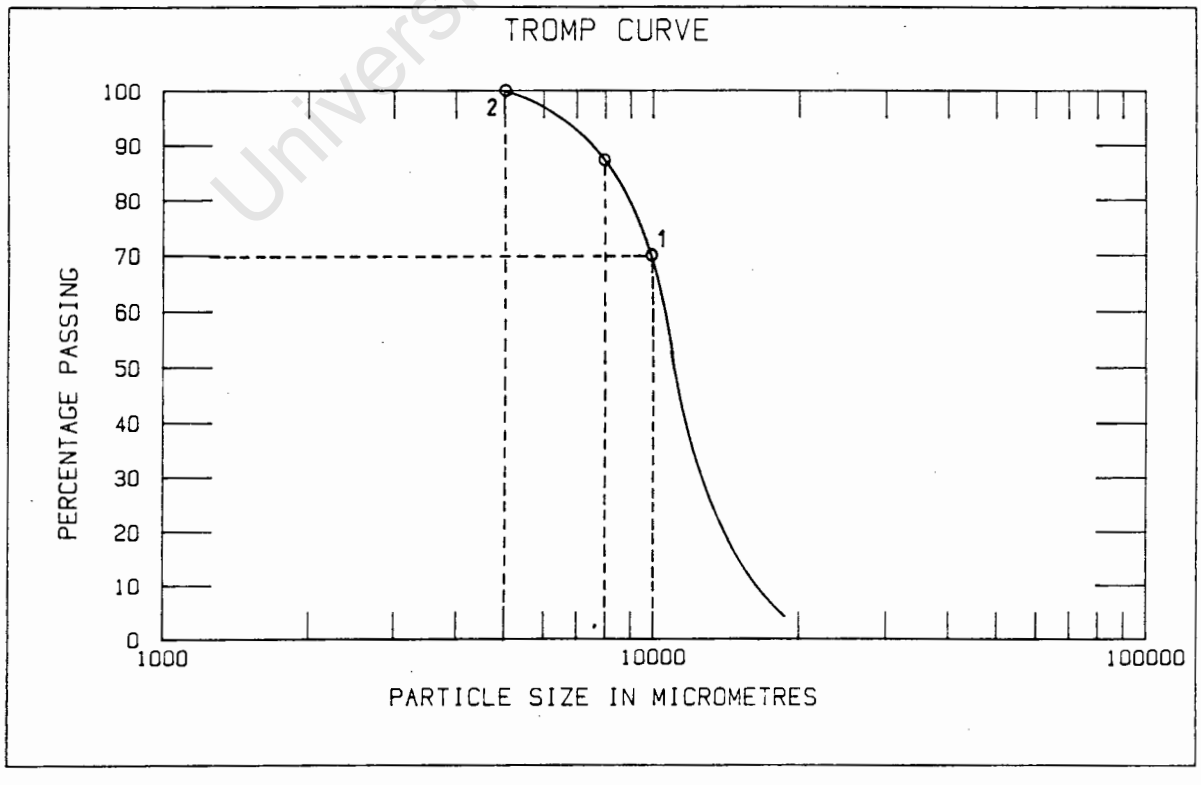

Figure 5.2 : Tromp curve

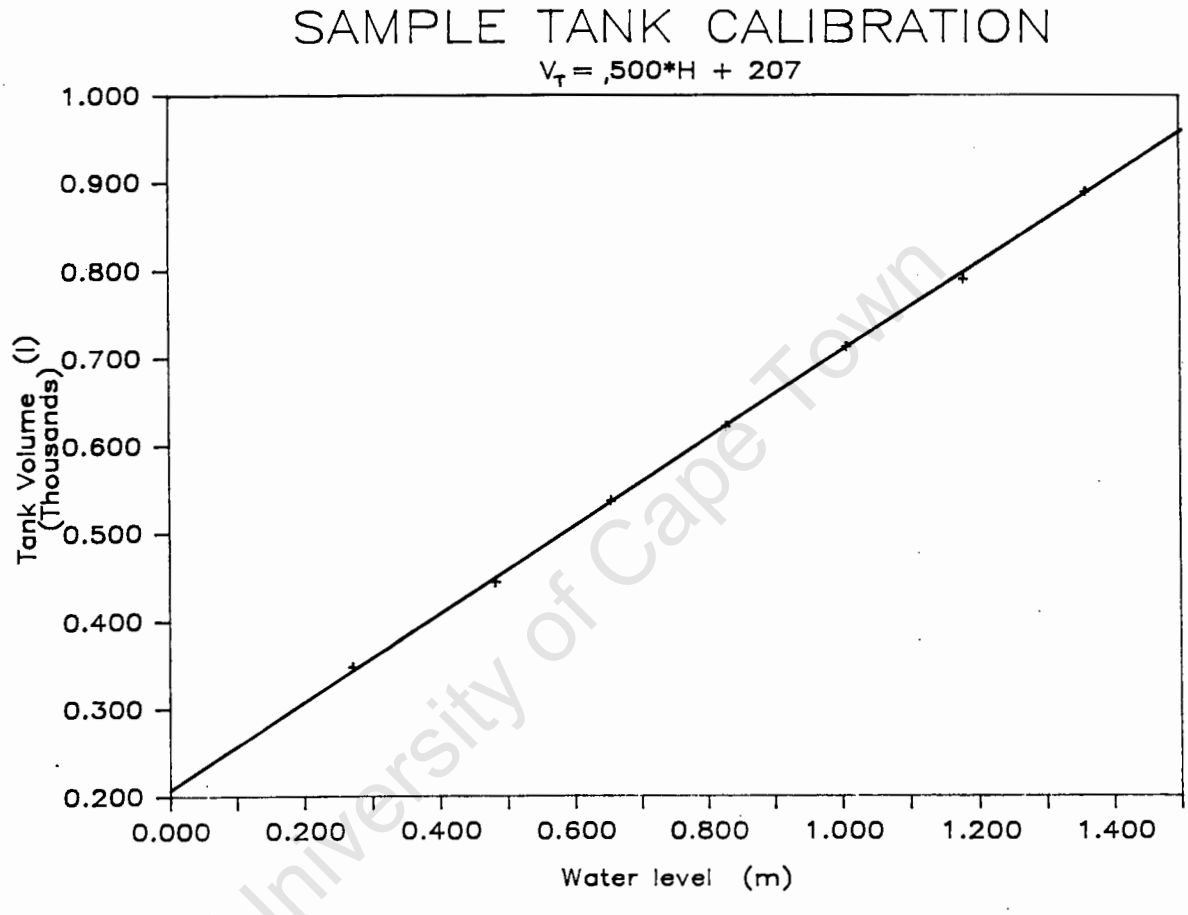

Figure 5.3 : 181 mm Test rig sample tank calibration

PRESSURE TRANSDUCER CALIBRATION

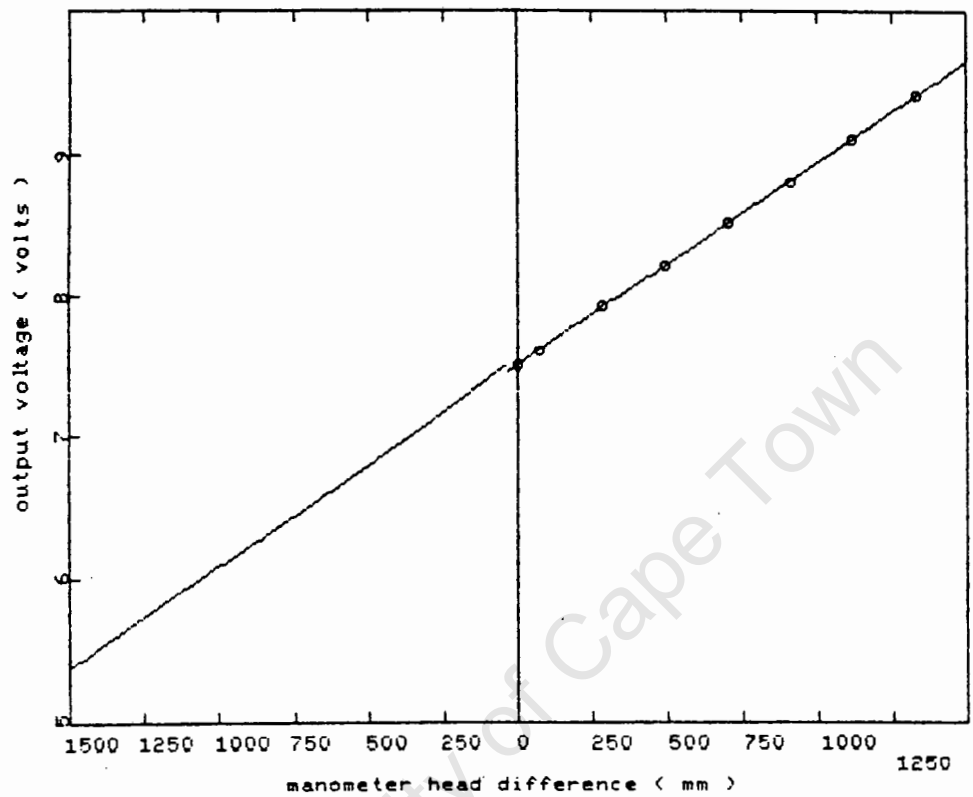

PRESSURE TRANSDUCER NUMBER : 1
OUTPUT VOLTAGE = (1.42404E-03 * DELTA h) + 7.508028

REGRESION COEFFICIENT R^2 = 1

DATE : 03-02-1987 TIME : 05:53:29

DELTA h (mm)	OUTPUT VOLTAGE (volts)
1332.0	9.4055
1117.0	9.0980
911.0	8.8047
704.0	8.5106
496.0	8.2145
288.0	7.9198
77.0	7.6172
0.0	7.5074

Figure 5.4 : Primary pressure transducer calibration

PRESSURE TRANSDUCER CALIBRATION

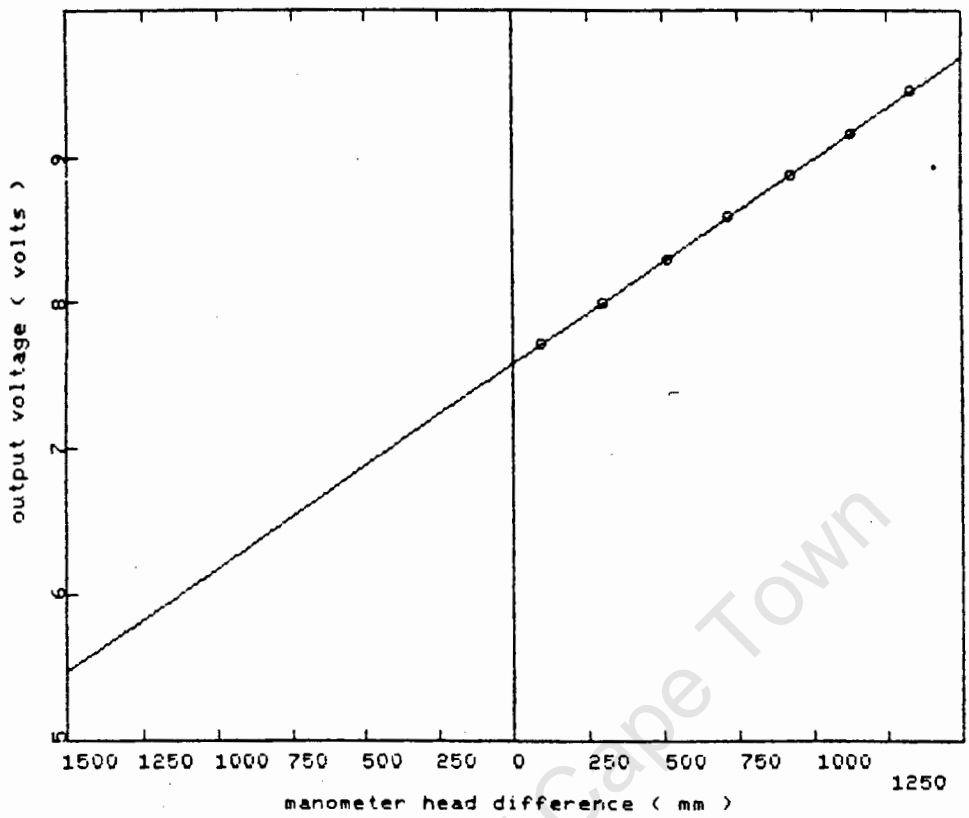

PRESSURE TRANSDUCER NUMBER = 4
OUTPUT VOLTAGE = (1.406288E-03 * DELTA h) + 7.580747

REGRESION COEFFICIENT R^2 = 1

DATE : 03-02-1987 TIME : 06:25:19

DELTA h (mm)	OUTPUT VOLTAGE (volts)
1334.0	9.4574
1133.0	9.1725
927.0	8.8850
720.0	8.5942
514.0	8.3022
303.0	8.0084
98.0	7.7178

Figure 5.5 : Secondary pressure transducer calibration

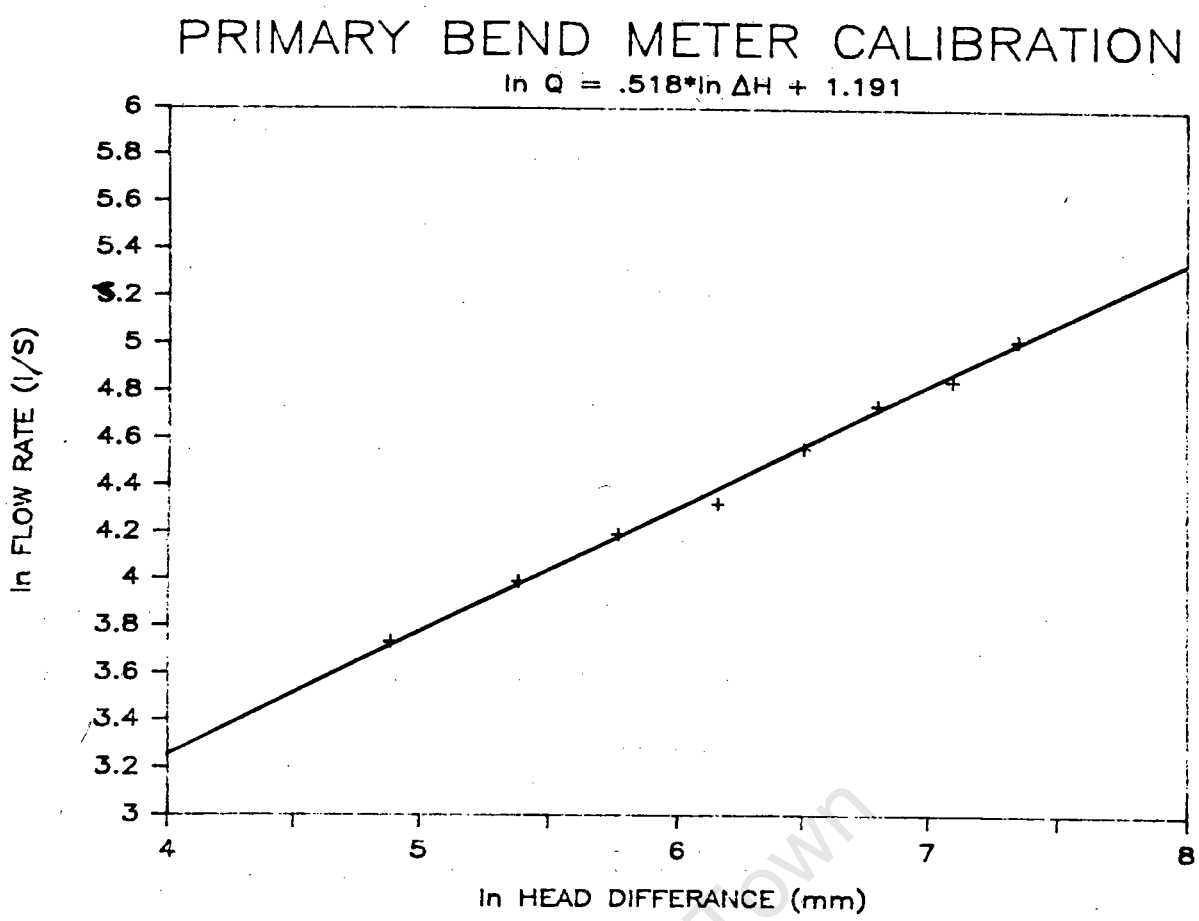

Figure 5.6 : Primary Bend meter calibration

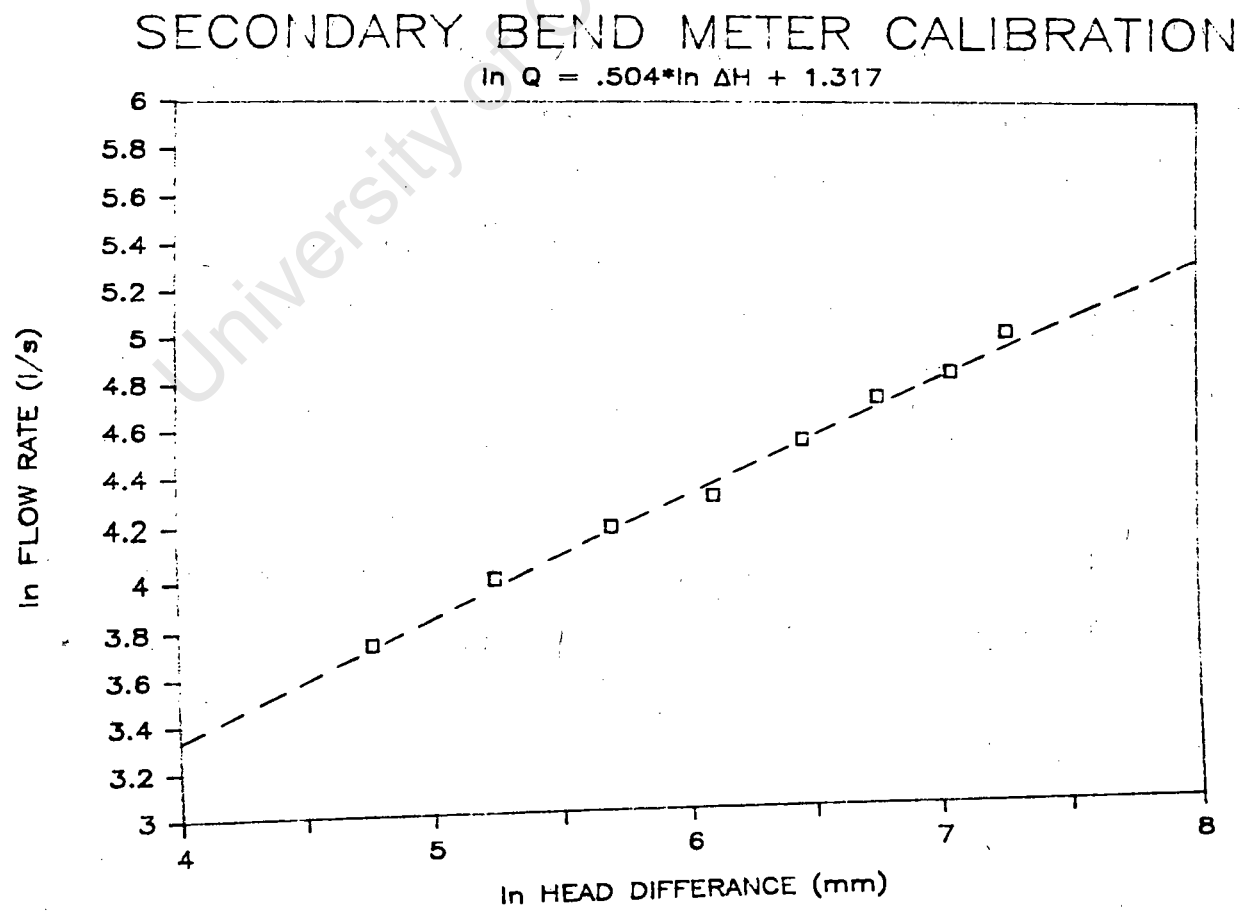

Figure 5.7 : Secondary bend meter calibration

6.2 TRACER PARTICLES

Coloured tracer particles were used in batched tests on all three separation devices to determine the effect of particle size and/or particle density. The particles varied in size and density but had a constant cylindrical shape. Table 6.1 gives a summary of the properties of each tracer particle.

Particle Size	Colour	Density (kg/m^3)	Terminal Settling Velocity (m/s)	SF
3,8	Orange	3 500	0,415	0,730
8	Orange	3 500	0,570	0,692
3,8	Purple	2 700	0,327	0,698
8	Purple	2 700	0,469	0,690
10	Purple	2 700	0,542	0,713

TABLE 6.1

6.3 INTERMEDIATE BULK SAMPLE

Intermediate bulk samples of approximately 6 kg of crushed granite, ranging from 4 mm to 100 mm were used in the converging elutriator tests.

The crushed granite was sieved into 6 particle size ranges. Each intermediate bulk sample was comprised of a recorded quantity of each size range as shown in Table 6.2.

A further intermediate bulk sample consisting of solitary particles and tracer particles was also used in the converging elutriator.

Particle Size Range (mm)	Mass (g)	Number
4 - 8	1200	
8 - 16	1200	
16 - 25	1000	
25 - 38		24
38 - 51		12
+ 51		8

TABLE 6.2

6.4 BULK SAMPLES

Different bulk samples of solid material were used in each test rig to determine the effect of concentration and/or particle size distribution, on the separation efficiency of the devices.

In the 181 mm test rig the bulk sample consisted of -17 mm dense phase submarine gravel and 17 - 100 mm submarine quartz pebbles. The solids density was measured at 2,90 g/cm^3 and had an initial particle size distribution as shown in Figure 6.1 from Lazarus & Rossouw (May 1988).

The solid material placed in the test tank of the 75 mm test rig had a smaller particle size range because of the limiting size of the spirosieve model. The sample was comprised of -25 mm quartz beach pebbles with a density of 2,70 g/cm^3 and an initial particle size distribution as shown in Figure 6.2 from Lazarus & Rossouw (March 1988).

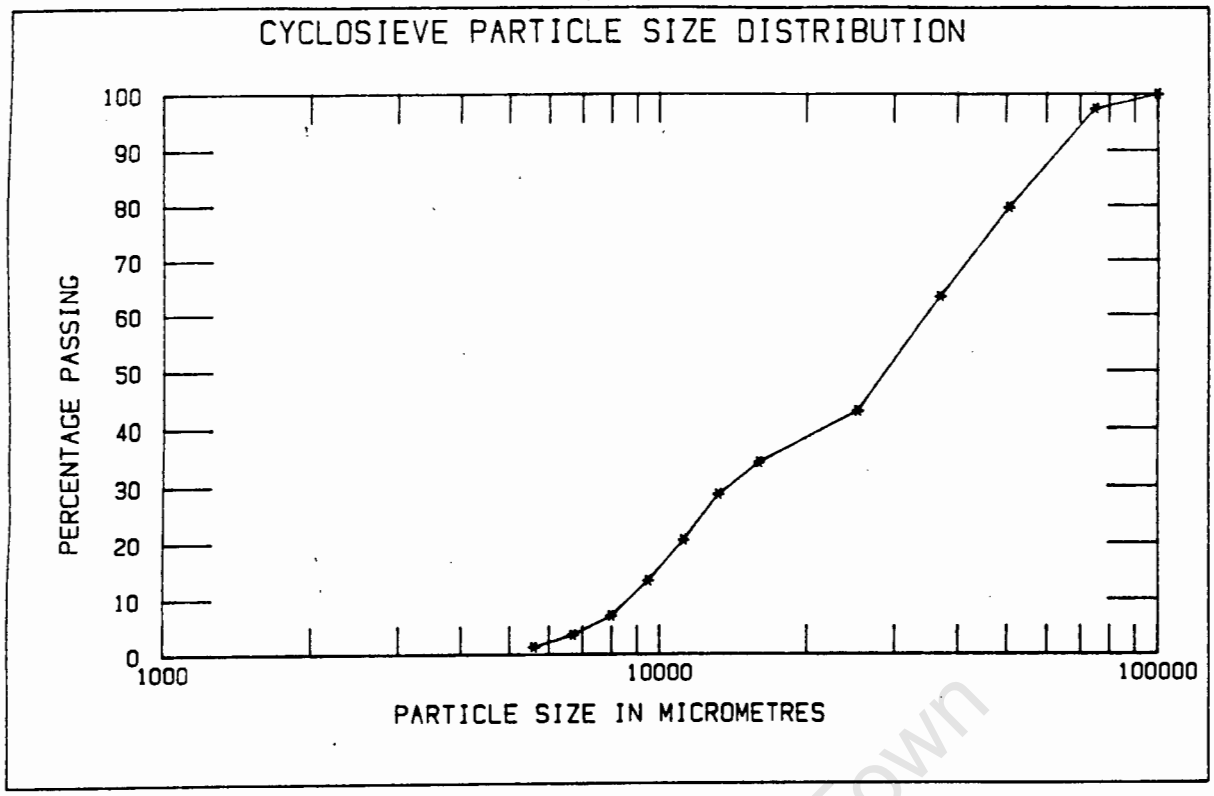

Figure 6.1 : 181 mm Test rig bulk sample particle size distribution (Lazarus & Rossouw, May 1988)

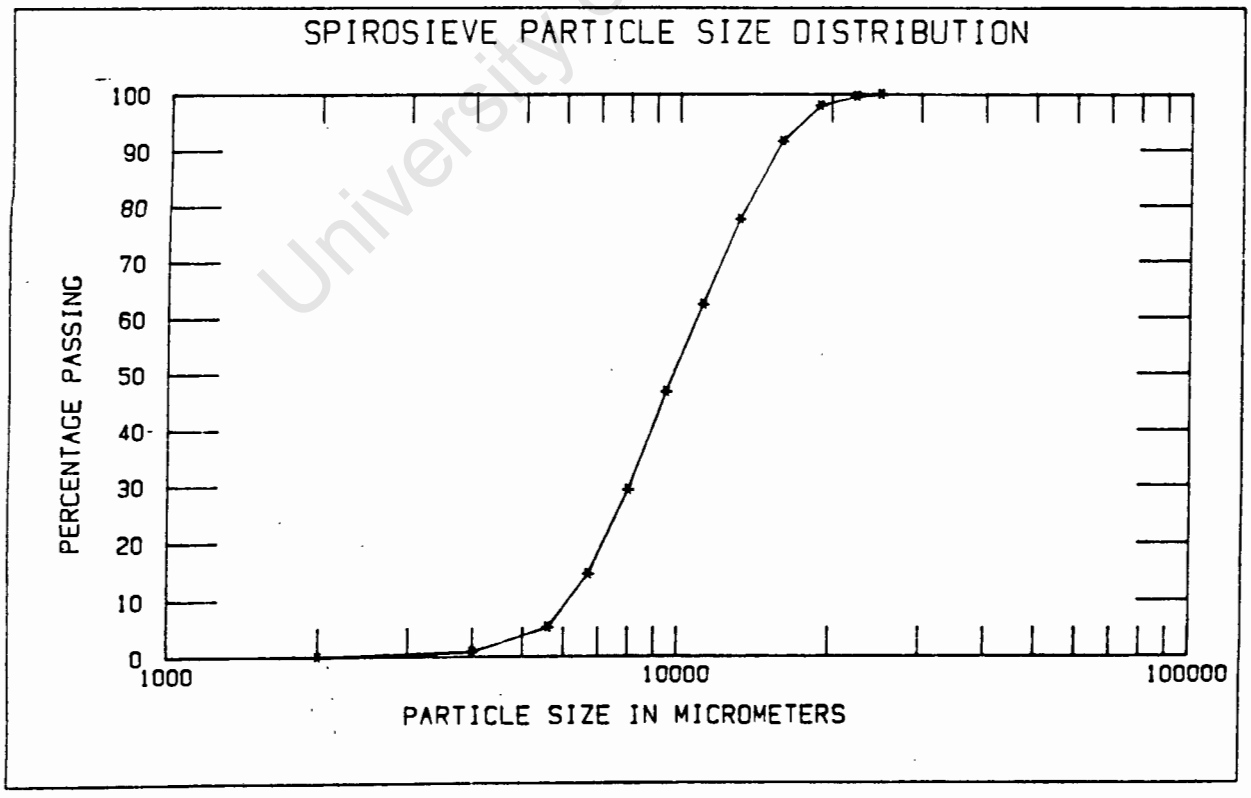

Figure 6.2 : 75 mm Test rig bulk sample particle size distribution (Lazarus & Rossouw, March 1988)

CHAPTER 7

EXPERIMENTAL PROCEDURE

INTRODUCTION

In order to determine the suitability of each device for underwater separation, various tests were carried out while varying different parameters. The parameters were :

Converging Elutriator - particle size
particle shape
particle density
elutriator geometry
elutriator velocities

Cyclosieve - particle size
particle density
solids concentration
screen geometry
primary inlet velocity
flow conditions

Spirosieve - particle size
particle density
velocity
solids concentration
particle size distribution
screen length
spirosieve orientation
presence of larger particles

This chapter covers the experimental procedure adopted while conducting tests to determine the effect of the above parameters on the separation efficiency of each device.

7.1 CONVERGING ELUTRIATOR

7.1.1 Solitary Particle Tests

Tests were conducted using solitary particles to determine the effect of *particle size and shape, and elutriation column velocity* on the separation efficiency.

Figure 7.1 (a), from Lazarus and Rossouw (July 1987), shows the geometry of the converging elutriator used for this series of tests.

With reference to Figure 3.2 the test procedure was as follows :

(a) With the system operating with clear water, all divertors were set so that the fine and coarse particles could be collected in the appropriate sample baskets.

(b) The primary flow was set 10 ℓ/s lower than the secondary flow so as to cause an upward flow in the annular disposal chamber.

(c) The flow rates and velocities were recorded.

(d) The solitary particles were individually introduced into the primary circuit via the primary inlet (B).

(e) The behaviour of each particle in the converging elutriator was observed through the perspex sections and recorded.

(f) When all the particles had been tested the divertors were returned to their original positions and the particles were collected.

Testing was continued by repeating (a) to (f) with different flow rates but always maintaining the 10 ℓ/s flow difference.

7.1.2 Intermediate Bulk and Batch Sample Tests

Tests were carried out using intermediate bulk samples of crushed granite, tracer particles/solitary particles, and batch samples of tracer particles. These tests were to investigate the effect of a change in *primary outlet velocity, elutriation geometry, upward annular disposal chamber velocity and particle density.*

The operating procedure was as follows :

(a) With the system operating with clear water, all divertors were set so that the fine and coarse particles could be collected in the appropriate sample baskets.

(b) The primary and secondary flow rates were set as required.

(c) The flow rates and velocities were recorded.

(d) A measured quantity of material was introduced into the primary circuit via valve (5).

(e) The behaviour of the particles in the converging elutriator were observed through the perspex sections and recorded.

(f) When the sample had passed through the system the divertors were returned to their original positions.

(g) The fines and coarse material was collected separately, dried, sieved, weighed and recorded.

The testing procedure varied slightly as each parameter was varied as follows :

1. Primary outlet velocity

The primary outlet velocity was varied by reducing the diameter of the primary outlet nozzle as in Figure 7.1 (b).

2. Elutriation geometry

The elutriation geometry was varied by changing the diameter and position of the primary outlet nozzle. The four geometric variations are shown in Figure 7.1.

3. Upward annular disposal chamber velocity

The annular disposal chamber velocity was varied once the optimum position of the outlet nozzle was found.

This was achieved by changing the ratio of primary flow to secondary flow resulting in an upward flow in the annular disposal chamber.

4. Particle density

The effect of a change in particle density was investigated by using batch samples of tracer particles with different densities, i.e. 2,70 g/cm^3 and 3,50 g/cm^3.

Tracer particles with a density of 3,50 g/cm³ were mixed with an intermediate bulk sample of the solitary particles (2,70 g/cm³), to determine the separation efficiency when 100% of the diamond density particles were separated.

7.2 CYCLOSIEVE

7.2.1 Batch Sample Tests

Batch samples of 8 mm tracer particles were used to investigate the effect of a change in *primary inlet velocity, flow conditions, screen geometry and particle density.*

With reference to Figure 3.3 the test procedure was as follows :

(a) With the system operating with clear water, all divertors were set so that the fine and coarse particles could be collected in the appropriate sample baskets.

(b) The primary and secondary flow rates were set as required.

(c) The flow rates and velocities were recorded.

(d) The flow patterns in the cyclosieve were observed through the clear perspex covers, and recorded.

(e) A measured quantity of tracer particles were introduced into the primary circuit via valve (5).

(f) Once the particles had been given sufficient time to pass through the system the divertors were returned to the normal position.

(g) The tracer particles were collected from each sample basket, counted and recorded.

The parameters to be investigated were varied as follows :

1. Primary inlet velocity

The primary inlet velocity was changed by altering the pump speed. The difference in flow rate between the primary inlet and secondary/fines outlet was kept constant during each test.

2. Flow conditions

The ratio of the secondary outlet flow to the primary inlet flow was varied by changing the relative pump speeds. This was done to create different flow conditions within the cyclosieve.

3. Screen geometry

The cyclosieve was dismantled so that the vertical screens could be changed to conical screens.

4. Particle density

Particle density was varied by using different density tracer particles.

7.2.2 Bulk Sample Tests

A bulk sample of marine gravel, as described in Section 6.4, was used to determine the effect of *particle size, solids concentration and different flow conditions* on the screening efficiency of the cyclosieve.

The test procedure was as follows :

(a) With the system operating with clear water, the bulk sample was emplied into the test tank.

(b) The primary and secondary flow rates were set as required.

(c) The flow rates and velocities were recorded.

(d) The flow patterns in the cyclosieve were observed through the clear perspex covers, and recorded.

(e) The fines and coarse outlets were diverted to the sample baskets for a short period (± 5 seconds), so as not to reduce the solids concentration in the system.

(f) The time of divertion was recorded.

(g) The coarse and fine material was collected, dried, sieved, weighed and recorded, so that the concentration, screening efficiency and particle size distribution could be calculated.

The variable parameters were changed as follows :

1. Particle size

The wide range of particle sizes in the bulk sample (Figure 6.1) allowed for the determination of the effect of particle size on screening efficiency.

2. Solids concentration

The solids concentration in the system was changed by adding more -17 mm material to the test tank.

3. Flow conditions

Different flow conditions were obtained by adjusting the ratio of the primary inlet flow to the secondary outlet flow.

7.3 SPIROSIEVE

7.3.1 Clear Water Tests

Before any solid material was tested in the spirosieve, clear water tests were carried out to determine the type of flow occurring in the spirosieve, i.e. smooth wall, partially-rough

wall or fully-rough wall turbulent flow with reference to the friction factor Reynolds number diagram for pipe flow.

With reference to Figure 3.4 the test procedure was as follows :

(a) The test tank (A) was filled with clear water and the pump (E) was started.

(b) The flow rate was set by adjusting the pump speed, and recorded.

(c) The head loss across the spirosieve was measured on the water over mercury manometer, and recorded.

Steps (b) and (c) were repeated at different flow rates and the associated head losses were recorded.

7.3.2 Batch Sample Tests

Batch samples of 3,8 mm tracer particles and marine gravel/ tracer particle mixtures were used to determine the effect of the following parameters :

- *velocity*
- *presence of larger particles*
- *particle density*
- *screen length*
- *spirosieve orientation.*

With reference to Figure 3.4 the test procedure was as follows :

(a) The straight suction inlet on the suction dredge head (B) was replaced with a 180° bend so that the suction inlet was facing upwards.

(b) The test tank (A) was filled with clear water and the system was started.

(c) The flow rate was set as required, and recorded.

(d) The fines and coarse flow were directed to the sample baskets, by diverting the gooseneck divertors (K_1 and K_2).

(e) A quantity of either tracer particles or a tracer particle/gravel mixture was introduced directly into the suction inlet.

(f) Visual observations of particle behaviour in the spirosieve were made, and recorded.

(g) When the sample had passed through the spirosieve the flow was directed back to the tank (A).

(h) The material in the fine and coarse baskets was collected, dried, sieved, weighed and recorded.

The parameters were varied as follows :

1. Velocity

   The velocity within the spirosieve was varied by changing the pump speed, resulting in a change in the flow rate.

2. Presence of larger particles

   The presence of larger particles on the separation of fines was investigated by introducing a mixture of small tracer particles and marine gravel into the system.

3. Particle density

   Tracer particles of varying density were used.

4. Screen length

   The screen length was shortened from 2,76 m to 2,02 m by blanking off the latter part of the screen with a solid barrier.

5. Spirosieve orientation

   The spirosieve was tested on its side to determine if this would affect the screening efficiency.

7.3.3 Bulk Sample Tests

A bulk sample of marine gravel, as described in Section 6.4, was used to investigate the effect of *particle size, solids concentration and particle size distribution.*

The test procedure was as follows :

(a) The 180° bend used in the batch sample tests was removed.

(b) The test tank (A) was filled with the bulk sample and water.

(c) Both the solids handling pump (E) and the jetting pump (P) were started.

(d) Valve (5) was opened until the jetting flow agitated the solids into suspension.

(e) The suction dredge head was lowered into the bulk sample.

(f) The flow rate was set as required and recorded.

(g) Visual observations of particle behaviour in the spirosieve were made, and recorded.

(h) The recirculating system was left to stabilise for 5 minutes before the fines and coarse flow were diverted to the sample baskets for a measured and recorded time period.

(i) The fine and coarse material was collected, dried, sieved, weighed and recorded.

The parameters were varied as follows :

1. Particle size

   The wide particle size range of the bulk sample provided a base for investigating the effect of particle size on the screening efficiency.

2. Solids concentration

   The solids concentration was varied by either raising or lowering the suction dredge head within the bulk sample.

3. Particle size distribution

   The particle size distribution was changed by adding 0,075 m^3 of 2 mm - 5 mm quartz stones to the existing bulk sample in the test tank.

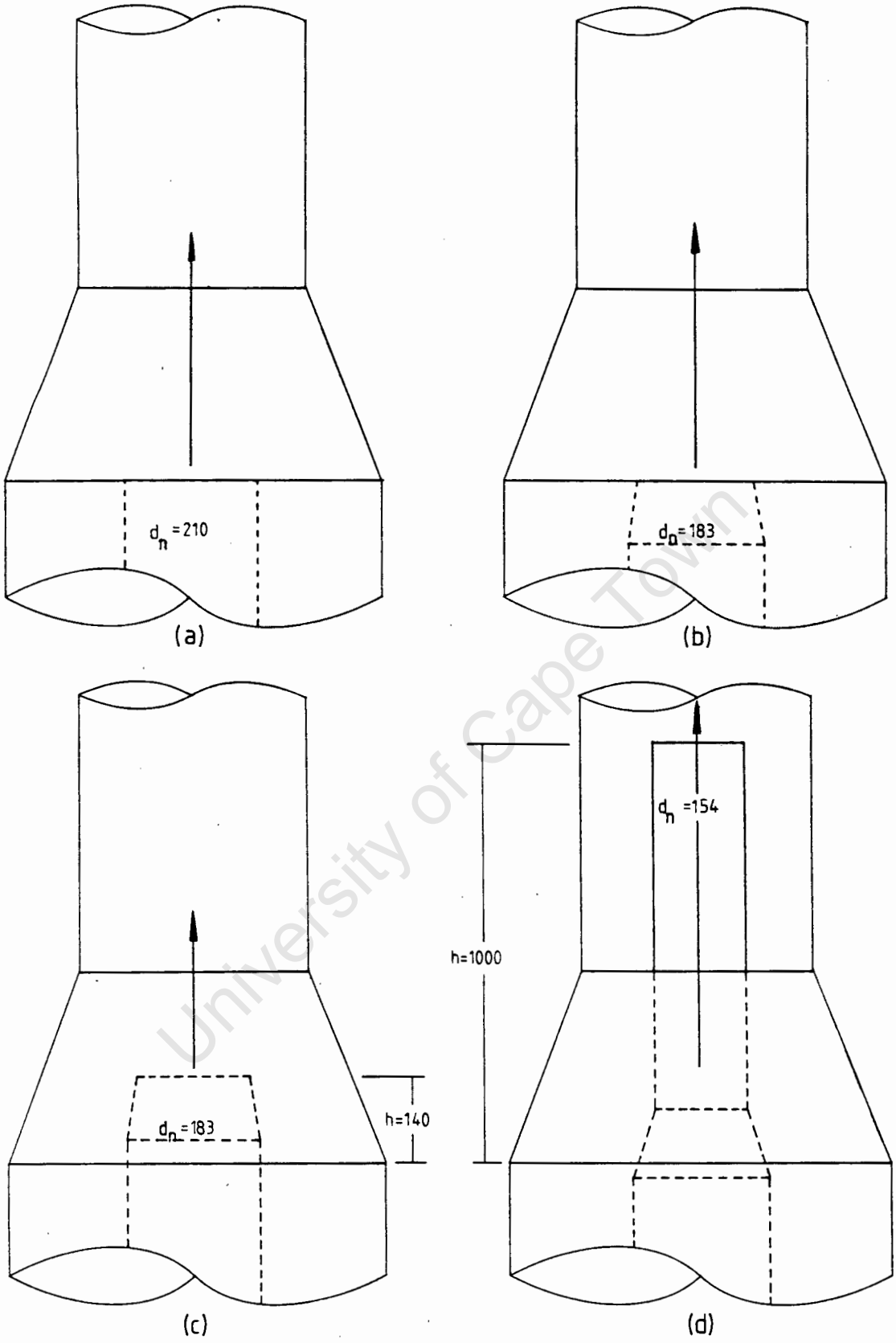

Figure 7.1 : Converging elutriation geometries
(Lazarus & Rossouw, July 1987)

CHAPTER 8

EXPERIMENTAL RESULTS AND OBSERVATIONS

INTRODUCTION

In this chapter, the experimental results and observations of the tests carried out on each separation device are presented.

Tabulated results of the experimental data are also presented in Appendices B, C and D.

8.1 CONVERGING ELUTRIATOR

8.1.1 Particle Size

Figure 8.1 to 8.3 represent the results of the solitary particle tests, at different elutration column velocities, to determine the effect of particle size on separation.

Most of the large rocks (50 mm - 60 mm) that passed out of the converging elutriator via the annular disposal chamber never entered the elutriation column (straight section).

The intermediate size rocks that were separated to waste, entered the elutriation column and only when they moved to the walls did they pass down and out via the annular disposal chamber. Some rocks recirculated for long periods between the walls and the higher velocity core before being separated.

8.1.2 Particle Shape

The effect of particle shape on the percentage particles entering the secondary circuit is shown in Figure 8.4 to 8.6 at different elutriation column velocities.

It was observed that the more irregular shaped rocks, i.e. lower shape factors, showed erratic behaviour in the elutriation column. A change in orientation would often result in a change in direction.

8.1.3 Elutriation Column Velocity

The effect that elutriation column velocity has on separation with solitary particles is shown in Figure 8.7.

Figure 8.8 shows the effect of a change in elutriation column velocity with an intermediate bulk sample of granite.

At all velocities small gravel particles were seen to move down the elutriation column in the wake of the larger rocks. Some smaller particles never entered the elutriation column but were separated out while still in the converging section.

Considerable turbulence was evident at the start of the elutriation column, especially at the higher velocities.

8.1.4 Primary Outlet Velocity

Figures 8.9 to 8.11 show the effect of an increased primary outlet nozzle velocity of approximately 32%.

At an elutriation column velocity of 0,82 m/s a greater amount of turbulence was observed at the higher velocity.

The turbulence continued to occur at the lower elutriation column velocities but at a position higher up in the elutriation column.

8.1.5 Elutriator Geometry

The elutriator geometry was varied as is shown in Figure 7.1 (a), (b) and (c) and the test results for an elutriation column velocity of 0,71 m/s are shown in Figure 8.12.

The test results with the Figure 7.1 (d) geometry are shown in Figure 8.13.

As the outlet nozzle was moved closer to the elutriation column a decrease in turbulence was observed.

8.1.6 Annular Disposal Chamber Velocity

Figures 8.14 and 8.15 show the effect of varying the annular velocity, with the elutriation geometry as in Figure 7.1 (d).

In Figure 8.14 the primary outlet nozzle flow was varied to produce a change in the annular flow, while in Figure 8.15 the secondary flow was varied.

8.1.7 Particle Density

Figure 8.16 is a plot of the percentage particles entering the secondary circuit versus annular velocity, with particle density as the variable parameter.

8.1.8 General Separation Trends

Figure 8.17 shows the separation efficiency of the converging elutriator when 100% of all 8 mm diamond density (3,50 g/cm^3) particles were entering the secondary circuit, i.e. passing to the ship.

Some smaller particles, including the 8 mm diamond density particles, moved into the outer coflow region with the larger rocks. They settled *slowly* until reaching the annular disposal chamber from where they were carried upwards by the annular flow. These particles recirculated between the two regions but were eventually all drawn back into the higher velocity central core and passed up the elutriation column.

Figure 8.18 is an experimental/theoretical plot of the separation efficiency when 100% of all 16 mm diamond density particles are passing.

8.2 CYCLOSIEVE

8.2.1 Vertical Screen

1. **Primary inlet velocity**

Figure 8.19 shows the effect that the primary inlet velocity has on screening. For this test the primary inlet flow (Q_p) and secondary outlet flow (Q_s) were equal.

It was observed that part of the inlet flow was deflected across the top of the cyclosieve, which resulted in a high degree of turbulence.

At the lower inlet velocities (< 4,5 m/s) the inlet jet began to strike the screen directly and only a thin layer of rotating water was observed on the screen.

2. **Flow conditions**

The effect on the screening efficiency, resulting from a change in the amount of water that is removed via the secondary outlet, is shown in Figure 8.20.

With $Q_p - Q_s = 44\ \ell/s$ a large mass of rotating water was observed in the cyclosieve, especially at the higher inlet velocities. The free vortex discharge via the coarse outlet was very strong. It was also noted that there was a considerable flow of water from the outer chamber back through the screen holes.

At $Q_p - Q_s = 20\ \ell/s$ a thinner layer of rotating water was observed on the screen. This layer of water covered only 6/8 of the screening surface at a 4,18 m/s inlet velocity. The amount of water flowing back through the screen holes was minimal.

8.2.2 Conical Screen

Figure 8.21 shows the change in screening efficiency when the screens were changed from vertical to conical.

At the higher inlet velocities (> 4,5 m/s) a layer of water was pushed up onto the solid section above the screen (see Figure 2.11(3)). This rotating layer of water neutralised *part* of the deflected inlet flow that was observed using vertical screens.

1. Primary inlet velocity

   Figure 8.22 shows the effect that a change in the inlet velocity has on the screening efficiency.

   As was the case with the vertical screens, the inlet jet strikes the screen directly at velocities below 4,5 m/s.

2. Variable secondary flow

   Changing the secondary flow while keeping the primary flow constant results in different flow conditions within the cyclosieve.

This is shown in Figure 8.23, as well as its effect on the screening efficiency.

It was observed that an almost non-aerated condition was obtained when the secondary flow rate was very much less than the primary inlet flow. The rotational velocity of the large mass of water appeared to be slightly slower than that of the thin layer of water.

3. Particle density

Figure 8.24 is a plot representing the effect that a change in particle density has on the percentage particles passing through the screen.

4. Particle size

Figure 8.25 is the Grade Efficiency Curve (Tromp Curve), showing the percentage particles passing plotted against the particle size.

Refer to Section 5.1.3 for an explanation of the Grade Efficiency Curve (Tromp Curve).

5. Flow conditions

The effect that the different flow conditions have on the screening efficiency is shown in Figure 8.26.

With the thin layer of rotating water on the screen, small and large rocks bounced off the screen and back through the water, into the air core and down the coarse outlet.

6. Solids concentration

Figure 8.27 is a graph of the particle size distribution and tromp curve, at three different solids concentrations.

The change in the particle size distribution was due to particle degradation caused by wear and the addition of -17 mm gravel to raise the solids concentration.

8.3 SPIROSIEVE

8.3.1 Clear Water Tests

Figure 8.28 represents the head loss per meter length of the spirosieve plotted against the average velocity.

These results were analysed as described in Appendix F and are presented on the friction factor versus Reynolds number diagram in Figure 8.29. Also shown on this graph are circular pipes with relative roughnesses of 0,02 and 0,05.

8.3.2 Velocity

The effect that a change in the average velocity has on the screening efficiency is shown in Figure 8.30.

8.3.3 Presence of larger particles

The effect of larger coarse material on the screening efficiency of fines was investigated and is shown in Figure 8.31.

8.3.4 Particle Density

The recorded change in screening efficiency, using different density tracer particles, is presented in Figure 8.32.

8.3.5 Screen Length

The effect that a shorter screen length had on the screening efficiency is shown in Figure 8.33.

8.3.6 Orientation

Figure 8.34 shows the percentage particles passing at different velocities for two different orientations of the spirosieve.

8.3.7 Particle Size

Figure 8.35 shows the tromp curve and particle size distribution for a bulk sample of marine gravel.

It was observed that the larger particles bounced off the screen and travelled through the bed into clear water before being forced back onto the screen again.

It was observed that individual screen holes became blocked with gravel but unblocked almost immediately when other rocks impinged on them. This resulted in a constant blocking and unblocking action during bulk sample tests.

8.3.8 Solids Concentration

Figures 8.36 and 8.37 show the effect that an increase in solids concentration has on the screening efficiency.

In the tests from which Figure 8.36 was derived, both the velocity and particle size distribution were kept constant.

In the Figure 8.37 tests, the particle size distribution changed slightly between tests because of material degradation due to wear.

The velocities in both tests were approximately equal and above the velocity (2,5 m/s) where screening efficiency began to decrease in the batch sample tests.

8.3.9 Particle Size Distribution

Figure 8.38 represents the results of tests carried out to determine the effect of an increase in the percentage fines on the screening efficiency.

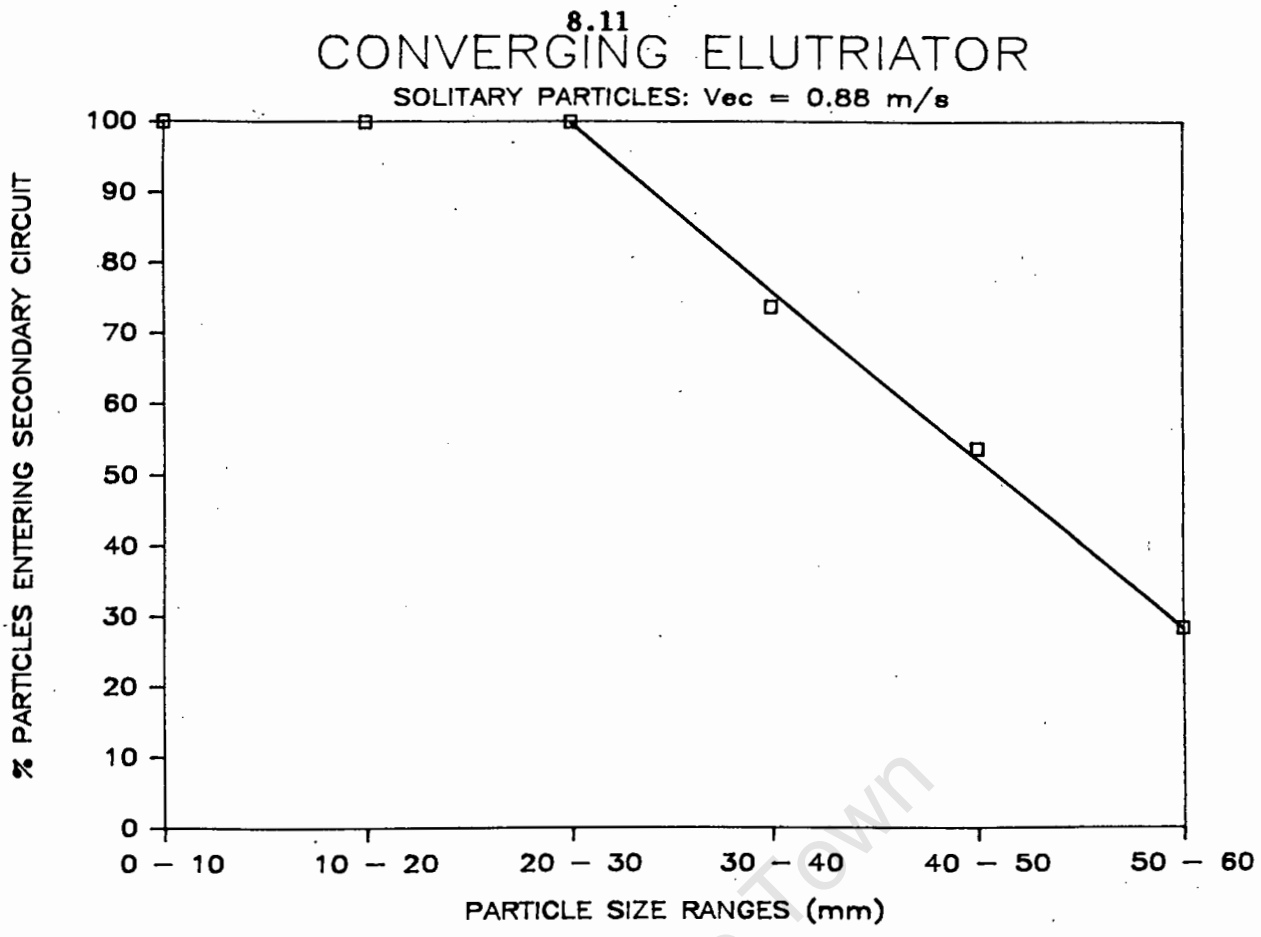

Figure 8.1 : % Particles entering secondary circuit vs particle size ranges

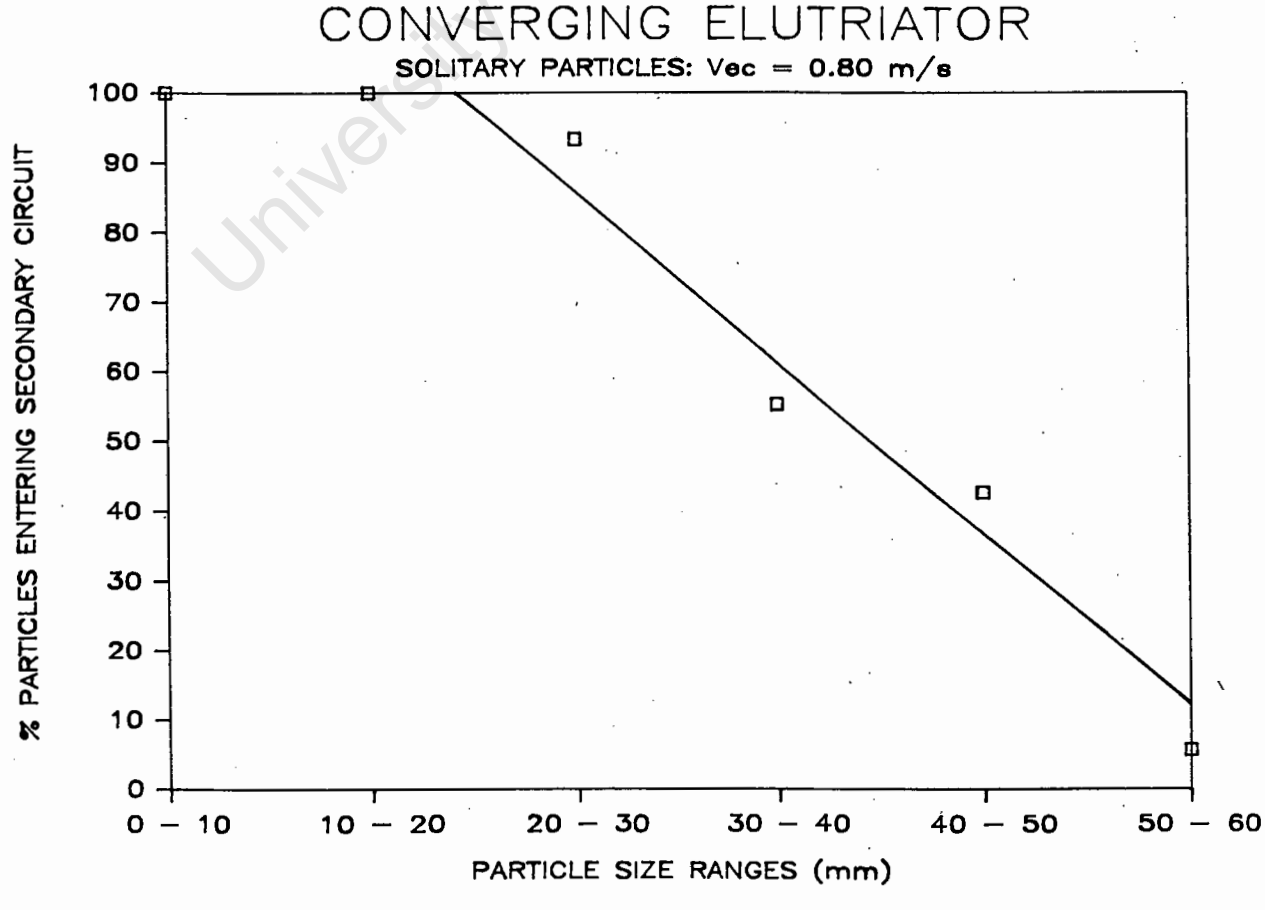

Figure 8.2 : % Particles entering secondary circuit vs particle size ranges

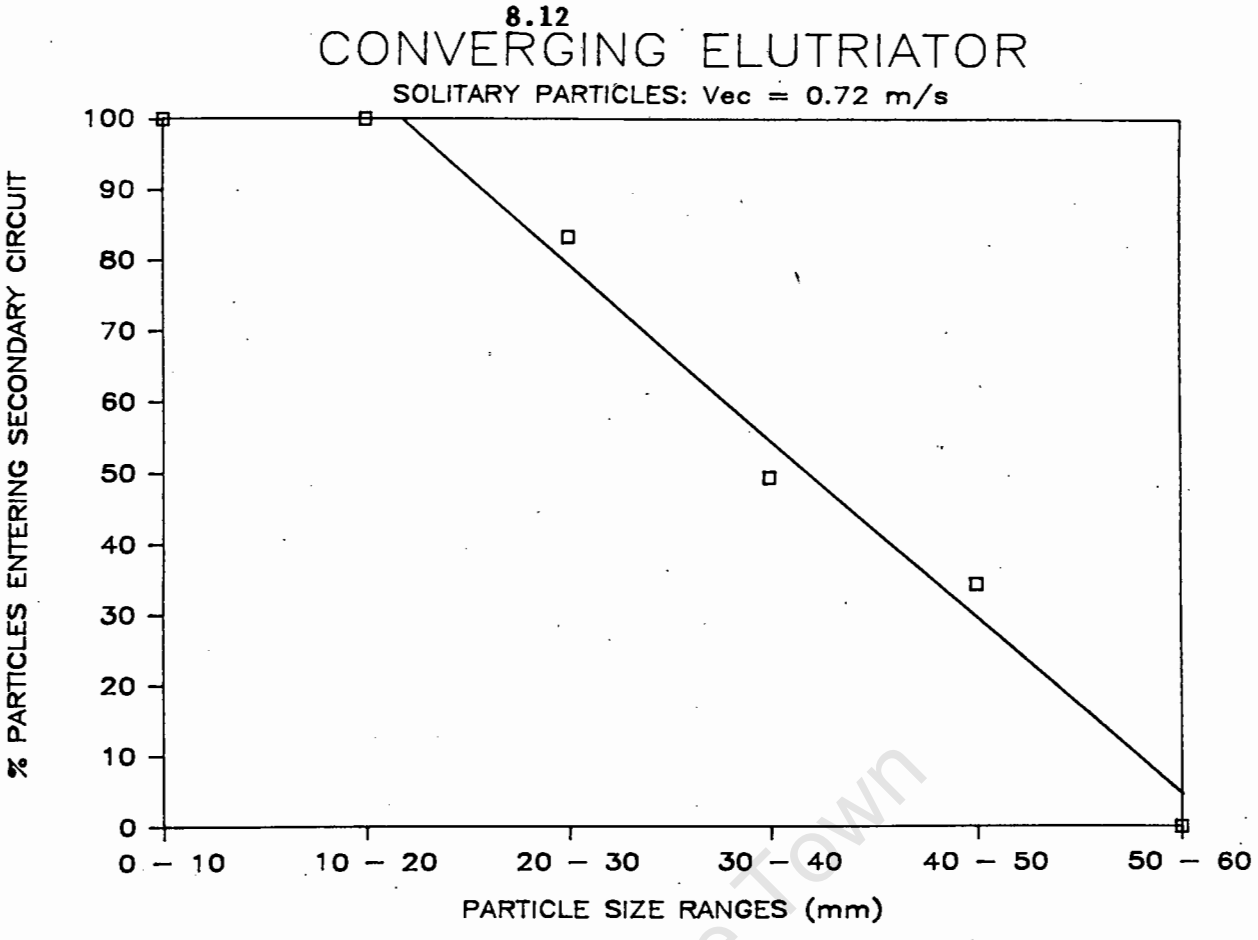

Figure 8.3 : % Particles entering secondary circuit vs particle size ranges

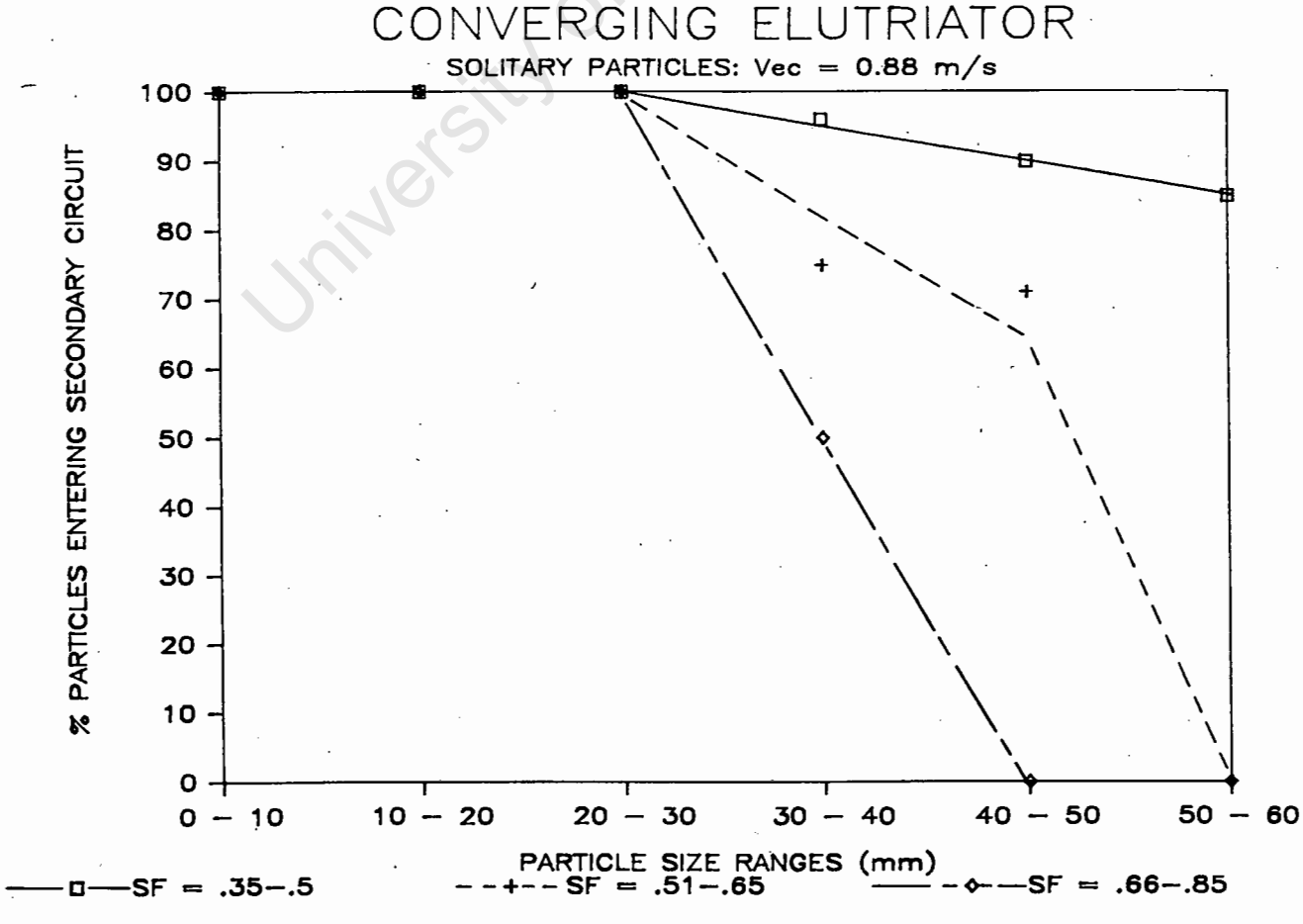

Figure 8.4 : % Particles entering secondary circuit vs particle size ranges for variable particle shape

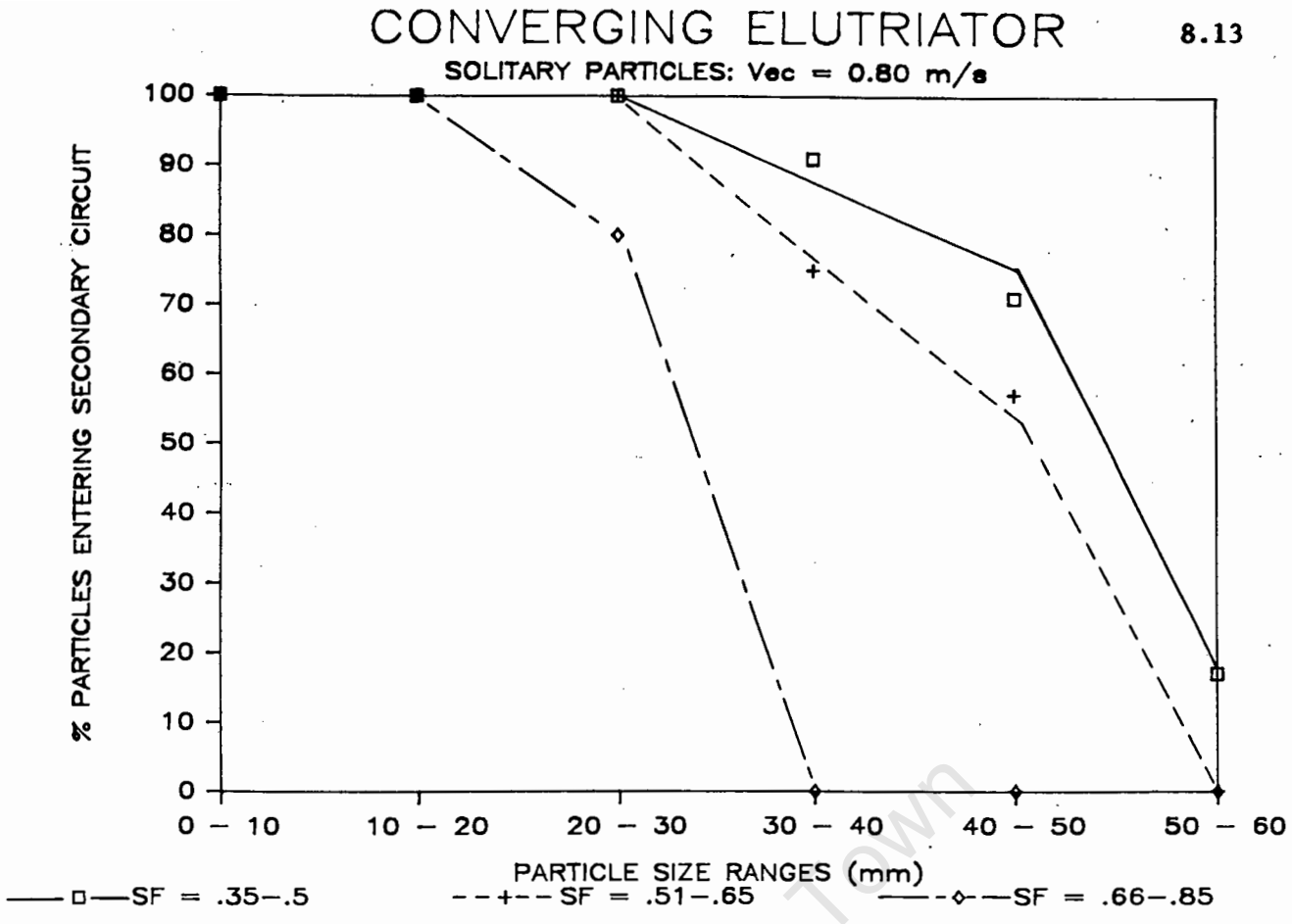

Figure 8.5 : % Particles entering secondary circuit vs particle size ranges for variable particle shape

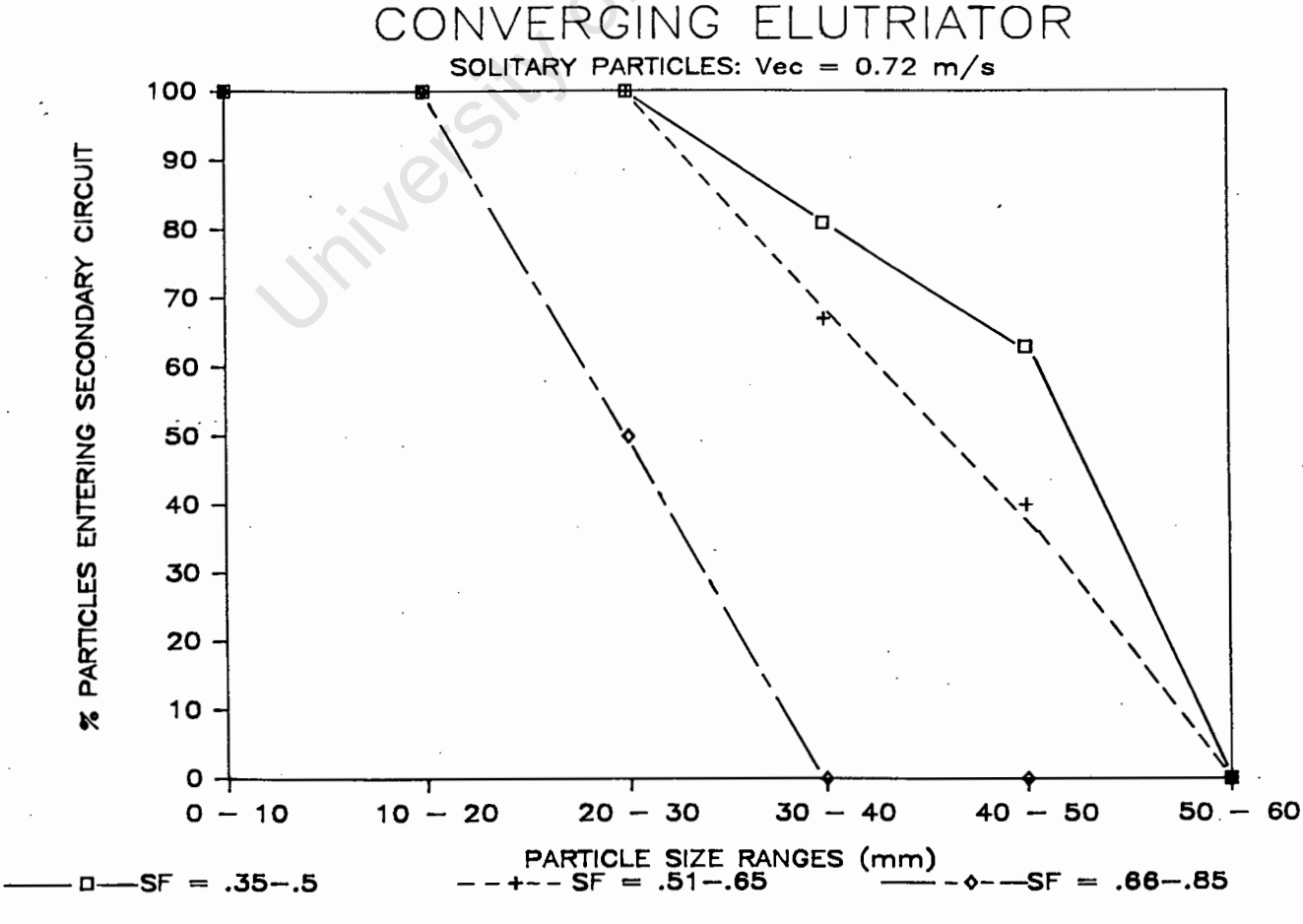

Figure 8.6 : % Particles entering secondary circuit vs particle size ranges for variable particle shape

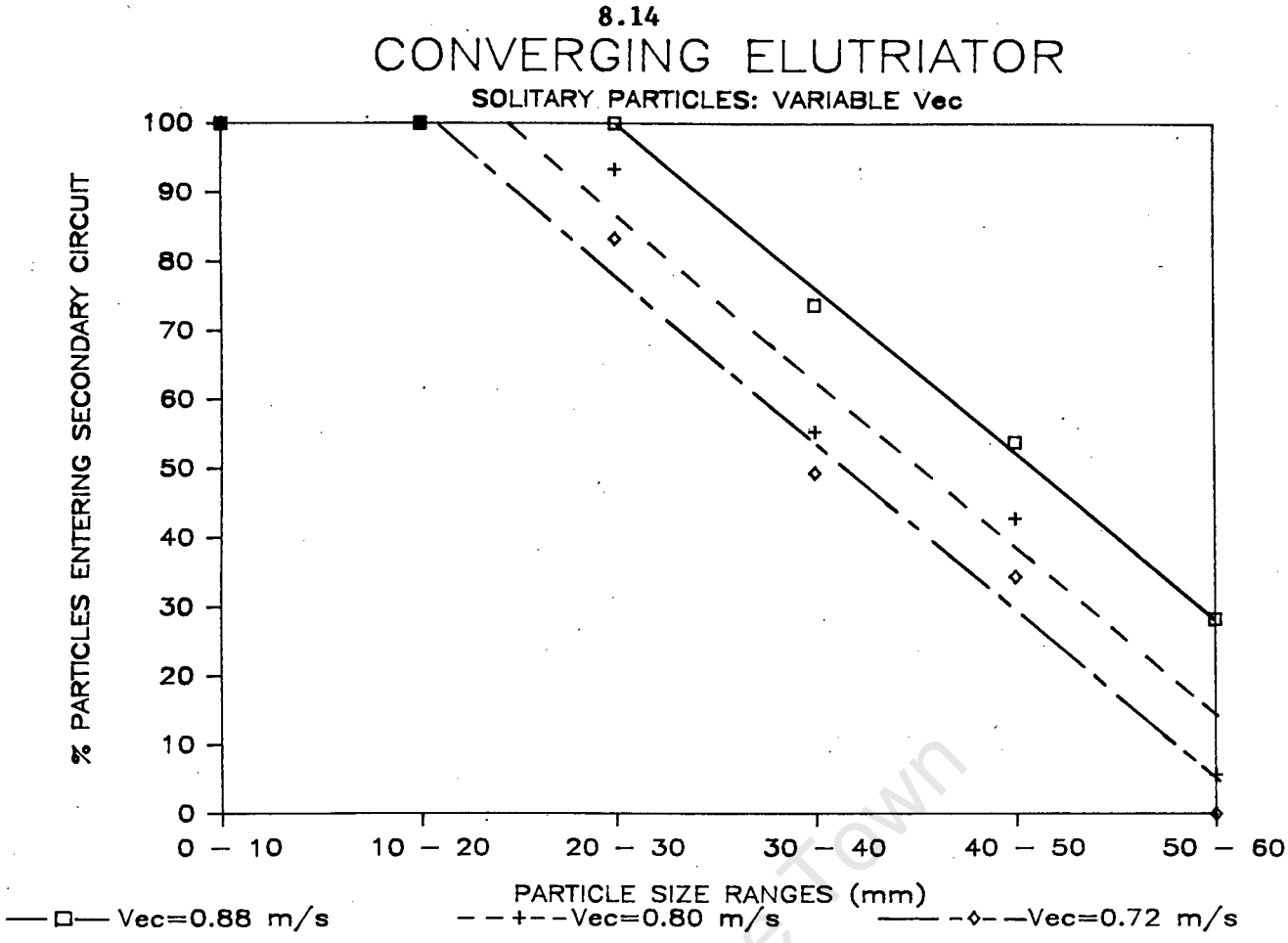

Figure 8.7 : % Particles entering secondary circuit vs particle size ranges for variable elutriation column velocity

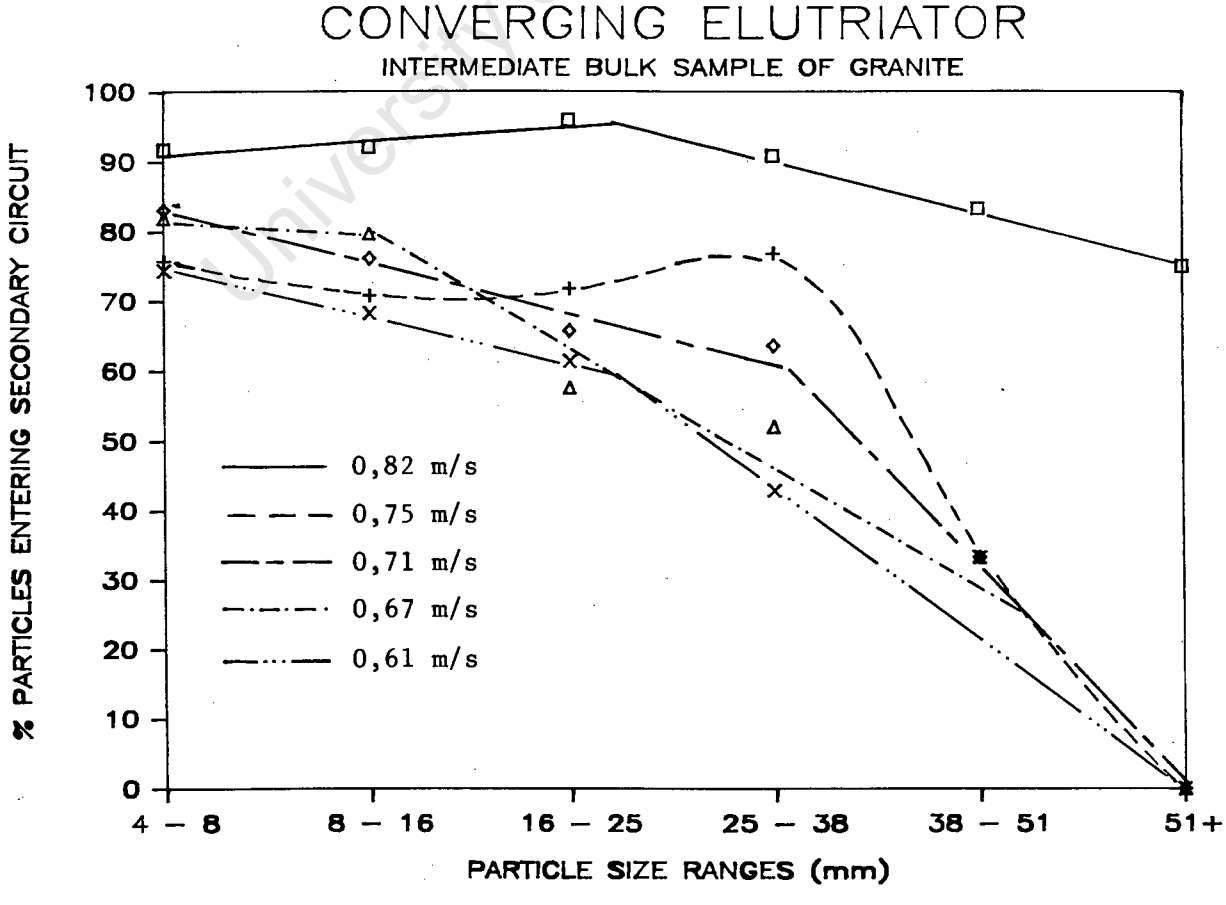

Figure 8.8 : % Particles entering secondary circuit vs particle size ranges for variable elutriation column velocity

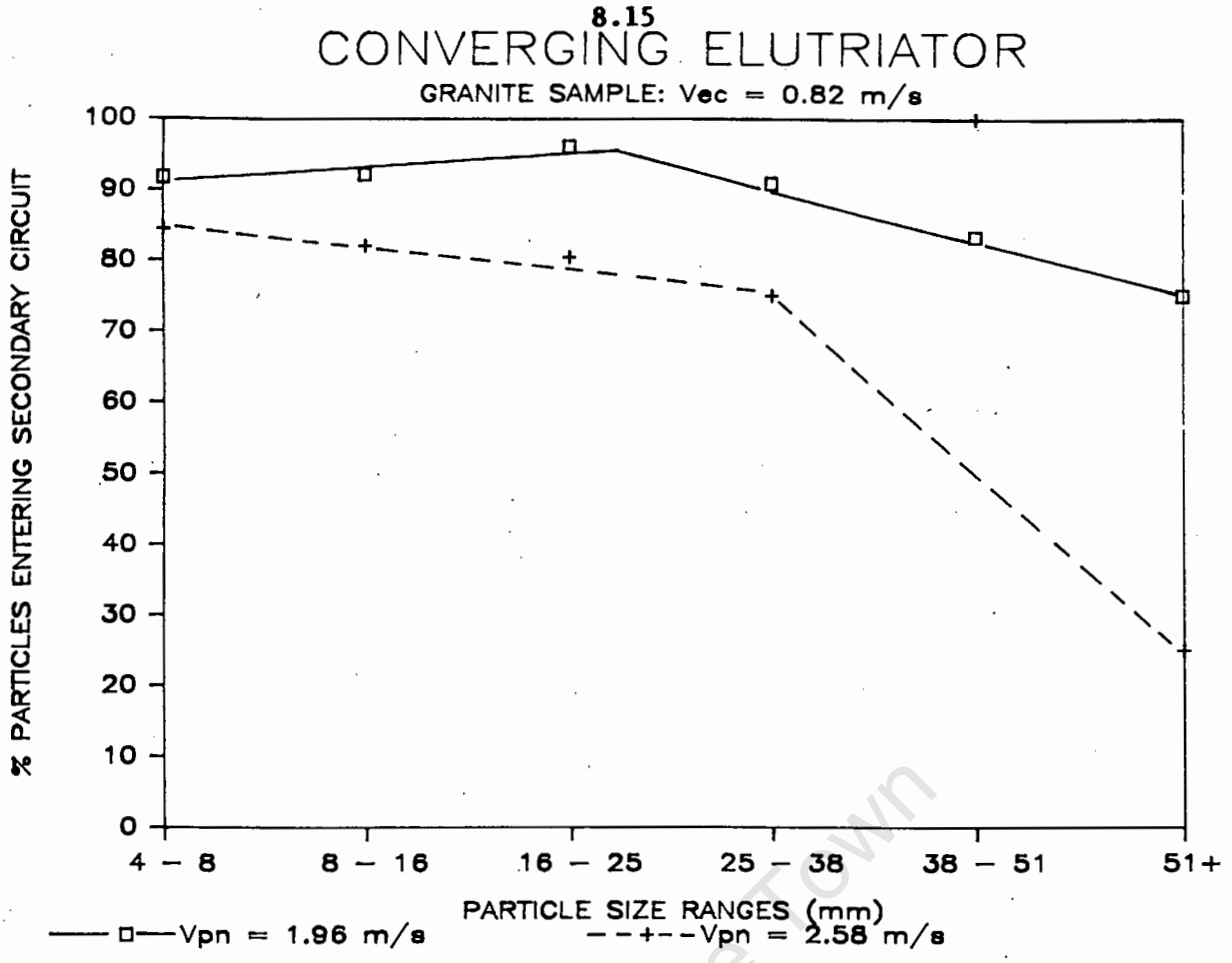

Figure 8.9 : % Particles entering secondary circuit vs particle size ranges for variable primary outlet velocity

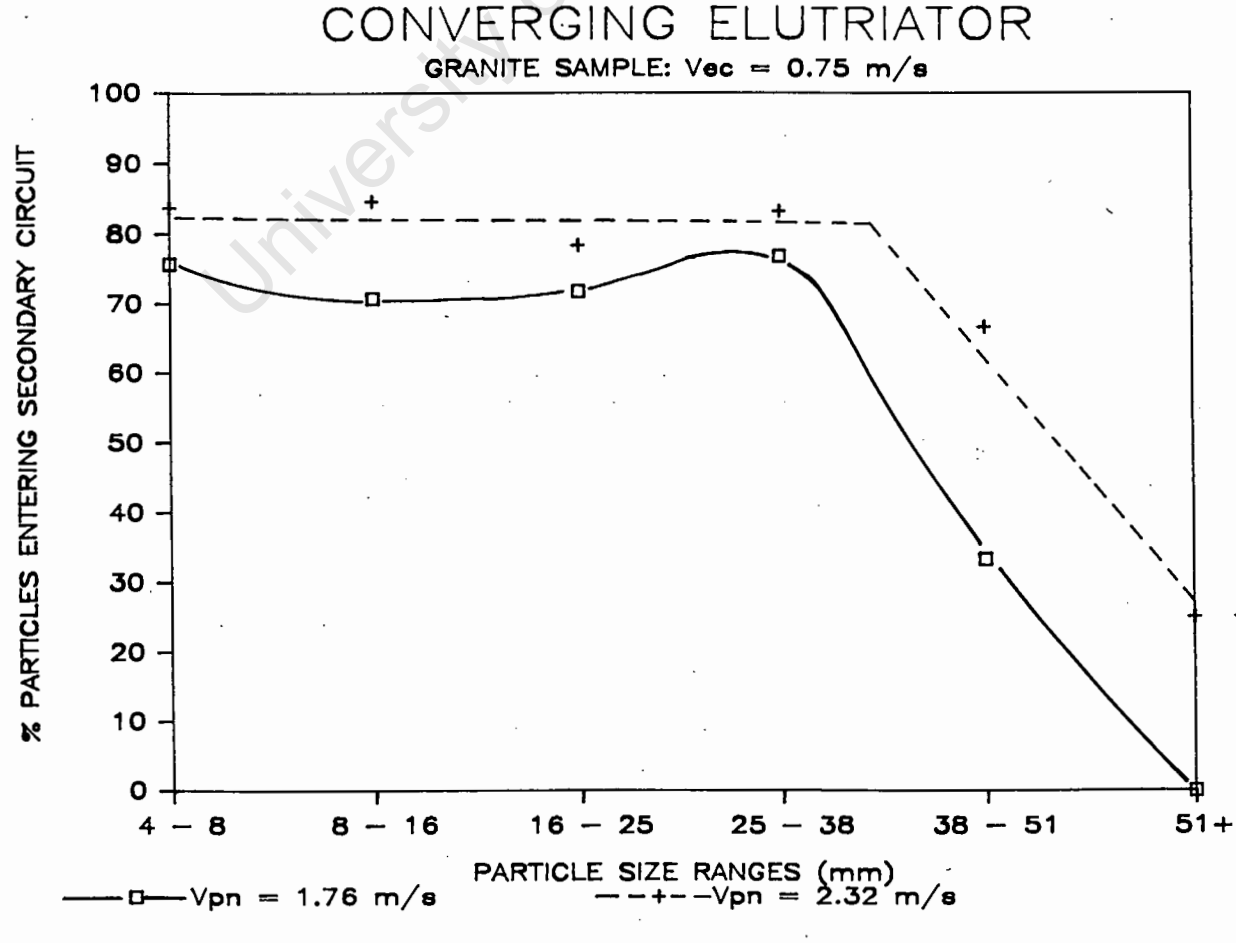

Figure 8.10 : % Particles entering secondary circuit vs particle size ranges for variable primary outlet velocity

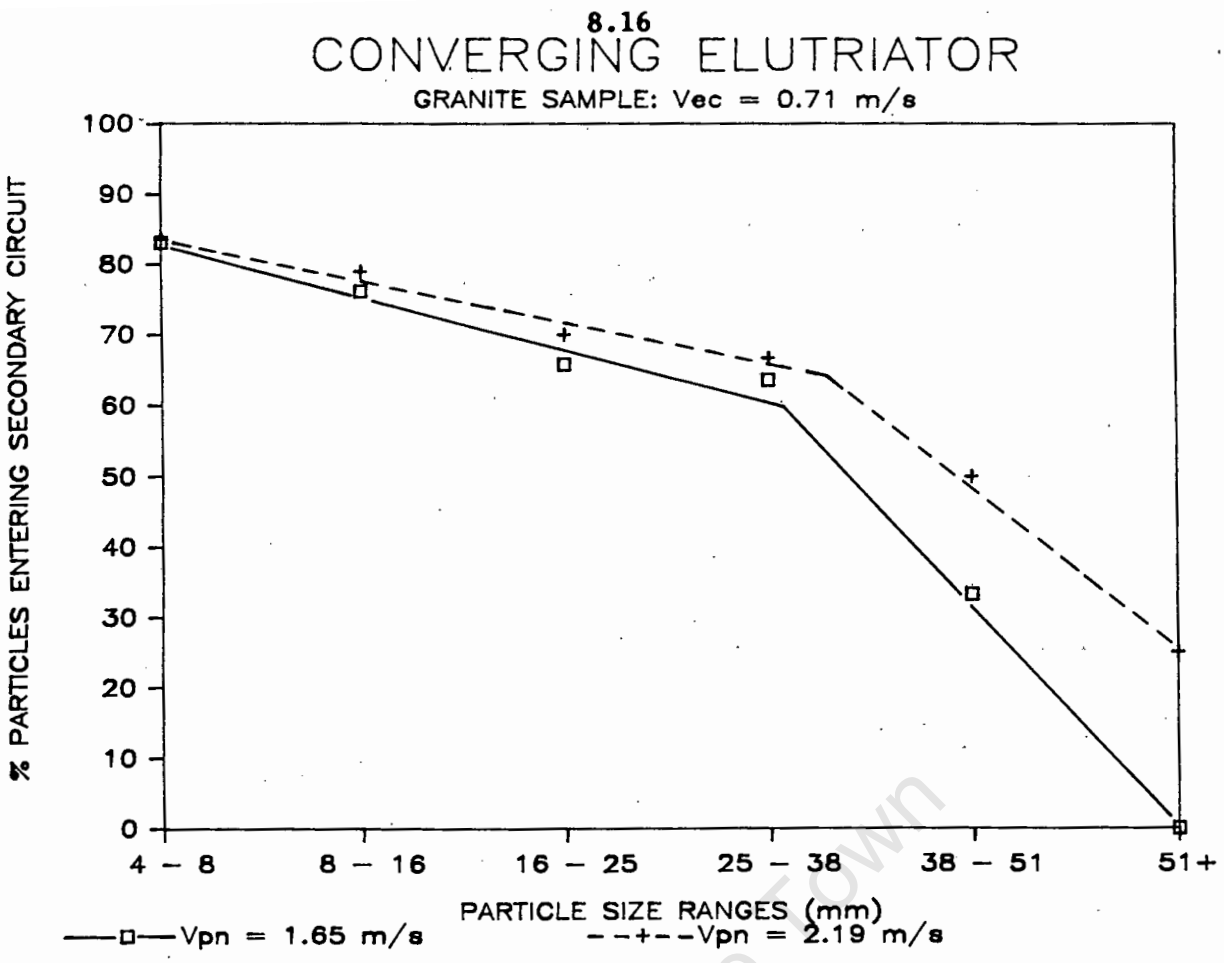

Figure 8.11 : % Particles entering secondary circuit vs particle size ranges for variable primary outlet velocity

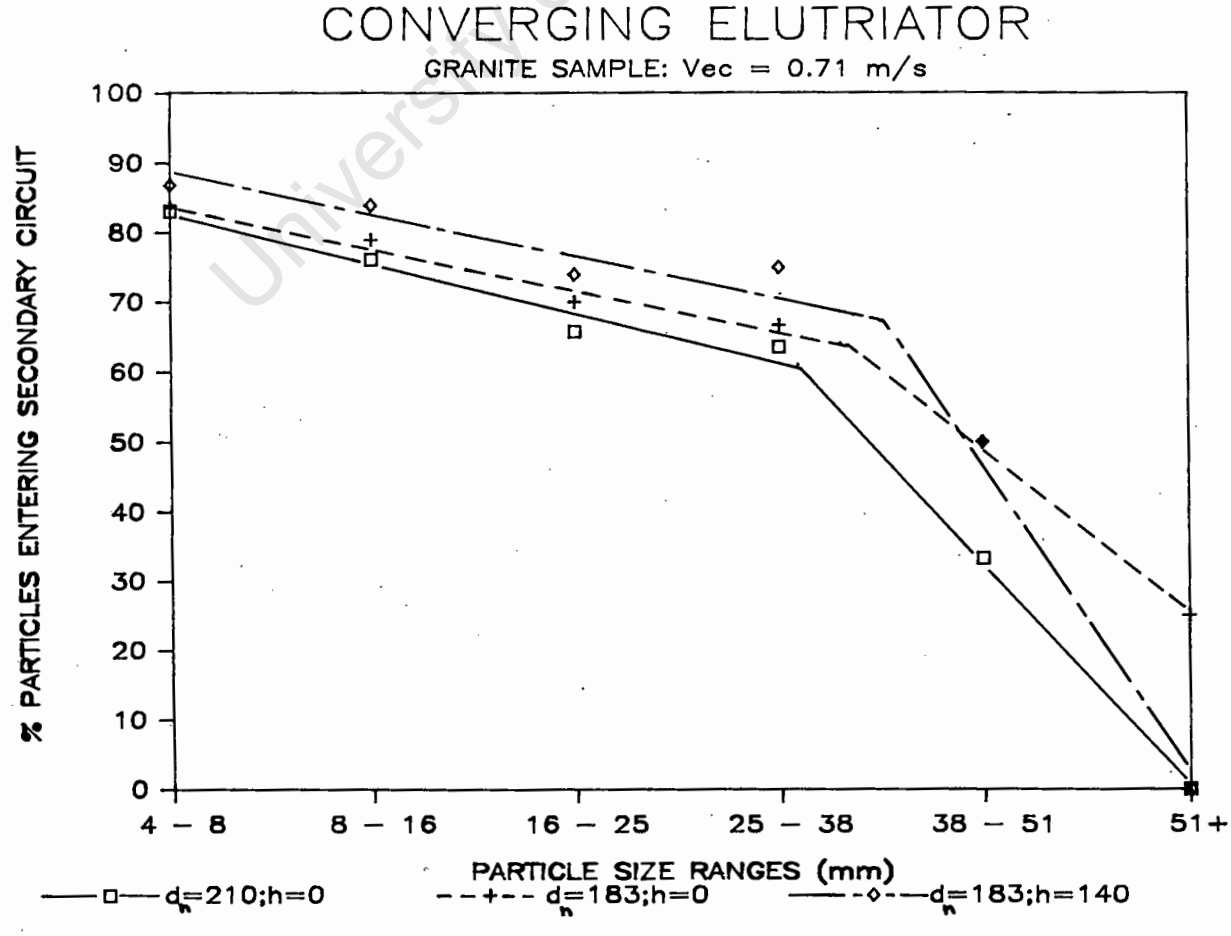

Figure 8.12 : % Particles entering secondary circuit vs particle size ranges for variable elutriation geometry

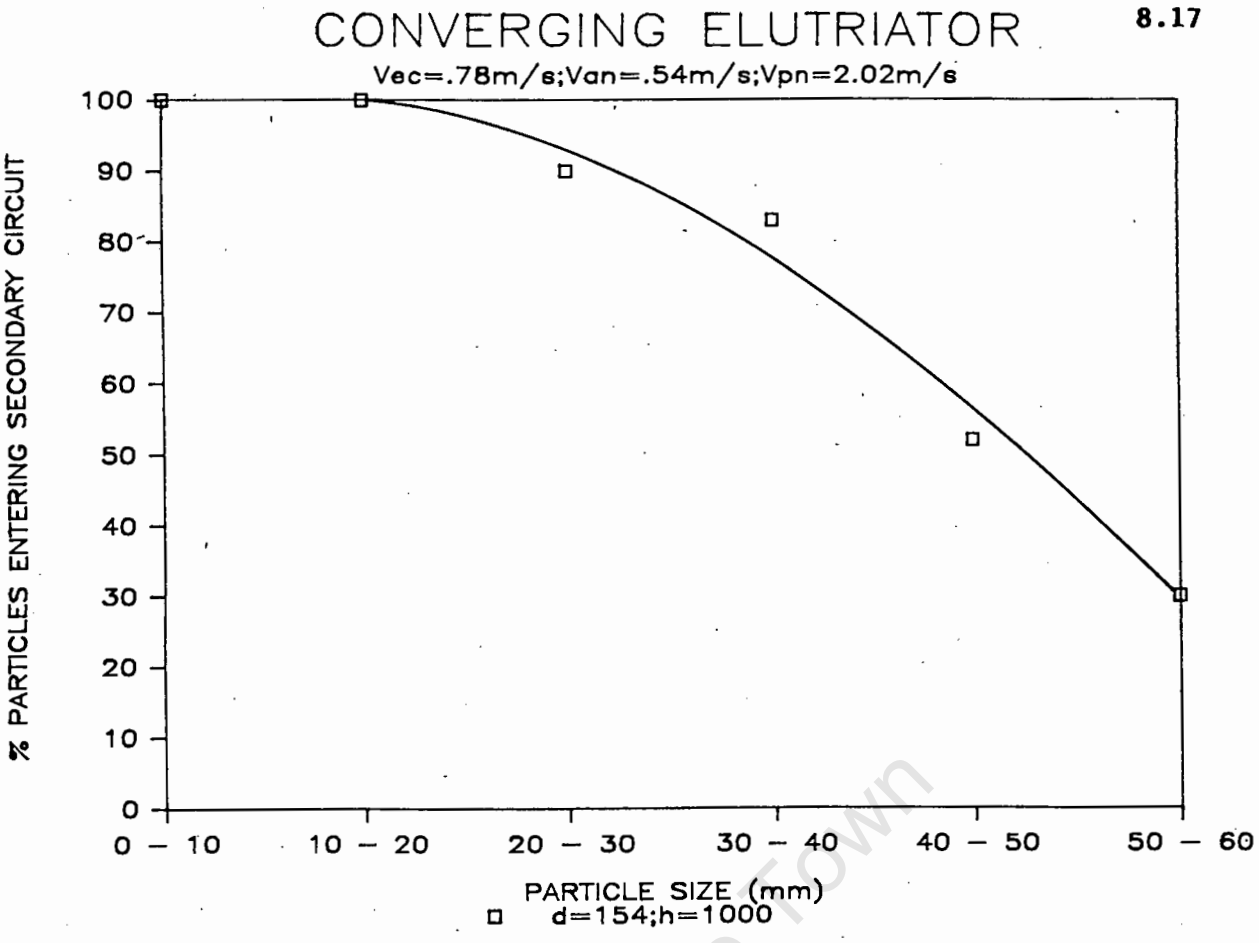

Figure 8.13 : % Particles entering secondary circuit vs particle size for variable elutriation geometry

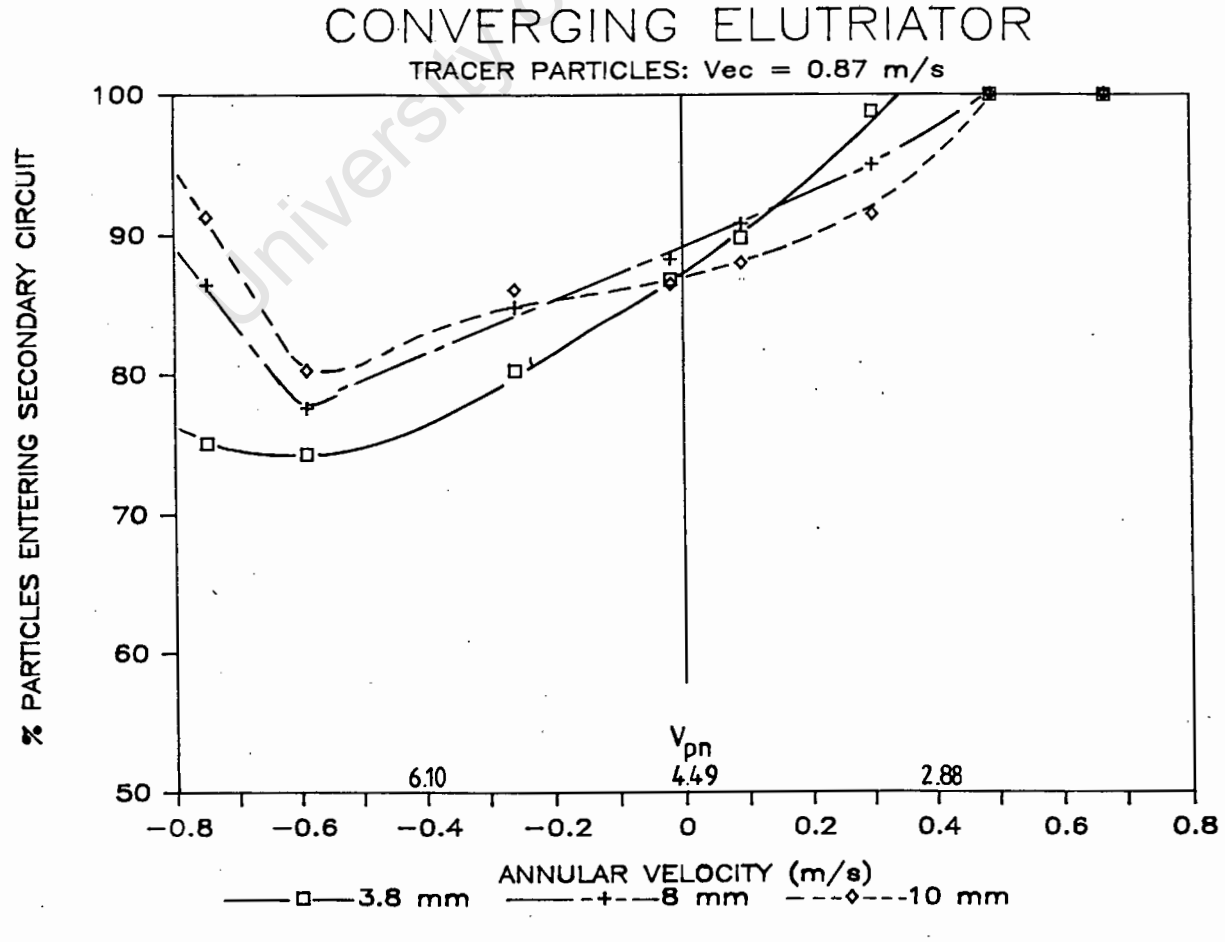

Figure 8.14 : % Particles entering secondary circuit vs annular velocity

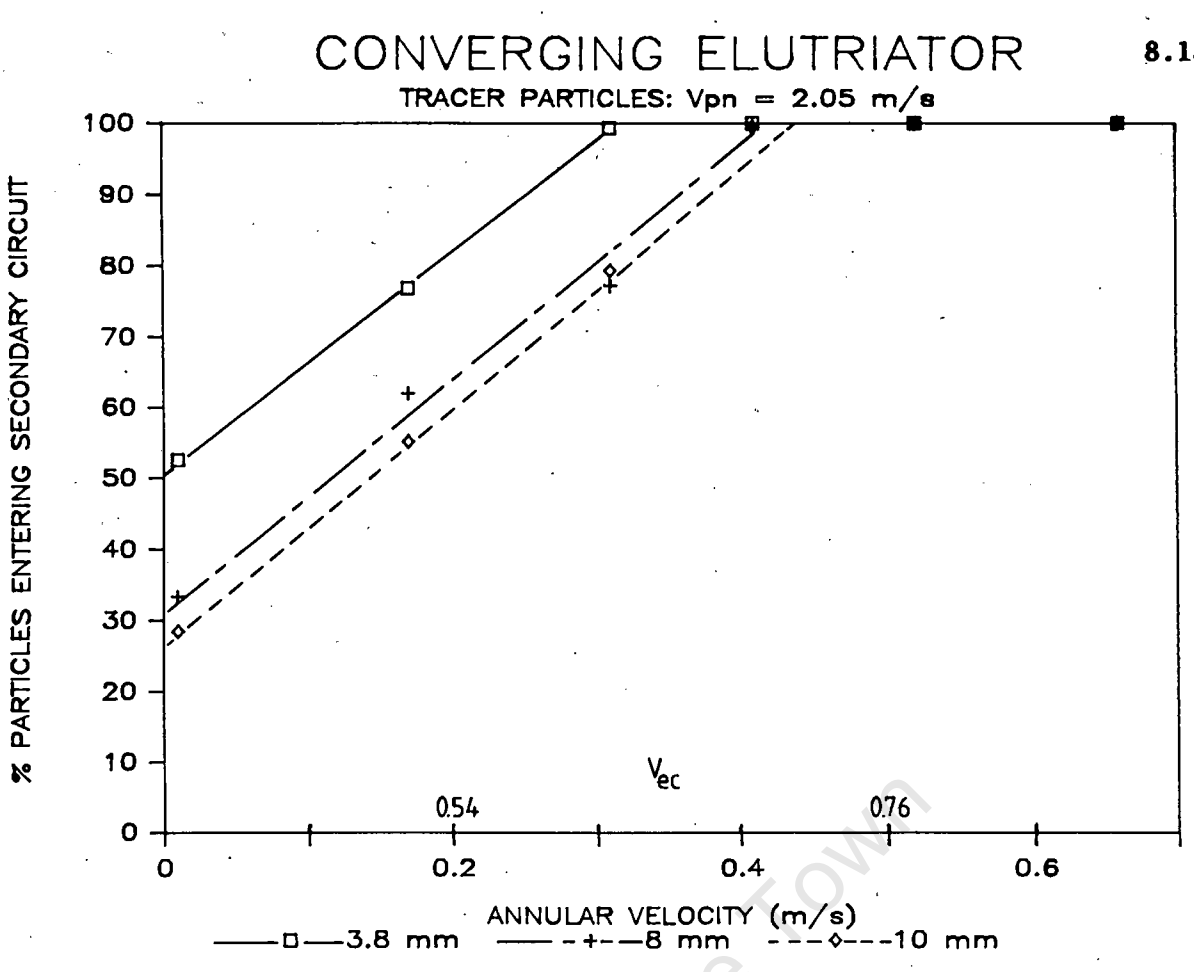

Figure 8.15 : % Particles entering secondary circuit vs annular velocity for variable annular velocity

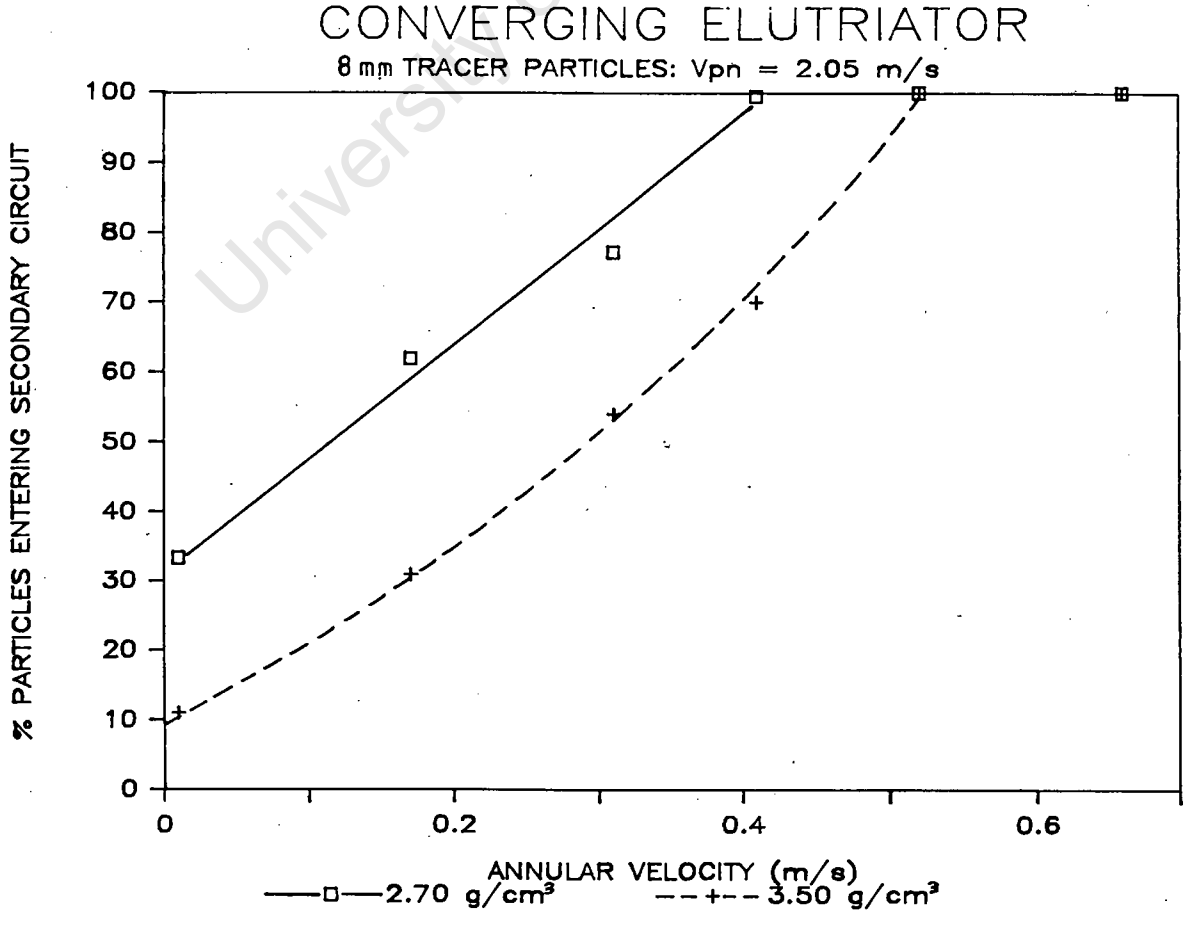

Figure 8.16 : % Particles entering secondary circuit vs annular velocity for variable particle density

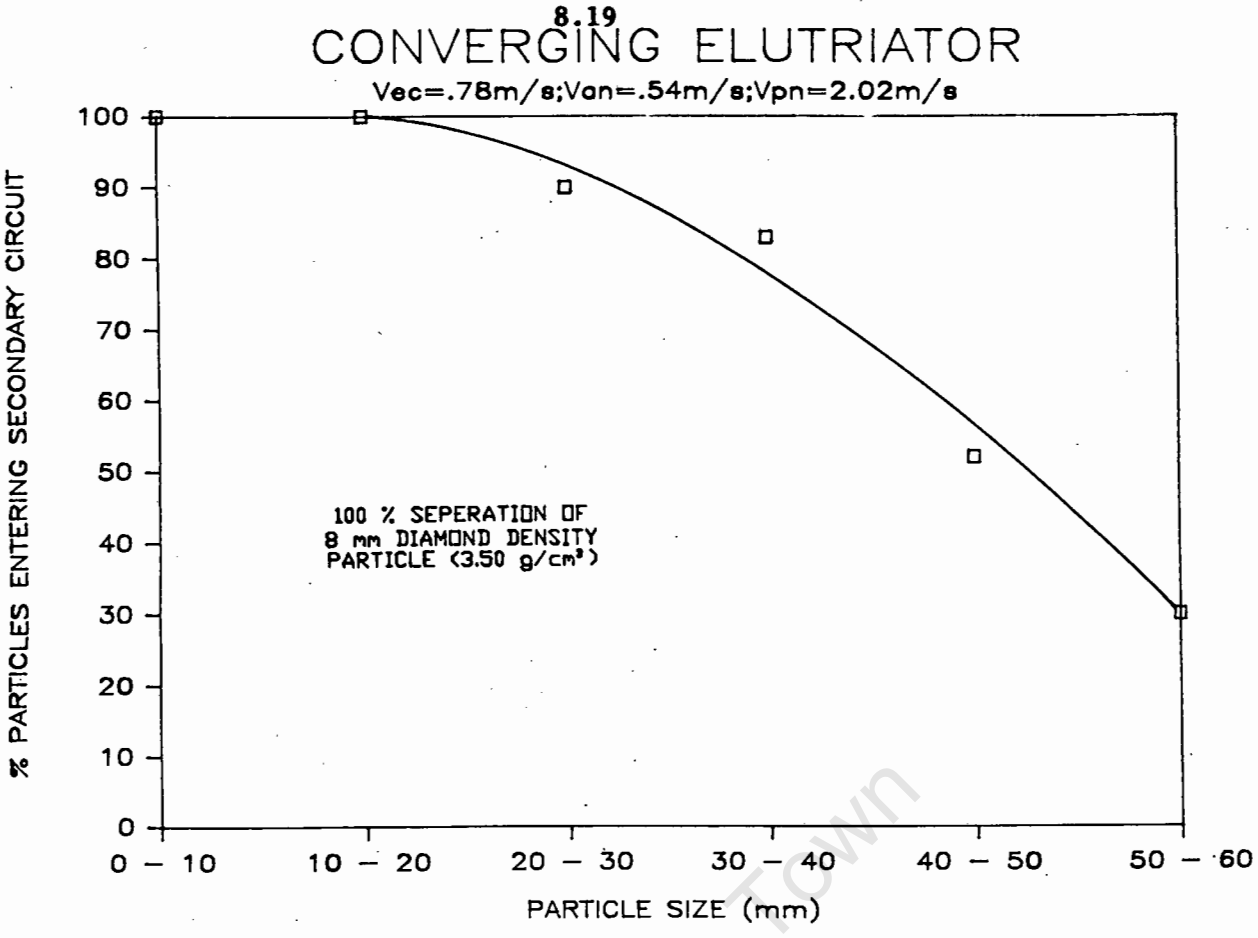

Figure 8.17 : % Particles entering secondary circuit vs particle size for general separation efficiency

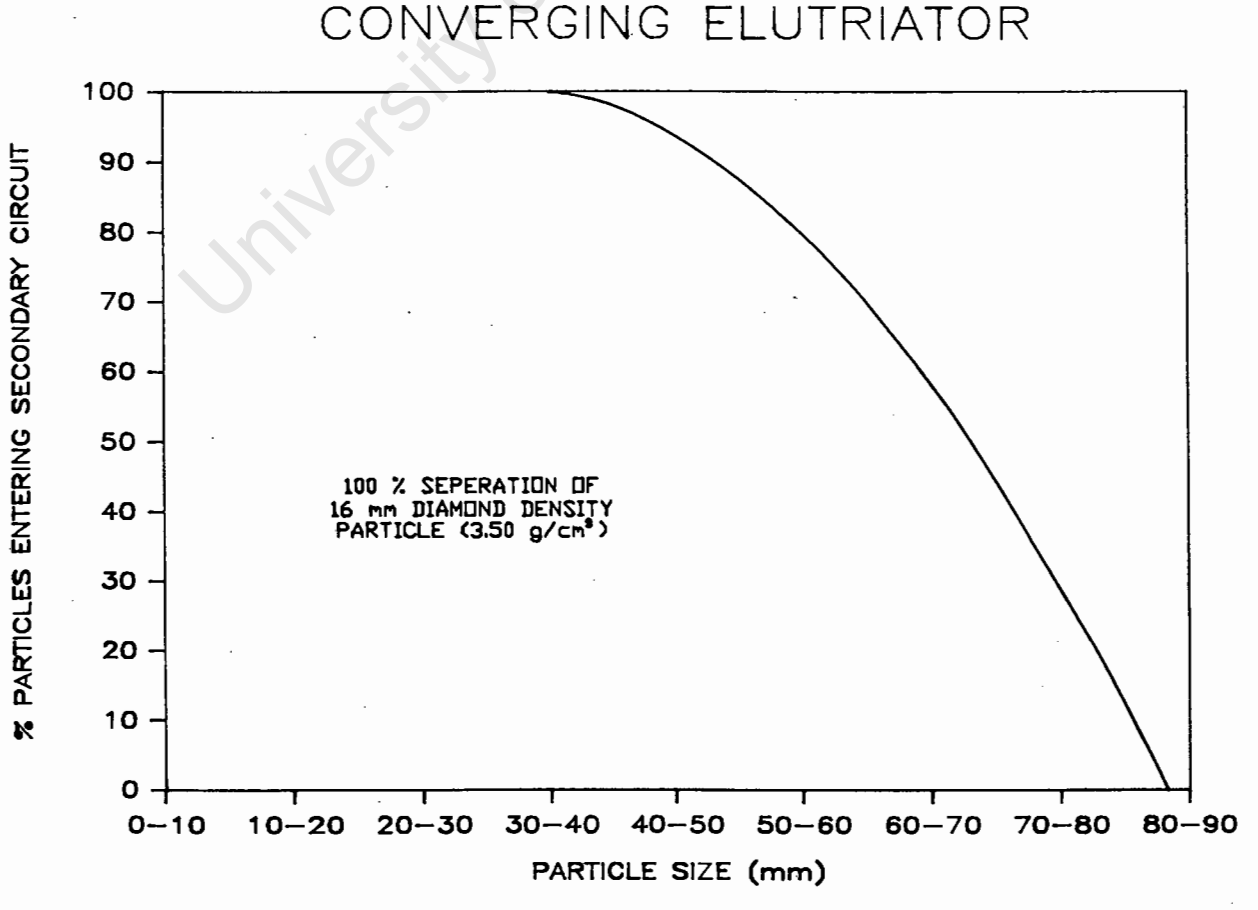

Figure 8.18 : % Particles entering secondary circuit vs particle size for estimated separation efficiency

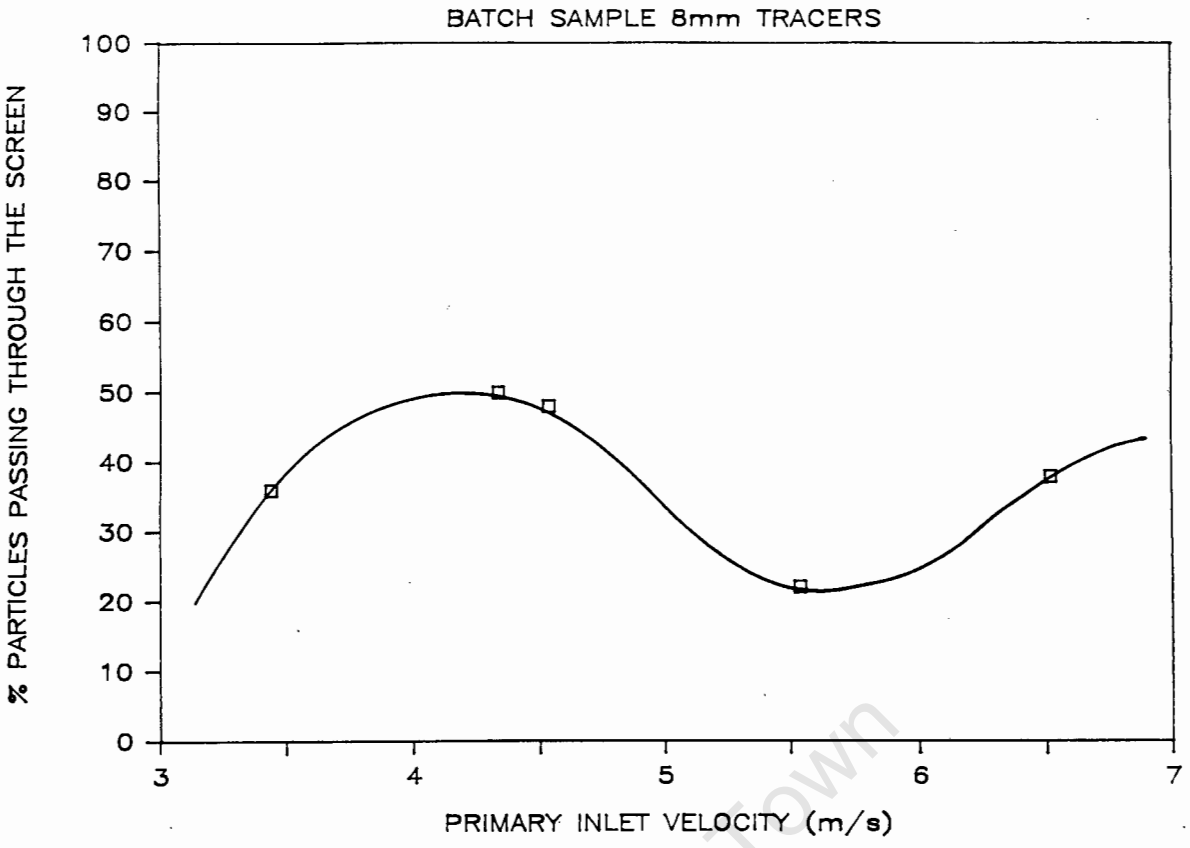

Figure 8.19 : Variable primary inlet velocity

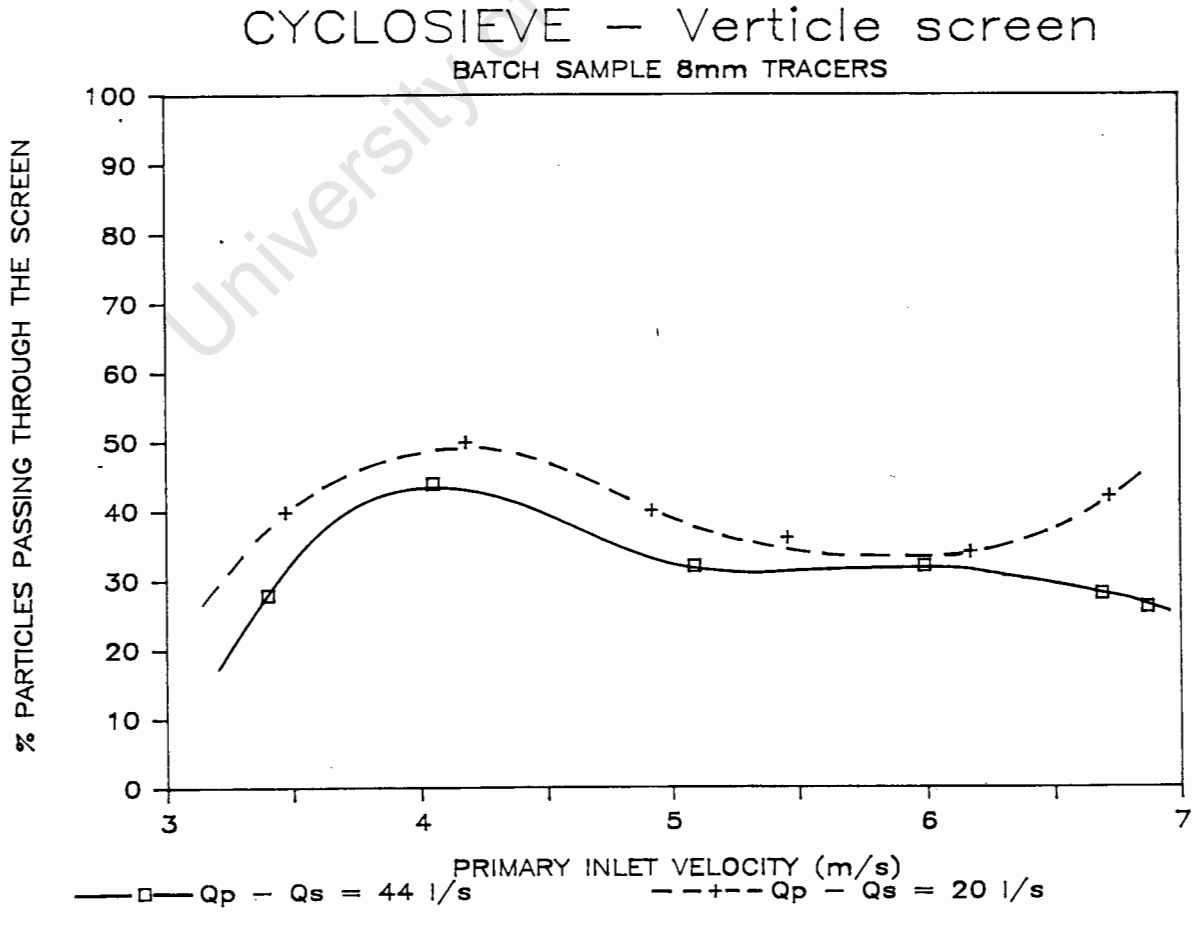

Figure 8.20 : Variable flow conditions

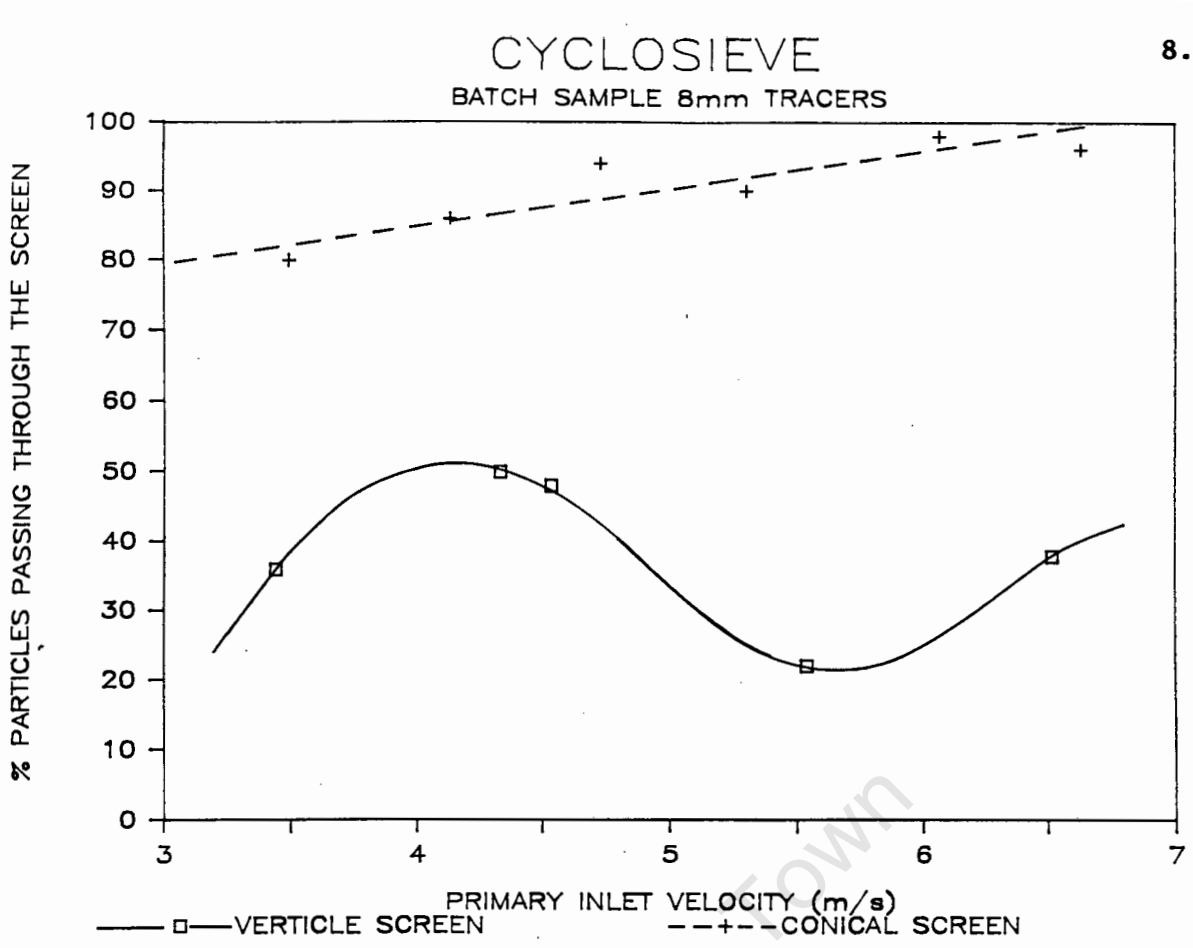

Figure 8.21 : Variable screen geometry

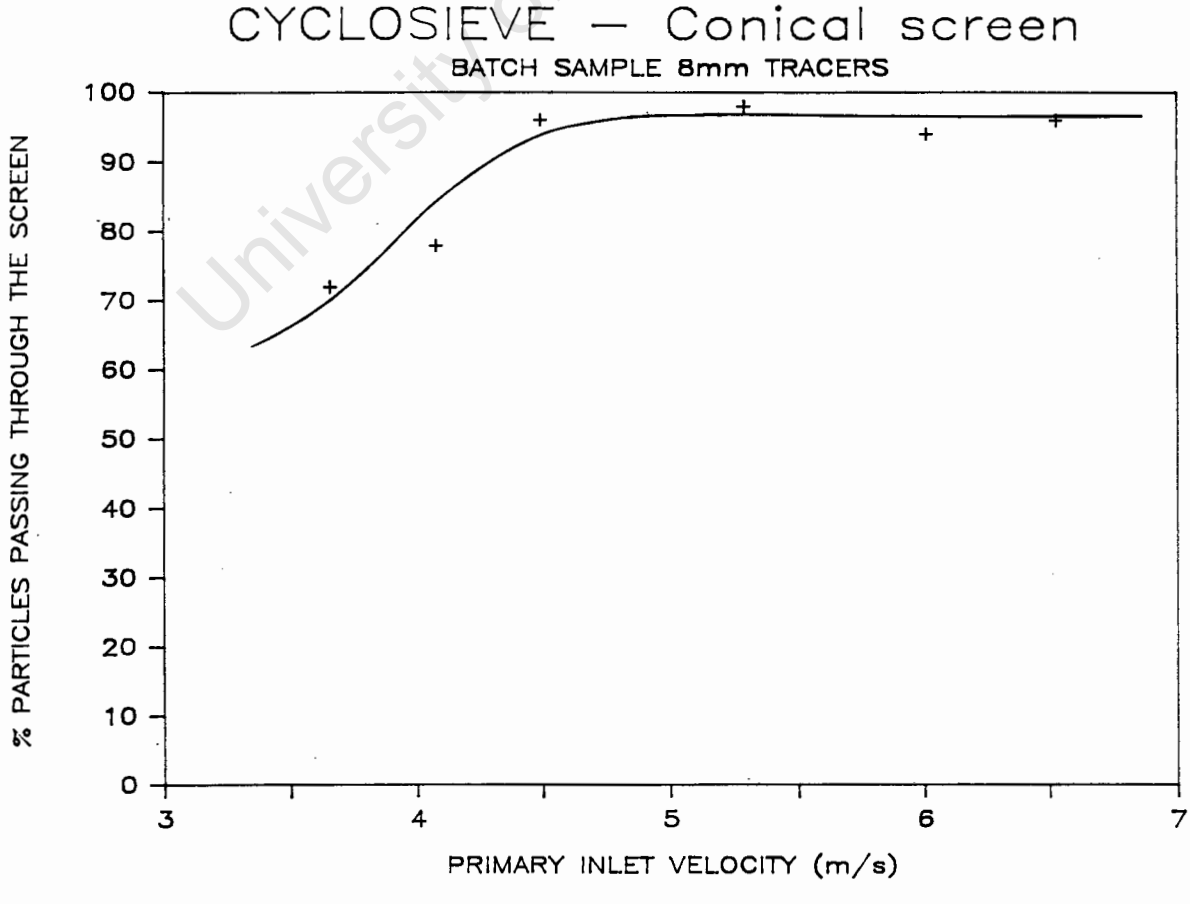

Figure 8.22 : Variable primary inlet velocity

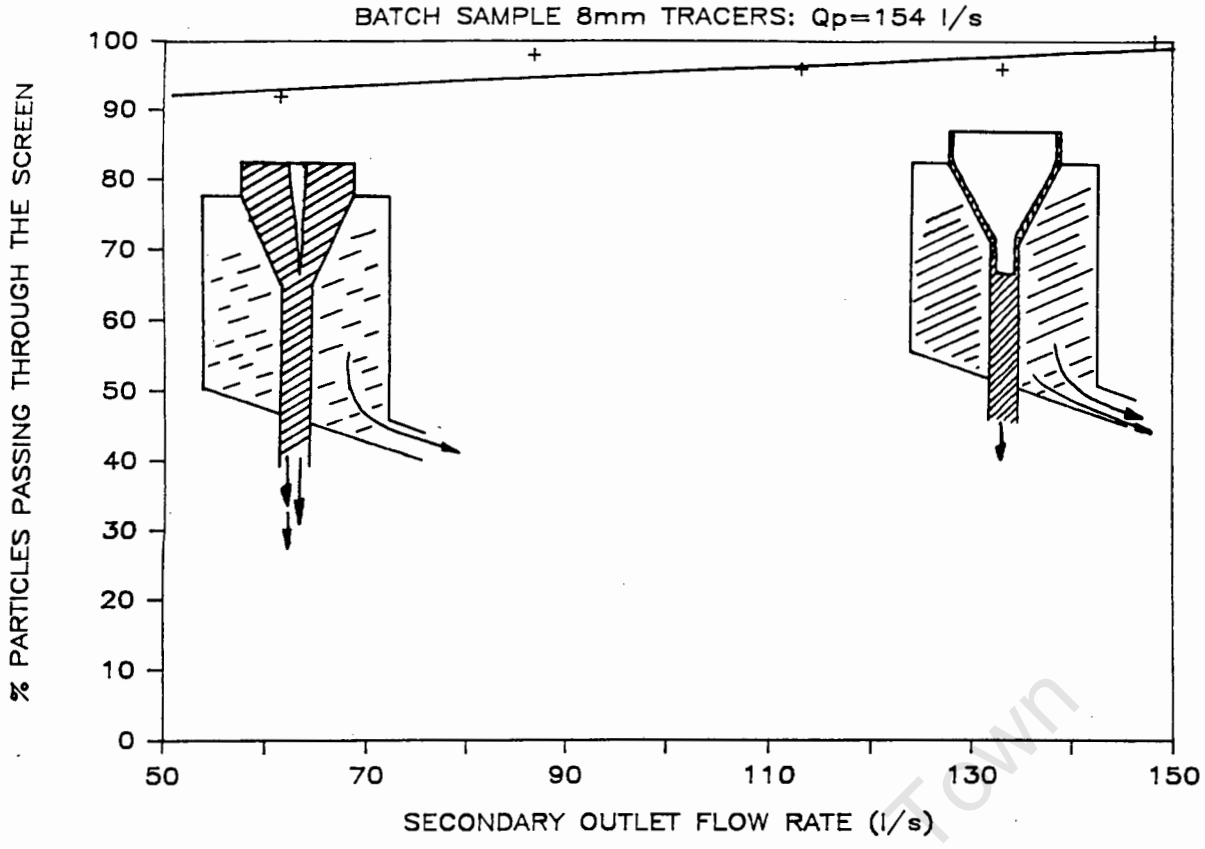

Figure 8.23 : Variable secondary flow

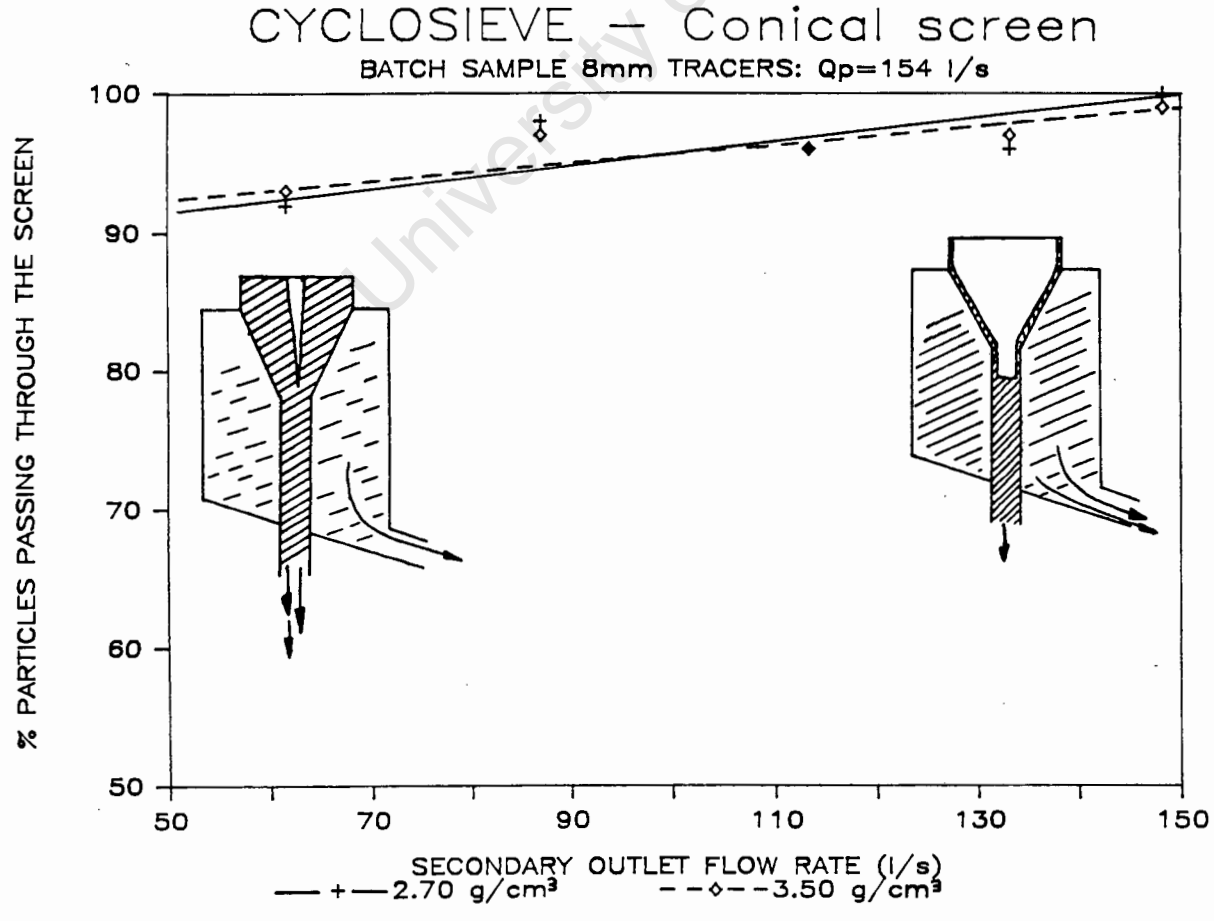

Figure 8.24 : Effect of particle density

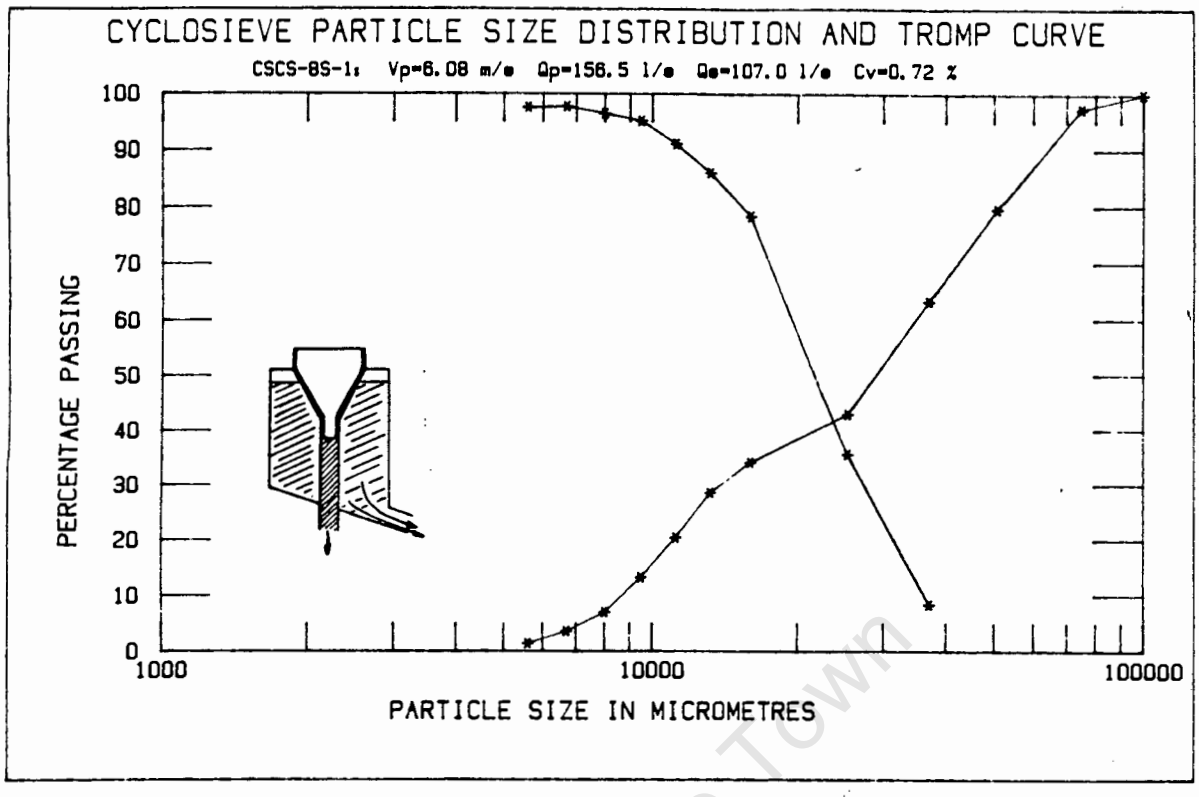

Figure 8.25 : Effect of particle size

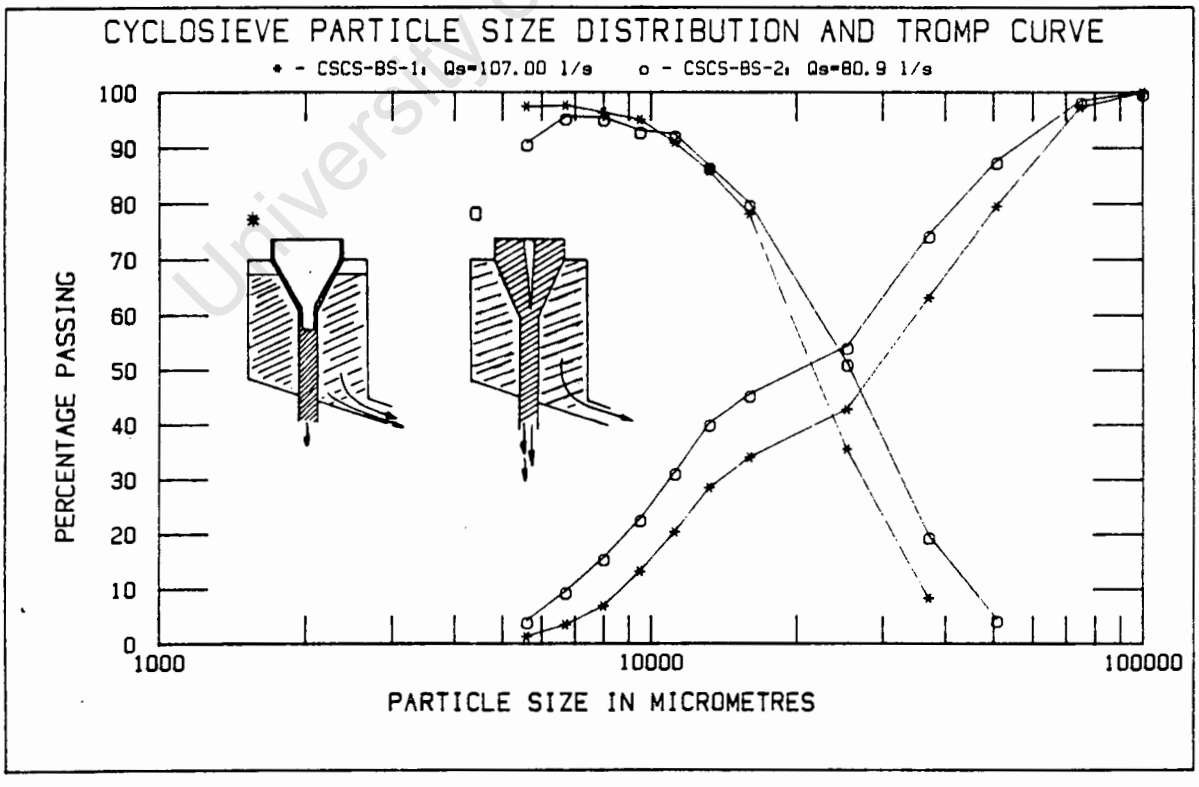

Figure 8.26 : Variable flow conditions

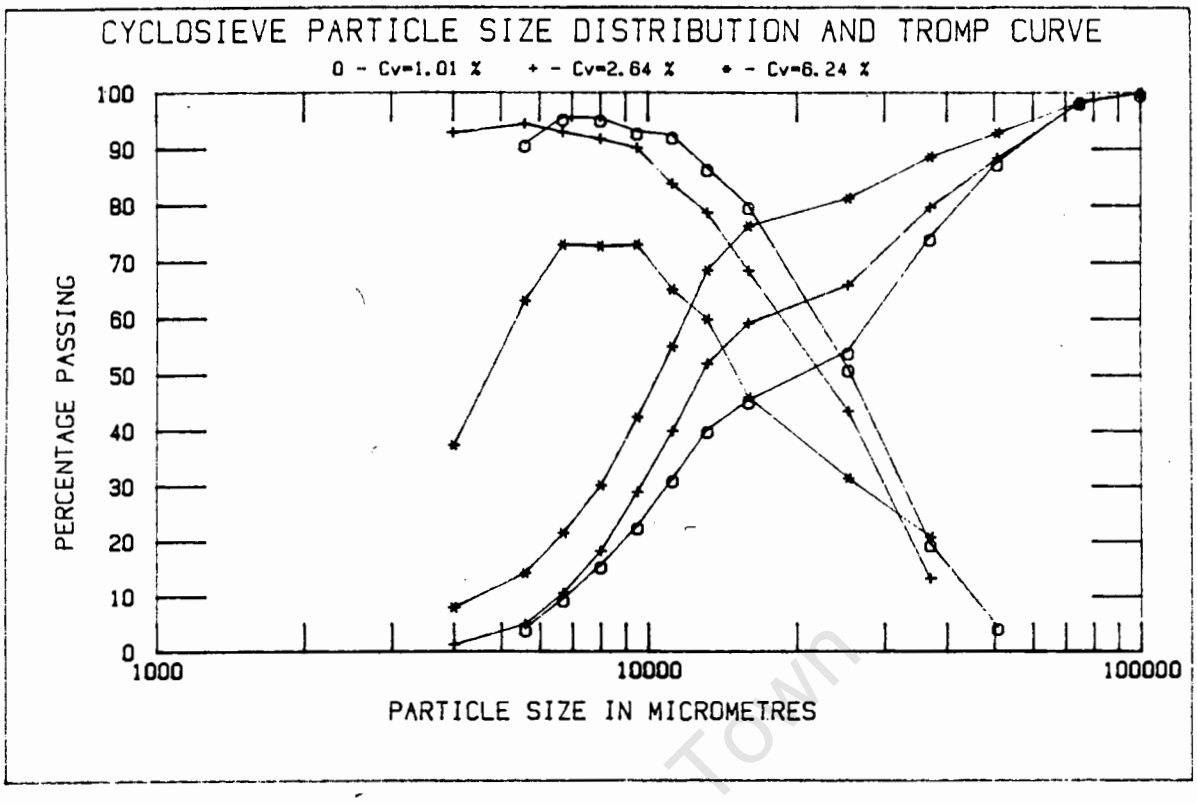

Figure 8.27 : Effect of variable concentration

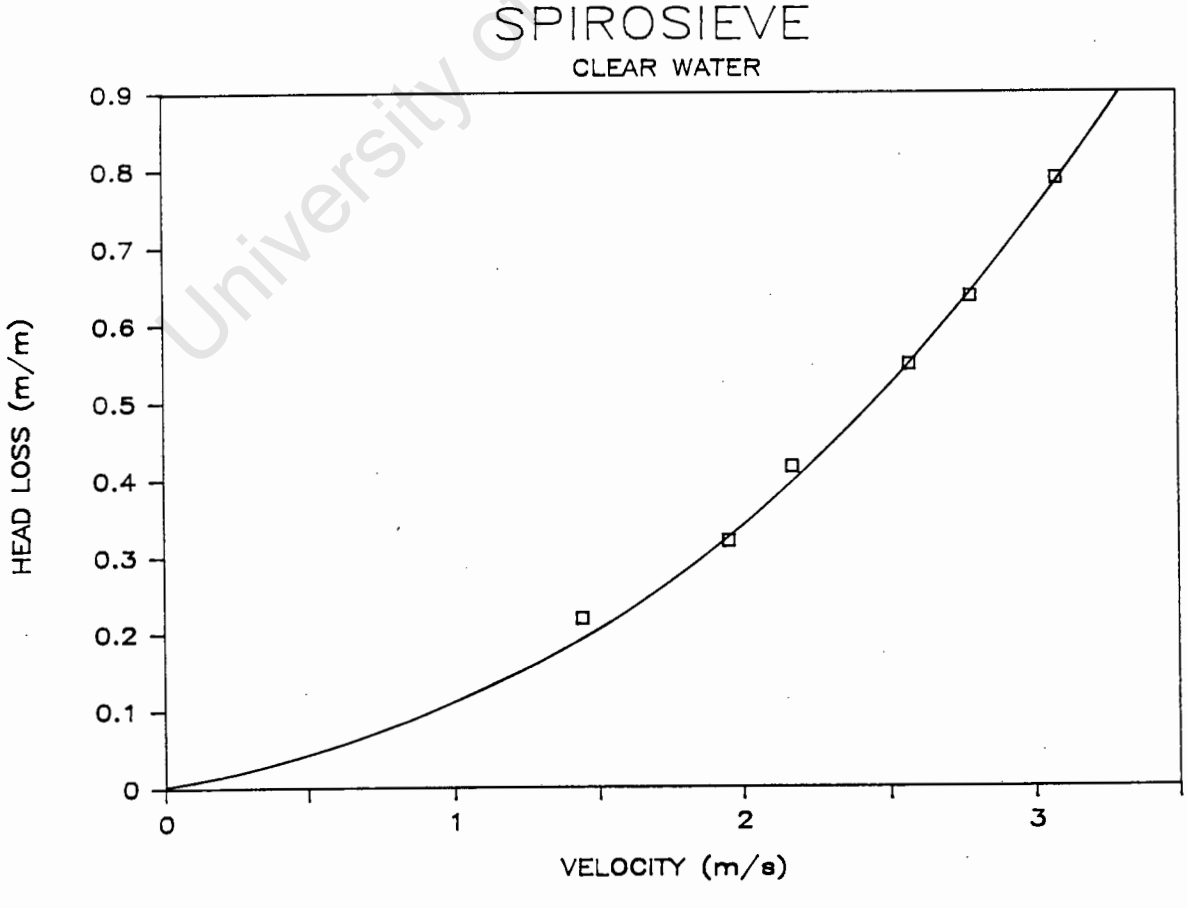

Figure 8.28 : Head loss across spirosieve

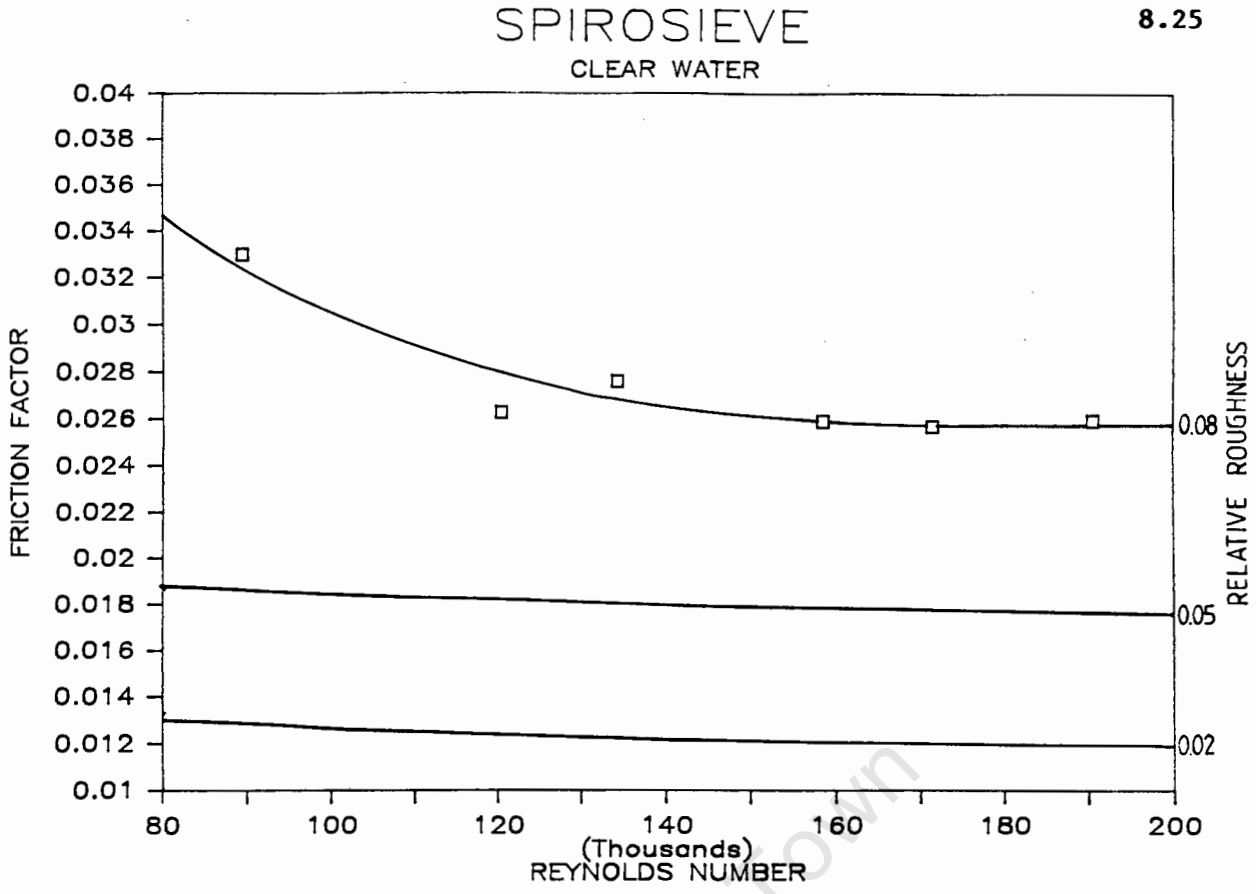

Figure 8.29 : Friction factor vs. Reynolds number

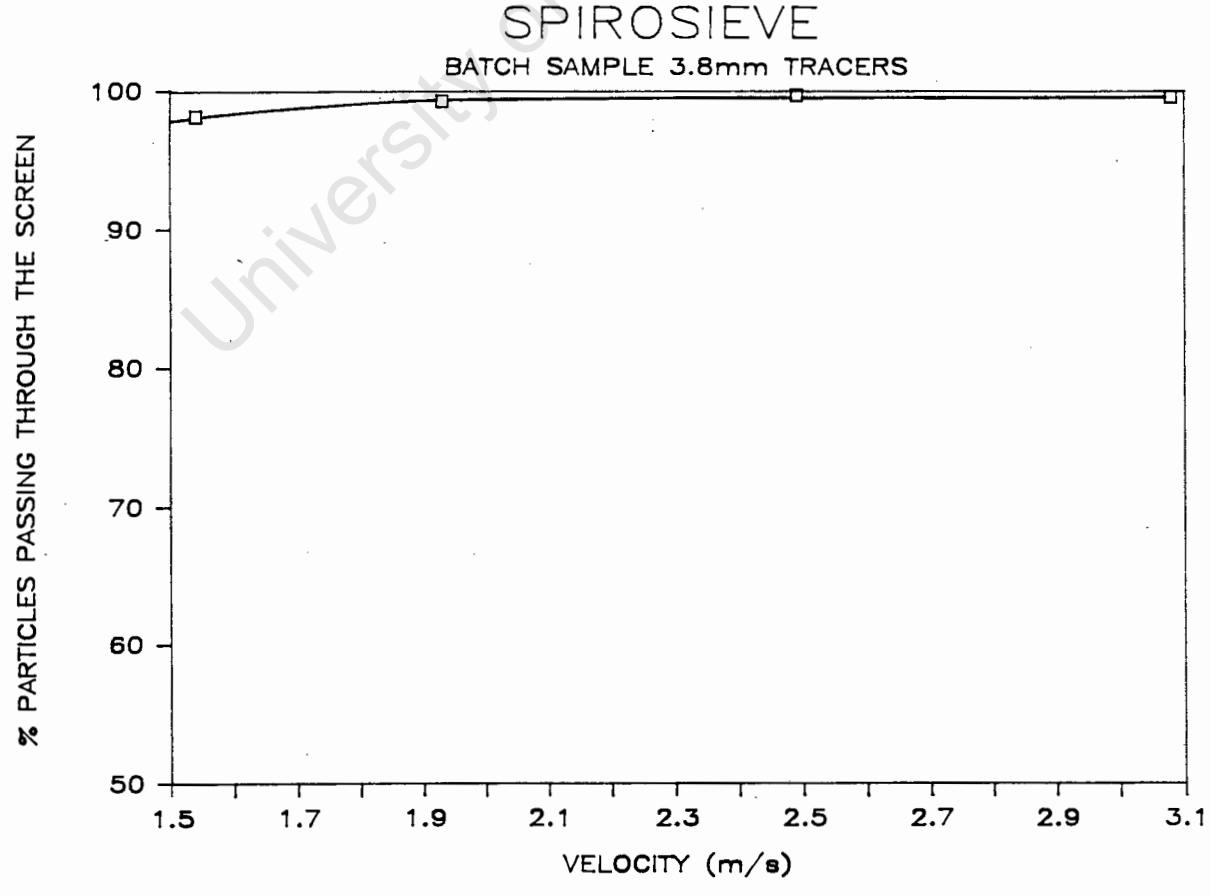

Figure 8.30 : Effect of variable velocity

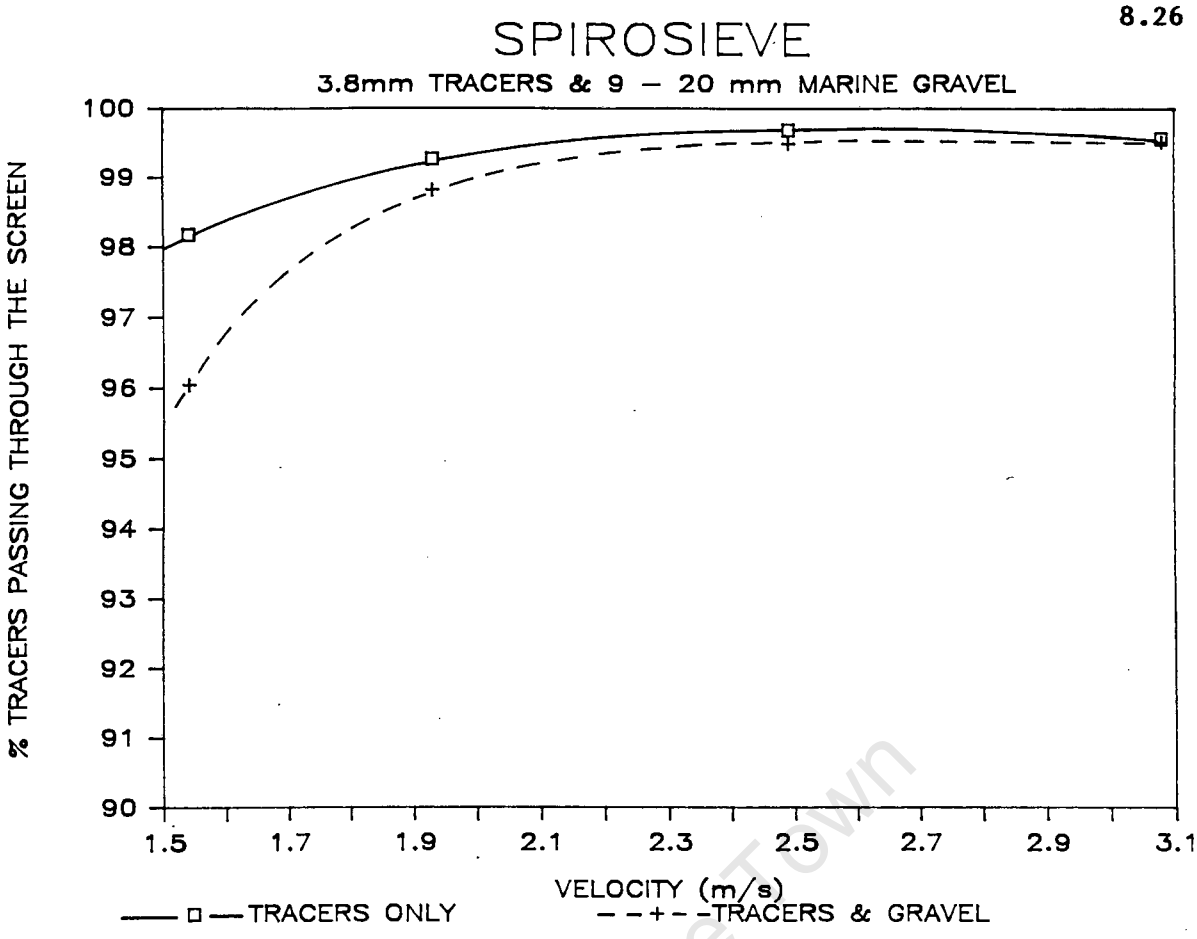

Figure 8.31 : The effect of the presence of larger particles

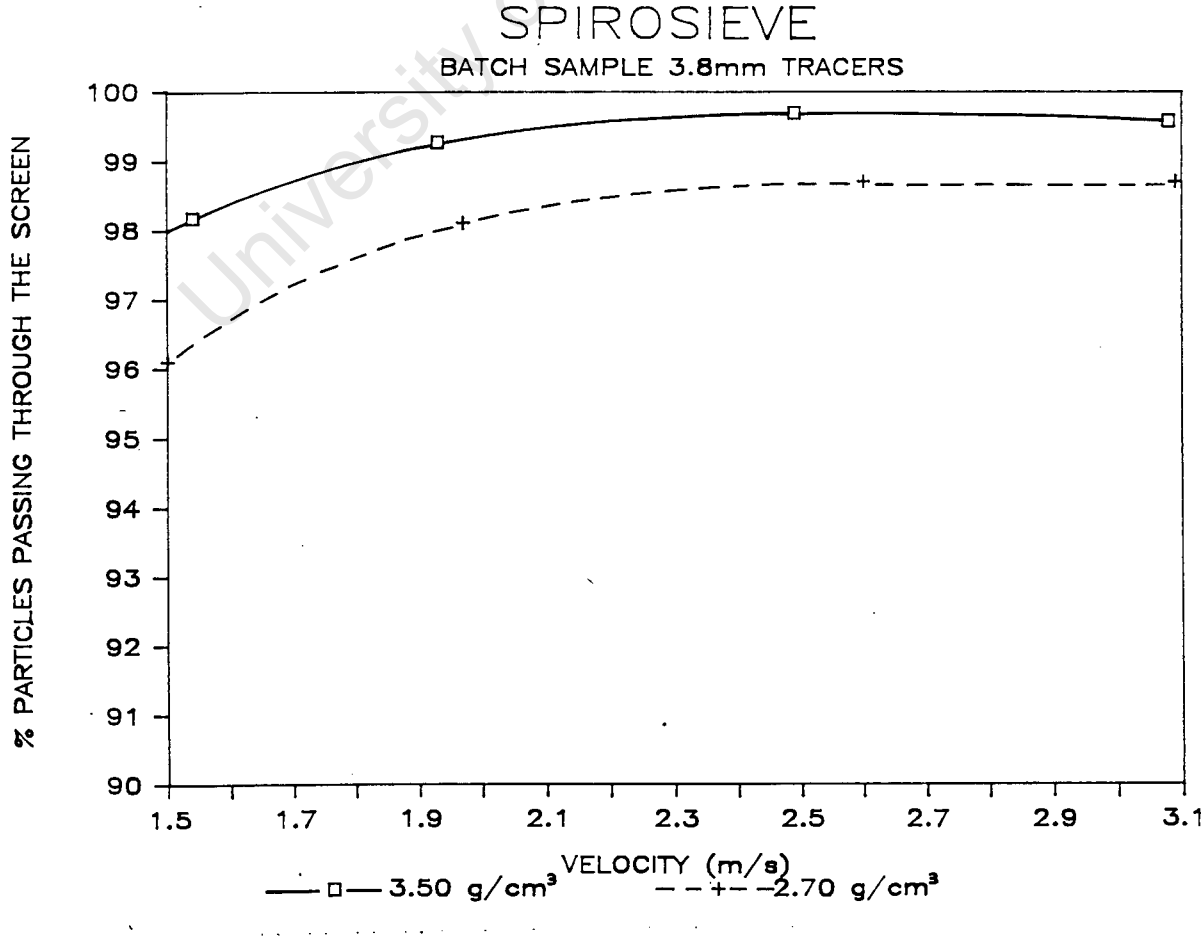

Figure 8.32 : Variable particle density

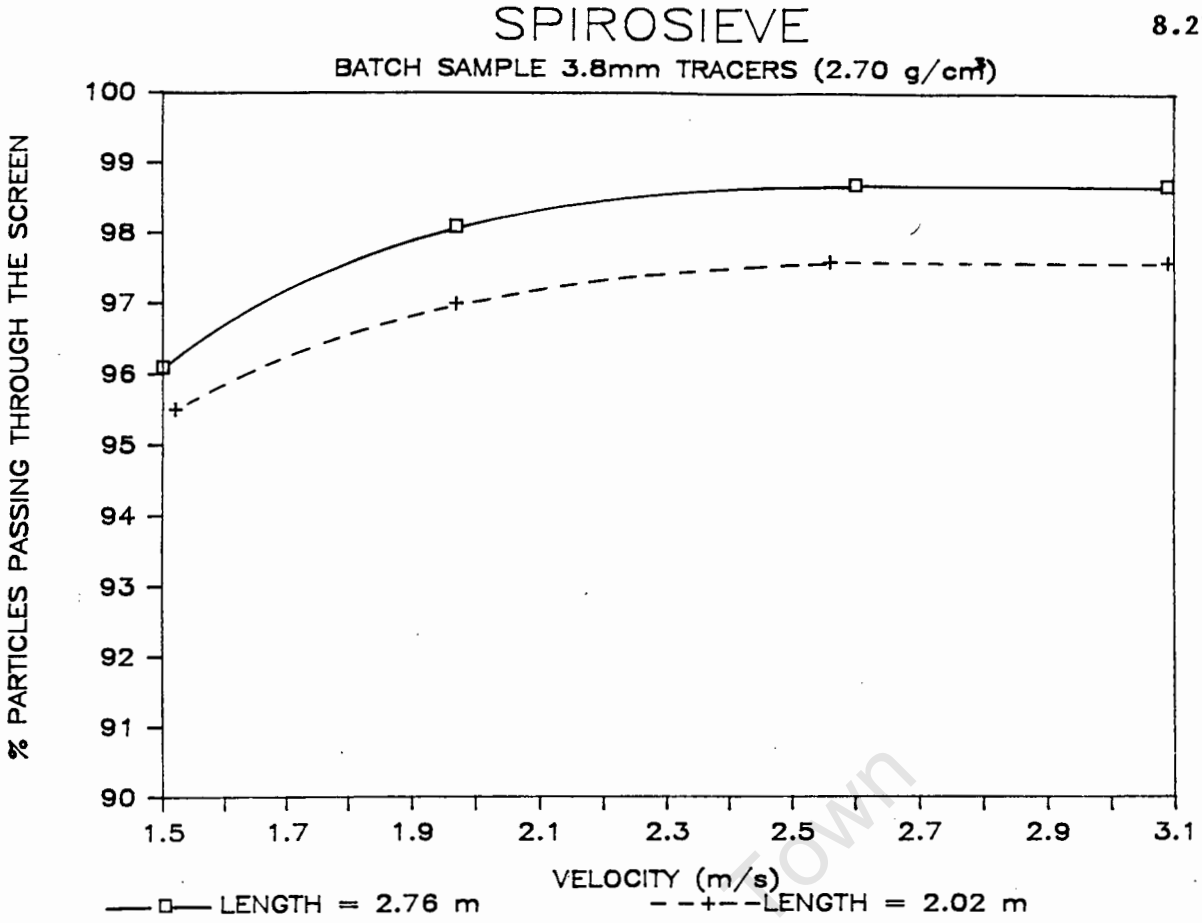

Figure 8.33 : Effect of screen length

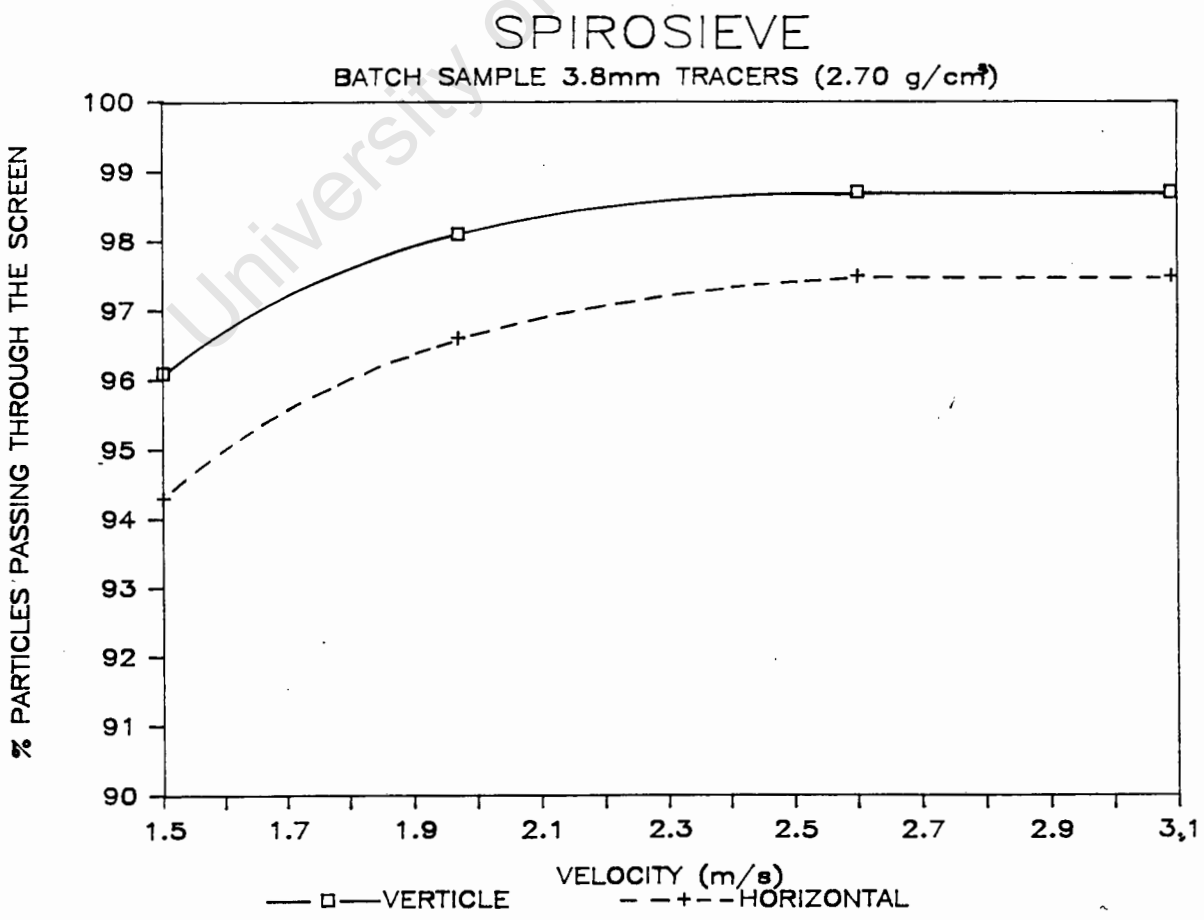

Figure 8.34 : The effect of spirosieve orientation

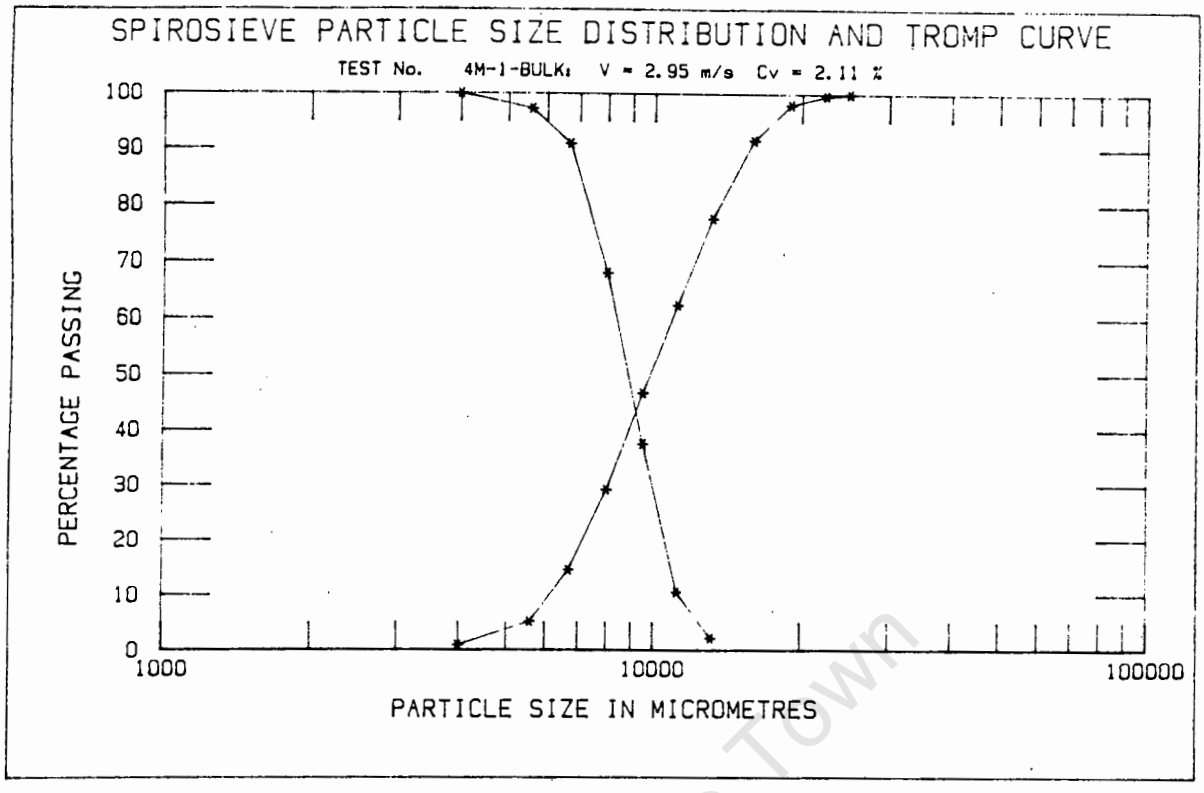

Figure 8.35 : The effect of particle shape

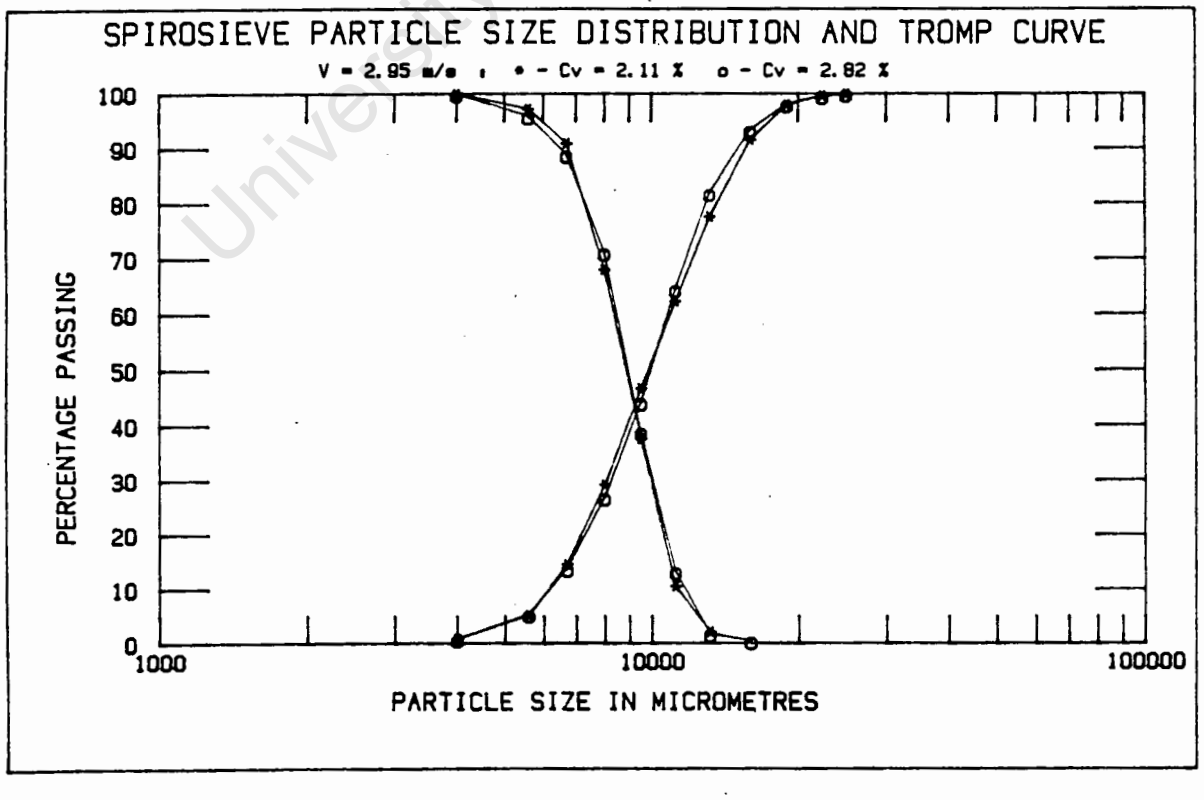

Figure 8.36 : Effect of variable concentration

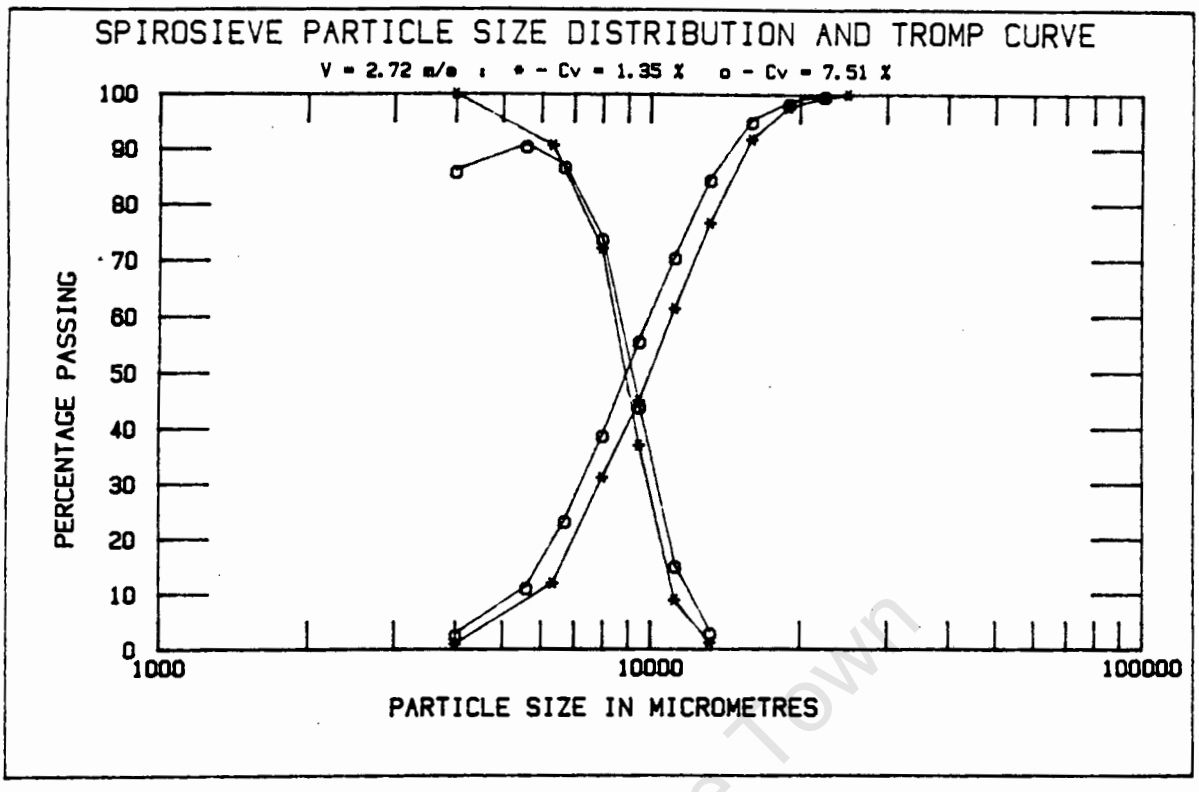

Figure 8.37 : The effect of variable concentration

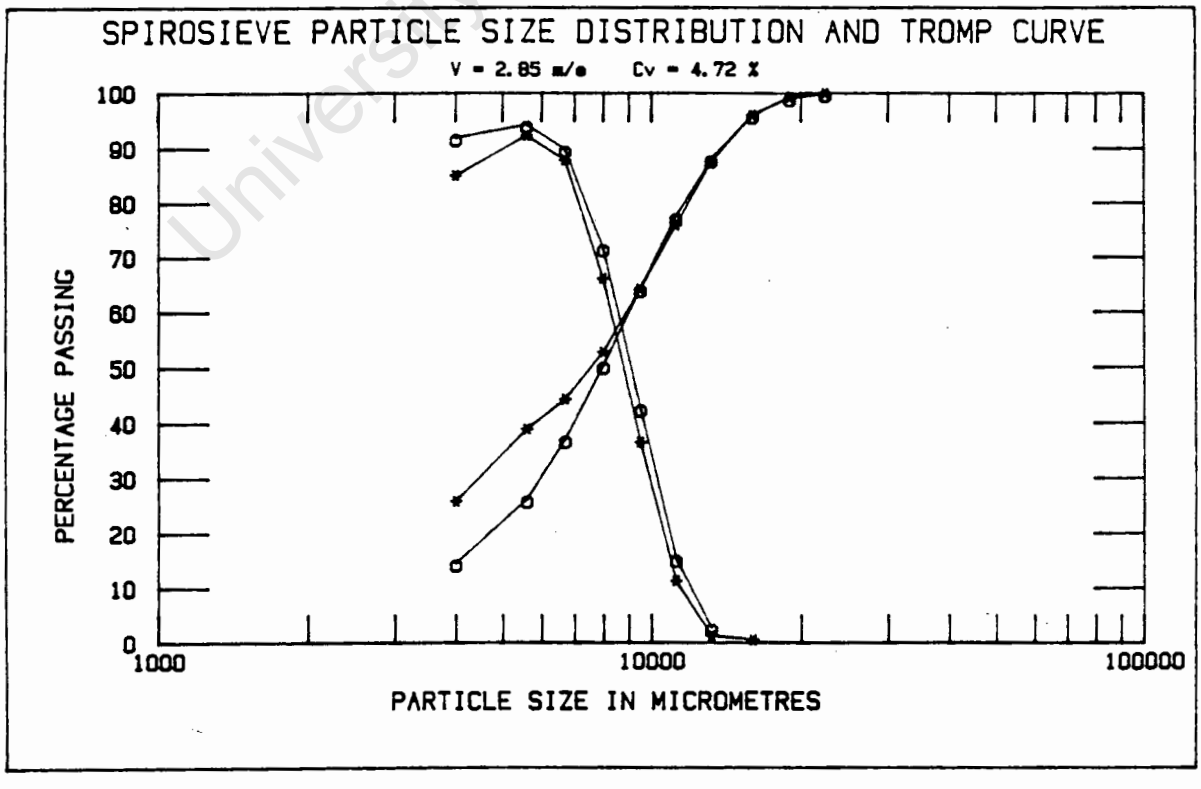

Figure 8.38 : Effect of an increase in the percentage fines

CHAPTER 9

DISCUSSION

INTRODUCTION

In this chapter, the experimental results and observations from the tests conducted on each separation device are discussed.

9.1 CONVERGING ELUTRIATOR

9.1.1 Particle Size

Referring to Figures 8.1 to 8.3, as was expected, an increase in particle size resulted in a decrease in the percentage particles entering the secondary circuit.

The relationship is fairly linear and can be attributed to the fact that solitary particles were used resulting in no interaction between particles.

9.1.2 Particle Shape

An increase in the particle shape factor resulted in a decrease in the separation efficiency at all elutriation column velocities, as is indicated in Figures 8.4 to 8.6.

The shape factor has a major effect on the separation efficiency, especially at the higher particle sizes.

At elutriation column velocities of 0,80 m/s and 0,72 m/s an 85% difference in the percentage particles passing, at a size range of 30-40 mm, was recorded for the complete shape factor range.

9.1.3 Elutriation Column Velocity

Figure 8.7 shows that a decrease in the elutriation column velocity results in a decrease in the percentage particles passing at all size ranges above 10-20 mm.

A more erratic trend was recorded in the intermediate bulk sample tests, as is indicated in Figure 8.8.

The decrease in separation efficiency at the lower size ranges is attributed to the interaction between the large and small particles. This is confirmed by the observed loss of smaller particles in the wake of larger rocks.

The turbulence observed at the start of the elutriation column may have been due to the jet striking the sides of the converging section before entering the straight section.

9.1.4 Primary Outlet Velocity

The primary outlet nozzle diameter was reduced in an attempt to prevent the jet from striking the sides of the converging section. This also resulted in a 32% velocity increase which would propel the sample further into the converging elutriator.

With reference to Figure 8.9, this change resulted in a decrease in separation efficiency at the higher elutriation column velocity, which corresponded to the observed high degree of turbulence.

Figures 8.10 and 8.11 indicate an increase in percentage particles passing at all size ranges.

9.1.5 Elutriator Geometry

The change in elutriator geometry resulted in two flow changes, i.e. higher primary nozzle velocity and higher annular velocity.

Figure 8.12 shows that the changes indicated in Figure 7.1(a), (b) and (c) resulted in an increase in the separation efficiency. The largest increase was recorded when the outlet nozzle was moved closer to the elutriation column (Figure 7.1(c)). This was due to the increased annular disposal chamber velocity and the decrease in the observed turbulence.

The geometry was then changed to that shown in Figure 7.1(d), which resulted in a much higher annular disposal chamber velocity. Figure 8.13 shows that the higher annular disposal chamber velocity resulted in 100% passing of all particles less than 20 mm.

9.1.6 Annular Disposal Chamber Velocity

Figure 8.14 shows that as the primary outlet flow was increased, resulting in a decrease in the annular velocity, the percentage particles entering the secondary circuit decreased.

When the primary outlet nozzle velocity exceeded 4,49 m/s and the annular flow was downwards, the percentage larger particles passing up the elutriation column was greater than that of the smaller particles.

This was due to the fact that the larger particles have a greater surface area and mass, and therefore a higher momentum in the high velocity jet to carry them further into the elutriation column.

The smaller particles are also more inclined to pass into the downward coflow due to the high degree of turbulence at the high primary nozzle velocities.

For 100% passing of the 10 mm particles a primary outlet velocity of approximately 2,5 m/s and an annular velocity of 0,5 m/s was required.

Referring to Figure 8.15, a decrease in screening efficiency was also recorded when the annular velocity decreased due to a decrease in the secondary flow rate.

The relationship was linear because the primary outlet nozzle velocity was kept constantly low (V_{pn} = 2,05 m/s).

For 100% passing of the 10 mm particles an elutriation column velocity of approximately 0,75 m/s was required.

9.1.7 Particle Density

Figure 8.16 confirms that an increase in the particle density results in a decrease in the separation efficiency.

At 100% passing the difference in the annular velocity for the two densities was approximately 0,1 m/s which corresponds to the measured difference in settling velocities (refer to Table 6.1).

9.1.8 General Separation Trends

Referring to Figure 8.17, the effect that particle density, shape, size and the interaction between particles has on the separation efficiency is shown (SF = 0,35-0,85).

To separate 100% of all 8 mm diamonds to the surface ship, 100% of -20 mm rocks and 30% of 50-60 mm rocks need to be raised to the ship as well.

The annular and elutriation column velocities had to be raised by 0,4 m/s and 0,3 m/s respectively above that indicated in Section 9.1.6. This was to account for the higher settling velocity of the 8 mm diamond density particles.

The fact that the smaller particles settled *slowly* in the coflow region indicates that there was no strong flow reversal.

The primary pump was not able to supply enough power to raise a bulk sample of marine gravel up the risers because of the low primary flow needed to create an upward annular flow. Nor was the annular disposal chamber large enough to allow the larger rocks to settle.

For these reasons Figure 8.18 was produced from the experimental results and theoretical settling velocity versus particle size curve for an average shape factor of 0,6.

This was done by displacing the separation curve in Figure 8.17 to the right by the theoretical difference in particle size, between a diamond and quartz density particle, having the settling velocity of a 16 mm diamond.

It is predicted that for 100% passing of all -16 mm diamond density particles, 100% of -35 mm rocks and approximately 20% of the 80 mm rocks will have to be raised to the surface ship.

This estimated separation efficiency does not take into account any marine gravel with very low shape factors. Therefore, if the average shape factor was lower then the curve would be further displaced to the right.

9.2 CYCLOSIEVE

9.2.1 Vertical Screens

1. **Primary inlet velocity**

Referring to Figure 8.19, the greatest screening efficiency was obtained when the inlet flow was striking the screen directly and not at the higher inlet velocities.

This was because a large proportion of the water and particles passed directly through the screen holes.

The turbulence caused by the inlet flow being deflected across the top of the cyclosieve, and the resulting loss of rotational energy, would account for the decrease in screening at the high velocities.

2. Flow conditions

With reference to Figure 8.20, an increase in screening efficiency was recorded when more water was removed via the secondary/fines outlet.

This was unexpected, as it was predicted in Section 2.2.3, that the particle residence time and screening length would be greater when under sub-marine conditions, i.e. thicker layer of water on the screens.

However, the observation that only 6/8 (270°) of the screening surface was covered with a thin layer of water at 4,18 m/s when under aerated conditions, corresponds well with the predicted value of 275° at 4,42 m/s (Section 2.2.3).

9.2.2 Conical Screens

Figure 8.21 shows that the change from vertical screens to conical screens resulted in a large increase in the screening efficiency.

The conical screen and the high centrifugal force caused the rotating water to settle more slowly than was the case with the vertical screen. This resulted in the water and particles completing more revolutions of the screen before passing out the coarse outlet.

The rotating layer of water near the inlet that was described in Section 8.22, reduced the deflection of the inlet flow, thereby increasing the rotational energy.

1. Primary inlet velocity

With reference to Figure 8.22, the decrease in the screening efficiency below 2,5 m/s inlet velocity was due to the decrease in rotational energy (centrifugal force) when the inlet jet began to strike the conical screen directly.

2. Variable secondary flow

Referring to Figure 8.23, a decrease in the secondary outlet flow resulted in the formation of a large mass of rotating water with a small central air core and a very small decrease in the screening efficiency. This was due to the slight decrease in the rotational velocity.

At the higher secondary flow rate, i.e. when very little water was removed via the coarse outlet, a thin layer of rotating water formed on the screen. This was because the majority of the water was drawn off through the screen holes.

3. Particle density

Figure 8.24 shows that particle density has no marked effect on the screening efficiency compared with the centrifugal force, flow conditions and inlet velocity.

4. Particle size

Figure 8.25 shows that an increase in particle size resulted in a decrease in the screening efficiency at the indicated flow conditions.

No gravel greater than 37,1 mm passed through the screen but the percentage passing for particles between 4 mm and 5,6 mm was only 97,5%.

These smaller particles were lost because they were deflected off the screen with the large rocks, as was described in Section 8.22 (4).

The accumulative percentage passing of all particles less than 16 mm was 89,6%.

5. Flow conditions

With reference to Figure 8.26, the different flow conditions resulted in a 1% increase in the accumulative percentage passing of all particles less than 16 mm. However, the larger mass of rotating water also resulted in two other major screening efficiency changes.

It was thought that the larger mass of rotating water would prevent the smaller particles from being deflected off the screen and to waste, thereby improving the screening efficiency.

Firstly, the percentage larger rocks (> 10 mm) being deflected off the screen and to waste decreased when an almost sub-marine flow condition was created. Secondly, the percentage smaller rocks (< 10 mm) passing to waste increased under the sub-marine conditions.

This trend can be explained by comparing the cyclosieve with a hydrocyclone.

Figure 9.1 and 9.2 show the two major forces acting on a single particle in a large mass of rotating water, such as that found in a hydrocyclone and the cyclosieve respectively.

In general, a particle in a hydrocyclone is subjected to two opposing forces: an outward centrifugal force (F_c) and an inward drag force (F_d).

$$F_c = \frac{\pi\, d_p^3\, (\rho_s - \rho_\ell)}{6\, r}\; v_{(t)}^2$$

(where d_p is the particle diameter, r is the instantaneous distance of the particle from the centre of the hydrocyclone and $v_{(t)}$ the tangential velocity).

Although the drag force is a function of the inward radial velocity $v_{(r)}$, the exact relationship depends on whether the flow is laminar or turbulent. Indications are that laminar conditions are approximated and Stokes' law is assumed because of the low values of $v_{(r)}$ and d_p, giving :

$$F_d = 3\pi\, d_p\, \mu\, v_{(r)}$$

When F_d exceeds F_c a particle will move inwards and may leave through the vortex finder. The split of particles is, therefore, dependent on the relative values of $v_{(r)}$ and $v_{(t)}$. (Kelly & Spottiswood, 1982 & Svarovsky, 1984).

The same forces exist in the cyclosieve, except that because the value of d_p is greater, either Allens or Newtons law must be assumed, giving

$$F_d = 5{,}5\ (\rho\ \mu\ v_{(r)}^3\ d_p^3)^{\frac{1}{2}} \quad - \text{ Allens law}$$

$$(1 < R_{ep} < 1\ 000)$$

or

$$F_d = 0{,}173\ \rho\ v_{(r)}^2\ d_p^2 \quad - \text{ Newtons law}$$

$$(R_{ep} > 1\ 000)$$

However, when the secondary outlet flow is reduced in the cyclosieve to create the required sub-marine flow conditions, less water passes through the screen holes and there is a slight decrease in the tangential velocity and F_c.

This must also result in an increase in the inward radial flow towards the free vortex at the coarse outlet, and therefore an increase in $v_{(r)}$ and F_d.

F_c is further reduced by a greater amount than F_d, at a smaller particle size, because of the respective powers to which d_p is raised.

All of these factors would explain why there was a decrease in screening efficiency at the smaller particle size range under sub-marine flow conditions.

6. Solids concentration

With reference to Figure 8.29, an increase in solids concentration resulted in a large decrease in the screening efficiency.

This was most noticeable at a solids concentration of 6,24% by volume when the percentage passing of particles between 2 mm and 4 mm was only 37,4%.

The overall accumulative percentage passing of particles less than 16 mm decreased to 62%.

9.3 SPIROSIEVE

9.3.1 Clear Water Tests

With reference to Figure 8.29, the flow within the spirosieve is clearly fully-rough wall turbulent, with the curve extending

beyond the upper limits of the normal friction factor Reynolds number diagram for pipe flow. The passageway through the spirosieve is as rough as a pipe with a relative roughness of 0,08.

9.3.2 Velocity

Referring to Figure 8.30, a decrease in velocity (centrifugal force) below 2,5 m/s resulted in a small decrease in the screening efficiency.

Between 2,5 m/s and 3,1 m/s the percentage particles passing remains constant at 99,8%.

It is expected that at higher velocities the screening efficiency may even decrease due to the decrease in the particle residence time.

The loss of 0,2% of the tracer particles could be due to secondary flow, as was discussed in Section 2.3.3, or too short a screen length.

9.3.3 Presence of Larger Particles

With reference to Figure 8.31, the presence of larger marine gravel had very little effect on the screening efficiency above 2,5 m/s.

Below 2,5 m/s, a decrease in the percentage tracers passing through the screen was recorded. This is due to the decrease in centrifugal force resulting in a decrease in stratification and therefore less smaller particles reaching the screen.

9.3.4 Particle Density

Figure 8.32 shows that a decrease in particle density resulted in a decrease in the screening efficiency of approximately 1,2% between 2,5 m/s and 3,1 m/s.

This is a distinct advantage as the heavier diamond particles are more easily screened than the marine gravel.

9.3.5 Screen Length

Referring to Figure 8.33, the 27% decrease in screen length resulted in a 1,2% decrease in the screening efficiency.

This can be best described by a comparison with a land based screen where similar results are found. Referring to Figure 9.3 from Kelly & Spottiswood (1982), Region III has a small through-put because the bed is excessively deep and presentation for passage is severely restricted. This is due to the high quantity of oversize material and insufficient stratification. In Region II maximum screening occurs because the bed thickness is decreased.

Region I is characterised by insufficient particles to form a monolayer on the screen. The particles tend to have excessive unrestrained motion and very little stratification occurs.

It was Region I that was shortened, resulting in only a small decrease in screening efficiency.

9.3.6 Orientation

Figure 8.34 shows that when the spirosieve was horizontal there was a decrease of approximately 1,2% in the screening efficiency at velocities greater than 2,5 m/s.

This is due to the change in the resultant centrifugal force caused by the gravity component, and the fact that the percentage passings versus velocity (centrifugal force) is not a linear relationship, as was shown previously and in Figure 9.4.

It can be seen from Figure 9.4 that at 5,71 g's (2,75 m/s), the decrease in the centrifugal force (F_c) in the top half of the spirosieve, results in a decrease in the screening efficiency. This decrease would actually be larger than that determined from the graph because the particle residence time would not increase as it does with decreasing velocity.

The resultant increase in F_c, due to the downward gravity component in the lower half of the spirosieve, does not result in an increase in the screening efficiency. This is due to the observed plateau after 2,5 m/s $(\frac{F_c}{F_g} = 4,72)$. This plateau was also due to the decrease in particle residence time at the higher velocity, therefore an increase would be expected because now only F_c is increased.

The average change in centrifugal force at 2,75 m/s is 0,560 g's. This was calculated by integrating the variable resultant centrifugal force in the top and bottom half of the spirosieve.

To summarise, the decrease in the screening efficiency in the top half of each revolution is therefore greater than the increase in the bottom half, because the relationship between percentage passing and velocity is not linear.

9.3.7 Particle Size

Figure 8.35 shows that an increase in particle size resulted in a decrease in the screening efficiency.

No particles larger than 13,2 mm passed through the screen and 100% passing was recorded for particles between 2 mm and 4 mm.

This was higher than that recorded for the batch sample of 3,8 mm tracers and is attributed to the observed stratification and the presence of the large amount of bigger particles against the screen.

The increase in the screening efficiency of smaller particles in the presence of larger particles is an indication that secondary flow conditions, as described in Section 2.33, were probably causing the batch tracer particles to pass back through the screen.

Either the secondary flow, or the effects of the secondary flow, are eliminated in the presence of larger particles.

9.3.8 Solids Concentration

With reference to Figures 8.36 and 8.37, an increase in solids concentration resulted in a decrease in the percentage particles passing through the screen. This was most noticeable in Figure 8.37 where the solids concentration increased by 6,16% and the screening efficiency decreased to 86,2% for particles between 2 mm and 4 mm.

At higher concentration the bed is considerably thicker, there is a large quantity of oversize material and therefore less stratification, resulting in a decrease in screening efficiency (as in Region III of Figure 9.3).

9.3.9 Particle Size Distribution

Figure 8.38 shows that an increase in the percentage fines resulted in a decrease in the overall screening efficiency especially at the lower particle size range.

This is because an increase in the amount of fines means that more particles have to travel through the gaps between the larger particles to reach the screen in the same time period.

An even larger decrease in screening efficiency could occur if the percentage fines increased to such an extent that the particles already screened came in contact with the outer side of the screen. This would prevent any further screening.

This is possible as the fines chamber has to be kept considerably smaller than the coarse chamber, to maintain the average velocity as well as prevent any blockages from occuring in the coarse chamber.

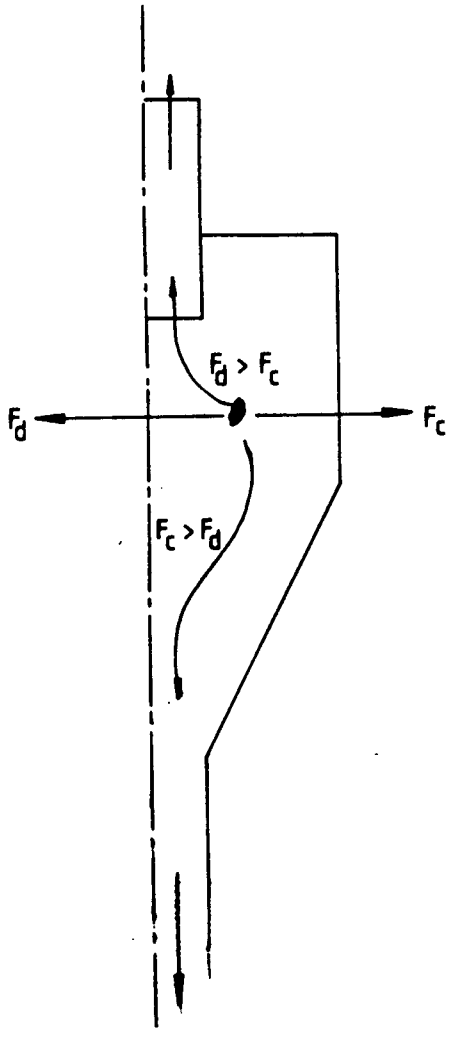

Figure 9.1 : Major forces in a hydrocyclone

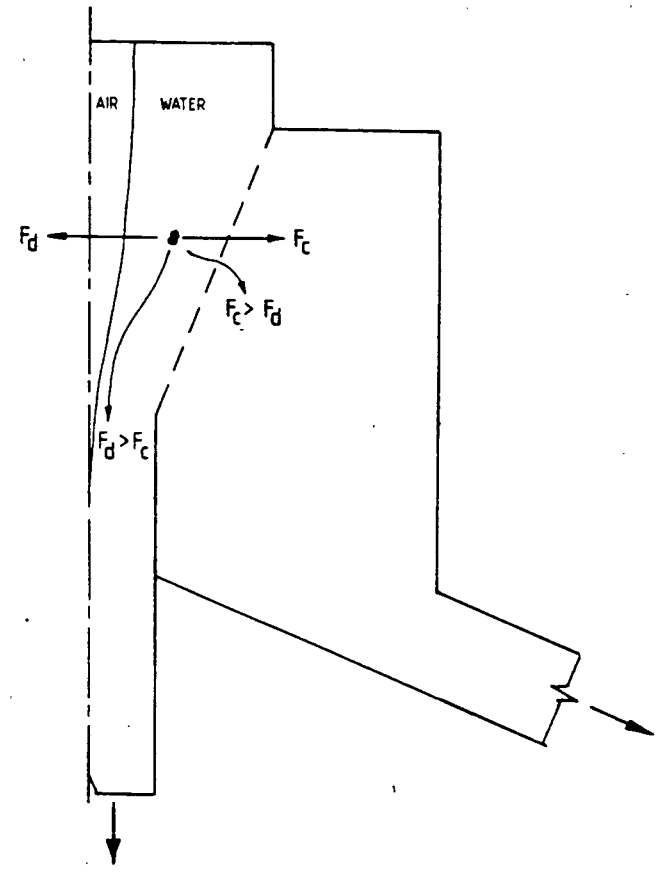

Figure 9.2 : Major forces in the cyclosieve

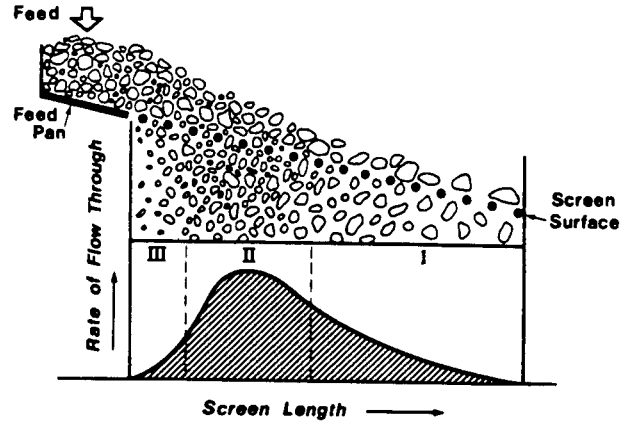

Figure 9.3 : Effect of screen length
(Kelly & Spottiswood, 1982)

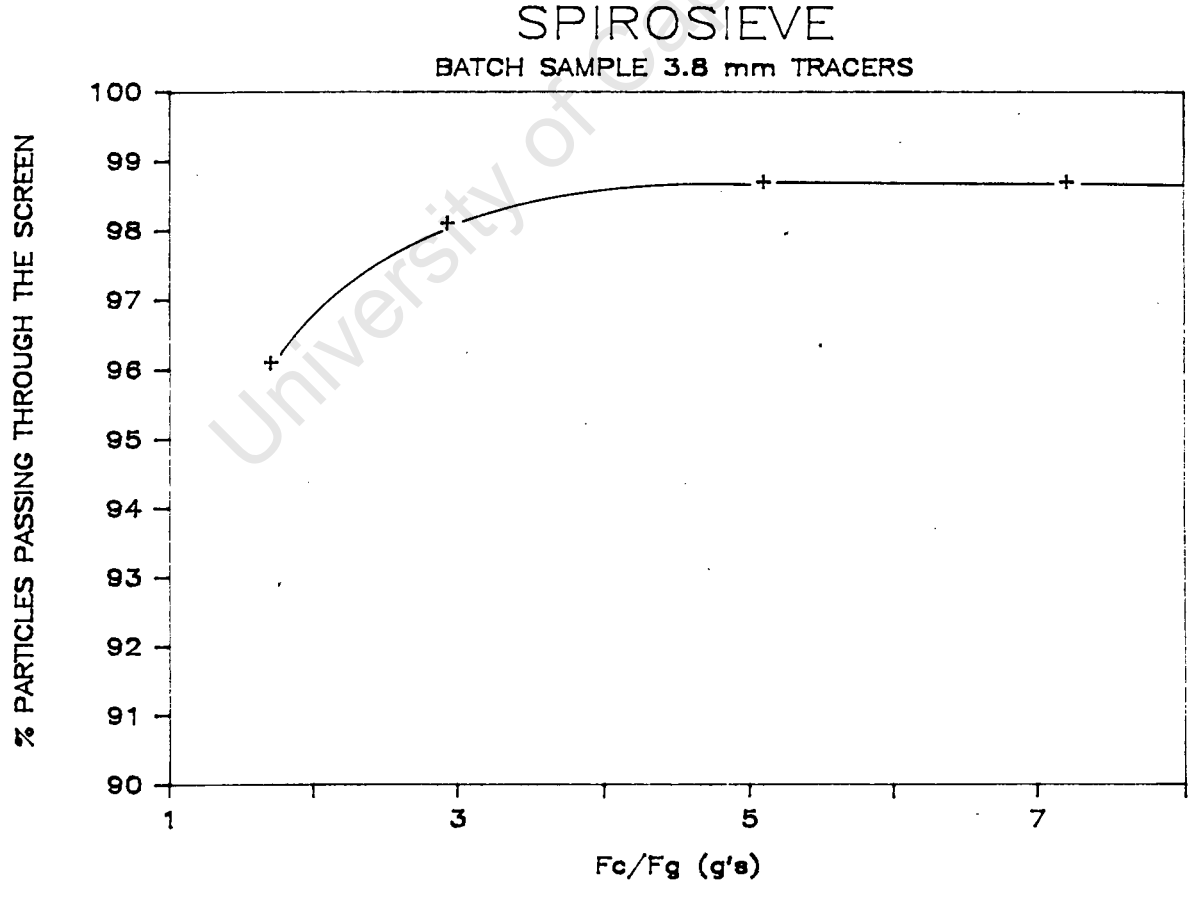

Figure 9.4 : The effect of centrifugal force

CHAPTER 10

CONCLUSIONS

1. The converging elutriator is unsuitable for the underwater separation of diamantiferous marine gravels in its present form for the following reasons:

   - Too large a size range of waste material needs to be removed to the surface ship because of the device's sensitivity to particle shape.

   - The higher density of diamonds, and therefore a greater settling velocity, has an adverse effect on the overall separation efficiency.

   - More water is removed with less material due to the required upward annular flow, therefore an additional dewatering pump is required.

   - The particle size at which separation takes place is sensitive to changes in velocity therefore extensive instrumentation will be required to monitor flow rates and pump speeds.

2. At the higher envisaged operating concentrations (C_v = ± 6%) the screening efficiency of the cyclosieve, in its present form, is reduced to a level where it cannot be considered as a feasible underwater screening device.

3. The screening efficiency can be improved by making the following changes:

   - The tangential primary inlet can be changed to that of an involute as shown in Figure 10.1.

   - The present screen holes can be changed to long slits in the same direction as the rotating water (Figure 10.2).

   - The central air core and part of the flow area can be replaced by a solid cone, as shown in Figure 10.3, thereby reducing the inward secondary flow that is affecting the screening efficiency.[1]

4. The construction and testing of the *spirosieve model* proved to be very successful because it was easy to observe the screening process and to make parameter changes such as screen length and orientation.

---

[1] This would essentially be converting the cyclosieve into a similar design to that of the spirosieve, where the central volume is a hollow cylinder.

5. The spirosieve is the most favourable device for the underwater separation of diamantiferous marine gravels, for the following reasons:

- The higher density of the diamonds improves the screening efficiency.

- Particle shape should have very little effect on the screening efficiency.

- The expected secondary flow or the resultant effects thereof, are eliminated.

- *Water and solids* are removed via the coarse outlet thereby reducing the mixture volume that is transported to the surface ship.

- The full scale unit would be fairly small and easily handled at sea.

- The flow is continous and is always in an upward direction, i.e. from the seabed towards the surface ship.

6. The degree of screening efficiency obtained with the *spirosieve model* is a good indication of its abilities as a full scale separation device, especially since it is believed that the percentage passing of fines can be improved by:

- Increasing the screen length and surface area.

- Increasing the degree of stratification.

- The removal of fines from the fines chamber at intermediate levels.

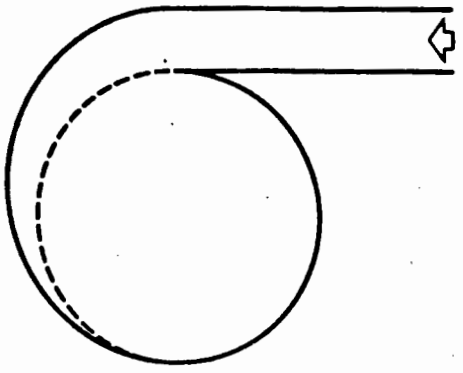

Figure 10.1 : Involute primary inlet
(Kelly & Spottiswood, 1982)

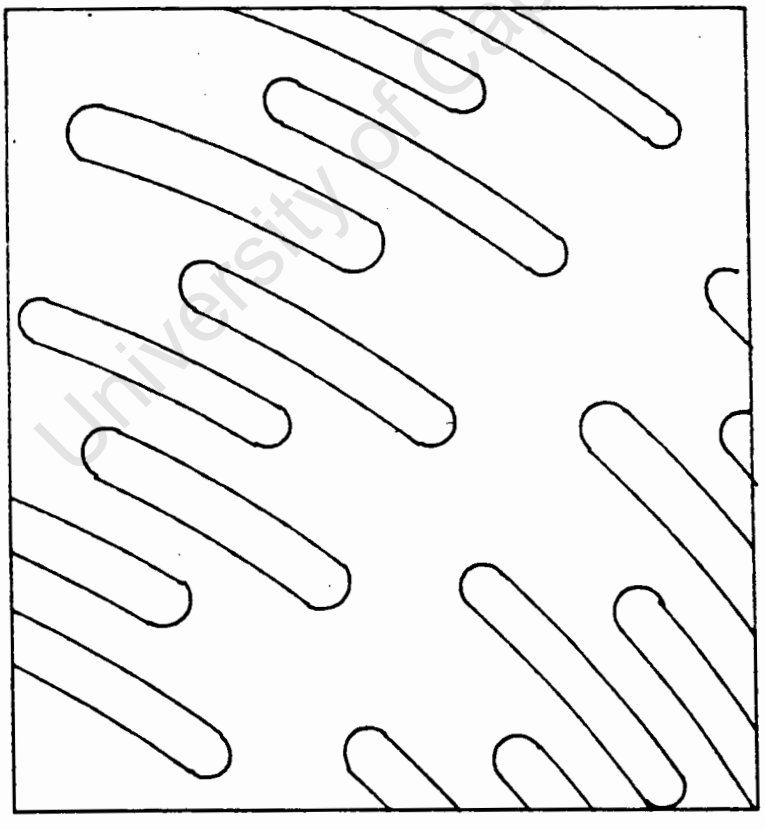

Figure 10.2 : Proposed screen configuration

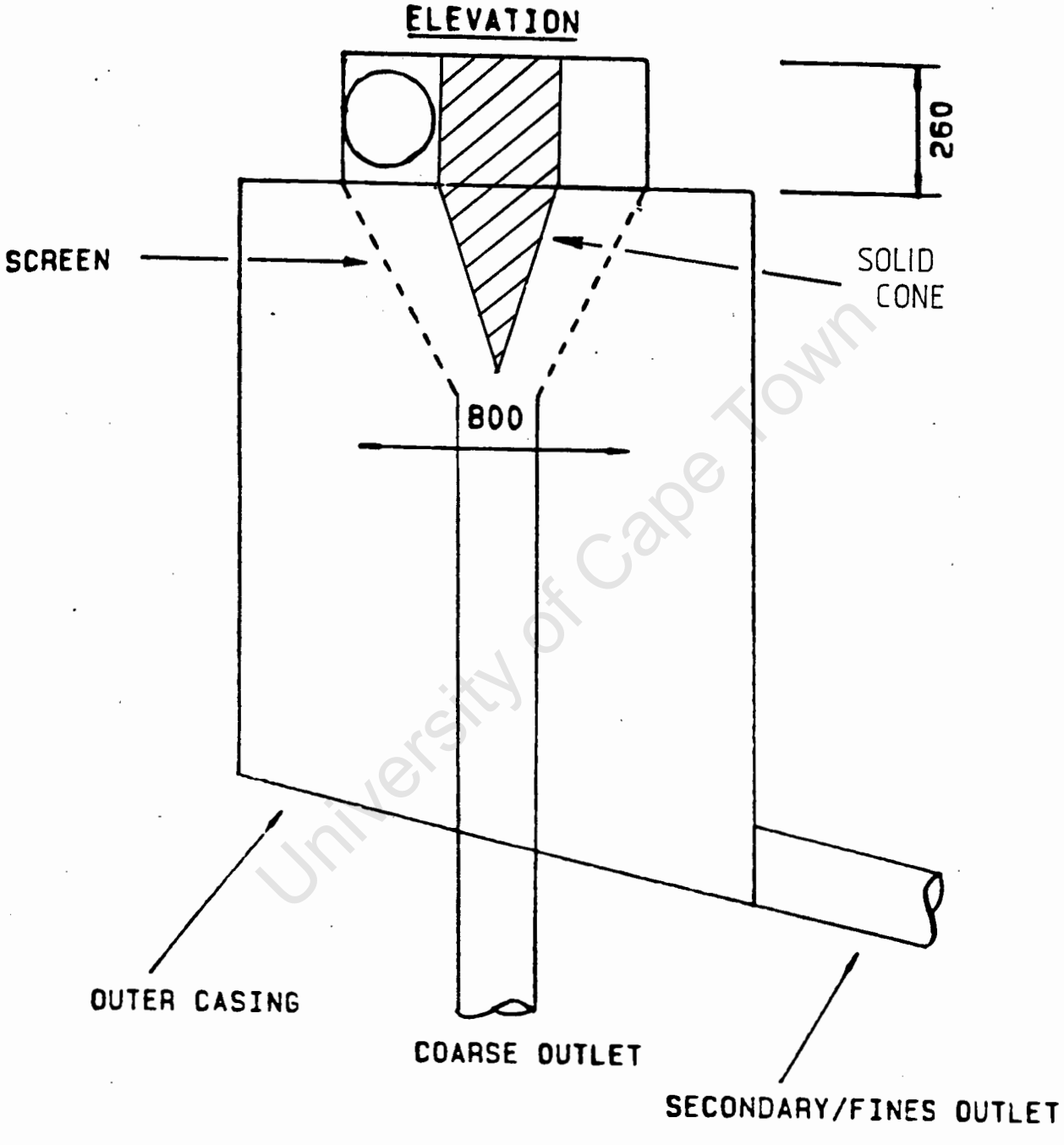

Figure 10.3 : Addition of solid cone to cyclosieve

CHAPTER 11

RESEARCH RECOMMENDATIONS

1. A larger scale spirosieve should be constructed in accordance with the design parameters presented in Appendix F.

   This device will allow the passage of rocks, within the coarse chamber, of up to 100 mm in diameter.

2. Similar tests to the ones conducted on the spirosieve model, should be carried out on the large scale spirosieve, to determine if the "larger scale" has any major effects on the screening efficiency.

3. Testing of the spirosieve model should continue, so as to optimise the ratio of open screen area to stratification, which is largely caused by the vertical bars.

4. It is also recommended that the spirosieve model be modified, so that a fines/water mixture can be removed and more water added at various positions along the screen length.

5. The model should then be tested with a higher percentage fines, to determine the effect on screening efficiency of removing fine material during operation.

6. All the information gained from the tests conducted on the spiro-sieve model should be used to improve the design of the larger scale spirosieve.

7. When enough information is known about the optimisation of the screening efficiency, and the effects of scaling up, then a full scale prototype spirosieve should be designed, constructed and tested before being implemented in an undersea environment.

REFERENCES

Bain, A.G. and Bonnington, S.T. (1970) The Hydraulic Transport of Solids by Pipeline, Perganon Press Ltd, Oxford.

Blevins, R.D. (1984) Applied Fluid Dynamics Handbook, Van Nostrand Reinhold Company Inc, New York.

Bovingdon, H.T. (1975) Screening - "State of the Art", Screening and Grading of Bulk Materials Conference Proceedings, London.

Brockett, F.H. and Petters, R.A. (1980) Proceedings of the Annual Conference of the Marine Technology Society, Washington DC (USA).

Kelly, E.G. and Spottiswood, D.J. (1982) Introduction to Mineral Processing, John Wiley & Sons, New York.

Lazarus, J.H. (1982) Particle Size and Settling Behaviour, Hydrotransport 8.

Lazarus, J.H. (1984) CE302 - Hydraulic Engineering Laboratory Manual, University of Cape Town.

Lazarus, J.H. and Rossouw, T.J. (1986-88) Underwater Screening Series of confidential reports for De Beers Marine, HTRU, University of Cape Town.

Richardson, J.F. and Zaki, W.N. (1954) The Sedimentation of a Suspension of Uniform Spheres under conditions of Viscous Flow, Transactions of the Institution of Chemical Engineers, Vol. 32, p.35.

Rossouw, T.J. (November 1986) Suction Dredge Head and Jetting Nozzles, BSc Thesis, University of Cape Town.

Schweitzer, P.A. (1979) Handbook of Separation Techniques for Chemical Engineers, McGraw-Hill, New York.

Smale-Adams, K.B. and Jackson, G.O. (1978-1979) Moving Into Deep Water Manganese Nodule Mining, Royal Society of London - Philosophical Transactions, p.290-.

Svarovsky, L. (1984) Hydrocyclones, Holt, Rinehunt & Winiston Ltd, Eastbourne.

Van Dooremalen, J.J.C.M. (1973) New Developments in Integrated Processing Systems on Sand and Gravel Dredges, World Mining Conference.

Annonymous (1979) Diamond Dredger Reap Inshore Harvest, The South African Shipping News and Fishing Industry Review.

APPENDIX A : Doppler Flow Meter Calibrations

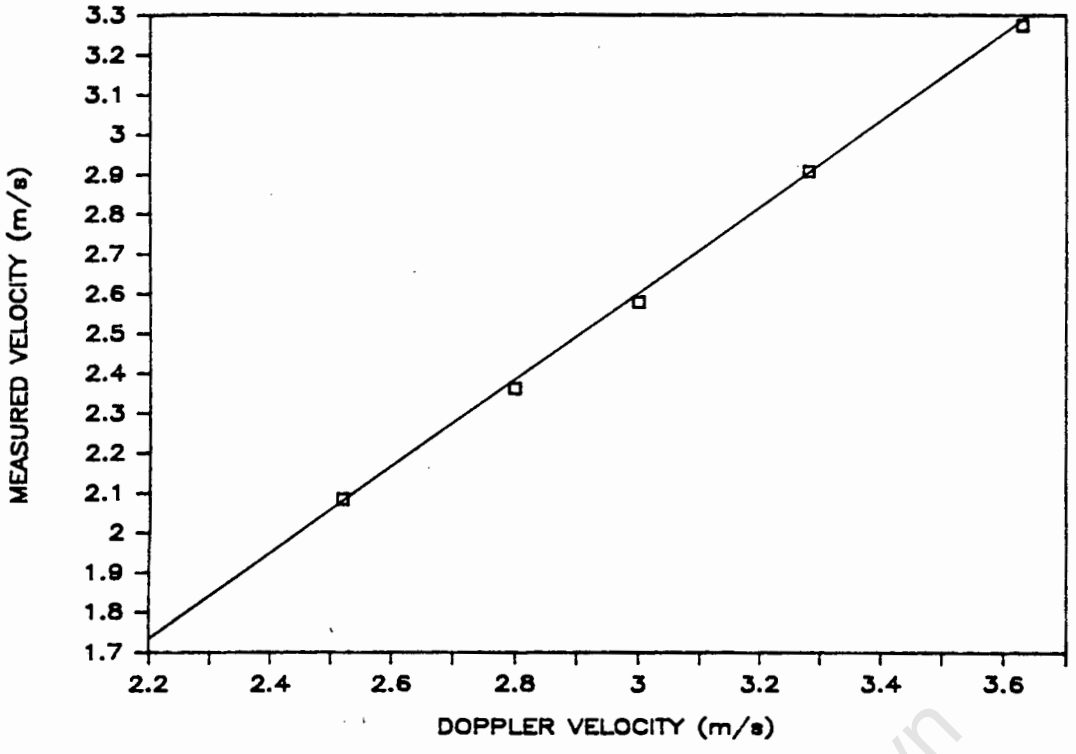

Figure A.1 : Primary Doppler flow meter calibration

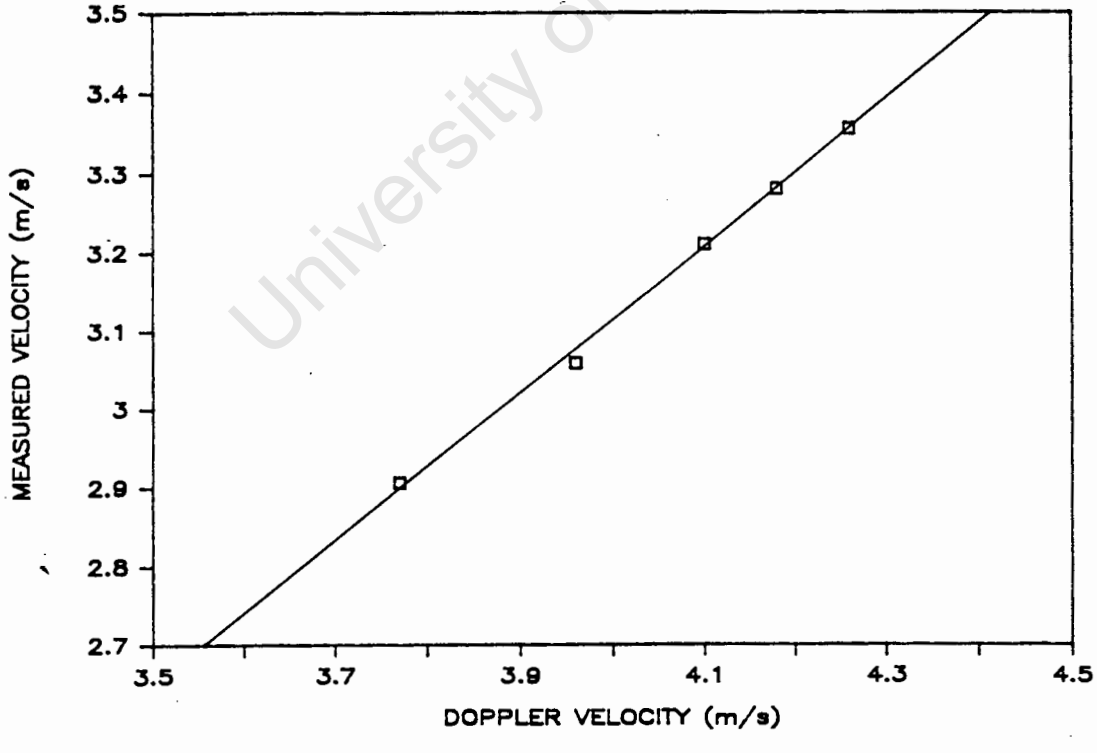

Figure A.2 : Secondary Doppler flow meter calibration

APPENDIX B : Converging Elutriator Experimental Results

SOLITARY PARTICLE TESTS			
PARTICLE SIZE RANGES (mm)	% PARTICLES ENTERING SECONDARY CIRCUIT ELUTRIATION COLUMN VELOCITY (m/s) 0.88	0.80	0.72
0 - 10	100	100	100
10 - 20	100	100	100
20 - 30	100	93.3	83.3
30 - 40	73.7	55.3	49.3
40 - 50	53.7	42.7	34.3
50 - 60	28.3	5.7	0

SOLITARY PARTICLE TESTS			
PARTICLE SIZE RANGES (mm)	% PARTICLES ENTERING SECONDARY CIRCUIT ELUTRIATION COLUMN VELOCITY 0.88 m/s SHAPE FACTOR .35-.50	SHAPE FACTOR .51-.65	SHAPE FACTOR .66-.85
0 - 10	100	100	100
10 - 20	100	100	100
20 - 30	100	100	100
30 - 40	96	75	50
40 - 50	90	71	0
50 - 60	85	0	0
Vec = 0.80 m/s			
0 - 10	100	100	100
10 - 20	100	100	100
20 - 30	100	100	80
30 - 40	91	75	0
40 - 50	71	57	0
50 - 60	17	0	0
Vec = 0.72 m/s			
0 - 10	100	100	100
10 - 20	100	100	100
20 - 30	100	100	50
30 - 40	81	67	0
40 - 50	63	40	0
50 - 60	0	0	0

INTERMEDIATE BULK SAMPLE OF GRANITE

Qs - Qp = 10 l/s ; d = 210 mm ; h = 0

PARTICLE SIZE RANGES (mm)	% PARTICLES ENTERING SECONDARY CIRCUIT — ELUTRIATION COLUMN VELOCITY (m/s) 0.82	0.75	0.71	0.66	0.61
4 - 8	91.8	75.8	83.2	82	74.5
8 - 16	92.2	70.8	76.2	79.7	68.3
16 - 25	96	71.8	65.8	57.6	61.4
25 - 38	90.9	76.9	63.6	52	42.9
38 - 51	83.3	33.3	33.3	33.3	33.3
51+	75	0	0	0	0
PRIMARY OUTLET NOZZLE VELOCITY (m/s)	1.96	1.76	1.65	1.48	1.34

INTERMEDIATE BULK SAMPLE OF GRANITE

Qs - Qp = 10 l/s ; d = 183 mm ; h = 0

PARTICLE SIZE RANGES (mm)	% PARTICLES ENTERING SECONDARY CIRCUIT — ELUTRIATION COLUMN VELOCITY (m/s) 0.82	0.75	0.71	0.66	0.61
4 - 8	84.5	83.8	83.7	80	84.2
8 - 16	82	84.8	79	70	72.5
16 - 25	80.4	78.4	70	69.2	75.8
25 - 38	75	83.3	66.7	66.7	41.7
38 - 51	100	66.7	50	0	0
51+	25	25	25	0	0
PRIMARY OUTLET NOZZLE VELOCITY (m/s)	2.58	2.32	2.19	1.92	1.75

INTERMEDIATE BULK SAMPLE OF GRANITE

Qs - Qp = 10 l/s ; d = 183 mm ; h = 140 mm

PARTICLE SIZE RANGES (mm)	% PARTICLES ENTERING SECONDARY CIRCUIT — ELUTRIATION COLUMN VELOCITY (m/s) 0.82	0.71	0.61
4 - 8	92.2	86.9	85.3
8 - 16	84.8	84	64.8
16 - 25	90	74	60.4
25 - 38	95	75	50
38 - 51	70	50	25
51+	33.3	0	0
PRIMARY OUTLET NOZZLE VELOCITY (m/s)	2.58	2.19	1.75

INTERMEDIATE BATCH SAMPLE OF TRACER PARTICLES					
Qs = 83.6 l/s ; Vec = 0.87 m/s					
ANNULAR VELOCITY Van (m/s)	PRIMARY OUTLET NOZZLE VELOCITY Vpn (m/s)	% PARTICLES ENTERING SECONDARY CIRCUIT PARTICLE SIZE (mm) 3.8	8	10
0.67	1.94	100	100	100
0.49	2.67	100	100	100
0.3	3.37	98.8	95	91.5
0.09	4.11	89.8	90.8	88
-0.02	4.55	86.8	88.3	86.5
-0.26	5.45	80.3	84.8	86.1
-0.59	6.71	74.3	77.6	80.3
-0.75	7.29	75.1	86.5	91.3

INTERMEDIATE BATCH SAMPLE OF TRACER PARTICLES						
Qp = 38.1 l/s ; Vpn = 2.05 m/s						
ANNULAR VELOCITY Van (m/s)	ELUTRIATION COLUMN VELOCITY Vec (m/s)	% PARTICLES ENTERING SECONDARY CIRCUIT PARTICLE SIZE (mm) (2.70 g/cm) 3.8	8	10	(3.5 g/cm) 3.8
0.66	0.87	100	100	100	100
0.52	0.77	100	100	100	100
0.41	0.69	100	99.5	99.5	70
0.31	0.62	99.3	77.2	79.3	54
0.17	0.52	76.8	61.9	55.1	30.9
0.01	0.4	52.6	33.3	28.5	11

INTERMEDIATE BULK SAMPLE OF SOLITARY PARTICLES & TRACER PARTICLES	
Vec = 0.78 m/s	
Van = 0.54 m/s	
Vpn = 2.02 m/s	
PARTICLE SIZE RANGE (mm)	% PARTICLES ENTERING SECONDARY CIRCUIT
0 - 10	100
10 - 20	100
20 - 30	90
30 - 40	83
40 - 50	52
50 - 60	30

APPENDIX C : Cyclosieve Experimental Results

CYCLOSIEVE TEST RESULTS

DATE: 16-10-87 PARTICLES: 8mm, 2,70g/cm³ COMMENTS:
50 particles

TEST NUMBER	BEND METER				SEPARATION		VORTEX DESCRIPTION
	PRIMARY FLOW (l/s)	SECONDARY FLOW (l/s)	PRIMARY VELOCITY (m/s)	SECONDARY VELOCITY (m/s)	% IN FINES SAMPLER	% IN COARSE SAMPLER	
CS-AF-VC-1	142,56	145,14	5,54	5,64	22	78	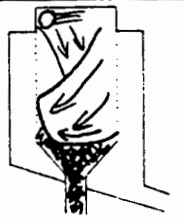
CS-AF-VC-1	167,71	168,54	6,52	6,55	38	62	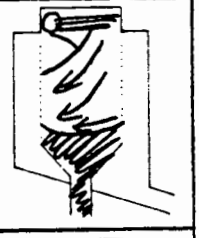
CS-AF-VC-3	111,58	117,36	4,34	4,56	50	50	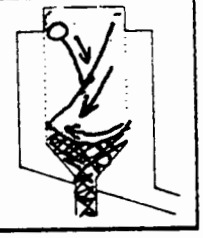

CYCLOSIEVE TEST RESULTS

DATE: 16-10-87 PARTICLES: 8mm, 2,7gcm³ COMMENTS:
50 particles

TEST NUMBER	BEND METER				SEPARATION		VORTEX DESCRIPTION
	PRIMARY FLOW (l/s)	SECONDARY FLOW (l/s)	PRIMARY VELOCITY (m/s)	SECONDARY VELOCITY (m/s)	% IN FINES SAMPLER	% IN COARSE SAMPLER	
CS-AF-VC-4	116,90	121,58	4,54	4,73	48	52	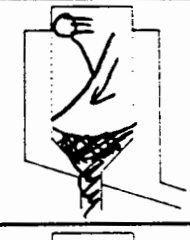
CS-AF-VC-5	88,43	95,42	3,44	3,71	36	64	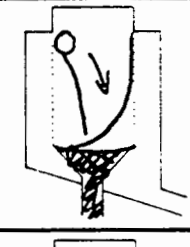
							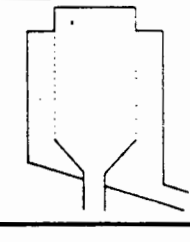

CYCLOSIEVE TEST RESULTS

DATE: 19-10-87 PARTICLES: 50; 8mm; 2,7g/cm³ COMMENTS: $Q_p - Q_s = \pm 44\ l/s$

TEST NUMBER	BEND METER				SEPARATION		VORTEX DESCRIPTION
	PRIMARY FLOW (l/s)	SECONDARY FLOW (l/s)	PRIMARY VELOCITY (m/s)	SECONDARY VELOCITY (m/s)	% IN FINES SAMPLER	% IN COARSE SAMPLER	
CS-A-VO-1	187,93	143,34	7,30	5,57	26	74	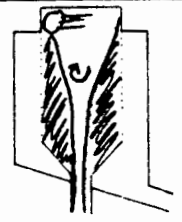
CS-A-VO-2	154,15	109,24	5,99	4.25	32	68	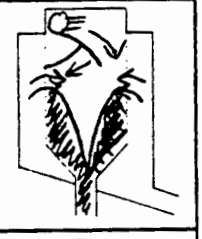
CS-A-VO-3	130,82	89,66	5,09	3,49	32	68	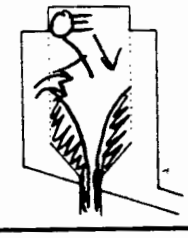

CYCLOSIEVE TEST RESULTS

DATE: 19-10-87 PARTICLES: 50; 8mm, 2,7g/cm³ COMMENTS:

TEST NUMBER	BEND METER				SEPARATION		VORTEX DESCRIPTION
	PRIMARY FLOW (l/s)	SECONDARY FLOW (l/s)	PRIMARY VELOCITY (m/s)	SECONDARY VELOCITY (m/s)	% IN FINES SAMPLER	% IN COARSE SAMPLER	
CS-A-VO-4	104,30	58,40	4,05	2,27	44	56	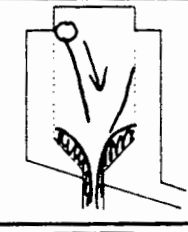
CS-A-VO-5	87,51	46,67	3,40	1,81	28	72	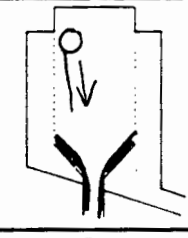
CS-A-VO-6	176,66	129,97	6,87	5,05	26	74	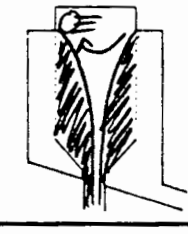

CYCLOSIEVE TEST RESULTS

DATE: 20-10-87 PARTICLES: 50; 8mm; 2,70g/cm³ COMMENTS: * Valve on C S open
* No → airflow
* -ve pressure

TEST NUMBER	BEND METER				SEPARATION		VORTEX DESCRIPTION
	PRIMARY FLOW (l/s)	SECONDARY FLOW (l/s)	PRIMARY VELOCITY (m/s)	SECONDARY VELOCITY (m/s)	% IN FINES SAMPLER	% IN COARSE SAMPLER	
CS-A-VO-7	172,09	128,49	6,69	4,99	28	72	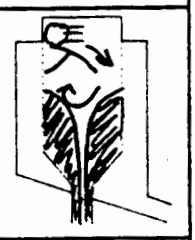
							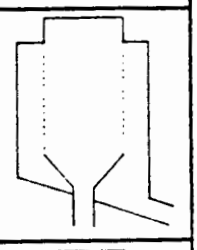
							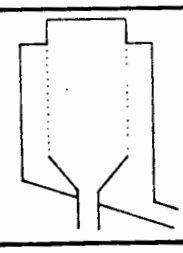

CYCLOSIEVE TEST RESULTS

DATE: 20-10-87 PARTICLES: 50; 8mm; 2,70g/cm³ COMMENTS: $Q_p - Q_s = \pm 20$ l/s

TEST NUMBER	BEND METER				SEPARATION		VORTEX DESCRIPTION
	PRIMARY FLOW (l/s)	SECONDARY FLOW (l/s)	PRIMARY VELOCITY (m/s)	SECONDARY VELOCITY (m/s)	% IN FINES SAMPLER	% IN COARSE SAMPLER	
CS-A-VO-8	172,92	153,01	6,72	5 95	42	58	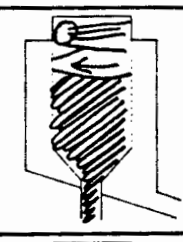
CS-A-VO-9	158,73	139,30	6,17	5,41	34	66	
CS-A-VO-10	140,48	120,12	5,46	4,67	36	64	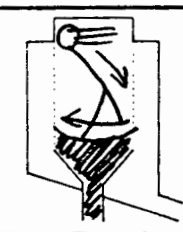

CYCLOSIEVE TEST RESULTS

DATE: 21-10-87 PARTICLES: 50;8mm, 2,70g/cm^3 COMMENTS: $Q_p - Q_s = 20\ell/s$

TEST NUMBER	BEND METER				SEPERATION		VORTEX DESCRIPTION
	PRIMARY FLOW (l/s)	SECONDARY FLOW (l/s)	PRIMARY VELOCITY (m/s)	SECONDARY VELOCITY (m/s)	% IN FINES SAMPLER	% IN COARSE SAMPLER	
CS-A-VO-11	126,57	105,45	9,92	4,10	40	60	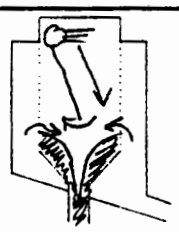
CS A-VO-12	107,57	88,48	4,18	3,44	50	50	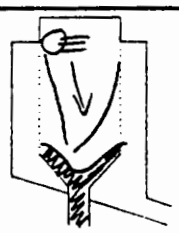
CS-A-VO-13	89,26	69,81	3,47	2,71	40	60	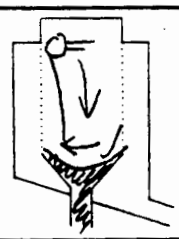

CYCLOSIEVE TEST RESULTS

DATE: 08-03-88 **PARTICLES:** 8 mm; 2,70 g/cm³ 20 particles **COMMENTS:**

TEST NUMBER	BEND METER				SEPARATION		VORTEX DESCRIPTION
	PRIMARY FLOW (l/s)	SECONDARY FLOW (l/s)	PRIMARY VELOCITY (m/s)	SECONDARY VELOCITY (m/s)	% IN FINES SAMPLER	% IN COARSE SAMPLER	
SSCS-AF-VC-1	136,48	135,92	5,35	5,28	90	10	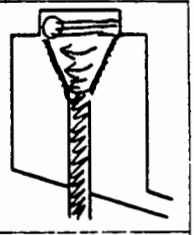
SSCS-AF-VC-2	156,11	156,22	6,07	6,07	98	2	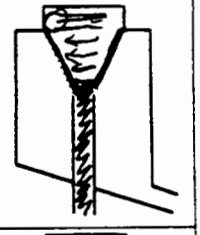
SSCS-AF-VC-3	170,68	167,087	6,63	6,494	96	4	

CYCLOSIEVE TEST RESULTS

DATE: **PARTICLES:** **COMMENTS:**

TEST NUMBER	BEND METER				SEPARATION		VORTEX DESCRIPTION
	PRIMARY FLOW (l/s)	SECONDARY FLOW (l/s)	PRIMARY VELOCITY (m/s)	SECONDARY VELOCITY (m/s)	% IN FINES SAMPLER	% IN COARSE SAMPLER	
SSCS-AF-VC-4	106,45	108,82	4,14	4,23	86	14	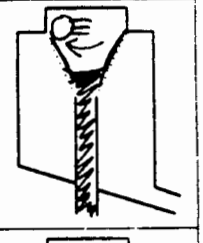
SSCS-AF-VC-5	89,88	91,67	3,49	3,56	80	20	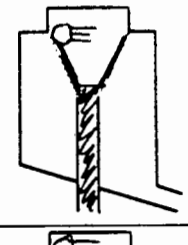
SSCS-AF-VC-6	121,860	121,07	4,74	4,71	94	6	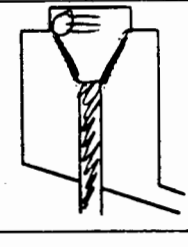

CYCLOSIEVE TEST RESULTS

DATE: 09-03-88 **PARTICLES:** 50, 8mm, 2,7g/cm³ **COMMENTS:** $Q_p - Q_s = \pm 45$ ℓ/s

TEST NUMBER	BEND METER				SEPARATION		VORTEX DESCRIPTION
	PRIMARY FLOW (ℓ/s)	SECONDARY FLOW (ℓ/s)	PRIMARY VELOCITY (m/s)	SECONDARY VELOCITY (m/s)	% IN FINES SAMPLER	% IN COARSE SAMPLER	
SSCS-A-VO-1	168,06	121,33	6,53	4,72	96	4	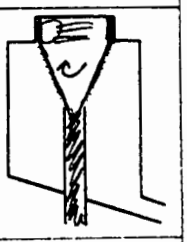
SSCS-A-VO-2	154,63	110,55	6,010	4,29	94	6	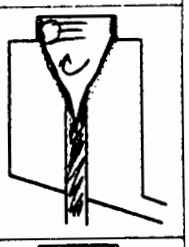
SSCS-A-VO-3	136,16	92,96	5,29	3,61	98	2	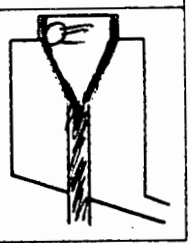

CYCLOSIEVE TEST RESULTS

DATE: 10-03-88 **PARTICLES:** 50; 8mm, 2,7g/cm³ **COMMENTS:** $Q_p - Q_s = \pm 45$ ℓ/s

TEST NUMBER	BEND METER				SEPARATION		VORTEX DESCRIPTION
	PRIMARY FLOW (ℓ/s)	SECONDARY FLOW (ℓ/s)	PRIMARY VELOCITY (m/s)	SECONDARY VELOCITY (m/s)	% IN FINES SAMPLER	% IN COARSE SAMPLER	
SSCS-A-VO-5	94,08	51,65	3,66	2,01	72	28	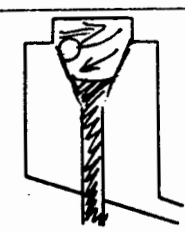
SSCS-A-VO-6	115,64	73,14	4,49	2,84	96	4	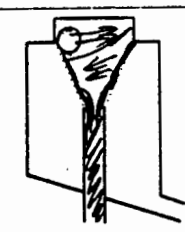
SSCS-A-VO-7	104,89	62,71	4,08	2,44	78	22	

CYCLOSIEVE TEST RESULTS

DATE: 11-03-88 **PARTICLES:** 50; 8mm ; 2,70g/cm³ **COMMENTS:** Full of water (small air vortex
Q_P = 153,600 V_P = 6,00

TEST NUMBER	BEND METER				SEPARATION		VORTEX DESCRIPTION
	PRIMARY FLOW (l/s)	SECONDARY FLOW (l/s)	PRIMARY VELOCITY (m/s)	SECONDARY VELOCITY (m/s)	% IN FINES SAMPLER	% IN COARSE SAMPLER	
SSCS-NA-VO-1	153,56	61,57	5,97	2,39	92	8	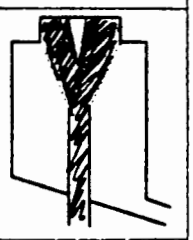
SSCS-NA-VO-2	156,04	86,95	6,06	3,38	98	2	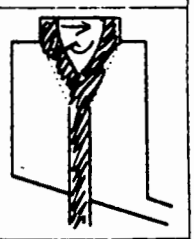
SSCS-NA-VO-3	155,44	113,38	6,04	4,41	96	4	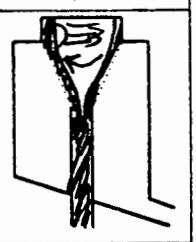

CYCLOSIEVE TEST RESULTS

DATE: 11-03-88 **PARTICLES:** 50; 8mm ; 2,70g/cm³ **COMMENTS:**

TEST NUMBER	BEND METER				SEPARATION		VORTEX DESCRIPTION
	PRIMARY FLOW (l/s)	SECONDARY FLOW (l/s)	PRIMARY VELOCITY (m/s)	SECONDARY VELOCITY (m/s)	% IN FINES SAMPLER	% IN COARSE SAMPLER	
SSCS-NA-VO-4	157,84	133,27	6,13	5,18	96	4	
SSCS-NA-VO-5	152,40	148,32	5,92	5,76	100	0	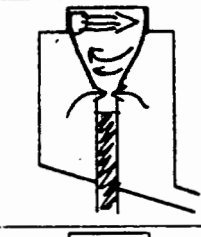
							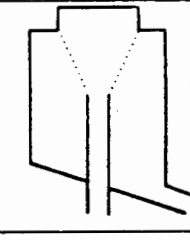

CYCLOSIEVE SIEVE ANALYSIS RESULTS

Qp = 156,48 l/s ; Qs = 106,97 l/s ; Cv = 0,72 % ; Screening 89,6% of -16mm

TEST No.	FINES (grams)										COARSE (grams)											
	4 | 5.6	5.6 | 6.7	6.7 | 8	8 | 9.5	9.5 | 11.2	11.2 | 13.2	13.2 | 16	16 | 25.4	25.4 | 37.1	37.1 | 50.8	4 | 5.6	5.6 | 6.7	6.7 | 8	8 | 9.5	9.5 | 11.2	11.2 | 13.2	13.2 | 16	16 | 25.4	25.4 | 37.1	37.1 | 50.8	50.8 | 75	75 | 100
CSCS-BOLK 1	330,9	641,3	998,3	1785,9	1971,2	2116,1	1293,6	940,0	511,6	—	8,4	15,1	37,5	92,4	195,1	348,5	361,5	1701,3	5611,3	4935,5	5365,2	796,2
				TROMP (%)									PARTICLE SIZE DISTRIBUTION (grams)									
	97,5	97,7	96,4	95,1	91,0	85,9	78,2	35,6	8,4	—	339,3	656,4	1035,8	1878,3	2166,3	2464,6	1655,1	2641,3	6122,9	4935,5	5365,2	796,2
													PARTICLE SIZE DISTRIBUTION (%)									
											1,4	3,6	7,0	13,3	20,5	28,6	34,1	42,9	63,2	79,6	97,4	100

Qp = 154,47 l/s ; Qs = 80,89 l/s ; Cv = 1,01 % ; Screening 90,6% of -16mm

TEST No.	FINES (grams)										COARSE (grams)											
	4 | 5.6	5.6 | 6.7	6.7 | 8	8 | 9.5	9.5 | 11.2	11.2 | 13.2	13.2 | 16	16 | 25.4	25.4 | 37.1	37.1 | 50.8	4 | 5.6	5.6 | 6.7	6.7 | 8	8 | 9.5	9.5 | 11.2	11.2 | 13.2	13.2 | 16	16 | 25.4	25.4 | 37.1	37.1 | 50.8	50.8 | 75	75 | 100
CSCS-BOLK 2	1767,7	2397,1	2660,8	3001,9	3578,3	3556,0	1936,1	2055,2	1812,5	281,4	177,8	110,3	127,4	222,4	794,0	544,6	485,5	1953,4	7369,8	6013,8	4958,5	688,6
				TROMP (%)									PARTICLE SIZE DISTRIBUTION (grams)									
	90,9	93,6	95,4	93,1	92,4	86,7	80,0	51,3	19,7	4,5	1945,5	2507,4	2788,2	3224,3	3872,3	4100,6	2421,6	4008,6	9182,3	6307,2	4958,5	688,6
													PARTICLE SIZE DISTRIBUTION (%)									
											4,3	9,7	15,8	22,9	31,4	40,3	45,6	54,4	74,5	87,7	98,5	100

CYCLOSIEVE SIEVE ANALYSIS RESULTS

Qp = 157,031/s ; Qs = 80,13 1/s ; Cv = 2,64 % ; Screening 84,8 % of -16mm

TEST No.	FINES (grams)											COARSE (grams)												
	2 | 4	4 | 5.6	5.6 | 6.7	6.7 | 8	8 | 9.5	9.5 | 11.2	11.2 | 13.2	13.2 | 16	16 | 25.4	25.4 | 37.1	37.1 | 50.8	2 | 4	4 | 5.6	5.6 | 6.7	6.7 | 8	8 | 9.5	9.5 | 11.2	11.2 | 13.2	13.2 | 16	16 | 25.4	25.4 | 37.1	37.1 | 50.8	50.8 | 75	75 | 100
C.S.C.S-BULK-3	5312	1474,4	2280,6	3016,1	4165,1	3964,8	4079,6	2130,2	1255,7	784,5	—	41,1	87,1	173,6	273,5	457,3	769,2	1105,7	980,2	1627,3	5111,4	3753,6	4237,3	760,6
					TROMP (%)										PARTICLE SIZE DISTRIBUTION (grams)									
	92,8	90,4	92,9	91,7	90,1	83,8	78,7	68,5	63,6	13,3	—	573,3	1561,5	2458,2	3289,6	4622,0	4734,0	5185,3	3110,4	2883,0	5895,9	3753,6	4237,3	760,6
															PARTICLE SIZE DISTRIBUTION (%)									
												1,3	5,0	10,7	18,3	29,0	40,0	52,1	59,3	66,0	79,7	88,4	98,2	100

Qp = 156,50 1/s ; Qs = 81,1 1/s ; Cv = 6,2,4 % ; Screening 62% of -16mm

TEST No.	FINES (grams)											COARSE (grams)												
	2 | 4	4 | 5.6	5.6 | 6.7	6.7 | 8	8 | 9.5	9.5 | 11.2	11.2 | 13.2	13.2 | 16	16 | 25.4	25.4 | 37.1	37.1 | 50.8	2 | 4	4 | 5.6	5.6 | 6.7	6.7 | 8	8 | 9.5	9.5 | 11.2	11.2 | 13.2	13.2 | 16	16 | 25.4	25.4 | 37.1	37.1 | 50.8	50.8 | 75	75 | 100
C.S.C.S-BULK-4	1351,6	1867,5	2087,6	2903,2	4190,5	3809,5	3791,0	1661,6	712,5	705,9	—	2316,8	1086,2	916,0	1086,3	1543,6	2033,6	2537,6	1909,3	1536,7	2656,8	1979,6	2363,3	783,3
					TROMP (%)										PARTICLE SIZE DISTRIBUTION (grams)									
	37,4	63,2	73,1	72,8	73,1	65,2	59,9	46,0	31,0	20,8	—	3698,0	2909,0	3803,6	3990,1	5736,1	5833,1	6375,6	3610,7	2269,2	3397,3	1979,6	2563,3	783,3
															PARTICLE SIZE DISTRIBUTION (%)									
												8,0	14,2	21,6	30,2	47,3	55,1	69,6	76,0	81,3	88,6	92,8	95,3	100

APPENDIX D : Spirosieve Experimental Results

HEAD LOSS OVER SPIROSIEVE FOR CLEAR WATER
(mean path length of 2.875 m)

VELOCITY (m/s)	HEAD LOSS (m)	HEAD LOSS (m/m)	f	Re
3.08	2.268	0.789	0.02598	190629
2.78	1.827	0.636	0.02569	171468
2.57	1.575	0.548	0.02591	158462
2.17	1.197	0.416	0.02762	134266
1.95	0.9198	0.32	0.02628	120420
1.44	0.63	0.219	0.03301	89371

BATCH SAMPLE TESTS ON SPIROSIEVE

3 kg ; 3.8 mm ;3.5 g/cm tracers

VELOCITY (m/s)	% PARTICLES PASSING
3.08	99.6
2.49	99.7
1.93	99.3
1.54	99.2

3 kg ; 3.8 mm ;3.5 g/cm tracers
& 5 kg ; 9-20 mm ; 2.70 g/cm
marine gravel

3.08	99.5
2.49	99.5
1.93	98.8
1.54	96

BATCH SAMPLE TESTS ON SPIROSIEVE	
3 kg ; 3.8 mm ;3.7 g/cm tracers	
VELOCITY (m/s)	% PARTICLES PASSING
3.09	98.7
2.6	98.7
1.97	98.1
1.5	96.1
3 kg ; 3.8 mm ;3.7 g/cm tracers screen length = 2.02 m	
3.09	97.6
2.56	97.6
1.97	97
1.5	95.5
3 kg ; 3.8 mm ;3.7 g/cm tracers horizontal orientation	
3.09	97.5
2.56	97.4
1.97	96.6
1.5	94.3

SPIROSIEVE SIEVE ANALYSIS RESULTS

V = 2,95 m/s Cv = 2,11 %

TEST No.	FINES (grams)									COARSE (grams)										
	2 | 4	4 | 5.6	5.6 | 6.7	6.7 | 8	8 | 9.5	9.5 | 11.2	11.2 | 13.2	13.2 | 16	16 | 19	2 | 4	4 | 5.6	5.6 | 6.7	6.7 | 8	8 | 9.5	9.5 | 11.2	11.2 | 13.2	13.2 | 16	16 | 19	19 | 22.4	22.4 +
4M-1-BULK	108,4	506,5	1019,5	1201,0	793,7	198,3	40,0	—	—	—	10,5	112,1	565,1	1319,9	1682,6	1801,3	1685,3	779,4	198,2	42,2
			TROMP (%)								PARTICLE SIZE DISTRIBUTION (grams)									
	100,00	97,22	90,09	68,00	37,55	10,54	2,17	—	—	108,4	521,0	1131,6	1766,1	2113,6	1880,9	1841,3	1685,3	779,4	198,2	42,2
											PARTICLE SIZE DISTRIBUTION (%)									
										0,90	5,22	14,59	29,23	46,74	62,33	77,59	91,55	98,01	99,65	—

V = 2,94 m/s Cv = 2,82 %

TEST No.	FINES (grams)									COARSE (grams)										
	2 | 4	4 | 5.6	5.6 | 6.7	6.7 | 8	8 | 9.5	9.5 | 11.2	11.2 | 13.2	13.2 | 16	16 | 19	2 | 4	4 | 5.6	5.6 | 6.7	6.7 | 8	8 | 9.5	9.5 | 11.2	11.2 | 13.2	13.2 | 16	16 | 19	19 | 22.4	22.4 +
5M-1-BULK	48,4	238,5	413,4	519,6	371,5	150,0	17,4	3,1	—	—	10,1	51,6	211,1	585,4	975,9	944,2	634,7	261,2	83,2	21,8
			TROMP (%)								PARTICLE SIZE DISTRIBUTION (grams)									
	100,0	95,9	88,9	71,1	38,8	13,3	1,8	0,5	—	48,4	248,6	465,0	730,7	956,9	1125,9	961,6	637,9	261,2	83,2	21,8
											PARTICLE SIZE DISTRIBUTION (%)									
										0,9	5,4	13,8	26,9	44,2	64,5	81,9	93,4	98,1	99,6	—

SPIROSIEVE SIEVE ANALYSIS RESULTS

V = 2,68 m/s Cv = 7,51 %

TEST No.	FINES (grams)									COARSE (grams)										
	2 | 4	4 | 5.6	5.6 | 6.7	6.7 | 8	8 | 9.5	9.5 | 11.2	11.2 | 13.2	13.2 | 16	16 | 19	2 | 4	4 | 5.6	5.6 | 6.7	6.7 | 8	8 | 9.5	9.5 | 11.2	11.2 | 13.2	13.2 | 16	16 | 19	19 | 22.4	22.4 +
SM-2-Bulk	2668	823,3	1112,4	1210,7	788,5	242,1	48,0	—	—	42,7	82,4	164,6	424,2	991,0	1333,0	1422,8	1118,6	355,4	135,8	—
			TROMP (%)								PARTICLE SIZE DISTRIBUTION (grams)									
	86,2	90,9	87,1	74,1	44,3	15,4	3,3	—	—	309,5	905,7	1277,0	1634,9	1779,5	1575,1	1470,8	1118,6	355,4	135,8	—
											PARTICLE SIZE DISTRIBUTION (%)									
										2,9	11,5	23,6	39,1	55,9	70,8	84,8	95,4	98,7	100,0	—

V = 2,90 m/s Cv = 4,71 %

TEST No.	FINES (grams)									COARSE (grams)										
	2 | 4	4 | 5.6	5.6 | 6.7	6.7 | 8	8 | 9.5	9.5 | 11.2	11.2 | 13.2	13.2 | 16	16 | 19	2 | 4	4 | 5.6	5.6 | 6.7	6.7 | 8	8 | 9.5	9.5 | 11.2	11.2 | 13.2	13.2 | 16	16 | 19	19 | 22.4	22.4 +
SM-3-Bulk	1800,1	996,2	385,1	456,7	342,5	108,4	12,3	3,3	—	319,0	82,9	53,7	233,9	595,4	848,8	989,6	684,6	263,3	68,4	—
			TROMP (%)								PARTICLE SIZE DISTRIBUTION (grams)									
	85,0	92,3	87,8	66,1	36,5	11,3	1,3	0,5	—	2119,1	1079,1	438,8	690,6	937,9	957,2	961,9	687,9	263,3	68,4	—
											PARTICLE SIZE DISTRIBUTION (%)									
										25,8	38,9	44,3	52,8	64,2	75,9	87,6	96,0	99,2	100,0	—

V = 2,80 m/s Cv = 4,74 %

TEST No.	FINES (grams)									COARSE (grams)										
	2 | 4	4 | 5.6	5.6 | 6.7	6.7 | 8	8 | 9.5	9.5 | 11.2	11.2 | 13.2	13.2 | 16	16 | 19	2 | 4	4 | 5.6	5.6 | 6.7	6.7 | 8	8 | 9.5	9.5 | 11.2	11.2 | 13.2	13.2 | 16	16 | 19	19 | 22.4	22.4 +
SM-5-BULK	884,9	728,2	606,2	630,4	391,7	134,9	19,3	—	—	77,6	44,2	73,7	248,4	526,7	740,2	681,6	531,3	205,9	50,0	—
			TROMP (%)								PARTICLE SIZE DISTRIBUTION (grams)									
	91,9	94,3	89,8	71,7	42,7	15,4	2,8	—	—	962,5	772,4	719,9	878,8	918,4	875,1	700,9	531,3	205,9	50,0	—
											PARTICLE SIZE DISTRIBUTION (%)									
										10,6	26,2	37,1	50,4	64,3	77,5	88,1	96,1	99,2	100,0	—

APPENDIX E : Spirosieve Clear Water Force Balance

CALCULATIONS OF FRICTION FACTORS AND REYNOLDS NUMBERS FOR SPIROSIEVE CLEAR WATER TESTS

With reference to the diagram below, a force balance is applied to an internal volume of fluid having length L and dimensions b and d as shown.

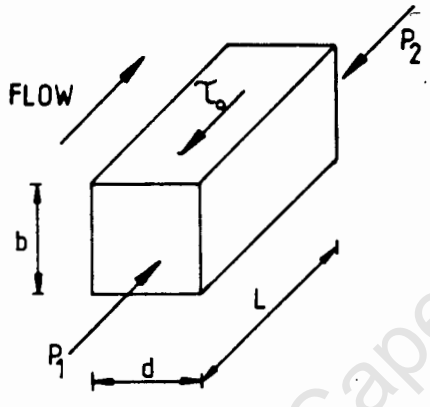

$(P_1 - P_2) = \Delta P$ (pressure loss)

$\Delta P\ b\ d = \tau_o\ (2b + 2d)\ L$

$\therefore$ the shear stress $\tau_o = \dfrac{\Delta P\ b\ d}{(2b+2d)L}$ (1)

friction factor $f = \dfrac{\tau_o}{\frac{1}{2}\ \rho\ \bar{v}^2}$ (2)

where $\bar{v}$ is the mean velocity

substituting (1) into (2) gives

$$f = \frac{\Delta P\ b\ d}{\rho \bar{v}^2 L(b+d)} \quad (3)$$

Reynolds Number $R_e = \frac{4Q}{\nu p}$

where p is the wetted perimeter

$$\therefore R_e = \frac{4Q}{10^{-6}\ (2b+2d)} \qquad (4)$$

By substituting in the values of b, d and L and the experimentally measured values of Q, $\bar{v}$ and ΔP into equations (3) and (4), a plot of friction factor versus Reynolds Number is obtained, as in Figure 8.29.

APPENDIX F : Design of Large Scale Spirosieve

DESIGN OF THE LARGE SCALE SPIROSIEVE

The large scale spirosieve was designed to be tested in the existing 181 mm diameter test rig, with a bulk sample of marine gravel similar to that which was used in the cyclosieve tests, i.e. 2 mm - 100 mm size range.

The required dimensions of the rectangular conduit are 250 mm x 150 mm. The screen would be made of 3 horizontal 16 mm square profile bars, with circular verticals at 45° spacings, and must be interchangeable with other screens.

This would result in a total flow area of 0,0367 m^2 and at a flow rate of 500 m^3/hr, an average velocity of 3,78 m/s.

It was shown in the batch sample tests on the spirosieve model that no improvement in the screening efficiency was gained when the velocity exceeded 2,5 m/s.

$$\frac{F_c}{F_g} = \frac{v^2}{R_g} = 4,72 \text{ g's (at 2,5 m/s)}$$

It was decided to design the larger scale spirosieve so that a centrifugal force of approximately 5,5 g's could be attained.

$$\therefore \quad R = \frac{v^2}{5,5g} = 0,265 \text{ m}$$

Figure F1 shows the dimensions of the final design, resulting in an $\frac{F_c}{F_g}$ ratio of 5,56 g's.

Figure F1

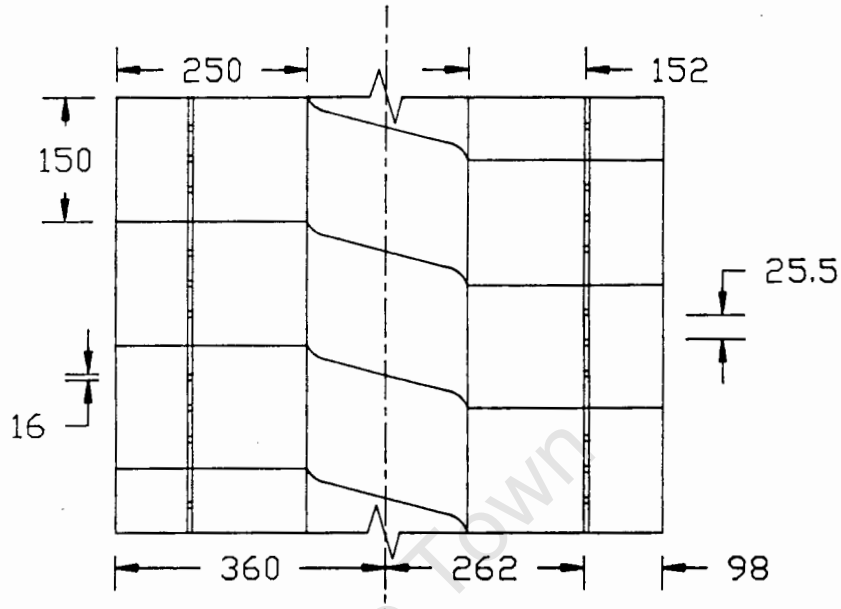

The total area of the screen was designed by using the present rato of the model screen area and solids flow rate, and the expected solids flow rate (at C_v = 6%)

At 2,72 m/s (5,56 g's) the flow rate (Q) in the model is 43,2 m^3/hr, and at C_v = 6% this yields a solids flow rate of 2,59 m^3/hr. The total screen area is 0,1224 m^2.

The expected solids flow rate in the full scale spirosieve is 30 m^3/hr, resulting in a required screen area (A_s) of 1,418 m^2.

With a screen height of 0,150 m the screen should be 9,453 m long or a total of 5,7 revolutions.

An elevation from the design drawings of the large scale spirosieve is shown in Figure F.2.

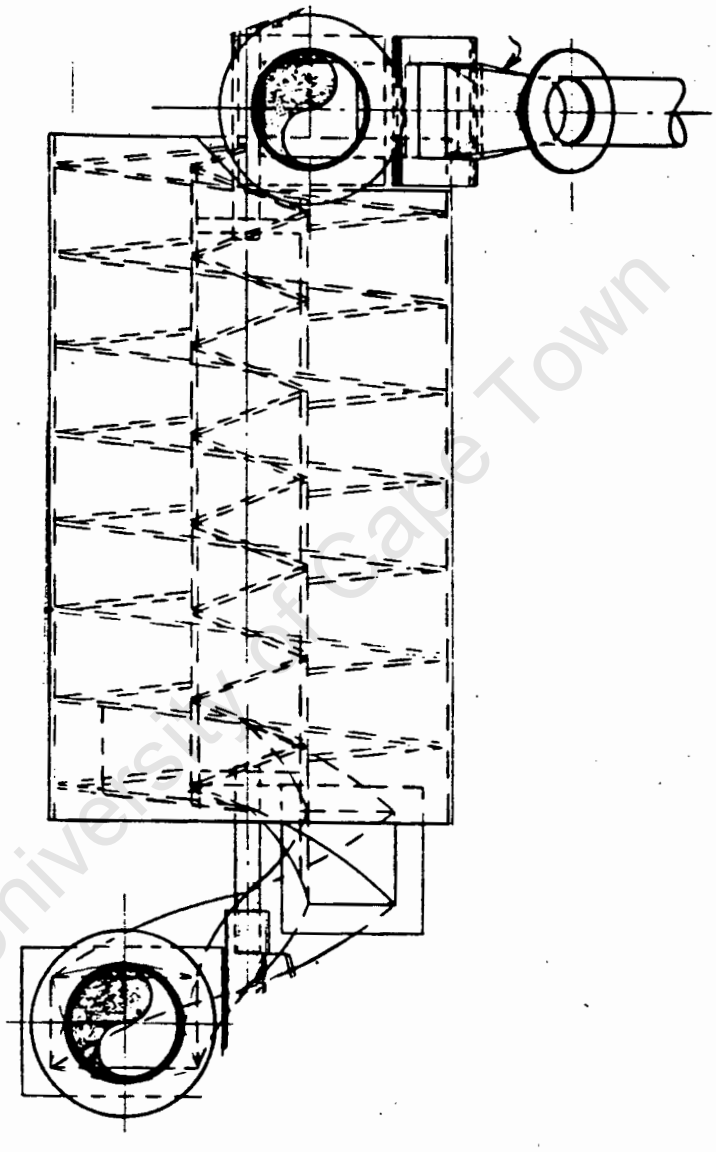

Figure F2